Author/s:
Chan, Kah Lok

Title:
Elucidating epigenetic mechanisms of cancer immune evasion

Date:
2023-03

Persistent Link:
https://hdl.handle.net/11343/336560

Elucidating epigenetic mechanisms of cancer immune evasion

Kah Lok Chan

ORCID: 0000-0002-9620-5558

Submitted in total fulfilment of the requirements for the degree of

Doctor of Philosophy

March 2023

Sir Peter MacCallum Department of Oncology

Faculty of Medicine, Dentistry and Health Sciences

The University of Melbourne

Abstract

Cancer immunotherapies have revolutionised the management of a wide range of haematological and solid organ malignancies, due to their potential to induce durable remissions in a proportion of responders. However, primary or acquired resistance remains problematic for the majority of patients, and typically arises from tumour-intrinsic properties that reduce immunogenicity or extrinsic factors promoting an immunosuppressive tumour microenvironment. Effective tumour antigen presentation via major histocompatibility proteins (MHC-I and/or MHC-II) to immune effector cells is a critical component of the adaptive anti-cancer response and genetic disruption of the MHC-I and/or MHC-II antigen presentation pathways, either through inactivating mutations or transcriptional silencing, is a well-recognised cause of resistance to both pharmacological and cellular immunotherapies.

In this thesis, I explore epigenetic mechanisms of MHC-I and MHC-II repression in cancer and identify an evolutionarily conserved role for Polycomb repressive complex 2 (PRC2) in MHC-I silencing. I also discover two key mechanisms of MHC-II regulation in acute myeloid leukaemia and melanoma: transcriptional repression of MHC-II pathway genes by the C-terminal binding protein (CtBP) co-repressor complex, and post-translational regulation of CIITA, the master regulator of MHC-II expression, by the FBXO11-containing E3 ubiquitin ligase complex. Targeting of these repressive pathways efficiently upregulates cell surface MHC expression and augments *in vitro* and *in vivo* adaptive immune responses. These findings provide valuable biological insights into mechanisms of cancer immune evasion and establish the scientific rationale for further pre-clinical and translational studies of these novel therapeutic strategies to overcome immunotherapy resistance via restoration of tumour antigen presentation.

Declaration

This declaration is to certify that:

a. This thesis comprises only my original work towards the PhD, except where indicated in the Preface,
b. Due acknowledgement has been made in the text to all other material used,
c. This thesis is fewer than 100,000 words in length, exclusive of tables, maps, bibliographies and appendices

Kah Lok Chan

Cancer Epigenetics Laboratory

Peter MacCallum Cancer Centre, Melbourne, Australia

The Sir Peter MacCallum Department of Oncology

Faculty of Medicine, Dentistry and Health Sciences

The University of Melbourne

Parkville, Australia

March 2023

Preface

This thesis includes experiments performed with the assistance of others. I would like to thank the following people for their contributions:

- A/Prof Marian Burr and Ms Christina Sparbier for collaboration on the MHC-I project and assistance with the MHC-II project
- Dr Enid Lam, Ms Miriam Yeung, Dr Yih-Chih Chan, Dr Dane Vassiliadis and Ms Andrea Gillespie for all of the bioinformatic analysis
- Dr Sylvain Garciaz for performing the whole-genome CRISPR screen in OCI-AML3 cells
- Dr Omer Gilan and Dr Charles Bell for curating the human epigenetic CRISPR screen libraries and designing the cloning protocol
- Ms Juliana Gomez, Dr Nishi Kumari and Dr Chelisa Cardinez for assistance with the MHC-II project, particularly experiments relating to melanoma cell lines and FBXO11 mechanism
- Dr Doen Ming Ong and Dr Fiona Brown for assistance with EHMT1/2 inhibitor treatment of patient AML samples
- Dr Jamie Kuzich for assistance with co-culture experiments

Figures in Chapter 1 were created in BioRender. The remainder of the experimentation and written work is my own.

Publications

Key publications related to PhD and referred to in thesis:

- **Chan KL**, Gomez J, Cardinez C, … , Wei AH, Burr ML*, Dawson MA*. *Inhibition of the CtBP complex and FBXO11 enhances MHC class II expression and anti-cancer immune responses.* **Cancer Cell** 2022;40(10):1190-1206. [Figures in Chapters 4 and 5 are adapted from this publication, as permitted by Cell Press policy.]
- Burr ML, Sparbier CE*, **Chan KL***, … , Lehner PJ, Sutherland KD, Dawson MA. *An evolutionarily conserved function of polycomb silences the MHC class I antigen presentation pathway and enables immune evasion in cancer.* **Cancer Cell** 2019;36(4):385-401. [Figures in Chapter 3 are adapted from this publication, as permitted by Cell Press policy.]

Contributions to other Dawson laboratory projects during PhD:

- Sparbier CE, Gillespie A, Gomez J, Kumari N, Motazedian A, **Chan KL**, … , Lam EYN, Burr ML*, Dawson MA*. *Targeting Menin disrupts the KMT2A/B and polycomb balance to paradoxically activate bivalent genes.* **Nat Cell Biol** 2023;25(2):258-272.
- Garciaz S, Guirguis AA, Muller S, Brown FC, Chan YC, Motazedian A, Rowe CL, Kuzich JL, **Chan KL**, … , McArthur K, Rodriguez R, Dawson MA. *Pharmacological reduction of mitochondrial iron triggers a non-canonical BAX/BAK dependent cell death.* **Cancer Discov** 2022;12(3):774-791.
- Macpherson L, Anokye J, Yeung MM, Lam EYN, Chan YC, Weng CF, Yeh P, Knezevic K, Butler MS, Hoegl A, **Chan KL**, … , Voss AK, Thomas T, Dawson MA. *HBO1 is required for the maintenance of leukaemia stem cells.* **Nature** 2020;577(7789):266-270.

(* = equal contribution)

Acknowledgements

Completing a PhD would not have been possible without the assistance of so many people, who have facilitated and shared in the highs and also provided much-needed strength during the lows.

I am incredibly grateful to my principal supervisors, **Mark Dawson** and **Marian Burr**, for their constant support and guidance throughout my PhD. Mark, thank you for giving me this once-in-a-lifetime opportunity to work with you and your amazing lab – it has been an immensely challenging, but equally rewarding, experience and I have enjoyed every second of it. Marian, thank you for being so generous with your time and patiently sharing your wealth of scientific knowledge with a complete novice. I have learned so much from both of you and look forward to witnessing the continued success of your labs in the years to come.

To my co-supervisor, **Constantine (Con) Tam**, thank you for your mentorship and considered advice over many years, which notably includes encouraging me to undertake this PhD! To my mentor, **Ashley Ng**, thank you for continually being a valuable sounding board for all things research- and career-related, over many cherished cups of coffee.

To the **Dawson lab**, thank you for five years of intellectual stimulation, laughter, inexhaustible patience and, most importantly, friendship. The lab is truly greater than the sum of its parts, which is a testament to everyone's love of science, determination to succeed and willingness to help others. I particularly want to thank **Christina Sparbier**, who taught me the fundamentals of laboratory science when I first joined the lab and with whom I have worked most closely during my PhD. Additionally, I would like to specifically thank **Sarah Ftouni**, **Paul Yeh**, **Kathy Knezevic**, **Enid Lam**, **Miriam Yeung**, **Katie Fennell**, **Yih-Chih Chan** and **Laura Macpherson** for their help and support. Thank you also to our external collaborators, including **Paul Beavis**, **Andrew Wei** and members of their labs for their critical help with key elements of this thesis.

I thank the **National Health and Medical Research Council (NHMRC)** and the **Haematology Society of Australia and New Zealand (HSANZ)**, who provided research funding. I am also grateful to **John Seymour**, **Ellen Maxwell** and **David Westerman** for enabling me to maintain my clinical and laboratory haematology skills during my PhD.

Finally, the time and effort invested in this PhD would only be possible due to the considerable encouragement, love and sacrifice from my family – particularly my parents, **Lai** and **Tho Lon**, and my sister, **See Mun**, who have unfailingly supported me at every stage of my training and career. I want to give special thanks to my wife, **Joy**, and our daughters, **Evie** and **Lara**, for their unwavering love and for putting up with all the long hours and weekends in the lab – I look forward to spending a lot more quality time with you now that the PhD is complete. Thank you also to my parents-in-law, **Jenny** and **Peter**, for their valued help and support during this lengthy journey. This thesis is dedicated to you all.

List of Abbreviations

5mC	5-methylcytosine
alloSCT	Allogeneic stem cell transplantation
AML	Acute myeloid leukaemia
APC	Antigen-presenting cell
APP	Antigen presentation pathway
ATF1	Activating transcription factor 1
B2M	β2-microglobulin
CAR	Chimeric antigen receptor
Cas9	CRISPR-associated protein 9
CBA	Cytometric bead assay
CD	Cluster of differentiation
CDR	Complementarity-determining region
CDYL	Chromodomain Y-like protein
ChIP	Chromatin immunoprecipitation
CHIP	Clonal haematopoiesis of indeterminate potential
CIITA	Class II transactivator
CIITApI	Class II transactivator, promoter 1
CIITApIII	Class II transactivator, promoter 3
CIITApIV	Class II transactivator, promoter 4
CLIP	Class II-associated Ii peptide
CML	Chronic myeloid leukaemia
CREB1	cAMP response element binding protein 1
CRISPR	Clustered regularly interspaced short palindromic repeats
crRNA	CRISPR RNA
CSD	Chromoshadow domain
CtBP	C-terminal binding protein
CTLA4	Cytotoxic T-lymphocyte-associated protein 4
DAMP	Danger-associated molecular pattern
DCs	Dendritic cells
dCas9	Nuclease-deficient Cas9
DFTD	Tasmanian devil facial tumour disease
DGE	Differential gene expression
DNA	Deoxyribonucleic acid

dsRNA	Double-stranded RNA
EGF	Epithelial growth factor
EMT	Epidermal-to-mesenchymal transition
ER	Endoplasmic reticulum
ERAD	Endoplasmic reticulum-associated degradation
ERV	Endogenous retroviral element
E:T	Effector:target
ETOH	Ethanol
EZH2	Enhancer of zeste homolog 2
FACS	Fluorescence-activated cell sorting
FBXO11	F-box only protein 11
FP	Fluorescent protein
GFP	Green fluorescent protein
GITR	Glucocorticoid-induced TNF receptor-related protein
GLP	G9a-like protein
GVHD	Graft-versus-host disease
GVL	Graft-versus-leukaemia
GVT	Graft-versus-tumour
H2AK119ub	Histone 2A lysine 119 monoubiquitination
H3K4me3	Histone 3 lysine 4 trimethylation
H3K9me1	Histone 3 lysine 9 monomethylation
H3K9me2	Histone 3 lysine 9 dimethylation
H3K9me3	Histone 3 lysine 9 trimethylation
H3K27ac	Histone 3 lysine 27 acetylation
H3K27me2	Histone 3 lysine 27 dimethylation
H3K27me3	Histone 3 lysine 27 trimethylation
HDAC	Histone deacetylase
HLA	Human leukocyte antigen
HP1	Heterochromatin protein 1
HSC	Haematopoietic stem cell
ICI	Immune checkpoint inhibitor
ICOS	Inducible co-stimulatory molecule
IFN	Interferon
IFNAR	Interferon-α/β receptor

Ig	Immunoglobulin
Ii	Invariant chain
IL	Interleukin
Indels	Insertions and deletions
IP-MS	Immunoprecipitation-mass spectrometry
IRAEs	Immune-related adverse effects
IRF1	Interferon regulatory factor 1
ISRE	Interferon-stimulated response element
ITIM	Immunoreceptor tyrosine-based inhibitory motif
JHDM	Jumonji domain-containing histone demethylase
KAP1	Krüppel-associated box interacting protein 1
KIR	Killer inhibitory receptor
KO	Knockout
LINE	Long interspersed nuclear element
LSD1	Lysine-specific demethylase 1
LXR	Liver-X nuclear receptor
MARCH	Membrane-associated RING-CH-type finger
MAVS	Mitochondrial antiviral signalling protein
MBD	Methyl-CpG-binding domain
mSCLC	Mouse small cell lung cancer
MDA5	Melanoma differentiation-associated protein 5
MDS	Myelodysplastic syndrome
MDSC	Myeloid-derived suppressor cell
MHC	Major histocompatibility complex
MHC-I	Major histocompatibility complex class I
MHC-II	Major histocompatibility complex class II
MOI	Multiplicity of infection
MPI	Median pixel intensity
NFκB	Nuclear factor kappa B
NFY	Nuclear factor Y
NHEJ	Non-homologous end joining
NK	Natural killer
NLRC5	NOD-like receptor family CARD domain containing 5
NLS	Nuclear localisation signal

OVA	Ovalbumin
PAMP	Pathogen-associated molecular pattern
PBMC	Peripheral blood mononuclear cell
PBS	Phosphate-buffered saline
PD-1	Programmed cell death protein 1
PD-L1	Programmed death ligand 1
PDGF	Platelet-derived growth factor
PE	Paired-end (sequencing)
PEV	Position effect variegation
PP2A	Protein phosphatase 2A
PRC1	Polycomb repressive complex 1
PRC2	Polycomb repressive complex 2
PRR	Pattern-recognition receptor
PVDF	Polyvinylidene fluoride
qRT-PCR	Quantitative real-time polymerase chain reaction
RFX	Regulatory factor X
rhIL-2	Recombinant human IL-2
RIC	Reduced-intensity conditioning
RMS	Root mean square
RNA	Ribonucleic acid
RREB1	Ras-responsive element binding protein 1
SCF	SKP1-CUL1-F-box (E3 ubiquitin ligase complex)
SCLC	Small cell lung cancer
scRNA-seq	Single-cell RNA sequencing
sgRNA	Single guide RNA
SHP2	SH2 domain-containing tyrosine phosphatase 2
SLAM	Signalling lymphocyte activation molecule
SMAC	Supramolecular activation cluster
SUV	Suppressor of variegation
TAM	Tumour-associated macrophage
TAP	Transporter associated with antigen presentation
TCR	T cell receptor
TIL	Tumour-infiltrating lymphocyte
TKI	Tyrosine kinase inhibitor

TME	Tumour microenvironment
tracrRNA	Trans-activating CRISPR RNA
T_{reg}	Regulatory T cell
TTD	Tandem Tudor domain
UMAP	Uniform manifold approximation and projection
UMI	Unique molecular identifier
V(D)J	Variable, diversity and joining (immunoglobulin gene segments)
WB	Western blot
WIZ	Widely interspaced zinc finger-containing protein
WT	Wildtype
X2BP	X2 box-binding protein

Table of Contents

List of Figures

List of Tables

Chapter 1 – Introduction

1.1 Cancer immunotherapy – a rapidly expanding frontier

The field of cancer immunotherapy has experienced an exciting renaissance in recent years, driven by the development and incorporation of many novel treatments into clinical practice, including immune checkpoint inhibitors (ICIs), bispecific antibodies and chimeric antigen receptor T (CAR-T) cells. These notable advances have revolutionised the therapeutic landscape for a variety of solid organ and haematological malignancies, due to their broad applicability, manageable toxicity profile and capacity to induce strikingly durable remissions in a proportion of responders. Considerable ongoing research efforts are focused on expanding the scope of existing immunotherapies, as well as bringing promising pre-clinical technologies such as therapeutic cancer vaccines to the bedside[1].

The successes achieved thus far illustrate the capacity of the immune system to exert and maintain robust anti-cancer responses. The immune system comprises innate and adaptive arms, both of which have the ability to recognise and eliminate tumour cells. However, with the exception of engineered bispecific antibodies and CAR-T cells, the majority of immunotherapies rely on presentation of tumour neoantigens to effector cells of the adaptive arm, facilitating cytotoxic T cell killing and the subsequent formation of immunological memory, which sustains disease control.

Despite the significant potential that immunotherapies have shown to date, the majority of patients treated with these interventions exhibit primary or acquired resistance. Both genomic and non-genomic resistance mechanisms have been identified, all of which enable tumour cells to evade the adaptive immune response[2]. Genomic resistance mechanisms typically impair the ability of tumour cells to present antigen to and activate immune effector cells, including mutations in the antigen presentation pathway (APP) or the interferon signalling pathway[2]. Of particular interest, however, are epigenetic processes that facilitate transcriptional silencing of essential APP components, which have been recently identified but hitherto remain incompletely understood. Characterising these key resistance mechanisms will not only provide important mechanistic insights into cancer immune evasion, but may permit effective restoration of antigen presentation and anti-tumour immunity via an expanding range of investigational therapies targeting various chromatin modifiers[3]. A more detailed overview of anti-tumour immunity, cancer epigenetics and their intersection at the clinical interface is presented below.

1.2 The immune system

Components of innate and adaptive immunity are defined by the types of receptors utilised for target recognition and how these are generated. The innate immune system relies on a limited number of germline-encoded receptors, which predominantly recognise foreign pathogens as well as endogenous cellular danger signals[4,5]. In contrast, the diverse T cell and B cell receptor repertoires that underpin adaptive immunity are generated somatically, with subsequent selection for pathogen-specific receptors by clonal expansion following exposure to the antigens that they target[6]. These features give rise to complementary functions of innate and adaptive immunity, whereby the innate arm generates a rapid initial reaction to infection, establishing preliminary control and providing time for specific effector cells of the adaptive arm to be selected, expand and contribute to the ongoing immune response. In addition, the innate and adaptive arms directly synergise on multiple levels to refine and potentiate each other's function, further strengthening host defences.

1.2.1 Innate immune system

The innate immune system encompasses both cellular and non-cellular components. Cellular components include natural killer (NK) cells, phagocytes (neutrophils, monocytes, macrophages and dendritic cells [DCs]), mast cells, basophils and eosinophils, while non-cellular components include antimicrobial peptides, inflammatory cytokines and the complement system[7].

Central to innate immune function is the ability to discriminate between "infectious non-self" and "non-infectious self"[8]. This principally occurs through the recognition of pathogen-associated molecular patterns (PAMPs), which are highly conserved molecular structures found across large groups of micro-organisms, such as bacterial lipopolysaccharide, peptidoglycan, mannans, viral double-stranded RNA and fungal glucans. These structures interact with a variety of pattern-recognition receptors (PRRs) that are expressed on innate immune cells or secreted into fluid compartments of the body, triggering a number of downstream reactions including phagocytosis, complement activation, pro-inflammatory signalling and induction of apoptosis[4]. Subsequently, an alternative model was proposed, arguing that the main role of the immune system was to sense and protect against danger, rather than distinguish between self and non-self[5]. This led to the discovery of danger-associated molecular patterns (DAMPs), which are corresponding structures released into the extracellular space following sterile tissue damage, as seen in cancer, ischaemia or autoimmunity[9,10].

Defects in innate immunity can lead to recurrent life-threatening infections, such as in chronic granulomatous disease, which is caused by mutations affecting the NADPH oxidase complex required for effective phagocytic function[11]. However, while the innate immune system is effective at eliminating conventional extracellular pathogens like bacteria and fungi, it is less able to sense and neutralise intracellular microbial infection and is also restricted by the genetically encoded repertoire of PRRs. These limitations are overcome by the adaptive immune system, which has evolved in vertebrates as a sophisticated second line of defence.

1.2.2 Adaptive immune system

The hallmark of the adaptive system is immunological memory, which enables it to rapidly recognise previously encountered antigenic stimuli and generate a highly specific and more powerful response. This phenomenon underpins the protective effect of vaccination and contrasts with the innate immune response, which is largely stereotypic even with repeated antigen challenge.

B and T lymphocytes are the key cells that mediate adaptive immunity. Although B and T lymphocytes differ in terms of ontogeny, cell surface marker expression and function, they both display transmembrane receptors that enable immune activation following cognate antigen binding. B cells serve a critical role in producing immunoglobulins to effect humoral immunity, while various T cell subsets fulfil a range of vital functions, including direct killing of infected or malignant host cells, activation of other immune cells, cytokine production and immune regulation.

1.2.2.1 B cell development and function

Initial stages of B cell development occur in primary lymphoid tissue (bone marrow and fetal liver) and subsequently progress in secondary lymphoid tissues (lymph nodes and spleen). Early B cell differentiation is characterised by ordered rearrangement of variable (V), diversity (D) and joining (J) gene segments of the immunoglobulin heavy chain locus, as well as rearrangement of the V and J gene segments of the immunoglobulin light chain locus[12]. The large number of possible V(D)J combinations generates the diverse primary repertoire of heavy and light chains, which are assembled to form the B cell receptor. An intact B cell receptor comprises two heavy chains and two light chains, as well as a transmembrane region that bears an intracellular signalling motif.

Following expression of the B cell receptor, immature B cells migrate to secondary lymphoid tissues. Upon cognate antigen binding within the lymph node germinal centre, B cells are activated, proliferate and undergo somatic hypermutation, which induces a high number of point mutations within the complementarity-determining regions (CDRs) of the variable segments of the heavy and light chains, thereby producing a range of B cells with varying specificity for the target antigen[13]. B cells with the highest specificity are selected over time, leading to affinity maturation and enhancement of future antigen recognition. The second key process that takes place in the germinal centre is class switch recombination, which allows switching of the immunoglobulin isotype from the low-affinity IgM that is initially produced by activated B cells to other immunoglobulin classes (IgA, IgE and IgG) that have different biological properties, tissue distribution and function[14].

After activation and maturation, a proportion of B cells undergo terminal differentiation into antibody-secreting plasma cells. These immunoglobulins are secreted into extracellular compartments, where they bind to pathogens to neutralise their activity or enable their destruction through phagocytosis and/or complement activation. In addition to this central role in humoral immunity, B cells also contribute to T cell responses by functioning as antigen-presenting cells, expressing co-stimulatory molecules and producing immunomodulatory cytokines such as interferon gamma (IFN-γ), interleukin-6 and interleukin-10[15].

1.2.2.2 T cell development and function

T cells originate from common lymphoid progenitors that form within the bone marrow and migrate to the thymus. In the thymus, T cell precursors undergo a series of developmental steps leading to expression of a T cell receptor (TCR) and, for T cells possessing an αβ TCR, expression of a CD4 or CD8 co-receptor. Early T cells do not express a TCR and also lack CD4 and CD8 ("double negative"), then progress to a "double positive" stage where they express TCR, CD4 and CD8, before finally committing to either a $CD4^+/CD8^-$ or $CD4^-/CD8^+$ phenotype.

Generation of the TCR repertoire occurs in a very similar fashion to immunoglobulin gene rearrangement in B cells, involving recombination of V and J gene segments in the TCRα locus and V, D and J gene segments in the TCRβ locus. After formation and expression of the TCR, T cells undergo positive and negative selection steps based on their level of TCR binding affinity for self-peptides presented by cortical thymic epithelial cells – T cells that do not engage self-

peptide fail to proliferate ("death by neglect"), while strong self-peptide interactions induce T cell apoptosis to minimise the potential for autoimmunity[16].

In broad terms, $CD8^+$ T cells possess cytotoxic activity and function as immune effectors that kill target cells through Fas- or perforin/granzyme-induced apoptosis and/or inflammatory cytokine production, while $CD4^+$ T cells predominantly orchestrate and regulate immune responses through activation of various immune cell subsets, cytokine release and potentiation of B cell antibody production and $CD8^+$ T cell activity[17-19]. Depending on the surrounding cytokine milieu, naïve $CD4^+$ T cells can differentiate into a variety of T helper cell subsets with distinct transcriptional programs, cytokine production and function[20]. A small subset of $CD4^+$ T cells also possess cytotoxic activity, while a separate fraction of $CD4^+$ T cells differentiate into regulatory T cells that limit immune responses to maintain peripheral tolerance and prevent autoimmune disorders. After activation and clonal proliferation due to encountering cognate antigen, a proportion of $CD4^+$ and $CD8^+$ T cells persist as circulating and tissue-resident memory T cells that rapidly trigger an enhanced, anamnestic response upon antigen re-exposure[21], thereby forming the basis of adaptive immunity.

1.2.3 T cell activation

To ensure appropriately directed adaptive immune responses, T cell activation is tightly regulated and requires a coordinated series of cellular signals. Incomplete initiation of this process instead results in T cell anergy, rendering them functionally inactive and unable to respond to subsequent stimulation.

1.2.3.1 Signal 1: TCR and peptide-MHC binding

The critical first step in T cell activation is the recognition of target antigen peptides, which are expressed on major histocompatibility complex (MHC) molecules by antigen-presenting cells (APCs). $CD8^+$ T cells recognise processed fragments of intracellular proteins presented via MHC class I (MHC-I), which is found on virtually all normal nucleated cells in the human body, whereas $CD4^+$ T cells recognise fragments of internalised extracellular peptides presented via MHC class II (MHC-II), which is restricted to professional APCs such as DCs, macrophages and B cells.

Binding of the TCR to a peptide-MHC complex induces conformational changes and polarisation of the T cell, leading to the formation of an immunological synapse between the T cell and APC. The immunological synapse comprises the central TCR-MHC complex surrounded by concentric

clusters of T cell and APC adhesion molecules as well as co-stimulatory or inhibitory receptors, known as supramolecular activation clusters (SMACs)[22]. The adhesion molecules, which include integrins and the signalling lymphocyte activation molecule (SLAM) family of proteins, enable sustained antigen engagement and directed secretion of cytokines and cytolytic granules into the synaptic cleft, while co-stimulatory and inhibitory molecules modulate the outcome of TCR-APC interaction and are a key target for modern cancer immunotherapies.

1.2.3.2 Signal 2: Co-stimulation

The second signal required for T cell activation is provided by co-stimulatory molecules such as the B7 proteins CD80 (B7-1) and CD86 (B7-2), which are expressed on APCs and bind to CD28 on the T cell surface. Other co-stimulatory receptor-ligand pairs of note include 4-1BB/4-1BB ligand, B7-H2/ICOS (inducible co-stimulatory molecule) and CD40/CD40 ligand[23]. Provision of both signals 1 and 2 trigger induction of multiple downstream signalling processes, including the MAP kinase, NF-κB and PI3K-AKT-mTOR pathways, resulting in T cell proliferation, survival and stimulation of effector function[23]. Cell surface expression of co-stimulatory molecules is upregulated by infection, cellular stress and sensing of danger signals by the innate immune system, and in turn promotes expression of co-inhibitory molecules. The resulting dynamic interplay between co-stimulatory and co-inhibitory signalling facilitates tuning of T cell responses in a "tidal" fashion, with T cell activation driven by a dominant co-stimulatory signal that is subsequently superseded by co-inhibitory signalling to disable the immune response when it is no longer required[24].

1.2.3.3 Signal 3: Inflammatory cytokines

In addition to TCR engagement and co-stimulation, a third signal from inflammatory cytokines, such as interleukin-12 or type I interferons (IFN-α and IFN-β), is typically required for optimal $CD8^+$ T cell expansion and function[25], culminating in the release of cytotoxic proteins including perforin, which forms pores in the target cell membrane and allows subsequent uptake of granzymes, which induce caspase activation and target cell apoptosis[26]. Interleukin-1 has also been shown to have a similar stimulatory effect on naïve $CD4^+$ T cells[27]. These cytokines complement interleukin-2 (IL-2) that is secreted by activated T cells following signals 1 and 2, which functions in an autocrine and paracrine manner to augment effector T cell proliferation and differentiation. Interestingly, IL-2 also plays a critical role in the development, function and survival of regulatory T cells (T_{reg})[28], which form a specialised T cell subset that maintains immune homeostasis through suppression of autoreactive immune cells. This counterbalance further

illustrates how the immune system is carefully controlled to appropriately respond to threats while minimising the potential for autoimmunity.

1.2.4 Structure and function of MHC-I

MHC-I is comprised of a single heavy α-chain with three extracellular domains (α1, α2 and α3), which is non-covalently linked to β2-microglobulin (B2M). There are three classical paralogues of the MHC-I heavy chain (HLA-A, HLA-B and HLA-C), which are all encoded by genes on chromosome 6p, whereas *B2M* is located on chromosome 15. Non-classical MHC-I alleles (HLA-E, HLA-F and HLA-G) have also been identified, which have restricted tissue distribution, genetic diversity and function[29]. The *HLA-A*, *HLA-B* and *HLA-C* genes all display considerable polymorphism, particularly within exons 2 and 3, which encode the α1 and α2 domains that form the peptide-binding groove. This predominantly influences the peptide repertoire that is presented on the cell surface by MHC-I to $CD8^+$ T cells[30].

MHC-I presents short peptide fragments (typically 8-10 amino acids in length) generated from proteasomal degradation of intracellular proteins, which are transported into the endoplasmic reticulum (ER) by the transporter associated with antigen presentation (TAP) complex, formed by the two proteins TAP-1 and TAP-2. Within the ER, MHC-I molecules form a peptide-loading complex with TAP, ERp57 and the chaperone proteins tapasin and calreticulin, which stabilise MHC-I until peptide binding occurs. Stable peptide-MHC complexes are then shuttled to the cell surface for antigen presentation (**Figure 1.1**), while MHC-I molecules that do not bind peptides are eventually degraded.

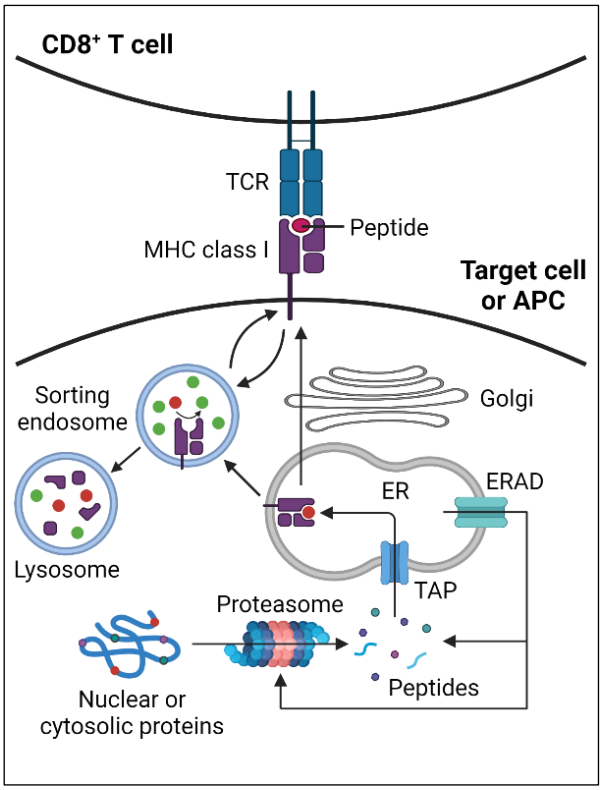

Figure 1.1. The MHC-I antigen presentation pathway.

Adapted from Neefjes *et al* (2011)[31]. Peptide fragments are generated through proteasomal degradation of intracellular proteins, which are loaded onto MHC-I within the endoplasmic reticulum and transported to the cell surface for presentation to $CD8^+$ T cells. ER, endoplasmic reticulum; ERAD, endoplasmic reticulum-associated degradation; TAP, transporter associated with antigen processing.

The TCR-MHC-I interaction is highly conserved, with the canonical docking conformation positioning the TCRα chain over the MHC-I α2 helix, while the TCRβ chain is above the MHC-I α1 helix[32]. This enables the hypervariable CDR3 loops of the TCR to contact and recognise the antigen within the MHC-I peptide-binding groove. Ultimately, MHC-I complexes at the cell surface are internalised and directed to either recycling endosomes or lysosomal degradation through the action of the membrane-associated RING-CH-type finger (MARCH) family of E3 ubiquitin ligases, particularly MARCH4 and MARCH9[33]. For recycled MHC-I, endosomal acidification induces release of bound peptide, allowing new peptides generated via the endocytic pathway to be loaded prior to transport back to the cell surface[31]. This forms the basis of antigen cross-presentation, the fundamental process through which APCs (predominantly DCs) can present fragments of extracellular proteins via MHC-I to activate $CD8^+$ cytotoxic T cells and stimulate adaptive immune responses in the setting of cancer, viral infection and vaccination.

1.2.5 Structure and function of MHC-II

MHC-II comprises a heterodimer of one α chain and one β chain, each of which contains two distinct domains. The α1 and β1 domains form the peptide-binding region and are anchored to the membrane-proximal α2 and β2 domains, respectively. As with MHC-I, there are three major paralogues of MHC-II, which are encoded by the *HLA-DR*, *HLA-DQ* and *HLA-DP* genes co-located with the MHC-I genes on chromosome 6p.

Peptides presented by MHC-II are larger in size (usually 13-25 amino acids in length)[34] and are typically formed through lysosomal degradation of extracellular proteins that are internalised via endocytosis or phagocytosis. MHC-II α and β chains are initially assembled in the ER together with the invariant chain (Ii), a chaperone protein that prevents ligand binding prior to downstream interaction with antigenic peptides. The Ii-MHC-II complex is transported to a late endosomal compartment where Ii is digested, leaving a class II-associated Ii peptide (CLIP) within the MHC-II peptide-binding groove. CLIP is then exchanged for an antigenic peptide by the HLA-DM protein, followed by transportation of the peptide-MHC-II complex to the cell surface (**Figure 1.2**).

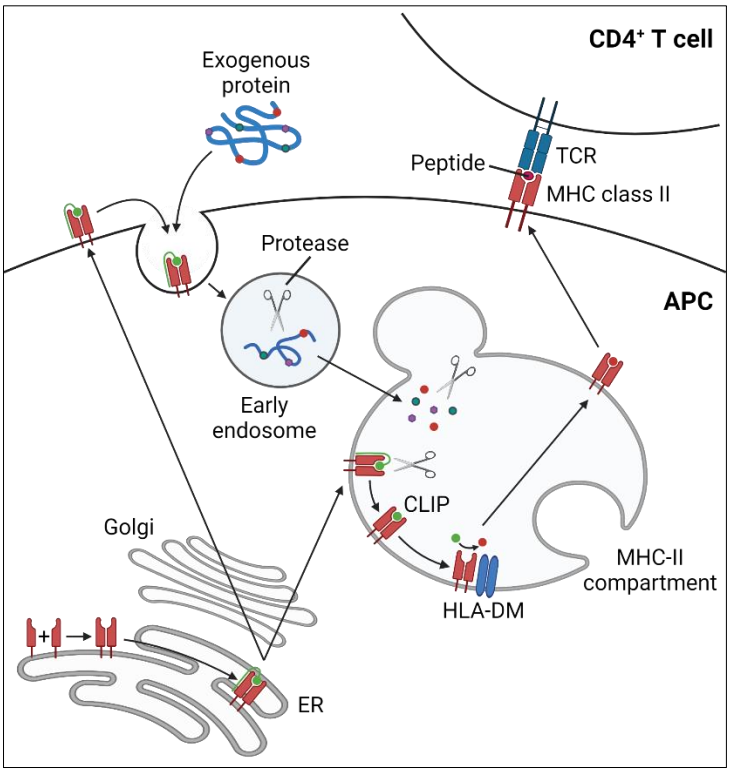

Figure 1.2. The MHC-II antigen presentation pathway.

Adapted from Neefjes *et al* (2011)[31]. Peptides presented on MHC-II are generated through lysosomal degradation of extracellular proteins that are internalised. Peptide fragments are

loaded onto MHC-II within a late endosomal compartment and transported to the cell surface for presentation to $CD4^+$ T cells. APC, antigen-processing cell; CLIP, Class II-associated invariant chain peptide; ER, endoplasmic reticulum.

Similar to MHC-I, peptide-MHC-II complexes are continuously recycled from the cell surface and are ubiquitinated by the E3 ubiquitin ligase MARCH1, targeting them for lysosomal degradation[35-37]. Peptide-MHC-II complexes can also be secreted from B cells or DCs in exosomes via a ubiquitin-independent mechanism[38], which can be taken up and used by MHC-II-deficient APCs to prime naïve $CD4^+$ T cells[39].

1.2.6 Regulation of MHC-I and MHC-II expression

Given their essential roles in immune function, the expression of MHC-I and MHC-II genes are tightly controlled through the interaction of specific transcription factors with conserved regulatory elements. For MHC-I genes, the key regulatory elements are the SXY module, the interferon-stimulated response element (ISRE) and the proximal enhancer A; the latter two facilitate inducible transcription of MHC-I through IFN-γ and NF-κB, respectively, and are not typically found at MHC-II gene promoters (**Figure 1.3**).

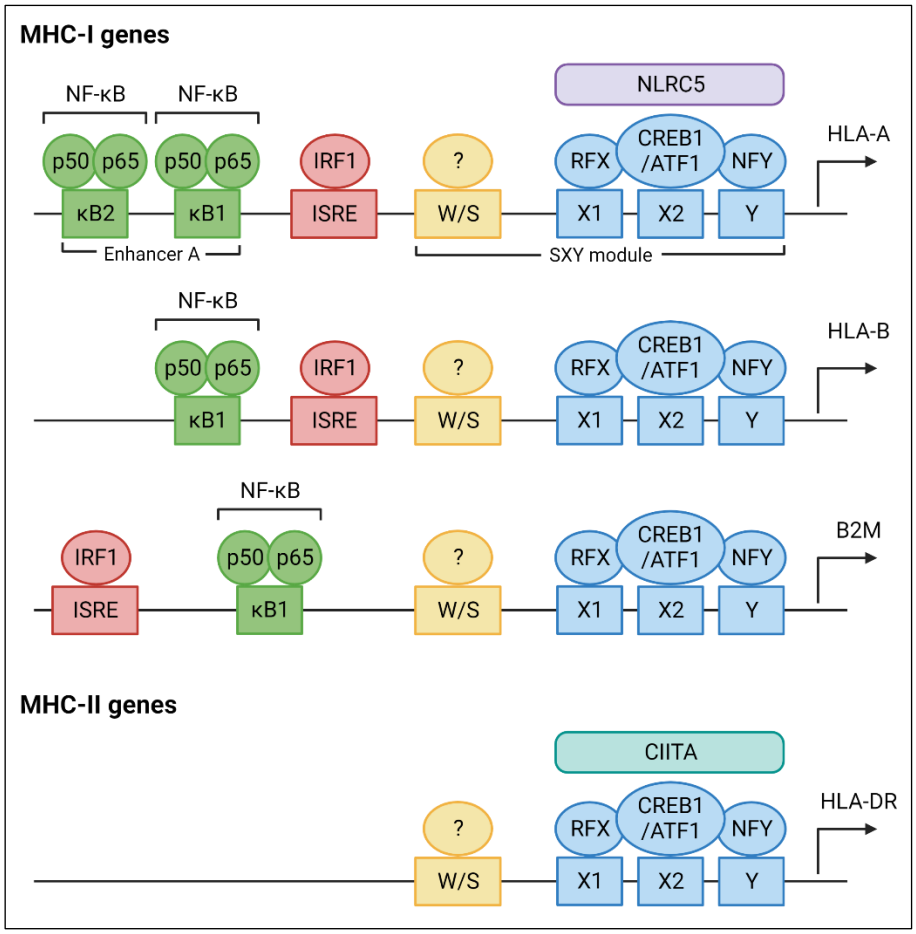

Figure 1.3. Promoters of MHC-I and MHC-II genes.

Adapted from Vijayan *et al* (2019)[40]. The promoter regions of MHC-I and MHC-II genes contain conserved regulatory elements, including the SXY module and, for MHC-I genes, an ISRE and proximal enhancer A. Transcription factors are recruited to the DNA motifs within the SXY module, forming an MHC enhanceosome that enables binding of NLRC5 and CIITA, which are transactivators that function as the master regulators of MHC-I and MHC-II expression, respectively. ATF1, activating transcription factor 1; CIITA, Class II Major Histocompatibility Complex transactivator; CREB1, cAMP response element binding protein 1; IRF1, interferon regulatory factor 1; ISRE, interferon-stimulated response element; NF-κB, nuclear factor kappa B; NFY, nuclear factor Y; NLRC5, NOD-like receptor family CARD domain containing 5; RFX, regulatory factor X.

The SXY module comprises four conserved, *cis*-regulatory DNA motifs, termed the W/S, X1, X2 and Y boxes, that are located at the proximal promoters of MHC genes and recruit additional transcription factors to form a key MHC enhanceosome complex. These transcription factors include the regulatory factor X (RFX) complex, which binds to the X1 box and comprises core RFX5, RFXAP and RFXANK subunits, as well as the X2 box-binding protein (X2BP) complex,

containing members of the CREB/ATF transcription factor family, and nuclear factor Y (NFY), which has NFYa, NFYb and NFYc subunits[41]. This enhanceosome collectively acts as a platform to facilitate binding of the master regulators of MHC-I and MHC-II gene expression, which are the transactivators NOD-like receptor family CARD domain containing 5 (NLRC5) and the Class II Major Histocompatibility Complex transactivator (CIITA). NLRC5 and CIITA are regarded as master regulators due to their essential requirement for MHC-I[42-45] and MHC-II[46] expression and the close correlation of NLRC5 and CIITA levels to cell surface MHC-I[47] and MHC-II expression[48], respectively. Notably, while the overall composition of the enhanceosome is similar, the preferential binding of NLRC5 or CIITA to their respective sets of MHC genes is determined by differences in the S box sequence[49].

Although MHC-I is expressed on virtually all nucleated cells in the body, the level of expression varies across tissue types and is considerably lower in organ systems and cellular contexts where immune activation is undesirable, such as the central nervous system and placenta[50]. These tissue-specific differences in MHC-I expression appear to be predominantly orchestrated by the balance between constitutively active enhancers and the variable activity of upstream silencing elements at MHC-I genes[51,52]. While levels of transcription inversely correlate with the cellular concentration of these silencing elements, clearly establishing their role in negative regulation of MHC-I, their exact mechanism of action and how they interact with enhancer factors remain incompletely characterised[51,52].

In contrast to the ubiquitous expression of MHC-I, constitutive MHC-II expression is restricted to professional APCs, but can also be induced in non-APCs following exposure to stimuli such as IFN-γ[53]; which functions by increasing CIITA levels in the absence of an ISRE at other MHC-II genes. The tissue-specific restriction of MHC-II expression is in part facilitated by the existence of three cell-specific isoforms of CIITA[54] – promoter 1 (CIITApI) is found in DCs, while promoter 3 (CIITApIII) is expressed in B lymphocytes and promoter 4 (CIITApIV) facilitates IFN-inducible MHC-II expression in non-haematopoietic cells[55]. MHC-II expression is also controlled by the recruitment of epigenetic modifiers such as histone deacetylases (HDACs), which block CIITA-mediated transactivation at MHC-II genes and can be overcome by the use of HDAC inhibitors to induce MHC-II upregulation[56-58]. Additionally, DNA hypermethylation at the CIITApIV promoter inhibits constitutive and inducible MHC-II expression in trophoblast cells[59-61], helping to prevent foetal rejection. Less is known about the epigenetic regulation of CIITA in other cellular contexts, although notably BLIMP-I represses CIITApIII and other MHC-II pathway genes

during terminal B cell differentiation into plasma cells[62], which is thought to relate to its ability to recruit HDACs and/or the histone methyltransferase EHMT2 (G9a). Understanding these physiological mechanisms of MHC-I and MHC-II regulation is important, particularly as they may be utilised and/or subverted to facilitate cancer immune evasion via MHC loss and impairment of antigen presentation.

1.3 Cancer immunotherapies

1.3.1 Immune checkpoint inhibitors

Co-inhibitory molecules are collectively described as "immune checkpoints", in recognition of their capacity to block T cell activation and restrain the adaptive immune response. The discovery of immune checkpoints has been effectively leveraged in the haematology/oncology setting through development of ICIs, which are monoclonal antibodies that bind to these receptors and abrogate their function, thereby boosting anti-cancer immunity. The best-known immune checkpoint molecules are cytotoxic T-lymphocyte-associated protein 4 (CTLA4) and the programmed cell death protein 1 (PD-1)/programmed death ligand 1 (PD-L1) axis, for which 6 monoclonal antibodies are currently funded on the Australian Pharmaceutical Benefits Scheme to treat a range of haematological and solid-organ malignancies. Remarkably, the potential scope for these immunotherapies continues to expand, with hundreds to thousands of active clinical trials examining additional cancer types and applications, as well as exploring targeting of novel checkpoints and inhibitory pathways[63].

1.3.1.1 CTLA4

CTLA4 was initially identified as a member of the immunoglobulin superfamily expressed primarily in activated cytotoxic T cells[64] and is also constitutively present on T_{reg} cells. Subsequent work demonstrated that CTLA4 has significantly greater affinity for CD80 (and to a lesser extent, CD86) than CD28[65], thereby blocking co-stimulatory signalling through competitive binding. In addition, CTLA4 induces cytoskeletal changes to increase T cell motility and disrupt engagement with target APCs[66] and also facilitates internalisation of CD80 and CD86[67], further impairing capacity for CD28 co-stimulation. Finally, CTLA4 recruits phosphatases such as SH2 domain-containing tyrosine phosphatase 2 (SHP2)[68] and protein phosphatase 2A (PP2A)[69], which inhibit phosphorylation of intracellular activation signals and promotes T cell tolerance and anergy[70].

This critical role in negative regulation of T cell responses was further characterised through generation of *Ctla4*-deficient mice, which rapidly developed uncontrolled lymphoproliferation and fatal, multiorgan autoimmune damage[71,72]. Ipilimumab, a monoclonal antibody to CTLA4, was the first ICI to enter clinical practice, with efficacy initially demonstrated in patients with metastatic melanoma and ovarian carcinoma[73,74] and later extending to a range of non-haematological malignancies, especially in combination with PD-1/PD-L1 inhibition[75].

1.3.1.2 PD-1/PD-L1 axis

PD-1 was first identified in studies of a T cell hybridoma cell line and was initially thought to be a protein related to programmed cell death[76]. Subsequent work found that PD-1 is expressed on all T cells at activation[77], negatively regulating T cell responses via binding to its cognate ligands, PD-L1 and PD-L2, and signalling through the immunoreceptor tyrosine-based inhibitory motif (ITIM) in its cytoplasmic tail[78]. This results in recruitment of the SHP1 and SHP2 phosphatases, which dephosphorylate and inactivate critical effectors of T cell activation signalling[79,80]. If the activating stimulus is cleared, PD-1 levels decrease in response; however, in the setting of chronic inflammatory states or cancer where there is persistent activation, PD-1 expression remains high, contributing to an exhausted T cell phenotype[81-84].

PD-L1 is expressed on a wide range of haematopoietic and non-haematopoietic cells and is therefore more relevant to a cancer context, whereas PD-L2 expression is mainly confined to DCs, macrophages and B cells[85]. As with CTLA4 inhibition, while targeting of PD-1 and/or PD-L1 using a variety of monoclonal antibodies has the potential to induce significant anti-cancer immune responses[86,87], their efficacy can be limited by the development of immune-related adverse events and resistance remains a common problem.

1.3.1.3 Efficacy and toxicity of immune checkpoint inhibitors

With over a decade of clinical experience in ICI use across a broad range of cancer contexts, it is now well recognised that response rates range from approximately 15-30% in most solid tumours and up to 45-60% in more immunogenic malignancies, such as melanoma and colorectal carcinoma with high microsatellite instability[88]. While these response rates may seem underwhelming when taken in isolation, it is important to note that alternatives in the pre-ICI era were limited to chemotherapy or immune cytokines, such as IL-2 or alpha-interferon, which were ineffective and toxic[89]. As an example, single-agent dacarbazine was the prior standard of care for metastatic melanoma, which had an overall response rate of less than 20% and a median

duration of response (and overall survival) of approximately 6 months[90]. In comparison, for modern-day combination ICI regimens, the median overall survival is greater than 5 years[91], unequivocally establishing the superiority of ICIs in this setting.

Consistent with their mechanism of action, the adverse effect profile of ICIs differs significantly from conventional chemotherapeutic agents and predominantly comprises autoimmune toxicity which may affect virtually any organ system in the human body. While the specific frequencies of immune-related adverse effects (IRAEs) vary between ICIs, the most common IRAEs include diarrhoea, colitis, endocrinopathies, rash and hepatitis[92]. However, the incidence of fatal adverse effects is low, ranging from 0.36% for anti-PD-1 monotherapy to 1.23% for anti-PD-1/PD-L1 and anti-CTLA4 combinations[93]. Depending on the type and severity of IRAE, management usually involves ICI discontinuation with or without immunosuppression.

1.3.2 Cellular immunotherapies

In contrast to ICIs that augment the function of endogenous T cells, cellular immunotherapies involve adoptive transfer of allogeneic or modified autologous immune cells to induce anti-cancer responses. Methods to enhance the efficacy of autologous products include *ex vivo* expansion and re-infusion of tumour-infiltrating lymphocytes (TILs), of which at least some are likely to recognise cancer-associated antigens[1]. However, the presence and activity of such TILs are critical assumptions that may not hold true for all patients and therefore restrict the efficacy and applicability of this approach.

Newer strategies involve engineering T cells to express a CAR containing a TCR that recognises a cancer-specific antigen, as well as co-stimulatory and CD3ζ signalling domains[94]. CAR-T cells have shown remarkable efficacy, particularly for haematological malignancies such as B cell lymphoproliferative disorders[95-97] – this is due in large part to the typically ubiquitous expression of the targeted CD19 antigen on B cells and relatively low morbidity of the prolonged B cell aplasia that accompanies durable responses, which can also be mitigated through supplementation of humoral immunity via immunoglobulin infusions[98]. Importantly, given the engineered TCR directly binds its target antigen, CAR-T cells function independently of MHC expression, which is an important distinction from the majority of other immunotherapies. This key strength may also be a vulnerability, however, as target antigen loss is a common and presently insurmountable mechanism of CAR-T resistance[99]. Additionally, the need for tumour-specific target antigens hampers broader utilisation of this technology, although considerable

ongoing research is focused on identifying and testing novel targets for other haematological and solid organ malignancies.

1.3.2.1 Allogeneic stem cell transplantation

As the earliest established form of cellular immunotherapy, initial iterations of allogeneic stem cell transplantation (alloSCT) involved treating patients with haematological malignancies using myeloablative doses of chemotherapy and/or radiotherapy, followed by re-infusion of mobilised haematopoietic stem cells (HSCs) from a related donor (ideally a sibling) or an unrelated, HLA-matched donor. This enabled delivery of anti-neoplastic therapies at otherwise lethal doses, with the infused HSCs reconstituting a new immune system that would also help to eradicate any residual disease and maintain remission through the formation of immunological memory[100]. Subsequently, to improve tolerability and access for older and other higher-risk patients, non-myeloablative or reduced-intensity conditioning (RIC) regimens were developed, focused on creating a permissive bone marrow niche for donor engraftment and primarily harnessing the immune graft-versus-tumour (GVT) effect[101-103]. Other notable advances include the utilisation of stem cells from umbilical cord blood or haploidentical donors, which provide viable alternatives in patients for whom a fully-matched sibling or unrelated donor cannot be found[104]. Consequently, following the first reports of successful alloSCT in the late 1960s and early 1970s[105,106], the range of indications for alloSCT has expanded considerably to include adverse-risk acute leukaemias, myelodysplastic syndromes, myeloproliferative neoplasms and lymphomas, as well as non-malignant conditions such as bone marrow failure syndromes and haemoglobinopathies[107].

Typically, a suitable alloSCT donor should match the recipient at both alleles of all major MHC-I loci (*HLA-A*, *HLA-B* and *HLA-C*) as well as the MHC-II loci *HLA-DRB1* and *HLA-DQB1*, referred to as a 10/10 match. This optimises the likelihood of engraftment and reduces the incidence and severity of graft-versus-host disease (GVHD)[108], which is a manifestation of the transplanted graft also recognising normal recipient tissues as foreign and triggering multi-system immune damage, which can lead to significant transplant-related morbidity and even death. The GVT effect and GVHD therefore represent a double-edged sword, as the development of GVHD has been linked to superior anti-neoplastic control[109,110] and interventions to reduce the risk of GVHD, such as T cell depletion of the graft, can increase the chance of disease relapse[111,112]. Accordingly, careful treatment decisions are required to manage this delicate balance and generate optimal, sustained GVT activity while minimising patient morbidity from GVHD.

Extending on the above clinical observations, pre-clinical studies clearly implicate T cells as a major driver of GVHD and, by extension, GVT effects. Using murine models of leukaemia and alloSCT, it was shown that allogeneic $CD8^+$ T cell-mediated GVHD requires recognition of recipient antigens presented on recipient APCs[113], a role that can subsequently be performed by donor APCs, likely via cross-priming[114]. Interestingly, donor APCs were dispensable for graft-versus-leukaemia (GVL) effects in this paper, although this finding may be specific to the particular *in vivo* model used as other groups have demonstrated the importance of donor APCs in GVL[115,116], particularly since recipient APCs are eliminated following alloSCT.

Other *in vitro* experiments have demonstrated that, aside from classical APCs, leukaemic blasts can also present antigenic peptides to $CD4^+$ T cells via MHC-II. For example, tumour cells from patients with chronic myeloid leukaemia (CML) induced proliferation of allogeneic $CD4^+$ T cells specifically recognising fragments of the *BCR::ABL* p210 fusion protein, a process that could be blocked using an anti-HLA-DR monoclonal antibody[117]. Subsequent work showed that cytotoxic $CD4^+$ T cells also recognise CML cells in an antigen- and HLA-DR-specific manner, although this unexpectedly augmented, instead of inhibited, CML cell growth[118]. This observation contrasts with an expanding body of evidence supporting a contribution from cytotoxic $CD4^+$ T cells to immune control of a range of haematological[119,120] and non-haematological[121-124] malignancies. Based on *in vivo* experiments with cytotoxic $CD8^+$ T cells in a CML mouse model, the ability of effector immune cells to facilitate tumour eradication or progression may depend on antigen load, as the $CD8^+$ T cells were able to eliminate low-level disease but promoted leukaemia proliferation when a heavy burden of disease was present, due to high-level IFN-γ secretion from activated immune cells[125]. This is consistent with clinical practice, where alloSCT is maximally effective when leukaemia patients are in complete remission following initial cytoreductive therapy, and has no role in the setting of uncontrolled disease[126].

In addition to the established role of T cells, donor NK cells have been reported to eliminate leukaemia cells in the setting of T cell-depleted haploidentical alloSCT[127]; however, the exact mechanism of NK alloreactivity is not well established[128]. Given NK cells are known to express killer inhibitory receptors (KIRs) that require MHC-I binding on target cells to prevent cytolysis, it is theorised that donor NK cells recognise and target recipient leukaemia cells lacking one or more MHC-I alleles that are present in the donor. Although potentially attractive as a strategy to boost GVL responses, especially since NK cells do not promote GVHD, further work is required to determine optimal ways to promote donor NK cell alloreactivity in anti-cancer contexts.

Current barriers that will need to be overcome include diminished NK cell efficacy in the setting of tumour bulk[129], as well as downregulation of activating receptor ligands on tumour cells in response to NK cell exposure[130-132].

1.3.3 Role of MHC-II in immunotherapy responses

In an era defined by the widespread incorporation of cancer immunotherapies into clinical practice, there is increasing recognition of the prognostic importance of MHC-II expression on tumour cells, especially in terms of predicting therapeutic responses and improved patient survival outcomes[133]. Interestingly, this is not limited to cancers arising from professional APCs that constitutively express MHC-II, such as diffuse large B cell lymphoma[134] and Hodgkin lymphoma[135], but also includes epithelial and cutaneous malignancies where the cell of origin does not normally express MHC-II, such as non-small cell lung cancer[136], breast cancer[137,138], serous ovarian cancer[139] and melanoma[140,141]. From histological analysis of patient biopsy specimens, tumour cell MHC-II expression correlates with an increase in TILs[137-140] and absence of lymphovascular invasion[138], linking the prognostic benefit observed from clinical trials to more direct evidence of improved immune responses. However, given one group also showed an enhancement in interferon signalling[138], it is unclear from these studies whether MHC-II expression is driving the immune response or merely secondary to interferon induction.

Attempts to determine the consequences of tumour cell MHC-II expression through *in vivo* models have shown conflicting results, although the majority are concordant with the above clinical analyses and support increased anti-cancer immunity. The predominant methods to induce MHC-II upregulation were CIITA overexpression and IFN-γ stimulation, which led to tumour rejection and/or growth inhibition across a variety of murine cancer cell lines, including sarcoma[142,143], breast carcinoma[144,145], colonic carcinoma[146] and lung adenocarcinoma[146]. Notably, using depletion studies, $CD4^+$ and $CD8^+$ T cells were the key adaptive immune cells required for tumour rejection[145]. Additionally, immune responses could still occur even in the absence of DCs[146], which are the classical APCs involved in T cell activation and implies that the MHC-II^+ tumour cells may directly present antigen to and activate $CD4^+$ T cells instead.

Conversely, isolated studies have shown that MHC-II upregulation via CIITA overexpression can accelerate tumour growth in a murine lung cancer model, although MHC-I was also increased and it was hypothesised that this may have a confounding effect via mitigation of NK cell cytotoxicity[147]. In another study, while MHC-II expression induced tumour rejection as

previously shown in a sarcoma cell line[142], co-expression of the invariant chain Ii potentiated tumour growth compared to CIITA-expressing cells alone[148]. Although it is plausible that Ii expression may block normal antigen presentation via the MHC-II pathway, this may be a phenomenon related to Ii overexpression at likely supraphysiological levels. Overall, the weight of evidence supports tumour cell MHC-II expression enhancing adaptive anti-tumour immunity via classical $CD4^+$ and $CD8^+$ T cell activation, leading to favourable immunotherapy outcomes.

1.4 Mechanisms of resistance to cancer immunotherapy

Clinically, immunotherapy resistance follows two main patterns – either primary resistance, where there is no response to treatment, or a period of initial response followed by subsequent progression due to disease adaptation enabling immune escape[149]. For both of these patterns, mechanisms of resistance may be classified according to whether they are intrinsic or extrinsic to the tumour cell.

1.4.1 Intrinsic mechanisms of immunotherapy resistance

Since ICIs targeting CTLA4 or the PD-1/PD-L1 axis block the normal function of these inhibitory proteins to promote immune killing of tumour cells, they remain critically dependent on antigen presentation via MHC-I to activate T cells. A major tumour-intrinsic mechanism of resistance therefore involves disabling antigen presentation via mutations or downregulation of key components of the MHC-I APP. One such component is B2M, for which biallelic genomic inactivation has been recurrently shown to disrupt antigen presentation and contribute to ICI resistance in up to 29.4% of longitudinal patient cohorts analysed[150-153]. Mutations in other MHC-I APP genes, including *TAP1*[154,155], *TAP2*[156] and *TAPBP*[157], have also been identified, mainly in isolated reports or small case series, and sometimes in conjunction with *B2M* and/or MHC-I heavy chain mutations. As shown above, these mutations may either be present at baseline, resulting in primary immunotherapy resistance, or are more typically seen as a specific, acquired lesion at disease progression in the absence of large-scale genomic changes affecting the MHC locus on chromosome 6. Notably, a case series of *B2M*-mutated, microsatellite instability-high colorectal cancer patients showed that a proportion still derived clinical benefit from ICI therapy, although no patients achieved a complete response and, for the majority, the duration of treatment was short (< 6 months)[158]. This may be due to the fact that not all *B2M* mutations led to complete loss of MHC-I expression, as well as intra-tumoral heterogeneity and selective clearance of a *B2M*-wildtype, $MHC\text{-}I^+$ compartment. γδ T cells have also been shown to

contribute to immunotherapy responses in MHC-I-deficient cancers[159], providing at least partial compensation for loss of conventional $CD8^+$ αβ T cell-mediated immunity.

MHC-I expression can also be downregulated through transcriptional silencing. This can occur via hypermethylation of MHC-I APP gene promoters[47,160-162]. *CIITA* promoter hypermethylation has also been observed as a mechanism of MHC-II silencing in non-haematological[163,164] and T cell malignancies[165]. In contrast to mutational loss, epigenetic inactivation of MHC-I and/or MHC-II can be overcome through the use of DNA methyltransferase inhibitors, leading to restoration of cell surface MHC expression and augmented immune responses[163,164,166-170]. Similar effects can also be seen with other epigenetic modifiers, including histone deacetylase inhibitors[170-173] and the histone demethylase LSD1[174]. An important caveat is that these pharmacological inhibitors often induce MHC upregulation and immune effects via reactivation of endogenous retroviral elements (ERVs), leading to production of double-stranded RNA structures that trigger a cell-intrinsic interferon response[174-176] as opposed to direct effects on MHC genes (**Figure 1.4**).

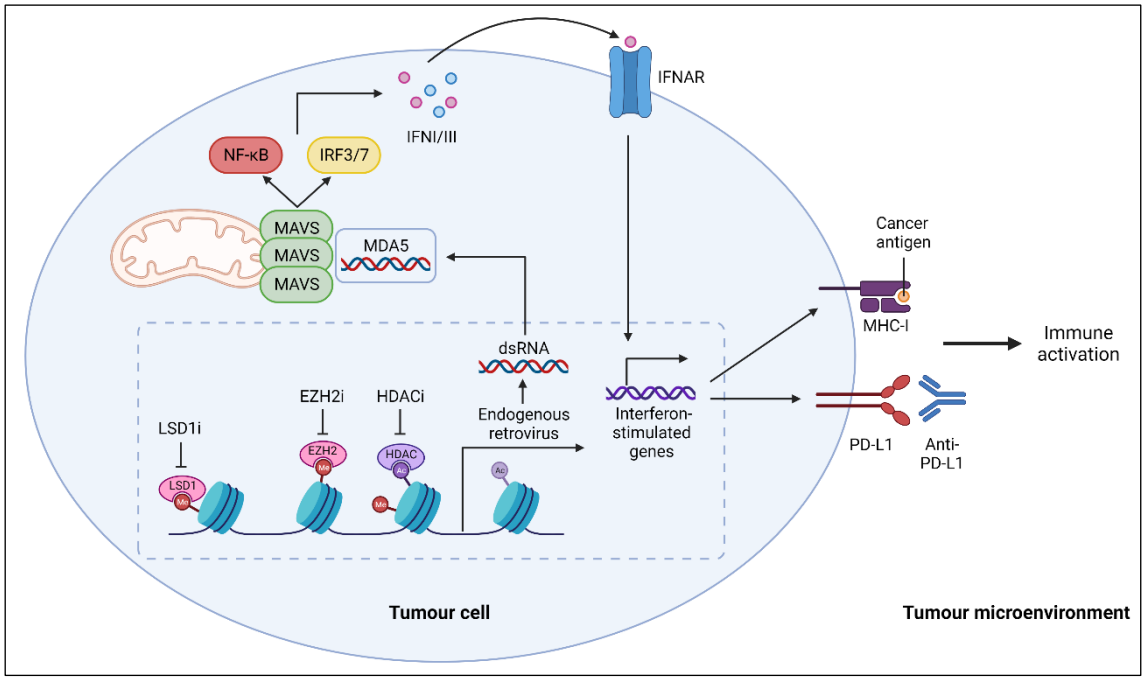

Figure 1.4. Epigenetic therapies reactivate endogenous retroviral elements and trigger a cell-intrinsic interferon response.

Adapted from Fennell *et al* (2019)[177]. A range of epigenetic therapies, such as inhibitors of EZH2, HDACs and LSD1, have been shown to reactivate silenced ERVs, resulting in formation of dsRNA molecules that are sensed by innate pattern recognition receptors such as MDA5. This triggers intracellular signalling pathways that induce a cell-intrinsic interferon response,

leading to upregulation of immune molecules such as MHC-I on the cell surface. dsRNA, double-stranded RNA; EZH2, enhancer of zeste homolog 2; HDAC, histone deacetylase; IFNAR, interferon-α/β receptor; IRF, interferon regulatory factor; LSD1, lysine-specific demethylase 1; MAVS, mitochondrial antiviral signalling protein; MDA5, melanoma differentiation-associated protein 5; NF-κB, nuclear factor kappa B; PD-L1, programmed death ligand 1.

Instead of downregulating MHC-I, an alternative method of blocking T cell activation is to reduce tumour neoantigen formation through a variety of mechanisms, including silencing or copy number loss of genes encoding neoantigenic mutations, as well as immunoediting or selection of less immunogenic clones[178]. Another rare but intriguing way to facilitate both is via cancer de-differentiation[179] or phenotypic switching[180,181] to a cell type characterised by low or absent MHC-I expression and/or loss of lineage antigens that confer immunogenicity. Additionally, IFN-γ signalling is another cornerstone of the adaptive anti-cancer immune response that can be disabled by mutations within essential pathway genes, such as *JAK1*, *JAK2*, *IRF1* or the IFN-γ receptor (*IFNGR1* or *IFNGR2*)[150,182-184].

Finally, alterations in intracellular signalling pathways can affect MHC-I and/or MHC-II expression, induce upregulation of inhibitory ligands and impact the surrounding tumour environment. A key example is upregulation of PD-L1 and/or PD-L2, which can not only be induced by genetic amplification of their respective genes[185,186], but also by activation of PI3K-AKT-mTOR[187,188] and EGFR[189] signalling, as well as MYC overexpression[190]. Amplification of the Ras-MAPK pathway (which lies downstream of EGFR) also suppressed tumour-specific MHC-I and MHC-II expression in triple-negative breast cancer cells[191] and lung cancer[192] and was associated with a reduction in TILs[191], while loss of the tumour suppressor PTEN activated PI3K-AKT signalling in melanoma and increased release of immunosuppressive cytokines such as VEGF, reducing TILs and conferring resistance to T cell-mediated apoptosis[193]. PI3K inhibition also enhanced IFN-γ induction of MHC-I and MHC-II expression in epithelial cell lines[194]. Similarly, melanomas with increased WNT/β-catenin signalling exhibit depletion of $CD103^+$ DCs via reduced production of the chemokine CCL4, impairing T cell priming and tumour control[195]. Of these signalling pathways, the EGFR-Ras-MAPK and PI3K-AKT-mTOR pathways are targetable with currently available inhibitors, which represent potential combinatorial strategies to subvert this form of resistance.

1.4.2 Extrinsic mechanisms of immunotherapy resistance

Extrinsic mechanisms of resistance focus on non-malignant cells with immunosuppressive capacity within the tumour microenvironment (TME), including T_{reg} cells, myeloid-derived suppressor cells (MDSCs) and tumour-associated macrophages (TAMs).

1.4.2.1 Regulatory T cells

T_{reg} cells are characterised by a distinctive $CD4^+/CD25^+/FOXP3^+$ immunophenotype and play a critical physiological role in immune regulation and maintaining self-tolerance through expression of inhibitory ligands, including CTLA4 and LAG-3, and secretion of immunosuppressive cytokines such as IL-10, TGF-β and adenosine[196]. A number of studies have shown that an increased ratio of tumour-infiltrating T_{reg} cells compared to $CD8^+$ effector TILs is associated with inferior prognosis in breast[197] and ovarian cancer[198,199]. Importantly, not all $CD4^+/FOXP3^+$ T cells have a regulatory phenotype, as one group identified distinct suppressive $FOXP3^{+(hi)}$ and pro-inflammatory $FOXP3^{+(low)}/CD45RA^-$ T cell populations in colorectal cancer specimens, with predominance of the former subtype conferring inferior prognosis that can be mitigated when there is significant concurrent infiltration by the latter subtype[200].

A number of strategies targeting T_{reg} cells to boost anti-tumour immunity have been explored. In keeping with the constitutive expression of CTLA4 on T_{reg} cells, anti-CTLA4 ICIs have been shown to deplete intratumoural T_{reg} cells, correlating with disease response[201,202]. While it remains unclear whether anti-PD-1 monoclonal antibodies have a similar effect despite PD-1 also being expressed on T_{reg} cells, targeting the chemokine receptor CCR4 blocks T_{reg} migration into tumours[203]. Additionally, early studies suggest that anti-LAG-3 antibodies[204] and agonist antibodies for the glucocorticoid-induced TNF receptor-related protein (GITR)[205] and OX40 (CD134)[206,207] may also inhibit T_{reg} function and augment immune response, especially in combination with other ICIs; however, further work is required to validate these findings.

1.4.2.2 Myeloid-derived suppressor cells

MDSCs are defined as granulocytes and monocytes with immunosuppressive activity, although they largely share the same cell surface immunophenotype as their classical counterparts, with one notable difference being low/negative HLA-DR expression in monocytic MDSCs compared to classical monocytes[208]. Similar to T_{reg} cells, MDSCs exert their immunosuppressive function on B, T and NK cells through expression of cell surface inhibitory ligands and cytokine secretion. Granulocytic MDSCs preferentially secrete reactive oxygen species, peroxynitrite, arginine 1 and

PGE_2, while monocytic MDSCs express PD-L1 and secrete IL-10 and TGF-β[208,209]. In cancer, MDSCs are well-recognised to promote tumour angiogenesis and metastasis[210,211] and their presence is associated with inferior response to a range of immune therapies, including ICIs[212] and adoptive T cell transfer[213].

Recruitment of MDSCs to tumours can be blocked by targeting key chemokine receptors such as CXCR2[214-216] and they can be depleted, albeit in a relatively non-specific manner, using a range of conventional chemotherapy agents[217-219]. Novel methods of MDSC depletion include induction of differentiation with all-*trans* retinoic acid[220,221] or via agonism of liver-X nuclear receptor (LXR) and its transcriptional target ApoE, which significantly reduces MDSC survival and showed promising activity in an early-phase clinical trial[222]. Finally, preclinical models suggest that blocking the immunosuppressive functions of MDSCs may also be effective, such as via impairment of PGE_2 synthesis[223,224] or targeting the endoplasmic reticulum stress response to reprogram MDSCs into myeloid cells with pro-inflammatory, anti-cancer capacity[225].

1.4.2.3 Tumour-associated macrophages

TAMs originate from circulating monocytes that migrate into tissues and undergo further differentiation, as well as innate tissue-resident macrophages that originate from yolk sac-derived progenitors[226]. Depending on the signals received, TAMs can be activated to polarise into either M1 (classical) or M2 (alternative) types, with M1 polarisation associated with tissue damage and tumour cell killing and M2 polarisation associated with tissue repair and remodelling, as well as promotion of an immunosuppressive TME[227]. In keeping with this, a high proportion of infiltrating TAMs typically portends poor prognosis across a range of human cancers[227,228], consistent with a predominant M2 phenotype. M2 macrophages promote tumour cell proliferation and invasion by secreting a number of growth factors, including epithelial growth factor (EGF), platelet-derived growth factor (PDGF) and TGF-β[229,230]. Similar to MDSCs, they also release immunosuppressive cytokines[231,232] and can recruit T_{reg} cells via the chemokine CCL22[198].

Although chemokine targeting to block monocyte recruitment to tissues has shown promise in pre-clinical models, this has not translated into meaningful clinical benefits[227], possibly since this does not stop replenishment of TAMs from tissue-resident precursors. Alternative strategies to functionally inhibit TAM-mediated immunosuppression have therefore been investigated, including IL-1 blockade[233,234] and inflammasome inhibition[235]. Interventions to activate anti-

tumour macrophage activity also appear promising, including CD40 agonist antibodies[236,237] and anti-CD47 monoclonal antibodies[238-240], although these likewise require further validation through clinical trials.

1.5 Epigenetics and cancer

1.5.1 Overview of epigenetics

The classical definition of epigenetics encompasses heritable cellular phenotypes arising from chromosomal changes that occur independently of alterations in the DNA sequence. In a molecular biology context, this typically refers to chromatin-based modifications that control transcriptional activity at gene loci. In eukaryotic cells, the entire genome is packaged as chromatin, a macromolecular complex of DNA and histone proteins, with two main types of chromatin structure: euchromatin, which is loosely packed and contains the majority of active genes, and heterochromatin, which is highly condensed, relatively inaccessible and transcriptionally silent[241].

The basic functional unit of chromatin is the nucleosome, which comprises 147 base pairs of DNA wrapped around a histone octamer, made up of two each of the histone proteins H2A, H2B, H3 and H4. Both histones and DNA can be chemically modified to alter gene activity through the dynamic function of three classes of proteins: writers deposit modifications, readers recognise and bind to these modifications and erasers remove these modifications[241]. The nature and position of histone modifications are critically important and often associated with specific effects on gene transcription – for example, trimethylation of lysine 27 on histone H3 (H3K27me3) is a well-known repressive mark, while trimethylation of lysine 4 on histone H3 (H3K4me3) is associated with transcriptionally active genes[242].

Methylation of the 5th carbon on cytosines (5-methylcytosine, 5mC) within CpG dinucleotides is another fundamental mechanism of transcriptional regulation via covalent DNA modification – this frequently occurs within CpG islands, which are genomic regions that contain a large number of CpG repeats and can be found in approximately 70% of mammalian gene promoters[241]. Establishment and maintenance of DNA methylation are conducted by DNA methyltransferases (DNMT3A/B and DNMT1 respectively) and conversion of 5mC back to its unmodified state either occurs in a passive fashion via loss of methylation patterns across cell divisions, or actively through the function of the ten eleven translocation (TET) family of demethylases[243]. Loss-of-function mutations in these proteins are well-known to occur in haematological malignancies

such as AML (approximately 10% for *TET2*, up to 35% for *DNMT3A*)[244,245]. Additionally, in myelodysplastic syndromes (MDS), which often precede development of AML, aberrant hypermethylation of tumour suppressor gene promoters has been shown to contribute to leukaemic progression[246]. The subsequent clinical utilisation of hypomethylating agents such as azacitidine has led to improved survival outcomes in these diseases, especially adverse-risk MDS and older AML patients unfit for intensive chemotherapy[247,248].

Given how tightly controlled histone and DNA modifications are laid down and removed, it is not surprising that mutations in epigenetic regulators disrupt this careful balance and contribute to oncogenesis and neoplastic adaptation. Conceptually, this likely occurs in a cancer- and context-specific fashion, encompassing activation or de-repression of oncogenes, silencing of tumour suppressor genes and/or targeted modulation of other cellular pathways to promote therapeutic resistance. As outlined in the previous section, silencing of key components of the immune system is a major cause of immunotherapy resistance; thus, understanding epigenetic mechanisms of transcriptional repression is important to obtain potential insights into cancer immune evasion and how they may be subverted for therapeutic benefit.

1.5.2 Polycomb repressive complex 2

The Polycomb group of proteins form two conserved epigenetic complexes, Polycomb repressive complex 1 (PRC1) and Polycomb repressive complex 2 (PRC2), that have a critical role in mediating gene silencing. This is predominantly through post-translational histone modification, with PRC1 facilitating monoubiquitination of lysine 119 on histone H2A (H2AK119ub) and PRC2 enabling di- and trimethylation of lysine 27 on histone H3 (H3K27me2/3)[249]. PRC1 and PRC2 are functionally antagonised by the Trithorax group of proteins, which are primarily responsible for gene activation. The balance between PRC1/2-mediated repression and Trithorax-mediated activation enables coordinated patterns of gene expression and silencing during development and their maintenance throughout adulthood[250].

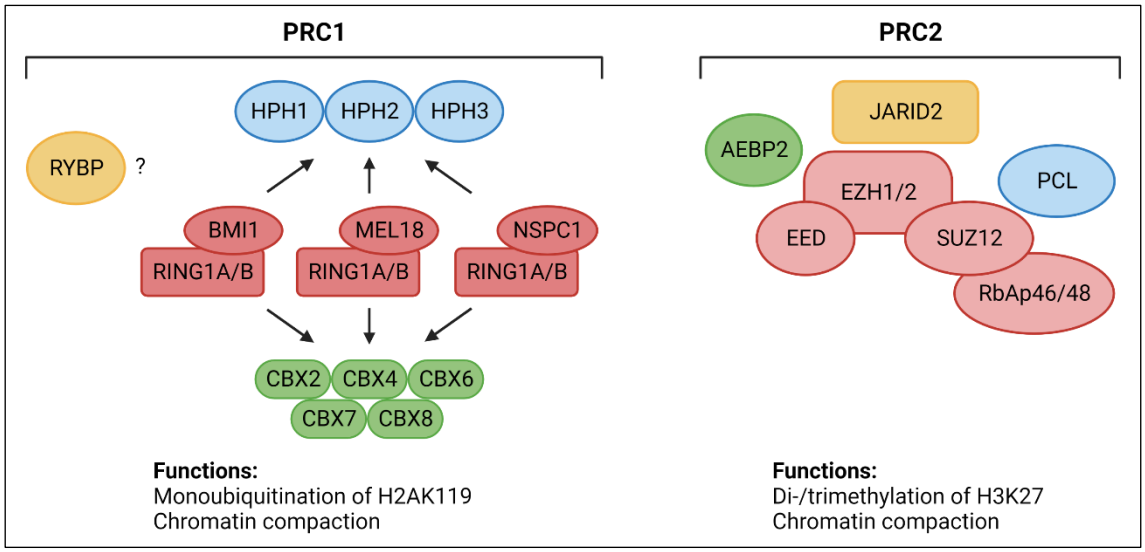

Figure 1.5. Composition of the Polycomb complexes PRC1 and PRC2.

Adapted from Margueron & Reinberg (2011)[249]. PRC1 and PRC2 are multiprotein complexes that comprise core components as well as facultative members that modulate their function. Monoubiquitination of histone H2A lysine 119, the central role of PRC1, is facilitated by the E3 ubiquitin ligases RING1A and RING1B. For PRC2, methylation of histone H3 lysine 27 is catalysed by the methyltransferases EZH1 and EZH2. Other PRC1/2 components play important roles in maintaining structural integrity of these complexes, as well as enabling binding to and inducing transcriptional repression of target genes.

Both PRC1 and PRC2 contain core complex components as well as a number of facultative members that modulate gene recruitment and enzymatic activity (**Figure 1.5**). PRC2 comprises four main proteins: EZH1/2, EED, SUZ12 and RbAp46/48 (RBBP7/4). EZH1 and EZH2 are SET-domain-containing histone methyltransferases that deposit the chromatin modification, while EED is a scaffolding protein that also binds and localises PRC2 to existing H3K27me3 marks in the genome, facilitating maintenance of a repressive chromatin state[251]. SUZ12 has a key role in maintaining PRC2 structural stability[252,253] and RBBP7/4 may help localise PRC2 to chromatin via its histone-binding ability[254]. Association of the core complex with accessory proteins gives rise to two mutually exclusive subcomplexes: PRC2.1, which also contains a polycomb-like homolog (one of the proteins PHF1, MTF2 or PHF19) and EPOP or PALI1/2; and PRC2.2, which contains AEBP2 and JARID2[255].

Polycomb-mediated repression occurs through a number of mechanisms, including chromatin compaction, which blocks RNA polymerase II recruitment and chromatin remodelling by the SWI/SNF complex[256]. In addition, Polycomb proteins block the histone acetyltransferase activity

of CBP and impairs acetylation of H3K27 (H3K27ac)[257], a mark of active gene enhancers. H3K27ac formation is also suppressed by H3K27me2, which is present on approximately 70% of total histone H3 in the form of large chromatin domains and, in doing so, is thought to prevent non-specific enhancer activation[258]. Finally, Polycomb complexes can facilitate formation of higher-order chromatin loops that stabilise repression of involved genes[259-261].

In cancer, PRC2 members have been implicated in a number of contexts – particularly EZH2, which is associated with more aggressive disease and poorer prognosis when overexpressed in prostate cancer[262] and breast cancer[263]. EZH2 is also commonly dysregulated in lymphoid malignancies, such as follicular lymphoma and germinal centre-type diffuse large B cell lymphoma[264], through gain-of-function mutations resulting in repression of BLIMP-1 and impaired terminal differentiation of germinal centre B cells[265]. In contrast, inactivating mutations in *EZH2* are commonly seen in T-cell acute lymphoblastic leukaemia, abrogating its role in developmental silencing of stem cell gene expression programs, including JAK/STAT signalling[266,267]. Illustrating how insights into molecular mechanisms of oncogenesis can be leveraged for therapeutic potential, tazemetostat, a potent and selective inhibitor of EZH2, has been approved by the FDA for treatment of both follicular lymphoma[268] as well as advanced epithelioid sarcoma with loss of function of INI1/SMARCB1, which results in dependence on EZH2[269]. While dysregulation of other core PRC2 components such as SUZ12 and EED have also been reported in cancer[270], these remain less well-studied to date and drug development efforts for EED, the other currently targetable PRC2 component, lag well behind those for EZH2.

1.5.3 Histone 3 lysine 9 methylation

Another key histone modification involved in transcriptional repression is methylation of histone 3 lysine 9, especially di- (H3K9me2) and trimethylation (H3K9me3). These modifications play a critical role in heterochromatin formation, especially constitutive heterochromatin, which comprises gene-poor, stably silenced DNA and is predominantly located in pericentromeric satellites and telomeric regions[271]. H3K9 methylation in these chromosomal regions functions as a binding site for heterochromatin protein 1 (HP1) family proteins[272-274], leading to recruitment of H3K9 methyltransferases, further H3K9 methylation and heterochromatin propagation[275]. Additionally, H3K9 methylation also plays a role in dynamic gene repression and facultative heterochromatin formation, such as in X chromosome inactivation[276].

1.5.3.1 Writers of H3K9 methylation

There are six mammalian H3K9 methyltransferases, which can be separated into three distinct families comprising two members each, with corresponding homologs for each family in mouse (*Mus musculus*), *Drosophila melanogaster* and *Caenorhabditis elegans*[277] (**Figure 1.6**).

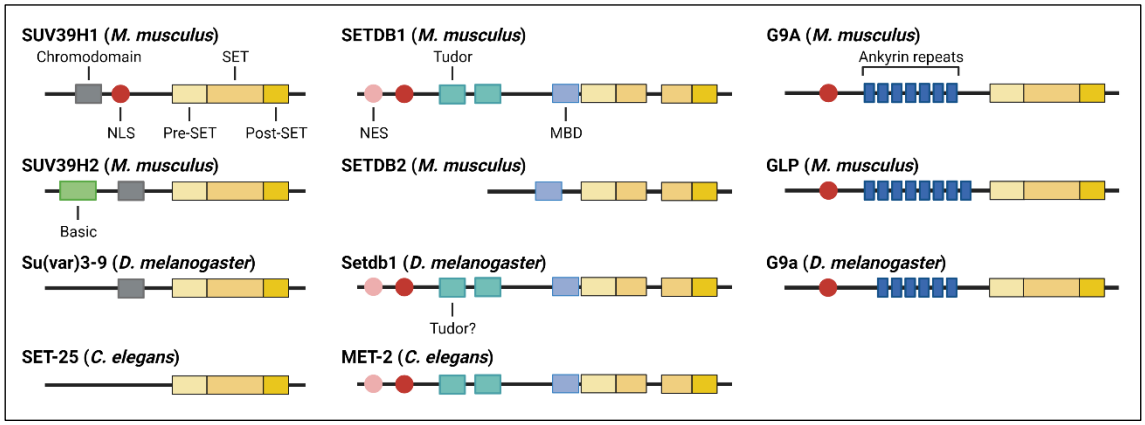

Figure 1.6. H3K9 methyltransferases.

Adapted from Padeken *et al* (2022)[277]. H3K9 methylation plays a crucial role in formation and maintenance of transcriptionally silent heterochromatin. Six mammalian H3K9 methyltransferases have been identified, with corresponding homologs also present in model organisms such as *Drosophila melanogaster* and *Caenorhabditis elegans*. MBD, methyl-CpG-binding domain; NLS, nuclear localisation signal.

The "suppressor of variegation" (SUV) family is named after the Drosophila H3K9 methyltransferase Su(var)3-9, which was identified as a suppressor of position effect variegation (PEV)[278]. This phenomenon was observed in *D. melanogaster* due to an inversion of the X chromosome that placed the euchromatic *white* gene near pericentromeric heterochromatin, leading to stochastic silencing of this gene and variegated loss of red eye facet colour[279]. PEV has subsequently been utilised as a genetic assay to identify key proteins required for heterochromatin formation.

The SUV family of H3K9 methyltransferases is characterised by a central SET domain possessing enzymatic activity, flanked by pre-SET and post-SET domains that are essential for its function (**Figure 1.6**). The mammalian homologs, SUV39H1 and SUV39H2, preferentially bind H3K9me1 and catalyse H3K9me2/me3 formation at pericentric heterochromatin[280], contributing to genomic stability and silencing of ERVs and long interspersed nuclear elements (LINEs)[281]. SUV39H1/H2 can also bind RNA transcribed from major satellite repeats[282,283], providing a

mechanism for formation of *de novo* heterochromatin at target sites where H3K9me1 is not constitutively present. Finally, SUV39H1/H2 interact with HP1 proteins[284] to maintain repression of methylated histones and re-establishment of constitutive heterochromatin following DNA replication.

The second family of H3K9 methyltransferases includes SETDB1, which differs from SUV39H1/H2 by the presence of a bifurcated SET domain[285] (**Figure 1.6**) and the ability to methylate unmodified H3K9, thereby being able to generate mono-, di- and trimethylated H3K9[286]. It plays a primary role in silencing of ERVs and other repetitive elements and is recruited to these sites by Krüppel-associated box interacting protein 1 (KAP1)[286]. SETDB1 also contains three Tudor domains that binds to histone H3 tails bivalently marked by H3K14 acetylation and H3K9 methylation – this is enriched in LINE elements and is proposed to mediate efficient silencing of these regions[287]. The second member of this family is SETDB2, which is closely related to SETDB1 although, like SUV39H1/H2, appears to preferentially bind and methylate H3K9me1[288].

The third family of H3K9 methyltransferases comprises euchromatic histone lysine methyltransferase 1 (EHMT1, otherwise known as G9a-like protein, GLP) and EHMT2 (G9a). While these two proteins share significant sequence homology and can form either homomeric or heteromeric complexes *in vitro*, they preferentially form heteromers *in vivo* and inhibition of either is sufficient to markedly deplete H3K9 methylation[289]. The SET domains for EHMT1 and EHMT2 are only able to catalyse H3K9me1 and H3K9me2, predominantly to silence genes within euchromatic regions[289-291], although they have also been reported to facilitate ERV repression[292].

EHMT1 and EHMT2 interact with a range of transcription factors that likely enable them to mediate their repressive activity in a context- and cell type-specific manner. One of the most notable examples is binding to the widely interspaced zinc finger-containing protein (WIZ), which links these two chromatin modifiers to the CtBP (C-terminal binding protein) co-repressor complex[293]. Additionally, through their interaction with the chromatin reader chromodomain Y-like protein (CDYL), they associate with the transcriptional repressor REST and histone deacetylases such as HDAC1 and HDAC2[294]. EHMT2 is also recruited by the transcription factor PRDM1 (BLIMP1) to control $CD8^+$ T cell fate in the setting of acute viral infection[295] and represses key developmental genes in liver cells via interaction with E4BP4[296] and SHP[297].

EHMT1 and EHMT2 contribute to oncogenesis in a number of cancer contexts, including silencing of tumour suppressor genes and regulation of cancer stemness – this usually arises in the setting of EHMT1/2 overexpression or through gain-of-function mutations[298]. Notably, EHMT2 represses the DKK family of Wnt antagonists in renal cell carcinoma[299], melanoma[300] and neuroendocrine tumours[301], driving tumour proliferation and oncogenesis. EHMT2 was also shown to maintain self-renewal and stemness in AML through regulation of HoxA9-dependent transcription[302]. Additionally, EHMT2 appears to play a role in cancer immune evasion, helping to establish an immunologically "cold" TME in melanoma[300] and blocking pro-inflammatory cytokine production in breast cancer[303]. In keeping with this, pharmacological EHMT2 inhibition enhanced ICI response in melanoma, which is postulated to reflect modulation of autophagy as well as IFN signalling via ERV reactivation[300,304].

In summary, the H3K9 methyltransferases collectively perform vital roles in formation and maintenance of heterochromatin, as well as stable repression of ERVs and also dynamic gene silencing to a lesser extent. Notable structural and functional differences between the three families of methyltransferases contribute to partitioning of their activity across the genome and raise the possibility of selective inhibition of these enzymes to induce transcriptional changes predominantly within a subset of target genes in defined chromosomal regions.

1.5.3.2 Readers and erasers of H3K9 methylation

As outlined above, the HP1 family of proteins (CBX1, CBX3 and CBX5 in humans) are the principal readers of H3K9 methylation and bind this modification via their amino-terminal chromodomain[272-274]. HP1 proteins also contain a related chromoshadow domain (CSD), which is separated from the chromodomain by a hinge region and facilitates homo- and heterodimerisation[305]. Through its CSD, HP1 proteins recruit H3K9 methyltransferases including SUV39H1, enabling methylation of H3K9 on neighbouring nucleosomes and a self-maintaining loop driving HP1 propagation and heterochromatin formation[275]. Interestingly, H3K9 methylation and HP1γ (CBX3) have also been shown to play a dynamic role in transcription elongation for active genes, being induced during gene activation and rapidly lost once transcription ceases[306]. The HP1 proteins therefore exhibit significant functional diversity, with both repressive and activating functions that are employed in a highly context-specific manner[307].

The E3 ubiquitin ligase UHRF1 (ICBP90) also recognises H3K9me3 via its tandem Tudor domain (TTD)[308] and interacts with DNMT1 to maintain DNA methylation. In addition to the TTD, UHRF1 also contains a PHD finger domain separated by a short linker sequence, which helps to enhance H3K9 binding[309,310]. Notably, mutations in the TTD, PHD finger or linker sequence disrupt the ability of UHRF1 to bind H3K9 and maintain DNA methylation[309], providing an interesting link between histone methylation and DNA methylation in maintenance of gene repression.

H3K9 demethylation is mediated by three classes of proteins with distinct but overlapping activity. The JHDM2 (Jumonji domain-containing histone demethylase 2) family contains JHDM2A-C , which demethylate H3K9me1 and H3K9me2[311], while the JHDM3 family contains five members (JHDM3A-E) that demethylate H3K9me2 and H3K9me3[312,313]. Lastly, PHF8, a member of the PHD finger protein family, is a demethylase for H3K9me1 and H3K9me2[314]. Through their demethylase function, these enzymes play an important role in transcriptional regulation, normal development as well as DNA repair[315].

1.5.4 The CtBP co-repressor complex

The founding member of the CtBP family was identified through a search for cellular proteins that bind to the C-terminal of the adenovirus E1A oncoprotein and was shown to negatively regulate tumorigenesis and disease transformation[316]. Subsequent work demonstrated the existence of two highly homologous proteins, CtBP1 and CtBP2, which are conserved in vertebrates and predominantly function as transcriptional co-repressors. In humans, the *CTBP1* gene is located on chromosome 4 and the *CTBP2* gene is located on chromosome 10, with alternative promoters and RNA splicing giving rise to structurally and functionally distinct isoforms of each protein[317].

CtBP proteins contain two key domains that facilitate its association with a broad range of DNA-binding proteins and transcriptional regulators. The first domain in the N-terminal cleft region engages with accessory proteins via binding to a consensus PLDLS motif, while a second surface groove on the dinucleotide-binding domain contains an RRT-binding motif. Proteomic studies have identified several classes of interactors that can form complexes with the core CtBP homo- or heterodimer, including DNA-binding proteins (ZEB1, RREB1, ZNF217), histone-modifying enzymes (HDAC1/2, EHMT1/2, LSD1), chromatin readers (CDYL) and other co-repressors (RCOR1/CoREST)[318]. Further biochemical analysis suggests that some of these proteins form exclusive subcomplexes that likely confer specificity of function depending on the DNA-binding

proteins and chromatin modifiers involved – one complex incorporates WIZ, CDYL and EHMT1/2, while another includes ZNF217, RCOR1, HDAC1/2 and LSD1[319].

In keeping with its diverse range of interacting proteins, the CtBP complex has been implicated in both pro-tumorigenic and tumour suppressive capacities. In terms of pro-tumorigenic potential, CtBP-dependent repression of pro-apoptotic genes was observed in colorectal cancer and osteosarcoma cell lines[320]. Additionally, recruitment of the CtBP complex by ZEB1 represses the epithelial marker E-cadherin and promotes epithelial-to-mesenchymal transition (EMT) and increased metastatic potential for a range of solid organ malignancies[321-324]. CtBP1/2 have also been shown to repress a number of tumour suppressors, including PTEN[325], Wnt[326,327] and the cyclin-dependent kinase inhibitor p16INK4a[328,329]. Conversely, loss of CtBP1 promoted tumour growth in androgen receptor-positive prostate cancer[330] and also facilitated melanoma progression[331,332]. Overall, the CtBP complex appears to play a predominantly pro-tumorigenic role, raising the possibility of targeting its function to disrupt multiple oncogenic pathways.

1.5.5 Immunomodulation with epigenetic therapies – can we do better?

As discussed in previous sections and recently comprehensively reviewed[3,333], epigenetic therapies have multifaceted effects on the anti-cancer immune response. These include enhancement of tumour cell immunogenicity, as well as modulation of the TME and the various immune cell subsets involved within. For many pharmacological inhibitors, including those targeting HDACs, DNMTs and LSD1, the predominant immune effect involves reactivation of repressed ERVs and other transposable elements, triggering a cell-intrinsic interferon response (**Figure 1.4**).

While epigenetic therapies have shown early promise in combination with ICIs, a key question is whether such broadly acting therapies are the most optimal way to augment anti-tumour immunity. For instance, targeting DNA methylation in a relatively non-specific fashion (e.g. through use of DNMT inhibitors like azacitidine) may also reactivate genes with immunosuppressive potential, such as *PD-L1*, *PD-L2* and *CTLA4*, which was associated with resistance to hypomethylating agent therapy in MDS/AML[334] although these co-inhibitory molecules are targetable with existing ICIs. There is also significant potential for additional off-target effects with these inhibitors, which may contribute to excessive toxicity particularly if used in combination with conventional chemotherapy, radiotherapy and/or other epigenetic modifiers[335].

Accordingly, identification and targeting of epigenetic mechanisms that selectively enable cancer immune evasion represents an ideal strategy to efficiently augment anti-tumour immunity with the widest therapeutic margin. Given the central importance of tumour antigen presentation to the majority of pharmacological and cellular immunotherapies, the work in this thesis focuses on reversing MHC-I and MHC-II silencing across a range of cancer contexts. For both MHC-I and MHC-II projects, unbiased CRISPR-Cas9 screens were performed to identify and validate key regulators of each pathway, followed by validation and dissection of the molecular mechanisms underpinning MHC-I and MHC-II repression. Finally, *in vitro* and *in vivo* functional studies confirm the validity and potential translational importance of these findings.

Chapter 2 – Materials and Methods

2.1 Materials

2.1.1 Buffers and bacterial growth media

Table 2.1: Stock solutions and bacterial media.

Name	Composition (per litre)
General buffers	
FACS wash (2%)	150 mM NaCl, 2.5 mM KCl, 10 mM Na_2HPO_4, 2 mM K_2HPO_4, 2% [v/v] FBS, 20 mM HEPES
FACS wash (5%)	150 mM NaCl, 2.5 mM KCl, 10 mM Na_2HPO_4, 2 mM K_2HPO_4, 5% [v/v] FBS, 20 mM HEPES
LB	10 g tryptone, 5 g yeast extract, 5 g NaCl
PBS	150 mM NaCl, 2.5 mM KCl, 10 mM Na_2HPO_4, 2 mM K_2HPO_4
Red cell lysis buffer (1X)	150 mM NH_4Cl, 10 mM $NaHCO_3$, 1 mM EDTA
SOC	20 g tryptone, 5 g yeast extract, 0.58 g NaCl, 0.19 g KCl, 10 mM $MgCl_2$, 10 mM $MgSO_4$ and 0.4% [w/v] glucose
TAE	40 mM Tris-acetate, 1 mM EDTA pH 8.0
TBE	90 mM Tris-borate, 2 mM EDTA pH 8.0
TBS	150 mM NaCl, 20 mM Tris-HCl pH 7.6
Western blot buffers	
Lysis buffer	1% SDS, 100 mM Tris-HCl pH 8.0, 1X Roche cOmplete EDTA-free protease inhibitor cocktail (catalogue number 4693132001)
Laemmli buffer (4X)	200 mM Tris-HCl pH 6.8, 20-35% glycerol, 1-2.5% sodium lauryl sulphate, 0.4% bromophenol blue
Running buffer (1X)	25 mM Tris-HCl, 190 mM glycine, 0.1% [w/v] SDS
Transfer buffer (1X)	25 mM Tris-HCl, 190 mM glycine, 20% [v/v] methanol
TBS-T	TBS with 0.05% [v/v] Tween-20
Skim milk blocking solution	5% [w/v] non-fat milk powder in TBS-T
ChIP buffers	
Lysis buffer	1% SDS, 10 mM EDTA, 50 mM Tris-HCl pH 8.0, 1X Roche cOmplete EDTA-free protease inhibitor cocktail (catalogue number 4693132001)

Modified RIPA buffer	1% Triton X-100, 0.1% Na deoxycholate, 90 mM NaCl, 10 mM Tris-HCl pH 8.0, 1X Roche cOmplete EDTA-free protease inhibitor cocktail (catalogue number 4693132001)
First wash buffer (low salt)	0.1% SDS, 1% Triton X-100, 2 mM EDTA, 150 mM NaCl, 20 mM Tris-HCl pH 8.0
Second wash buffer (high salt)	0.1% SDS, 1% Triton X-100, 2 mM EDTA, 500 mM NaCl, 20 mM Tris-HCl pH 8.0
Lithium chloride buffer	0.25 M LiCl, 1% NP-40, 1% Na deoxycholate, 1 mM EDTA, 10 mM Tris-HCl pH 8.0
TE buffer	10 mM Tris-Cl, 1 mM EDTA
Elution buffer	1% SDS, 0.1 M $NaHCO_3$
CUT&Tag buffers	
Wash buffer	20 mM HEPES pH 7.5, 150 mM NaCl, 0.5 mM spermidine, 1X Roche cOmplete EDTA-free protease inhibitor cocktail (catalogue number 4693132001)
Binding buffer	20 mM HEPES pH 7.9, 10 mM KCl, 1 mM $CaCl_2$, 1 mM $MnCl_2$
Antibody buffer	Wash buffer plus 0.05% digitonin, 2 mM EDTA, 0.1% BSA
Digitonin buffer	Wash buffer plus 0.1% digitonin
Dig-300 buffer	20 mM HEPES pH 7.5, 300 mM NaCl, 0.5 mM spermidine, 1X Roche cOmplete EDTA-free protease inhibitor cocktail (catalogue number 4693132001), 0.01% digitonin
Tagmentation buffer	Dig-300 buffer plus 10 mM $MgCl_2$
Stop buffer (2X)	Dig-300 buffer plus 40 mM EDTA, 0.2% SDS, 400 µg/mL proteinase K

2.1.2 Cell culture media and additives

Table 2.2: Cell culture media and additives.

Item	**Source**	**Catalogue #**
2-mercaptoethanol	Thermo Fisher Scientific	21-985-023
DMEM	Thermo Fisher Scientific	11965
Fetal bovine serum (HyClone™)	GE Life Sciences	SH30084.03
Gentamicin	Sigma-Aldrich	G1272
GlutaMAX™	Thermo Fisher Scientific	35050061

Opti-MEM	Thermo Fisher Scientific	31985
Penicillin/streptomycin	Thermo Fisher Scientific	15140122
Recombinant human IL-2 (rhIL-2)	National Institutes of Health	Ro 23-6019
Recombinant human IL-6	PeproTech	200-06
Recombinant murine IL-3	PeproTech	213-13
Recombinant murine stem cell factor	PeproTech	250-03
RPMI-1640	Thermo Fisher Scientific	11875
Schneider's Drosophila medium	Thermo Fisher Scientific	21720024

2.1.3 Chemicals and investigational compounds

Table 2.3: Chemicals and investigational compounds.

Item	**Source**	**Catalogue #**	***In vitro* Vehicle**
A-366 (GLP/G9a inhibitor)	Selleck Chemicals	S7572	Ethanol
EPZ011989 (EZH2 inhibitor)	Selleck Chemicals	S7805	Ethanol
OVA peptide (323-339)	GenScript	RP10610	ddH_2O
Raltegravir	Selleck Chemicals	S2005	DMSO
Recombinant human interferon gamma	Sigma-Aldrich	SRP3058	ddH_2O
Recombinant mouse interferon gamma	Abcam	ab123747	ddH_2O
SIINFEKL (OVA peptide 257-264)	Sigma-Aldrich	S7951	ddH_2O
UNC0638 (GLP/G9a inhibitor)	Selleck Chemicals	S8071	Ethanol

2.1.4 Antibodies

Table 2.4: Flow cytometry antibodies.

Antibody	**Species**	**Clone**	**Fluorochrome**	**Source**	**Catalogue #**
CD3	Human	UCHT1	BV510	BioLegend	300448
CD4	Human	OKT4	BV605	BioLegend	317438
CD8	Human	SK1	BUV737	BD Biosciences	612754
CD3	Mouse	17A2	PE/Cyanine7	BioLegend	100220
CD4	Mouse	GK1.5	BV650	BD Biosciences	563232
CD8	Mouse	53-6.7	PE	BioLegend	100708
HLA-A,B,C	Human	W6/32	Alexa Fluor 488	BioLegend	311413

HLA class I (Bw6)	Human	REA143	APC-Vio770	Miltenyi Biotec	130-099-837
HLA-DR,DP,DQ	Human	Tü39	Alexa Fluor 647	BioLegend	361704
HLA-DR	Human	L243	Alexa Fluor 488	BioLegend	307620
MHC class I (H-2Kb)	Mouse	AF6-88.5	Alexa Fluor 647	BioLegend	116512
MHC class II (1-A/1-E)	Mouse	M5/114.15.2	Alexa Fluor 647	BioLegend	107618

Table 2.5: ChIP, CUT&Tag and WB antibodies.

Antibody	**Species**	**Clone**	**Source**	**Catalogue #**	**Application**
Alpha tubulin	Mouse	DM1A	Invitrogen	62204	WB
CIITA (polyclonal)	Rabbit	-	Cell Signaling Technology	3793S	WB
FBXO11 (polyclonal)	Rabbit	-	Novus Biologicals	NB100-59826	WB
GAPDH	Rabbit	14C10	Cell Signaling Technology	2118S	WB
H3K9me2 (polyclonal)	Rabbit	-	Active Motif	39239	CUT&Tag
H3K27me3 (Lys27)	Rabbit	C36B11	Cell Signaling Technology	9733	WB, ChIP, CUT&Tag
HSP60	Mouse	C-10	Santa Cruz Biotechnology	sc-376240	WB
Human EZH2	Mouse	11/EZH2	Becton Dickinson Transduction Laboratories	612667	WB
Human MHC-I heavy chain	Mouse	HC10	Origene	AM33035PU-N	WB
IRF-1	Rabbit	D5E4	Cell Signaling Technology	8478	WB
Phospho-Stat1 (Tyr701)	Rabbit	58D6	Cell Signaling Technology	9167	WB

STAT1 (polyclonal)	Rabbit	-	Merck Millipore	06-501	WB

Table 2.6: Miscellaneous antibodies.

Antibody	Species	Clone	Source	Catalogue #	Application
CD3	Human	OKT3	eBioscience	16-0037-81	PBMC activation
CD28	Human	CD28.2	eBioscience	16-0289-81	PBMC activation
CD16/32	Mouse	93	BioLegend	101302	Fc blocking
IgG	Human	-	Sigma-Aldrich	I4506	Fc blocking

2.1.5 Cell lines

Table 2.7: Cell lines.

Cell Line	Species	Cell Type	Source	RRID
MOLM13	Human	AML	Dawson laboratory stock	CVCL_2119
MV4-11	Human	AML	Dawson laboratory stock	CVCL_0064
OCI-AML-3	Human	AML	Dawson laboratory stock	CVCL_1844
K-562	Human	CML	ATCC	CVCL_0004
HEK293-ET	Human	Embryonic kidney	Felix Randow (MRC-LMB, Cambridge, UK)	CVCL_6996
A375	Human	Melanoma	ATCC	CVCL_0132
LM-MEL-53	Human	Melanoma	ATCC	CVCL_UC56
WM852	Human	Melanoma	ESTDAB	CVCL_6804
IMR-32	Human	Neuroblastoma	Paul Ekert (MCRI, Melbourne, Australia)	CVCL_0346
Kelly	Human	Neuroblastoma	Paul Ekert (MCRI, Melbourne, Australia)	CVCL_2092
S2	Drosophila	Embryonic	ATCC	CVCL_Z232
MLL-AF9	Mouse	AML	Dawson laboratory stock	-

ATCC, American Type Culture Collection. MCRI, Murdoch Children's Research Institute. MRC-LMB, Medical Research Council Laboratory of Molecular Biology. RRID, Research Resource Identifier.

MOLM13, MV4-11, OCI-AML-3 and mouse MLL-AF9 cell lines were available as stocks within the Dawson laboratory (Peter MacCallum Cancer Centre, Melbourne, Australia). Cell lines were

authenticated by STR profiling through the Australian Genome Research Facility (Melbourne, Victoria). Key mutations for the myeloid leukaemia cell lines used are shown below.

Table 2.8: Key mutations for myeloid leukaemia cell lines.

Cell Line	Mutations
K-562	BCR-ABL gene fusion Homozygous for *TP53* c.406_407insC, p.(Gln136fs*13)
MLL-AF9	KMT2A-MLLT3 (MLL-AF9) gene fusion
MOLM13	KMT2A-MLLT3 (MLL-AF9) gene fusion FLT3-ITD
MV4-11	KMT2A-AFF1 (MLL-AF4) gene fusion FLT3-ITD
OCI-AML-3	*DNMT3A* c.2644C>T, p.(Arg882Cys) Heterozygous for *NPM1* c.860_863dupTCTG, p.(Trp288Cysfs*12)

2.1.6 Bacterial strains for plasmid DNA production

The NEB® Stable Competent *E. coli* strain (New England Biolabs, catalogue number C3040) was used for chemical transformation. Endura™ Electroccompetent Cells (Lucigen, catalogue number 60242) were used for electrical transformation. The genotypes of these bacterial strains are shown below.

Table 2.9: Bacterial genotypes.

Bacterial Strain	Genotype
NEB® Stable Competent *E. coli*	F' *proA+B+ lacI^q Δ(lacZ)M15 zzf::Tn10* (Tet^R) *Δ(ara-leu) 7697 araD139 fhuA ΔlacX74 galK16 galE15 e14- Φ80dlacZΔM15 recA1 relA1 endA1 nupG rpsL* (Str^R) *rph spoT1 Δ(mrr-hsdRMS-mcrBC)*
Endura™ Electrocompetent Cells	*recA13 supE44 ara-14 galK2 lacY1 proA2 rpsL20(Str^R) xyl-5 λ– leu mtl-1 F– mcrB mrr hsdS20(r_B–, m_B–)*

2.1.7 Vectors

The listed pHRSIN vectors were generated by subcloning, as outlined in the Methods section.

Table 2.10: Vectors.

Vector	Application	Addgene #
pMD2.G	Viral VSV-G envelope plasmid (a gift from Didier Trono)	12259
psPAX2	Lentiviral packaging plasmid (a gift from Didier Trono)	12260
gag/pol	Retroviral packaging plasmid (a gift from Tannishtha Reya)	14887
pcDNA3-myc-CIITA	Source for subcloning (a gift from Matija Peterlin)	14650
pCMVHA-EED WT	Source for subcloning (a gift from Kristian Helin)	24231
MSCVhygro-FLAG-Ezh2 WT	Source for subcloning (a gift from Kai Ge)	24926
MSCVhygro-FLAG-Ezh2 F667I	Source for subcloning (a gift from Kai Ge)	24927
pcDNA3.1-FLAG-HA-FBXO11	Source for subcloning (a gift from Adam Antebi)	52501
pcDNA3.1-FLAG-HA-FBXO11-ΔFbox	Source for subcloning (a gift from Adam Antebi)	52502
pKLV-U6gRNA(BbsI)-Puro$_{2A}$-BFP	Transfection into mammalian cells for gene knockout via CRISPR/Cas9 (a gift from Kosuke Yusa)	50946
Bassik human CRISPR knockout library	Whole-genome CRISPR screening (a gift from Michael Bassik)	101926-101934
Zuber mouse CRISPR knockout library	CRISPR screening with targeted epigenetic library (a gift from Johannes Zuber)	-
pHRSIN-P$_{SFFV}$-EZH2-P$_{PGK}$-Puro	Transfection into mammalian cells for protein expression	-

pHRSIN-P_{SFFV}-EZH2 F667I-P_{PGK}-Puro	Transfection into mammalian cells for protein expression	-
pHRSIN-P_{SFFV}-EED-P_{PGK}-Puro	Transfection into mammalian cells for protein expression	-
pHRSIN-P_{SFFV}-EED W364A-P_{PGK}-Puro	Transfection into mammalian cells for protein expression	-
pHRSIN-P_{SFFV}-Cas9-P_{PGK}-Blasticidin	Transfection into mammalian cells for protein expression	-

2.1.8 CRISPR guide RNA target sequences

Guide RNA target sequences for CRISPR/Cas9-mediated knockout of human (Table 2.11) and mouse (Table 2.12) genes are listed below. Safe control sgRNAs were also used, which target genomic locations with no annotated function.

Table 2.11: Human guide RNA target sequences.

Gene	sgRNA #	Target sequence
CDYL	1	GCGGTCCTGCTCTTAACG
	2	GGAGTGACTGCCAGCAAA
CIITA	1	GAGTTGGGGCCCCTAGAAGG
	2	GGAAGGTGATGAAGAGACCA
EHMT1	1	GCGGACGGTGAGACCAAT
	2	GCAGCATTTGCATGACTGC
EHMT2	1	GGGTTTCTTCACTACGAG
	2	GCGGGCTCGGTGGACCTT
FBXO11	1	GTGCACATGTAAAGCC
	2	GTTCAGGATGCATCATA
	3	GAGCCTCTTGTACCCCACCA
RCOR1	1	GGCCATTATTGGGGGCGG
	2	GCGGAGAGGGAGGAACAACG
RREB1	1	TGGCGATCGAGGGAGC
	2	TGCATGGTCAGCTGGTGCT
	3	GGGAAGGTCACAGAGAATGG
WIZ	1	GACCACCTGCGAGGTCTG

	2	GTGGCAGAGTCGGAAAGCAG
ZNF217	1	GCTCTCTTGGCAGTCCGA
	2	GCAGAACATGCAATCCAA
Safe targeting control	-	AATCATAAGGCAATCATC

Table 2.12: Mouse guide RNA target sequences.

Gene	sgRNA #	Target sequence
Fbxo11	1	GTGATTCCGTCTAATAAT
	2	GATGATGCATCCTGAACC
	3	GTTGCAGAAGAATCAGGTCC
Rcor1	1	GGTGGGACCCCAGTACCAAG
	2	GAGACAATCTTGGCATGT
	3	GCTATCGCCAAAGAGAAGCA
Rreb1	1	GACGTCGAATTCGCCCAT
	2	GCCAATCCGATTTGGTCC
	3	GCTCATTACTGCTGACATCA
Zfp217	1	GGCCCGTCCATGTACACG
	2	GATGCTGTGCCCATAAAA
	3	GAGCATGGCCGTGGCAGA
Safe targeting control	-	TTCGGCTGGTGTGCGTTCAC

2.1.9 PCR primers

Custom PCR primer oligonucleotides were purchased from Integrated DNA Technologies and resuspended as 100 µM stock solutions in nuclease-free H_2O.

Table 2.13: Human cDNA PCR primers.

Amplicon	Forward primer	Reverse primer
MHC class I primers		
B2M	TGACTTTGTCACAGCCCAAG	AGCAAGCAAGCAGAATTTGG
HLA-A	GGCCCTGACCCAGACCTG	GCACGAACTGCGTGTCGTC
HLA-B	CATCGTGGGCATTGTTGCTG	ACGCAGCCTGAGAGTAGC
HLA-C	CTGGCCCTGACCGAGACCTG	CGCTTGTACTTCTGTGTCTCC
NLRC5	CACTTGGAGGAGCTGGACTT	GTGAGTAAGCAAGGCCAAGG

PSMB8 (LMP7)	TCTCCAGAGCTCGCTTTACC	CACTCCATGCTGGAACTTGA
PSMB9 (LMP2)	CGTTGTGATGGGTTCTGATTCC	GACAGCTTGTCAAACACTCGGTT
TAP1	CCTGTGGCACAAACTCGGG	ATCTCCCCAAGAGAGGAGAGGA
TAP2	TCGACTCACCCTCCTTTCTC	ACTGCATCCTGGATCTCCC
MHC class II primers		
CD74	TCCCAAGCCTGTGAGCAAGATG	CCAGTTCCAGTGACTCTTTCG
CIITA	CAAGTCCCTGAAGGATGTGGA	ACGTCCATCACCCGGAGGGAC
HLA-DMB	TCCTTCAACAAGGATCTGCTG	CTTCCTCCACGTGATAGTCAC
HLA-DRA	TAAGGCACATGGAGGTGATG	GTACGGAGCAATCGAAGAGG
Primers for housekeeping genes		
ACTB	GCACAGAGCCTCGCCTT	CCTTGCACATGCCGGAG
GAPDH	ACAACTTTGGTATCGTGGAAGG	GCCATCACGCCACAGTTTC

Table 2.14: Human ChIP-qPCR primers.

Amplicon	**Forward primer**	**Reverse primer**
HLA-B promoter	TTGTGTAGGGAAACTGAGCACG	TGTCTCTACACCTCCATTCCCAG
NLRC5 promoter	ATCCACGTGATTTCTCGGCA	ACTGAAAGTAGAAGCCGCCG
GAPDH promoter	AAAGCCTGCCGGTGACTAAC	CACCCGGAGGAGAAATCGG
Negative control	CTTCAGGGTGACTCACAGGG	AGTTAAGGGGAAGCAGTGCC

2.1.10 DNA restriction enzymes

Table 2.15: DNA restriction enzymes.

Restriction Enzyme	**Manufacturer**	**Catalogue #**
BamHI	New England Biolabs	R3136 (High-Fidelity®)
EcoRI	New England Biolabs	R3101 (High-Fidelity®)
BbsI (BpiI)	Thermo Fisher Scientific	FD1014 (FastDigest™)
KpnI	New England Biolabs	R3142 (High-Fidelity®)
XhoI	New England Biolabs	R0146

2.1.11 Animals

All experimental mice used were between 6-12 weeks of age and housed in the pathogen-free animal facility at the Peter MacCallum Cancer Centre. The mouse strains used are outlined below.

Table 2.16: Mouse strains.

Strain	Genotype	Source
NSG	NOD.Cg-Prkdc<scid>Il2rg<tm1Wjl>	Bred in-house at Peter MacCallum Cancer Centre
OT-I	C57BL/6-Tg(OT-I)	Joseph Trapani, Peter MacCallum Cancer Centre
OT-II	C57BL/6-Tg(OT-II)	Walter and Eliza Hall Institute
Ptprc[a]	B6.SJL-Ptprc<a>Pepc<b>/BoyJ	Animal Resources Centre, Western Australia

2.1.12 Patient samples

Peripheral blood or bone marrow samples were obtained from patients following informed consent and under full ethical approval at each involved institute:

- Peter MacCallum Cancer Centre: HREC 11/102 and 11/88
- Alfred Hospital: HREC 575/19

2.2 Methods

2.2.1 Cell culture

All cell culture was carried out in sterile conditions in a standard Class II Biological Safety Cabinet. All cell lines were maintained in a humidified incubator at 37°C in 5% CO_2. All cell lines were maintained in 6-well plates and/or plastic flasks (25cm^2 or 75cm^2, Greiner Bio-One) and passaged every 48-72 hours to maintain a cell density between 1×10^5 to 2×10^6 cells/mL.

Primary murine haematopoietic progenitors and derived cell lines were cultured in RPMI-1640 supplemented with murine IL-3 (10 ng/mL), human IL-6 (10 ng/mL), murine SCF (50 ng/mL), 10% [v/v] fetal bovine serum, penicillin (100 units/mL), streptomycin (100 μg/mL) and GlutaMAX™ (2 mM). K-562, Kelly, LM-MEL-53, MOLM13, MV4-11, OCI-AML-3 and WM852 cells were cultured in RPMI-1640 supplemented with 10% [v/v] fetal bovine serum, penicillin (100 units/mL), streptomycin (100 μg/mL) and GlutaMAX™ (2 mM). A375, IMR-32 and HEK293-ET cells were cultured in DMEM supplemented with 10% [v/v] fetal bovine serum, penicillin (100 units/mL), streptomycin (100 μg/mL) and GlutaMAX™ (2 mM). S2 cells were cultured in Schneider's Drosophila medium supplemented with 10% [v/v] fetal bovine serum, penicillin (100 units/mL) and streptomycin (100 μg/mL). T cells isolated from mice were cultured in complete RPMI-1640 media, containing 10% fetal bovine serum, penicillin (100 units/mL), streptomycin (100 μg/mL), sodium pyruvate (1 mM), GlutaMAX™ (2 mM) and 2-mercaptoethanol (55 μM).

Cell cultures were cryopreserved in fetal bovine serum supplemented with 10% [v/v] DMSO. A controlled rate of cooling (-1°C/minute) was achieved by using Mr. Frosty™ Freezing Containers (Thermo Fisher Scientific) at -80°C.

2.2.2 Mycoplasma contamination testing

Cell lines were routinely tested for mycoplasma contamination by PCR. A 1 mL sample of media (containing a minimum of 10,000 cells) was obtained from cultures following at least 48 hours growth. These samples were centrifuged in 1.5 mL microcentrifuge tubes at 400 g for 4 minutes to pellet contents and the supernatants were aspirated. Cell pellets were lysed in 100 μL of QuickExtract™ solution (Lucigen) according to manufacturer's instructions and then diluted with 1.1 mL ddH_2O. Lysate aliquots (1 μL) were used as template DNA for PCR.

PCRs were carried out using a Mastercycler™ nexus gradient thermal cycler (Eppendorf) and MangoTaq™ DNA polymerase (Bioline) according to manufacturer's instructions. The primers (Table 2.17), reaction mix and protocol (Table 2.18) are detailed below. PCR products were run on a 2% [w/v] agarose gel, made by dissolving molecular-grade agarose (Bioline) in 100 mL TBE and adding 10 µL of SYBR™ Safe DNA Gel Stain (Thermo Fisher Scientific). The gel was poured into a mould, allowed to set and then mounted in an electrophoresis tank and covered with TBE. Mycoplasma contamination was present if a 520 bp band was detected in conjunction with a 375 bp cytochrome b band (positive PCR reaction control).

Table 2.17: PCR primers for mycoplasma testing.

Amplicon	**Forward primer**	**Reverse primer**
Mycoplasma	YGCCTGVGTAGTAYRYWCGC	GCGGTGTGTACAARMCCCGA
Cytochrome b	AAAAAGCTTCCATCCAACATCTCAG CATGA	AAACTGCAGCCCCTCAGAATGATAT TTGTC

M, adenine or cytosine. R, adenine or guanine. V, adenine or cytosine or guanine. W, adenine or thymine. Y, cytosine or thymine.

Table 2.18: PCR reaction mix and protocol for mycoplasma testing.

Mycoplasma PCR		
Reaction mix (made up to 25 µL in nuclease-free H_2O)	5 µL 5X MangoTaq™ buffer	0.5 µL 10 mM dNTP mix
	1.5 µL 25 mM $MgCl_2$	1 µL sample lysate
	1 µL 20 µM mycoplasma forward primer	
	1 µL 20 µM mycoplasma reverse primer	
	0.25 µL 20 µM cytochrome b forward primer	
	0.25 µL 20 µM cytochrome b reverse primer	
Enzyme	1.25 units Lucigen MangoTaq™ DNA polymerase	
PCR protocol	1. 95°C for 5 minutes 2. 95°C for 30 seconds, 53°C for 30 seconds, 72°C for 30 seconds (44 cycles) 3. 72°C for 5 minutes	

2.2.3 DNA cloning techniques

The DNA cloning techniques utilised in this work are described in general below, with specific applications detailed in subsequent sections.

Restriction enzyme digestion of DNA templates was performed according to manufacturer's instructions, comprising 5 µL 10X CutSmart® Buffer (New England Biolabs), 5 µg template DNA and 2 µL of each restriction enzyme, made up to a 50 µL reaction volume with nuclease-free H_2O. All digests were carried out at 37°C for 60 minutes, followed by heat inactivation of restriction enzymes at 65°C for 20 minutes. Digested vectors were also treated with 5 units of recombinant shrimp alkaline phosphatase (New England Biolabs) for 2 hours prior to the above heat inactivation step, in order to dephosphorylate the cut ends and minimise vector recircularisation.

Where possible, DNA fragments were inserted into vectors cut with two unique restriction enzymes to generate incompatible ends, thereby promoting correct insert orientation as well as further reducing vector recircularisation.

To maximise the successful generation of recombinant plasmids, both vector and insert fragments were purified by gel extraction to exclude the presence of undigested template DNA in the ligation reaction. Agarose gels (0.8% w/v) were made by dissolving molecular-grade agarose (Bioline) in 100 mL TAE and adding 10 µL SYBR™ Safe DNA Gel Stain (Thermo Fisher Scientific). The gel was poured into a mould, allowed to set and then mounted in an electrophoresis tank and covered with TAE. DNA samples were loaded onto the gel following addition of 6X Blue/Orange Loading Dye (Promega), with electrophoresis performed at 100 V. A 100 bp or 1 kb DNA ladder (Promega) was run alongside samples as a marker.

DNA fragments were excised from agarose gels using a clean scalpel blade, with excess agarose trimmed off to ensure the smallest gel slice possible. DNA extraction was then performed using the NucleoSpin® Gel and PCR Clean-up kit (Macherey-Nagel) according to manufacturer's instructions, with DNA eluted into 30 µL of nuclease-free H_2O per sample. Ligation of digested vectors and inserts was performed in molar ratios ranging from 3:1 to 1:10, using 10 µL reaction volumes with Quick Ligase™ (New England Biolabs) according to manufacturer's instructions.

2.2.4 Plasmid cloning

Wildtype EED was PCR amplified from pCMV HA EED WT (Addgene 24231, a gift from Kristian Helin)[336] and subcloned into pHRSIN-P_{SFFV}-eGFP-P_{PGK}-Puro via BamHI and XhoI, replacing the GFP. Mouse Ezh2 and Ezh2 F667I were subcloned into pHRSIN-P_{SFFV}-eGFP-P_{PGK}-Puro via BamHI and XhoI following PCR amplification from MSCVhygro-F-Ezh2 wildtype or F667I (Addgene 24926

and 24927, a gift from Kai Ge)[337]. For all constructs, the N-terminal tag (HA or FLAG) was removed during cloning. The EED W364A mutant was generated by site-directed mutagenesis of wildtype EED that had been subcloned into pcDNA3. Following sequence verification, EED W364A was subcloned into pHRSIN-P_{SFFV}-eGFP-P_{PGK}-Puro.

pcDNA3 myc CIITA (P#808) was a gift from Matija Peterlin (Addgene plasmid #14650)[338]. CIITA cDNA from pcDNA3 myc CIITA was subcloned into both pMSCV-IRES-mCherry fluorescent protein (FP) (a gift from Paul Beavis) and pMSCV-IRES-GFP (modified from pMSCV-IRES-mCherry FP, a gift from Paul Beavis) via EcoRI and XhoI sites. FLAG-HA-Fbxo11-pcDNA3.1- (Addgene #52501) and FLAG-HA-Fbxo11-ΔFbox-pcDNA3.1- (Addgene #52502) were a gift from Adam Antebi[339]. Wildtype FBXO11 and FBXO11 ΔFbox were PCR amplified from the above plasmids and subcloned into pHRSIN-P_{SFFV}-eGFP-P_{PGK}-Puro via BamHI and XhoI, replacing the GFP. An ovalbumin (OVA)-expressing retroviral vector was generated by PCR amplification of full-length chicken OVA from pcDNA3-OVA (Addgene #64599, a gift from Sandra Diebold & Martin Zenke)[340] and subcloned into pMSCV-IRES-GFP via EcoRI and XhoI sites.

2.2.5 Cloning of a human CRISPR library targeting epigenetic modifiers

To generate a targeted epigenetic CRISPR library, a bespoke set of ~15,300 sgRNAs was designed by members of the Dawson laboratory, targeting ~2,400 recognised chromatin regulators (6 sgRNAs per gene), as well as non-targeting and safe-targeting control sgRNAs[341]. The library was designed through a combination of searches for genes containing domains known to be enriched in transcriptional regulators and manual curation. The oligonucleotide pool was synthesised by CustomArray (GenScript) and each sgRNA contained a BsmBI DNA restriction site for downstream cloning as well as PCR primers to enable subpool amplification out of the master oligonucleotide pool.

Library sgRNAs were PCR amplified and cloned into the pKLV-U6gRNA(BbsI)-$_{PGK}$puro$_{2A}$BFP lentiviral sgRNA expression vector, which encodes puromycin and BFP selection markers. The ligated product was electroporated into two 25 µL aliquots of electrocompetent cells (Lucigen), which were then pooled and grown in 500mL LB overnight at 37°C before being extracted by Maxiprep (Macherey-Nagel). Serial dilutions of the bacterial culture was performed (maximum dilution 1:100,000) to ensure adequate library diversity, with a minimum of 100-500 colonies obtained per sgRNA. Low skewing of the library was confirmed by sequencing of the plasmid pool with a minimum average read coverage >1500X.

2.2.6 Bacterial transformation

Bacterial transformation for production of plasmid DNA was achieved through heat shock of NEB® Stable Competent *E. coli* or electroporation of Endura™ Electrocompetent Cells.

For chemical transformation, 20 µL of bacteria was thawed on ice prior to addition of 2 µL of a ligation reaction or 25 ng of plasmid DNA. Cells and DNA were mixed gently prior to incubation on ice for 5 minutes. Cells were then immersed in a 42°C water bath for 30 seconds and placed immediately back on ice for 2 minutes. Pre-warmed SOC media (380 µL) was then added to the mixture and placed in a 37°C rotary shaker-incubator for 30 minutes at 225 rpm. Following incubation, 50-400 µL of the transformation mixture was spread on a pre-warmed LB-ampicillin plate and incubated at 37°C overnight.

For electroporation, the ligation mixture was cleaned using the NucleoSpin® Gel and PCR Clean-up kit (Macherey-Nagel) and eluted in 15 µL nuclease-free H_2O prior to transformation. Bacteria were thawed on ice, with 1 µL of purified ligation mixture added to 25 µL of cells and transferred to a chilled Bio-Rad Gene Pulser® cuvette (0.1cm gap). Electroporation was then performed on a Bio-Rad GenePulser Xcell™ system using manufacturer settings (10 µF, 600 Ohms, 1800 V). The cells were resuspended in pre-warmed 975 µL Recovery Medium, transferred to a 1.5 mL microcentrifuge tube and placed in a 37°C rotary shaker incubator for 1 hour at 225 rpm. Following incubation, 50-200 µL of the transformation mixture was spread on a pre-warmed LB-ampicillin plate and incubated at 37°C overnight.

2.2.7 Bacterial culture

Single bacterial colonies were picked from plated cultures and grown in 10 mL LB (Miniprep) or 200 mL LB (Maxiprep) at 37°C overnight. To allow selection of bacteria transformed with plasmid DNA expressing the gene of interest, 100 µg/mL ampicillin was also added.

2.2.8 Plasmid purification from bacterial cultures

Plasmid DNA preparation from *E. coli* was performed using the QIAprep® Spin Miniprep Kit (QIAGEN) or the NucleoBond Xtra Kit (Maxiprep, Macherey-Nagel) according to manufacturer's instructions. Bacteria were harvested by centrifugation at 3,270 g for 15 minutes at room temperature prior to DNA extraction. DNA was eluted in 50 µL (Miniprep) or 1000 µL (Maxiprep) of nuclease-free H_2O. DNA concentration was determined by measurement of absorbance at

260 nm using a NanoDrop™ 2000 spectrophotometer (Thermo Fisher Scientific). DNA sequences were verified by Sanger sequencing performed by the Australian Genome Research Facility (Melbourne, Australia).

2.2.9 Viral production and transduction

For the production of virus particles, HEK293-ET cells were seeded at a density that ensured 70-80% confluency on the day of transfection. Lentivirus was prepared by combining the plasmid of interest and the packaging plasmids psPAX2 and pMD.G at a 0.5:0.35:0.15 ratio. Retrovirus was prepared by combining the plasmid of interest, structural pMD1-gag-pol plasmid and pMD.G envelope plasmid at a 0.75:0.22:0.03 ratio. Combined DNA was then resuspended in Opti-MEM (200 µL per well for 6-well plates, 1 mL per flask for T75 flasks). PEI transfection reagent (4 µg per 1 µg DNA) was added prior to incubation at room temperature for 10 minutes, followed by dropwise addition to the HEK293-ET cells. Supernatant containing viral particles was collected after 48-72 hours and filtered through a 0.45 µm filter prior to storage of viral aliquots at -80°C.

Viral transduction of target cells was achieved through spin infection. To enhance viral adsorption on target cell membranes, 8 µg/mL polybrene (Merck Millipore) was added to 5 x 10^5 target cells in a 6-well plate, followed by dropwise addition of harvested viral supernatant. Plates were then centrifuged at 900 g for 90 minutes at 25°C and incubated for 4-6 hours at 37°C. After incubation, the viral supernatant was replaced with fresh media to minimise polybrene toxicity.

For plasmids containing a fluorescent protein, its expression was checked by flow cytometry 48 hours post-transduction to assess transduction efficiency. For plasmids containing antibiotic resistance genes, the relevant antibiotic (for example, 2 µg/mL puromycin) was added 48 hours post-transduction to select transduced cells.

2.2.10 Flow cytometry and fluorescence-activated cell sorting

2.2.10.1 Flow cytometry

Cells were washed in PBS prior to Fc blocking with 5 µg human IgG (for human cells, Sigma-Aldrich) or 0.5 µg anti-mouse CD16/32 (for mouse cells, BioLegend) for 10 minutes at room temperature. Cells were then stained on ice for 20 minutes in 2% FACS wash buffer; antibodies used are listed in Table 2.4. After washing in 2% FACS wash buffer, samples were resuspended

in 2% FACS wash buffer with a viability dye (DAPI or propidium iodide). Data were acquired on a BD LSRFortessa™ or BD LSR II and analysed in FlowJo™.

2.2.10.2 Fluorescence-activated cell sorting (FACS)

Cells were washed and stained as outlined above, then passed through a 70 µm strainer prior to sorting on the BD FACSAria™ Fusion 3 or Fusion 5 cell sorters. Cells were sorted into a 1:1 mix of media and fetal bovine serum supplemented with 20 mM HEPES and 50 µg/mL gentamicin (Sigma-Aldrich). After sorting, cells were resuspended in fresh media supplemented with 50 µg/mL gentamicin until passage.

2.2.11 Quantitative real-time PCR

Total mRNA was prepared using the Qiagen RNeasy kit according to manufacturer's instructions. Extracted RNA was eluted into 30 µL of nuclease-free H_2O and quantified using a NanoDrop™ 2000 spectrophotometer (Thermo Fisher Scientific).

cDNA synthesis was performed using the SuperScript™ VILO™ kit (Life Technologies) in 20 µL reaction volumes, by adding 4 µL of the VILO™ master mix to 500 ng total RNA made up to 16 µL with nuclease-free H_2O. Samples were initially incubated at 25°C for 10 minutes, prior to cDNA synthesis during incubation at 42°C for 60 minutes. Reactions were inactivated by heating to 85°C for 5 minutes.

Quantitative real-time PCR (qRT-PCR) was performed in 96-well plates on an Applied Biosystems StepOnePlus™ system or in 364-well plates on a Roche LightCycler 480® Real-Time PCR System using Fast SYBR® Green reagents (Life Technologies). Primers utilised for qRT-PCR are listed in Table 2.13. The 10 µL reaction volume comprised 5 µL 2X Fast SYBR® Green master mix, 0.2 µL cDNA, 0.05 µL forward primer (200 µM), 0.05 µL reverse primer (200 µM) and 4.7 µL nuclease-free H_2O. All samples were run in triplicate. Relative expression levels were determined with the ΔCt method and normalised to *GAPDH*.

2.2.12 RNA sequencing

RNA was prepared using the Qiagen RNeasy kit according to manufacturer' instructions and then quantified using a Qubit fluorometer (Thermo Fisher Scientific). Libraries were prepared using the QuantSeq 3' mRNA-seq Library Prep kit (Lexogen) and sequenced on the NextSeq 500

(Illumina) using 75 bp single end chemistry. Library preparation, quality control and sequencing were performed by the Molecular Genomics Core Facility at the Peter MacCallum Cancer Centre.

Bcl2fastq (Illumina) was used to perform sample demultiplexing and to convert BCL files generated from the sequencing instrument into Fastq files. Reads were aligned to the human genome (G1k V37) using HiSAT2[342] and reads were assigned to genes using htseq-count[343]. Differential expression was calculated using DESeq2[344]. Genes with a false discovery rate corrected for multiple testing using the method of Benjamini and Hochberg below 0.05 and a log2 fold change greater than 1 were considered significantly differentially expressed. Scatterplots depicting log fold change differences between conditions were generated in R using the ggplot2 package and custom R code. Bioinformatic analysis of RNA sequencing data was performed by Dr Enid Lam, Dr Yih-Chih Chan and Ms Miriam Yeung (Dawson Laboratory, Peter MacCallum Cancer Centre).

2.2.13 Immunoblotting (Western blot)

Pellets containing approximately 1 x 10^6 cells were lysed in 60 µL of Western blot lysis buffer, after which 1.5 µL of Benzonase® (Sigma-Aldrich) was added to each sample to remove nucleic acids. Following incubation at room temperature for 10 minutes, 22 µL of loading dye solution (200 mM dithiothreitol in 4X Laemmli buffer) was added. Protein samples were denatured by boiling at 70°C for 10 minutes, then loaded into 10% or 4-15% Mini-PROTEAN® pre-cast gels (Bio-Rad) for electrophoresis in Tris-glycine running buffer at 100V. Pre-stained high molecular weight protein markers (Thermo Fisher Scientific) were run alongside the samples.

Proteins were transferred from polyacrylamide gels to Immobilon® polyvinylidene fluoride (PVDF) membranes (Merck Millipore) using the Trans-Blot® SD Semi-Dry Transfer Cell (Bio-Rad). Gels were soaked in transfer buffer and then sandwiched next to a PVDF membrane between two pieces of extra thick blot paper (Bio-Rad) within the transfer cell, such that the gel was facing the cathode and the PVDF membrane was facing the anode. Transfer was performed at 20V for 50-60 minutes.

For immunoblots visualised on X-ray film, membranes were then soaked in skim milk blocking solution for 1 hour prior to incubation with primary antibody diluted in skim milk blocking solution with gentle agitation overnight at 4°C. Membranes were washed 3 times in TBS-T for 5 minutes and then incubated with secondary antibodies conjugated with horseradish peroxidase

(Southern Biotech) diluted in skim milk blocking solution for 30-60 minutes. Membranes were again washed 6 times in TBS-T for 5 minutes, then incubated with SuperSignal™ West Pico PLUS chemiluminescent substrate (Thermo Fisher Scientific) according to manufacturer's instructions before exposure to X-ray film for protein detection.

For digital visualisation of immunoblots on the Odyssey® CLx Imaging System (LI-COR Biosciences), membranes were instead soaked in TBS Intercept® Blocking Buffer (LI-COR Biosciences) for 1 hour prior to incubation with primary antibody diluted in TBS Intercept® Blocking Buffer with 0.1% Tween-20 with gentle agitation overnight at 4°C. Membranes were washed 4 times in TBS-T for 5 minutes and then incubated with IRDye® secondary antibody (LI-COR Biosciences) diluted in TBS Intercept® Blocking Buffer with 0.1% Tween-20 and 0.01% SDS for 1 hour. Membranes were again washed 4 times in TBS-T and finally rinsed in TBS prior to imaging on the Odyssey® CLx for protein detection.

2.2.14 Imaging flow cytometry

Cells were fixed and permeabilized with eBioscience Transcription Factor Staining Buffer Set (Thermo Fisher Scientific, catalogue number 00-5523-00) according to manufacturer's instructions. Cells were blocked using 2.5% BSA in PBS for 30 minutes at room temperature. Antibodies for intracellular staining were diluted in permeabilization wash buffer supplemented with 0.1% BSA. Cells were incubated with intracellular antibody cocktail at 4°C overnight. The next day, cells were stained with appropriate fluorochrome-conjugated secondary antibodies for 1 hour at room temperature. Cell nuclei were stained with DAPI (Sigma-Aldrich) at 20 ng/mL for 10 minutes at room temperature. Cells were washed with PBS and re-suspended in PBS.

Data was acquired on an Amnis ImageStream X Mark II using 60X objective. At least 5000 images were collected for each sample. Post-acquisition spectral compensation and downstream analysis were performed using IDEAS® image analysis software (Amnis Corporation). To determine single cell populations and to separate from debris, doublets and aggregates, an initial gating strategy using Brightfield Area vs. Brightfield Aspect Ratio was performed. In-focus cells were selected using the Brightfield Gradient Root Mean Square (RMS) feature, which enables selection of high-quality images with RMS values > 50. The degree of shared localization and nuclear localization was calculated using the similarity feature, which is based on log-transformed Pearson's correlation coefficient. This measures the degree to which the masked areas associated to the images of the markers of interest are linearly correlated. High similarity

means that staining intensity of both images are high in the same pixels. Cells with a similarity score of ≥ 3 were classified as co-localized, as previously described[345-347]. Expression analysis was calculated using Median Pixel Intensity (MPI). Violin plots for summary graphs were created using RStudio software (RStudio Team, 2022).

2.2.15 Chromatin immunoprecipitation

Chromatin immunoprecipitation (ChIP) was performed on stably growing cell lines with approximately 20 x 10^6 cells harvested per condition. Cells were cross-linked with 1% formaldehyde (Sigma-Aldrich) for 15 minutes at room temperature, with gentle agitation on an orbital shaker. Cross-linking was stopped by the addition of 0.125 M glycine with gentle agitation on an orbital shaker for 5 minutes. Cells were then pelleted by centrifugation at 400 g for 5 minutes, washed twice with cold PBS and then lysed in 300 µL of ChIP lysis buffer. Lysates were sonicated in a Covaris ultrasonicator to shear DNA to an average fragment size of 500 bp. Chromatin was pelleted prior to resuspension in modified RIPA buffer, with an aliquot (4% of sample) stored as an input control. Immunoprecipitation was performed overnight at 4°C in modified RIPA buffer, using antibodies listed in Table 2.5.

The following day, 50 µL of Protein A Dynabeads® (Life Technologies) was added to each sample for 2 hours at 4°C to bind the antibody and associated chromatin. The magnetic beads were washed twice and resuspended in modified RIPA buffer prior to addition to samples. Chromatin-bound beads were serially washed with low salt and high salt wash buffers, followed by lithium chloride buffer and TE buffer. Chromatin was eluted off magnetic beads in 200 µL of elution buffer for 30 minutes at 65°C on a thermal shaker set at 1,000 rpm. The immunoprecipitated samples and input controls were then mixed with 1 µg RNase (Qiagen) and incubated at 65°C overnight on a thermal shaker set at 1,000 rpm to reverse cross-linking. DNA was purified using the MinElute® PCR purification kit (Qiagen) according to manufacturer's instructions, with samples and input controls eluted in 50 µL and 100 µL of nuclease-free H_2O, respectively.

For qRT-PCR analysis of immunoprecipitated DNA (ChIP-qPCR), analysis was performed in 96-well plates on an Applied Biosystems StepOnePlus™ system using Fast SYBR® Green reagents (Life Technologies), as outlined in section 2.2.9. The primers used are listed in Table 2.14. Fold enrichment of immunoprecipitated DNA at genes of interest were normalised to corresponding input controls and then compared to a negative control region.

2.2.16 CUT&Tag

CUT&Tag was performed as previously described[348]. MV4-11 cells (0.375 x 10^6 per condition) were mixed with Drosophila S2 cells (0.125 x 10^6 per condition) and then serially washed with PBS and CUT&Tag wash buffer at room temperature. Concanavalin A beads were activated by washing twice with binding buffer, after which 10 µL of activated beads were added to each sample and incubated for 10 minutes at room temperature. Bead-bound cells were then resuspended in 150 µL of antibody buffer with a 1:50 dilution of primary antibody and incubated for 2 hours at room temperature. Antibodies used are listed in Table 2.5.

The supernatant was then removed and the beads were washed twice with digitonin buffer prior to re-suspension in 50 µL of Dig-300 buffer with pAG-Tn5 enzyme for 1 hour at room temperature. The supernatant was again aspirated and the beads washed twice with Dig-300 buffer, followed by re-suspension in 50 µL Tagmentation buffer and incubation for 1 hour at 37°C. An equal volume of 2X stop buffer was then added and the samples were incubated at 55°C for 2 hours, then held at 4°C overnight.

The following day, the supernatant was taken and purified using the MinElute® PCR purification kit (Qiagen) according to manufacturer's instructions, with each sample eluted in 25 µL of elution buffer. To amplify libraries, 21 µL of eluted DNA was mixed with 2 µL of a universal i5 primer and 2 µL of a unique barcoded i7 primer, as well as 25 µL of NEBNext® HiFi 2X PCR Master Mix (New England Biolabs). Following 14 cycles of PCR amplification, clean-up was performed using 1.1 x volume of AMPure XP beads (Beckman Coulter), analysed on the Agilent 4200 TapeStation to determine size distribution of libraries and then sequenced on the NextSeq 500 (Illumina) using 75 bp paired end chemistry. Library preparation, quality control and sequencing were performed by the Molecular Genomics Core Facility at the Peter MacCallum Cancer Centre.

2.2.17 ChIP and CUT&Tag sequencing data analysis

Bcl2fastq (Illumina) was used to perform sample demultiplexing and to convert BCL files generated from the sequencing instrument into Fastq files. Adapters were trimmed from reads by trimmomatic[349], then aligned to the human genome (GRCh37) combined with fly genome (BDGP5) with bowtie2[350]. Samtools[351] was used to convert, sort and index bam files, and PCR duplicates were removed with picard. Peak calling was performed with MACS2[352] with default parameters, and deepTools[353] was used for normalisation. Genome-browser images of sequencing data was generated by converting files to TDF files with igvtools and viewing in

IGV[354]. Bioinformatic analysis of CUT&Tag sequencing data was performed by Dr Enid Lam (Dawson Laboratory, Peter MacCallum Cancer Centre).

2.2.18 In vivo procedures

All *in vivo* experiments were performed in accordance with ethical guidelines from the Peter MacCallum Cancer Centre Animal Ethics and Experimentation Committee (ethics approval number E615).

2.2.18.1 Bone marrow and spleen harvest

Mice were culled by cervical dislocation and bone marrow was harvested from pelvic bones, femurs and tibias. Bones were crushed using a mortar and pestle in cold PBS and passed through a 40 µm filter. Whole spleens were removed and mashed through a 40 µm filter. Bone marrow and spleen samples were centrifuged at 400 g for 5 minutes and then resuspended in 10 mL of red cell lysis buffer, incubated for 10 minutes at room temperature and washed twice with an equivalent volume of cold PBS. Cells were then taken into experimentation or cryopreserved in fetal bovine serum supplemented with 10% [v/v] DMSO.

2.2.18.2 Isolation and in vitro activation of OT-I CD8⁺ T cells and OT-II CD4⁺ T cells

For expansion of $CD8^+$ OT-I T cells, splenocytes were harvested from the spleen of OT-I mice and stimulated by incubation with 20 ng/mL of SIINFEKL (OVA peptide 257-264, Sigma-Aldrich) for 72 hours in complete RPMI-1640 media supplemented with rhIL-2 (which stimulates mouse T cells at similar concentrations to mouse IL-2[355]) at 100 units/mL (NIH). For expansion of $CD4^+$ OT-II T cells, splenocytes were harvested from the spleen of OT-II mice and stimulated by incubation with 300 nM $OVA_{323-339}$ peptide (GenScript) for 72 hours in complete RPMI-1640 media supplemented with rhIL-2 at 100 units/mL (NIH). After washing to remove the peptide, cells were re-cultured in media supplemented with rhIL-2 for an additional 3 days. Successful enrichment of $CD4^+$ and $CD8^+$ T cell populations was confirmed by flow cytometry staining for CD3, CD4 and CD8.

2.2.19 Processing of patient samples

Isolation and in vitro activation of human peripheral blood mononuclear cells (PBMCs)

Human PBMCs were isolated from donor buffy coat preparations from the Australian Red Cross Lifeblood by Ficoll-Paque® density gradient centrifugation and stimulated for 72 hours in

complete RPMI-1640 media with 600 units/mL rhIL-2 (NIH), 30 ng/mL anti-CD3 (OKT3, eBioscience) and 0.5 µg/mL anti-CD28 (eBioscience). After washing, cells were re-cultured in media supplemented with rhIL-2 for 1-3 days before experimental use. Successful enrichment of T cell populations was confirmed by flow cytometry staining for CD3, CD4 and CD8.

2.2.20 Single-cell RNA sequencing (scRNA-seq)

scRNA-seq of all primary patient AML samples was conducted on the 10X Chromium system using the 10X Genomics Chromium Next GEM 5' Single Cell Gene Expression Solution (10X Genomics). Cryopreserved samples (frozen after treatment with A-366 or vehicle control) were rapidly thawed at 37°C and viable cells were bulk sorted into Eppendorf tubes using a BD FACSAria Fusion cell sorter and propidium iodide viability dye. The cells were then washed twice with PBS + 1% BSA. All patient samples were pooled together and loaded onto a single lane of the 10X Chromium Single Cell Chip using TotalSeq-C anti-human Hashtag antibodies (BioLegend). Up to 1 million viable primary AML cells were resuspended in 100 µL of Hashing staining buffer (PBS + 2% BSA + 0.01% Tween). 1 µL of the relevant hashtag antibody was then added to the sample and stained on ice for 30 minutes. Cells were then washed 2 times with Hashing staining buffer and the cell concentration was determined. Hashtag-labelled samples were then pooled together at equal cell concentrations, spun down and resuspended in Suspension buffer (PBS + 0.04% BSA + 0.4 U/µL RNase Inhibitor (Roche)) at a final cell concentration suitable for superloading onto the 10X Chromium Single Cell Chip (>1500 cells per µL). The final cell suspension was put through a cell strainer and a final cell count was conducted for accuracy, with ~40,000 cells superloaded onto the 10X Chromium Single Cell Chip. Details of the Hashtag sequences and corresponding samples are listed below.

Table 2.19. scRNA-seq hashtags and corresponding patient samples.

Hashtag	Sequence	Sample
TotalSeq-C0251	GTCAACTCTTTAGCG	01-122-2020 vehicle control (ETOH)
TotalSeq-C0252	TGATGGCCTATTGGG	01-122-2020 A366
TotalSeq-C0253	TTCCGCCTCTCTTTG	01-010-2020 vehicle control (ETOH)
TotalSeq-C0254	AGTAAGTTCAGCGTA	01-010-2020 A366

Single cells were captured in droplet emulsions using the 10X Chromium Single-Cell Instrument and reverse transcription, cDNA amplification and library preparation were performed based on the manufacturer's protocol using the Chromium Single Cell 3' Library & Gel Bead Kit v3 (10X

Genomics). An additional primer that was specific for the oligo sequence conjugated to the Total-seq antibody was added during the reverse transcription stage. Following this, cDNA was amplified and the fraction containing the amplified Hashtags were separated from the full-length mRNA from each cell using SPRI beads (10X Genomics). These two fractions were then processed as separate cDNA libraries. Quality of final libraries was checked using the 2100 Bioanalyser (Agilent) and they were stored at -20°C until sequencing. Libraries were pooled at equimolar ratios and sequenced on the Illumina NovaSeq 6000 system (PE 150 bp reads, ~30-50,000 reads per cell). Hashtag libraries were sequenced on the Illumina NextSeq or the Illumina MiSeq (PE 75 bp reads, 5000 reads per cell).

2.2.21 scRNA-seq data analysis

Count matrices were generated from demultiplexed scRNA-seq fastq files using the 10X Genomics Cell Ranger v3.1.0 count pipeline against the hg38/GRCh38 genome (v3.0.0). scRNA-seq quality control was performed using Seurat v4 in R[356,357]. Low quality cells were removed by filtering out cells that had fewer than 500 genes or 1000 unique molecular identifiers (UMIs). Cells with greater than 15% mitochondrial RNA content were also removed. Multiplexed scRNA-seq samples containing TotalSeq-C hashtag oligo information were de-multiplexed using the CITE-seq-count v1.4.3 software and HTODemux methods within Seurat v4 using the default settings[358].

Where available, 10X scRNA-seq droplets containing doublet cells were identified based on hashtag oligo combinations with the HTODemux function in Seurat and were removed. Normalization of scRNA-seq datasets was performed using the SCTransform method[359] with percentage mitochondrial reads, S phase cell cycle score and G2M cell cycle phase score variables included in the regression model as sources of technical variation to remove except where indicated. Dimensional reduction, k-nearest neighbour graph construction and clustering were performed using Seurat v4 using default settings. The first 50 principal components were used to compute a non-linear dimensional reduction using the Uniform Manifold Approximation and Projection (UMAP) method[360]. Marker gene identification and differential gene expression analysis for clusters and groups of cells was performed using a Wilcoxon Rank-Sum test. Only groups that were comprised of at least 20 cells were considered for marker gene identification and DGE analysis. Bioinformatic analysis of scRNA-seq sequencing data was performed by Dr Dane Vassiliadis (Dawson Laboratory, Peter MacCallum Cancer Centre).

2.2.22 T cell cytotoxicity assays

2 x 10^4 MLL-AF9 or MV4-11 cells expressing CIITA cDNA, OVA peptide and/or *RREB1* sgRNA or corresponding vector controls were plated in 96-well flat clear bottom black plates (Corning) pre-coated with 5 µg/mL fibronectin (Merck). For MLL-AF9 co-cultures, $CD4^+$ OT-II T cells and/or $CD8^+$ OT-I T cells were added at the indicated effector:target (E:T) ratios, with each treatment set up in triplicate wells. For MV4-11 co-cultures, human PBMCs were added at the indicated E:T ratios, with each treatment set up in triplicate wells. Plates were incubated in the Incucyte® SX5 Live Cells Analysis System (Sartorius) at 37°C for 72 hours and set to acquire images measuring the fluorescent cell count (green and/or red) every 6 hours. Proliferation or depletion of tumour cells in each treatment was calculated by fold change of the fluorescent cell count at each timepoint, normalised to baseline (T_0).

2.2.23 Measurement of T cell cytokine secretion

1 x 10^5 MLL-AF9 cells, expressing CIITA cDNA and/or OVA peptide or corresponding vector controls, were co-cultured with 2 x 10^5 OT-II T cells in 96-well plates. Co-cultures were performed in triplicate for each condition. The cell culture media was collected after 24 hours of co-culture. Levels of T cell cytokines were measured using the BD Cytometric Bead Array Mouse IFN-γ and TNF Flex Sets, with data acquired on a BD FACSVerse and analysed using FCAP Array software.

Chapter 3 – PRC2 enables cancer immune evasion via MHC-I silencing

3.1 Introduction

This chapter describes the project within the Dawson laboratory, led by A/Prof Marian Burr, which discovered a critical role for the epigenetic complex PRC2 in transcriptional repression of MHC-I in cancer cells to evade T cell killing. Upon joining the laboratory at the commencement of my PhD, I had the opportunity to contribute to this project while learning fundamental cell and molecular biology techniques, which was recognised by joint second authorship on the resulting manuscript[361]. Some additional data not generated by me is included for context and will be acknowledged in the relevant figures and text.

3.1.1 Epigenetic dysregulation drives oncogenesis and immune evasion

The historical dogma in cancer biology is defined by the central tenet that malignancy develops through acquisition of one or more genomic mutations, which confer hallmark capabilities facilitating cell growth, tumour angiogenesis and metastasis[362]. Advances in molecular sequencing technologies have helped to unravel the mutational landscape of a multitude of cancer types, informing our understanding of disease pathophysiology and prognostication, as well as guiding potential targeted therapeutic avenues[363-371]. Through these discoveries, we now understand that mutations in key epigenetic pathways feature consistently across a wide range of cancers, affecting regulators of histone modification, DNA methylation and chromatin organisation. For example, follicular non-Hodgkin lymphoma is characterised by frequent mutations in the H3K4 methyltransferase *KMT2D* (72-89%), the H3K27 methyltransferase *EZH2* (17-27%) and the histone acetyltransferases *CREBBP* (32-70%) and *EP300* (9-19%)[372,373].

Similarly, within the spectrum of myeloid malignancies, the pre-leukaemic conditions of clonal haematopoiesis of indeterminate potential (CHIP) and MDS are enriched for mutations in *DNMT3A* and *TET2*, which regulate DNA methylation and demethylation respectively, as well as the chromatin regulator *ASXL1*[374]. Recurrent *DNMT3A* mutations have also been identified in pre-leukaemic HSCs; while the sequential acquisition of further driver mutations (such as *FLT3* and/or *NPM1*) are required for transformation to acute myeloid leukaemia, it is the *DNMT3A*-mutated HSCs that survive chemotherapeutic challenge and ultimately serve as a nidus for relapse[375,376]. Based on these insights, many novel therapies targeting epigenetic pathways are in development and have entered clinical trials[247,377-380] – some have even become standard of care in specific clinical situations, such as azacitidine (a DNA methyltransferase inhibitor) for high-risk MDS[247].

In addition to the established role for epigenetic regulators in oncogenesis and neoplastic progression, there is emerging evidence that they also contribute significantly to cancer immune evasion. This is partially based on the ability of epigenetic agents, including histone deacetylase inhibitors (HDACi) and azacitidine, to upregulate immunomodulatory pathways and sensitise cancer cells to immunotherapy[171,381,382]. Inhibition of the histone H3K4 demethylase LSD1 has also recently been shown to enhance anti-tumour immunity through induction of surface MHC class I expression and promotion of tumour infiltration by effector T cells, overcoming intrinsic anti-PD-1 resistance in a mouse melanoma model[174]. Furthermore, inhibition or genetic depletion of EZH2 has a potent immunogenic effect on the TME, reprogramming regulatory T cells towards a T-effector-like profile, augmenting T cell infiltration and cytotoxicity and improving the efficacy of ipilimumab in mouse models[383,384]. While these functional observations hold considerable promise in terms of informing potential combination therapies, the exact molecular mechanisms underpinning the interaction between epigenetic regulators and anti-tumour immunity have yet to be fully elucidated.

3.1.2 The CRISPR-Cas9 system

CRISPR-Cas9 is a genome editing technology derived from an adaptive antiviral defence mechanism found in prokaryotes, discovered after the identification of clustered regularly interspaced short palindromic repeats (CRISPR) in bacterial genomes[385,386]. The DNA spacer sequences found between the repeats often corresponded to fragments of bacteriophage viruses that were incorporated into the bacterial genome following infection and were subsequently shown to confer resistance to re-exposure with phages sharing sequence homology with the spacers[387].

In type II CRISPR systems, which utilise the activity of the endonuclease CRISPR-associated protein 9 (Cas9), the CRISPR sequences are initially transcribed as precursor CRISPR RNA (crRNA) and hybridise with a trans-activating CRISPR RNA (tracrRNA) sequence. This RNA duplex is then cleaved by endogenous RNase III to form a mature tracrRNA:crRNA product that complexes with Cas9 and directs it to induce site-specific double-strand DNA breaks[388]. The tracrRNA:crRNA hybrid can be replicated by synthetic single guide RNAs (sgRNAs) where the sequence recognition component is easily customised[389], thereby enabling highly efficient and precise modification of any gene of interest.

In eukaryotic cells, the DNA damage induced by Cas9 targeting may be repaired through non-homologous end-joining (NHEJ), which is an error-prone process that typically induces insertions and deletions (indels) and often causes frameshifts inactivating the gene. An alternative pathway is homology-directed repair, which can be harnessed in the laboratory by designing a single-strand DNA repair template to introduce specific mutations at the site of the double-strand break. Additionally, a modified, nuclease-deficient Cas9 (dCas9) can be used to selectively block gene transcription in the absence of DNA damage[390], or activate genes when the dCas9 is fused to a transcriptional activation domain[391]. The ability to apply this technology on a genome-wide scale enables screening approaches to answer fundamental biological questions in a robust and unbiased manner[392].

3.2 Results

3.2.1 Whole-genome CRISPR-Cas9 screens identify PRC2 as a key transcriptional repressor of MHC-I expression

To identify negative regulators of MHC-I expression, whole-genome positive-selection CRISPR-Cas9 screens were performed in K-562 cells (**Figure 3.1A**), a *BCR::ABL*-positive erythroleukaemia cell line that does not express cell surface MHC-I except in the context of IFN-γ stimulation (**Figure 3.1B**). The screens were performed using the Bassik Lab Human CRISPR-Cas9 Deletion Library, which contains ~220,000 sgRNA and includes 10 sgRNA targeting each of the ~20,500 protein-coding genes in the human genome, as well as sets of non-targeting sgRNAs and safe control sgRNAs that target genomic regions with no annotated function[393]. After transduction of the sgRNA library and puromycin selection of mutagenized cells, cells with MHC-I reactivation were enriched through serial FACS using both HLA-B-specific and pan-HLA-A/B/C antibodies. The top candidate hits in both screens were *EED* and *SUZ12*, which are core components of PRC2, as well as *MTF2*, which is a facultative PRC2.1 subunit that is involved in recruiting PRC2 to genomic targets[394] (**Figure 3.1C**).

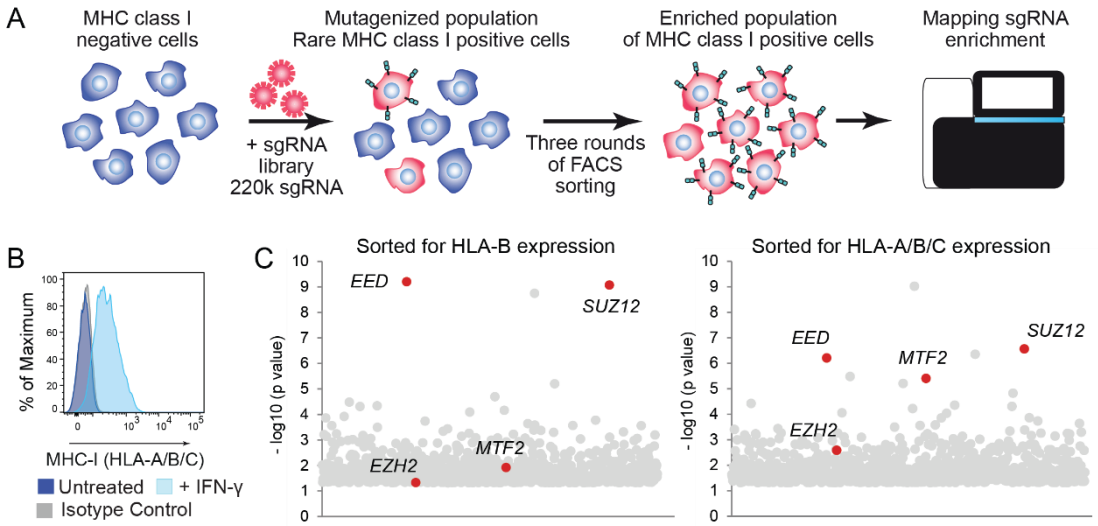

Figure 3.1. Whole-genome CRISPR screen overview and candidate hits.

(A) Schematic of CRISPR screen methodology in K-562 cells. **(B)** Cell surface MHC-I in K-562 cells in the presence or absence of IFN-γ 10 ng/mL for 24 hours. **(C)** Bubble plots show the top 1,000 enriched genes identified in the CRISPR screens. PRC2 genes are indicated in red. p values were calculated using the RSA algorithm[395]. Experiments performed by A/Prof Marian Burr.

The validity of the screen findings was confirmed through single gene knockout (KO) of *EED*, which efficiently induced cell surface MHC-I upregulation even in the absence of IFN-γ stimulation (**Figure 3.2A**). To further support a key role for PRC2 components in MHC-I repression, I next performed a series of complementation experiments for EED and EZH2. Separate K-562 *EED* and *EZH2* KO clones were generated by transiently expressing sgRNAs targeting these genes, while treating the transduced cells with raltegravir 2 nM for a total of 10 days to prevent lentiviral integration. Cells were selected with puromycin 2 µg/mL for 24 hours, starting 24 hours post-transduction, and then single cells were sorted by FACS to generate clones. Clones were verified by immunoblot for H3K27me3 and EZH2 and flow cytometry for cell surface MHC-I expression, while lentiviral integration was excluded through selection of BFP-negative and puromycin-sensitive cells.

I then cloned wildtype and functional mutants of both EED and EZH2, as described in **Section 2.2.4**. This included the *EED* W364A mutant, which disrupts binding of its aromatic cage to H3K27me3, preventing PRC2 recruitment and H3K27me3 propagation[251], as well as the *EZH2* F667I mutant, which alters a critical residue in its SET domain required for catalytic

function[337,396]. As expected, expression of wildtype EED cDNA in *EED* KO cells was sufficient to restore global H3K27me3 levels and MHC-I repression (**Figures 3.2A and 3.2B**), with similar findings also observed with expression of wildtype EZH2, but not the EZH2 F667I mutant, in *EZH2* KO cells (**Figure 3.2C**). While complementation of *EED* KO cells with the EED W364A mutant was able to preserve the PRC2 integrity and EZH2 stability, it was unable to reinstate H3K27me3 at MHC-I genes and associated transcriptional repression of MHC-I (**Figures 3.2D-F**). These findings collectively confirm the critical requirements for EZH2 catalytic activity and PRC2 structural integrity for MHC-I repression in these cells.

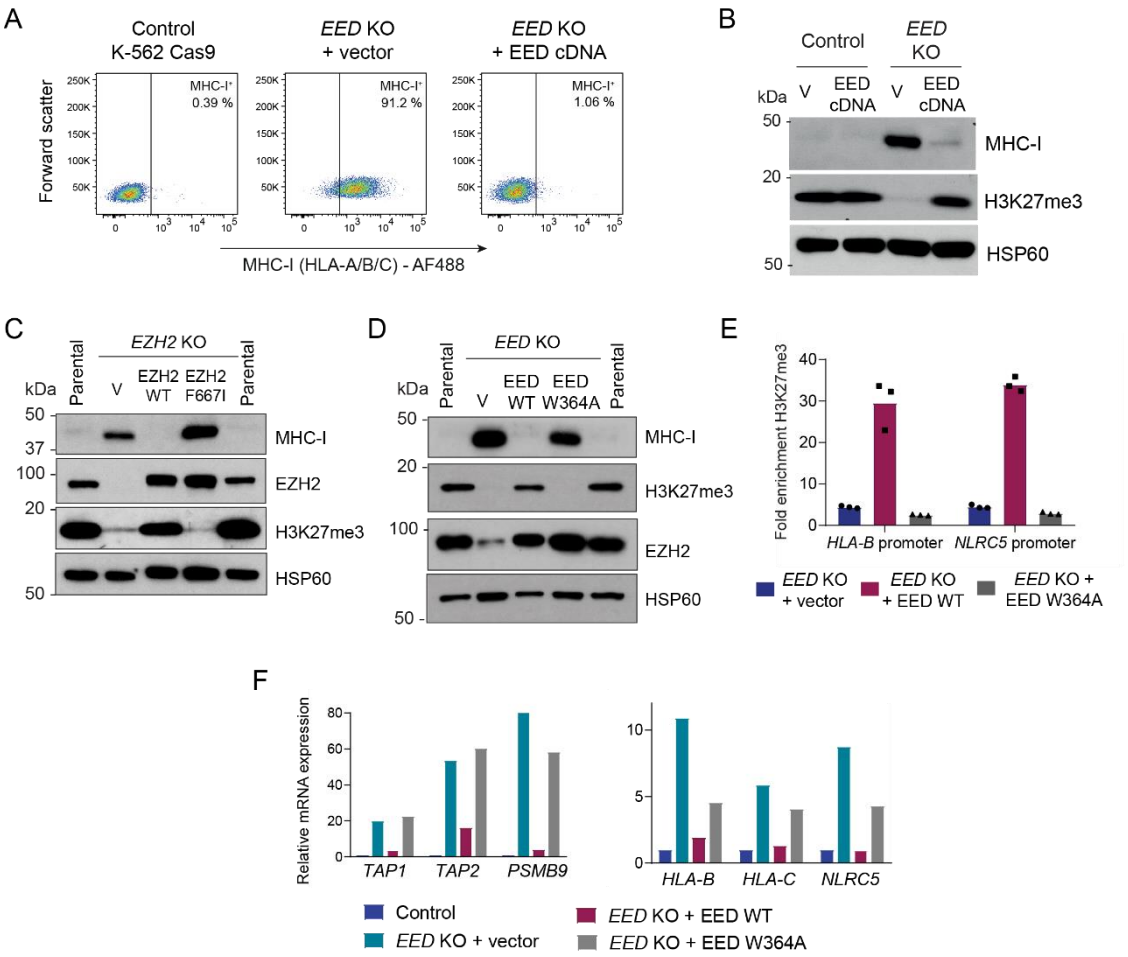

Figure 3.2. The PRC2 complex is a key transcriptional repressor of MHC-I genes.

(A and B) K-562 *EED* KO cells were transduced with EED cDNA or vector control (V) and analysed by flow cytometry (A) and immunoblot (B). **(C)** Immunoblot in K-562 *EZH2* KO cells transduced with lentiviral vectors encoding wildtype (WT) EZH2, EZH2 F667I or vector control (V). **(D-F)** K-562 *EED* KO cells were transduced with lentiviral vectors encoding wildtype (WT) EED, EED W364A or vector control (V). (D) Immunoblot. (E) H3K27me3 chromatin immunoprecipitation (ChIP) qPCR at MHC-I gene promoters. Fold enrichment was calculated

relative to the signal at the *GAPDH* promoter as a negative control. Bars show the mean of three technical replicates represented by points. (F) qRT-PCR analysis of MHC-I APP gene expression relative to control parental K-562 cells. Bars represent the mean of technical triplicates from a representative experiment.

Mirroring genetic disruption of PRC2, treatment of K-562 cells with EPZ-011989, a potent and selective pharmacological inhibitor of EZH2, effectively depleted H3K27me3 levels and increased transcription of multiple components of the MHC-I APP (**Figures 3.3A and 3.3B**). Prior studies have demonstrated that PRC2 inhibition in cancer cells leads to de-repression of ERVs and activation of an interferon "viral mimicry" response[397], which can increase MHC-I levels. This effect can be abolished through genetic disruption of *STAT1*, a central transcription factor in the IFN response pathway, as evidenced by the inability of *STAT1* KO cells to upregulate MHC-I in response to exogenous IFN-γ stimulation (**Figure 3.3C**). I then utilised an *EED* KO clone generated for the complementation experiments, which had been treated with raltegravir to block integration of the *EED*-targeting sgRNA. Expression of *STAT1*-targeting sgRNA in the *EED* KO clone effectively depleted STAT1 (**Figure 3.3D**) but did not block MHC-I upregulation (**Figure 3.3E**). Additionally, STAT1 phosphorylation was not detectable following EZH2 inhibition in the absence of exogenous IFN-γ (**Figure 3.3F**), confirming independence of this mechanism from IFN signalling. Taken together, these findings support a key role for PRC2 in mediating direct transcriptional repression of MHC-I APP components, unrelated to ERV reactivation, viral mimicry and IFN signalling.

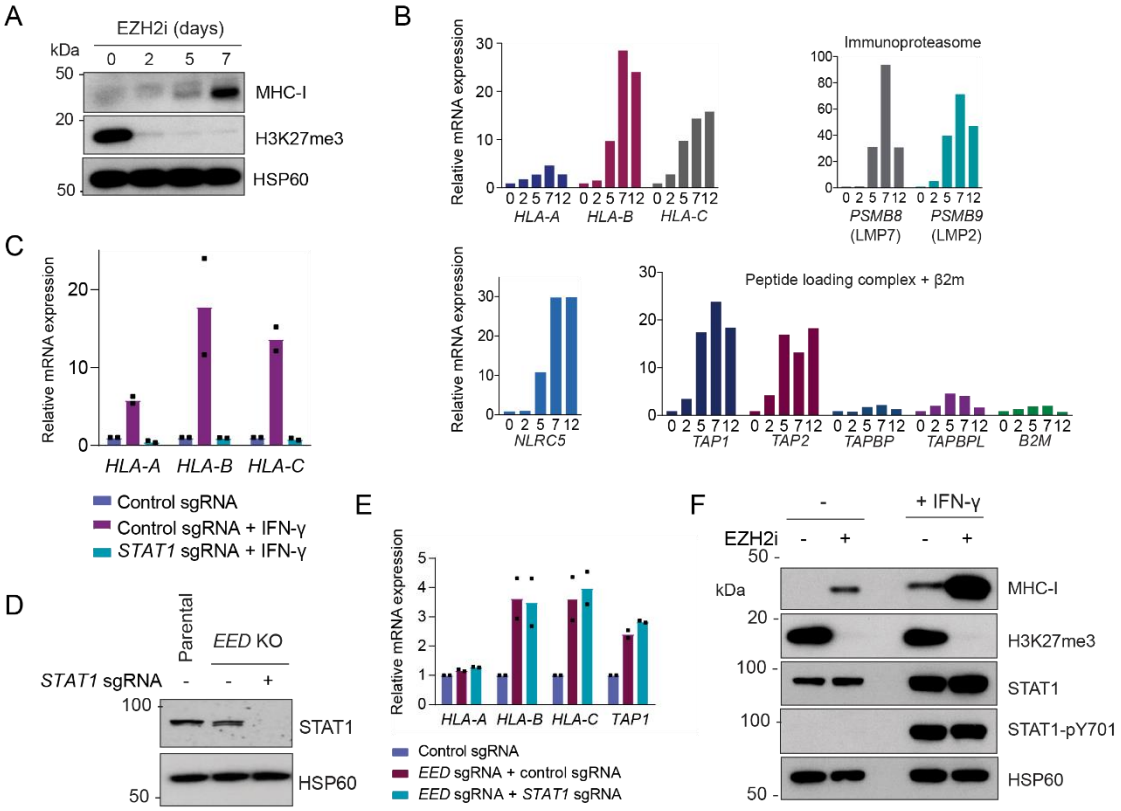

Figure 3.3. Genomic and pharmacological PRC2 targeting restore MHC-I expression independently of STAT1 signalling.

(A and B) K-562 cells incubated with EPZ-011989 3µM (EZH2i) for the indicated times were analysed by immunoblot (A) and qRT-PCR (B). For (B), bars represent the mean of technical triplicates from a representative experiment. **(C)** qRT-PCR analysis of K-562 cells expressing *STAT1* sgRNA or control sgRNA treated with or without IFN-γ 10 ng/mL for 24 hours. Bars indicate the mean fold change from independent experiments and points denote the mean of technical triplicates from individual experiments. **(D and E)** K-562 *EED* KO cells were transduced with control or *STAT1*-targeting sgRNA and analysed by immunoblot (D) and qRT-PCR (E) compared to parental control K-562 cells. For (E), bars indicate the mean fold change from independent experiments and points denote the mean of technical triplicates from individual experiments. **(F)** Immunoblot of Kelly cells treated with EPZ-011989 3µM for 10 days in the presence or absence of IFN-γ 10 ng/mL for 24 hours.

3.2.2 PRC2 coordinates silencing of the MHC-I antigen presentation pathway across multiple cancer types

Having established the key epigenetic mechanism of MHC-I repression in K-562 cells, I next wished to explore whether PRC2 also regulated MHC-I in other cancer types with constitutively low MHC-I expression. Analysis of sequencing data from the Cancer Cell Line Encyclopedia[398] showed that small cell lung cancer (SCLC) and neuroblastoma cell lines consistently exhibited the lowest expression of MHC-I APP genes out of all tumour types (**Figure 3.4A**). Importantly, both tumour types are of neuroendocrine origin and are characterised by high levels of EZH2 expression, which has been shown to contribute to oncogenesis and therapeutic resistance[399,400].

Consistent with my findings in K-562 cells, genetic and pharmacological PRC2 disruption significantly induced MHC-I expression in SCLC and neuroblastoma cell lines (**Figure 3.4B**). EZH2 inhibition also effectively upregulated MHC-I in a Merkel cell carcinoma cell line (**Figure 3.4B**), which is another neuroendocrine tumour that has been shown to suppress MHC-I expression as a means of escape from immune therapies[401].

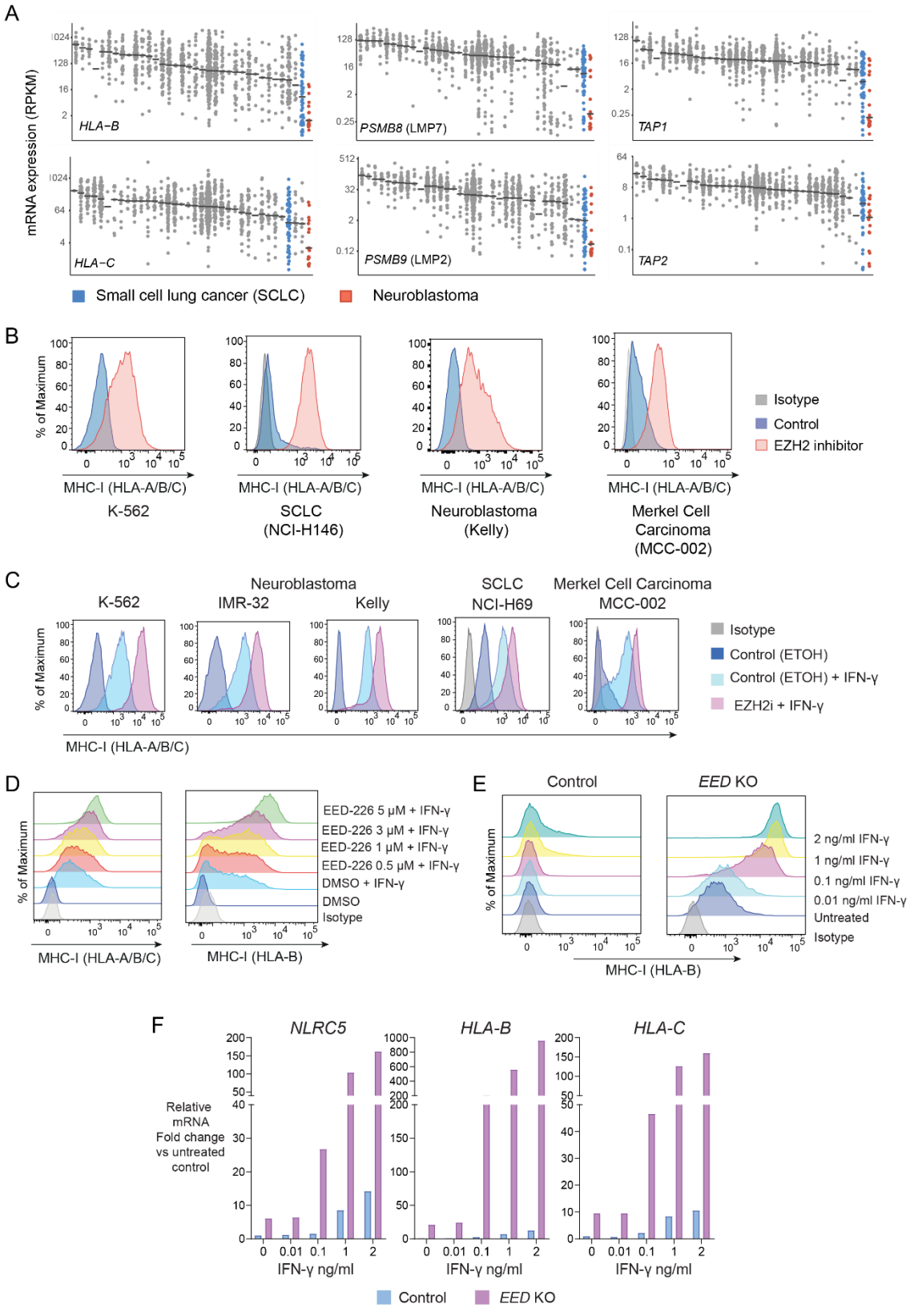

Figure 3.4. PRC2 maintains transcriptional repression and restricts interferon-induced activation of MHC-I in multiple MHC-I-low cancers.

(A) mRNA expression (reads per kilobase of transcript per million mapped reads) of MHC-I genes in 920 cancer cell lines in the Cancer Cell Line Encyclopedia. Each dot represents an

individual cancer cell line, clustered by tumour type (log_2 scale, black line indicates median). **(B)** Cell surface MHC-I in indicated cell lines treated with EZH2 inhibitor (GSK-503 5μM in NCI-H146 and EPZ-011989 3μM in K-562, Kelly and MCC-002) after 10 days of treatment. **(C and D)** Cell surface MHC-I following incubation with IFN-γ 10 ng/mL for 24 hours in indicated cell lines pre-treated with EPZ-011989 (C) and K-562 cells pre-treated with EED-226 (D). Analysis after 10 days of inhibitor treatment. **(E and F)** Cell surface MHC-I (E) and qRT-PCR analysis of MHC-I gene expression (F) in EED KO or parental control K-562 cells incubated with the indicated concentrations of IFN-γ for 24 hours. Experiments in panels B and C were performed with A/Prof Marian Burr and Ms Christina Sparbier.

In addition to reactivation of basal MHC-I expression, pharmacological PRC2 inhibition potentiated the induction of MHC-I seen in response to IFN-γ stimulation of multiple deficient cancer types (**Figure 3.4C**), with inhibitor titration studies confirming that this occurs in a dose-dependent manner (**Figure 3.4D**). Additionally, stably relieving PRC2-mediated transcriptional repression via *EED* KO also markedly reduced the threshold required to initiate MHC-I gene expression, with responses seen at IFN-γ doses well below what is required for MHC-I upregulation in an *EED*-wildtype state (**Figures 3.4E-F**). These data illustrate the evolutionarily conserved role of PRC2 in mediating MHC-I repression across multiple cancer types, particularly those of neuroendocrine origin. Disruption of PRC2 function not only facilitates MHC-I re-expression but also modulates IFN sensitivity, supporting potential combinatorial therapeutic strategies to optimise MHC-I upregulation and tumour immunogenicity.

3.2.3 Cancers deficient in MHC-I exploit PRC2 function to maintain bivalent chromatin modifications at MHC-I genes

PRC2 is the only epigenetic complex known to catalyse H3K27 di- and tri-methylation, with H3K27me3 functioning as a stable repressive chromatin mark[249]. Having shown that PRC2 targeting induces MHC-I expression, we next assessed the levels of repressive H3K27me3 and activating H3K4me3 modifications at MHC-I APP genes in the presence and absence of EZH2 inhibition. Remarkably, in the context of intact PRC2 function where MHC-I is silenced, both H3K27me3 and H3K4me3 marks were present at the promoters of MHC-I APP genes across a range of human cancer types, as well as cell lines derived from mouse SCLC and the Tasmanian Devil facial tumour disease (DFTD) (**Figure 3.5A**). DFTD is particularly notable as it is a rare example of cancer transmission between non-identical, immunocompetent individuals, where immune evasion occurs due to reversible downregulation of MHC-I expression[402].

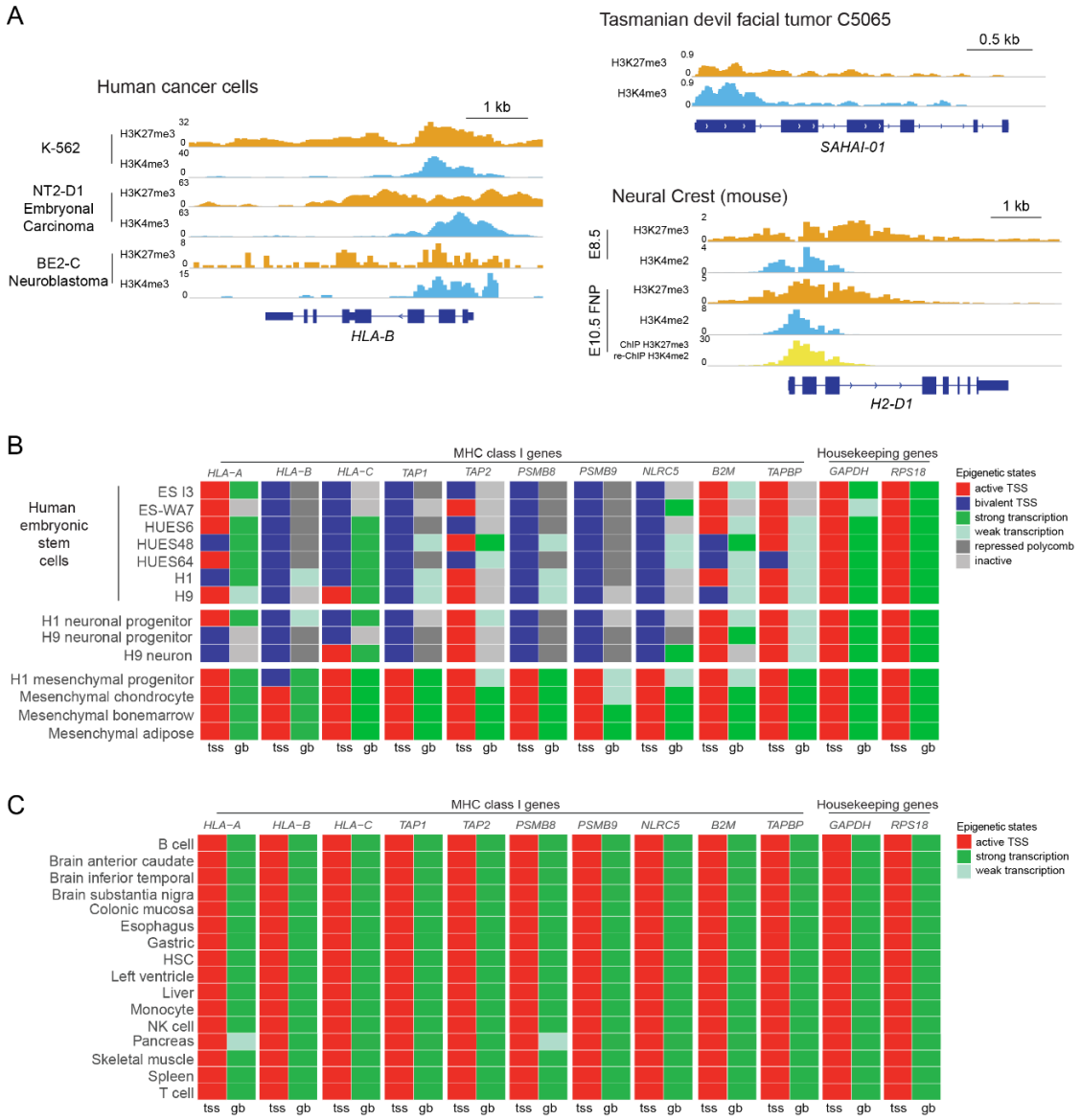

Figure 3.5. PRC2 maintains bivalency at MHC-I gene promoters in embryonic stem and neural progenitor cells and in MHC-I-low cancers.

(A) H3K27me3 and H3K4me3 modifications at MHC-I gene promoters in human and Tasmanian devil cancer cells and mouse neural crest cells. ChIP sequencing (ChIP-seq) in K-562 and Tasmanian devil cells was performed in-house by A/Prof Marian Burr and Ms Christina Sparbier. Neural crest data are from GEO:GSE89435[403], BE2-C from GEO:GSE80151[404] and NT2-D1 from GEO:GSE31755[405]. Y axes indicate reads per million (rpm). **(B and C)** Chromatin state discovery tracks in selected human embryonic stem and progenitor cells (B) and normal adult human tissues (C) generated using ChromHMM software integrating H3K27me3, H3K4me3, H3K27ac and H3K36me3 ChIP-seq data from the NIH Roadmap Epigenetics Mapping Consortium[406]. Generated chromatin annotation states for the transcriptional start site (tss) and gene body (gb) of the indicated genes are shown.

The bivalent chromatin state seen at MHC-I APP genes was initially described as a defining feature of developmental genes in embryonic stem cells[407], which remain repressed but poised for rapid activation or stable silencing depending on subsequent differentiation signals. In keeping with this observation, MHC-I gene promoters in human embryonic stem cells were also found to contain bivalent H3K27me3 and H3K4me3 marks, which was maintained in neural progenitor cells but resolved in favour of transcriptional activation following subsequent mesenchymal differentiation (**Figures 3.5B and 3.5C**).

3.2.4 PRC2 targeting restores cell surface MHC-I expression and overcomes resistance to T cell killing

To explore the functional consequences of inducing MHC-I upregulation in deficient cancer cells, we utilised a mouse model of SCLC (mSCLC) driven by conditional inactivation of *Tp53* and *Rb1*[408] and characterised by transcriptional repression of MHC-I that can be overcome by PRC2 targeting and/or IFN-γ stimulation (**Figures 3.6A and 3.6B)**. Cells derived from this model were engineered by A/Prof Marian Burr and Ms Christina Sparbier to express the chicken OVA protein, which is processed through the MHC-I APP to generate the SIINFEKL peptide. SIINFEKL is presented on mouse MHC-I (H-2Kb in C57Bl/6-derived strains) and is specifically recognised by the T cell receptor on $CD8^+$ T cells from OT-I transgenic mice (**Figure 3.6C**). In their subsequent co-culture experiments with OVA-expressing mSCLC cells and OT-I $CD8^+$ cytotoxic T cells, pre-treating the mSCLC cells with EZH2 inhibitor was sufficient to induce SIINFEKL:H-2Kb upregulation (**Figure 3.6D**) and activate OT-I T cells, resulting in release of pro-inflammatory cytokines (**Figure 3.6E**) and efficient tumour cell killing (**Figure 3.6F**), both of which were further potentiated with the addition of exogenous IFN-γ. These data illustrate the potential therapeutic utility of PRC2 targeting to restore MHC-I expression in deficient tumours and sensitise them to $CD8^+$ cytotoxic T cell killing.

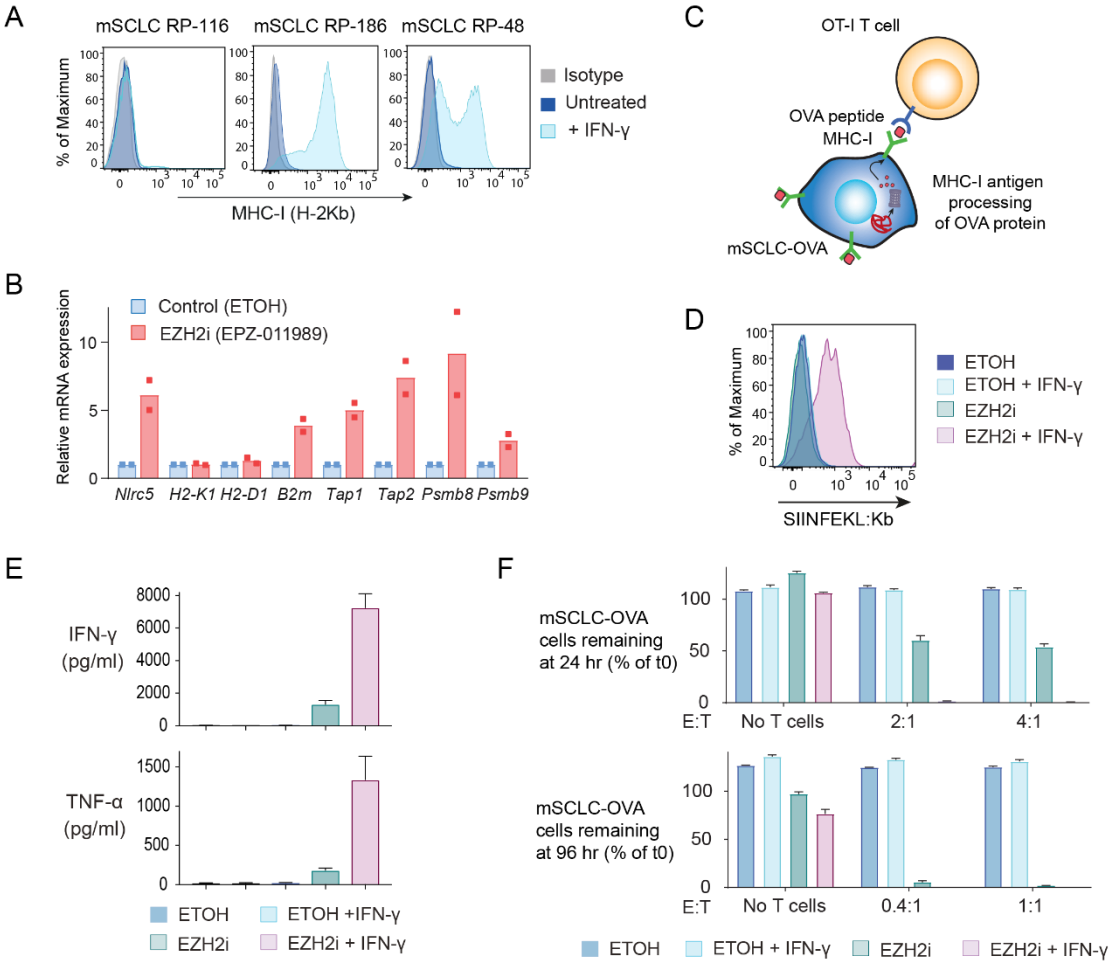

Figure 3.6. Pharmacological EZH2 inhibition overcomes resistance to T cell killing in SCLC. **(A)** Cell surface MHC-I in mSCLC cell lines in the presence or absence of IFN-γ 10 ng/mL for 24 hours. **(B)** qRT-PCR analysis of MHC-I genes in mSCLC RP-116 cells treated with EPZ-011989 3μM or vehicle control (ETOH) for 10 days. Bars depict the mean fold change in expression from independent experiments and points indicate the mean of technical triplicates from individual experiments. **(C)** Schematic of the mSCLC-OVA co-culture assay. Stable expression of full-length OVA in mSCLC cells allows functional evaluation of the intracellular MHC-I antigen-processing pathway. Processed OVA peptide bound to H-2Kb is presented at the tumour cell surface and recognised by antigen-specific OT-I T cells. **(D)** Cell surface SIINFEKL:Kb (MHC-I-bound OVA peptide) in OVA-expressing RP-116 cells, pre-treated with EPZ-011989 3μM or vehicle control (ETOH) for 10 days in the presence or absence of IFN-γ 10 ng/mL for 24 hours. **(E)** CBA assay for T cell effector cytokines following 24-hour co-culture with mSCLC-OVA cells, pre-treated as indicated. **(F)** Percent remaining live mSCLC-OVA cells following incubation with OT-I T cells at the indicated effector:target (E:T) ratios. Experiments performed by A/Prof Marian Burr and Ms Christina Sparbier.

As further validation of the clinical relevance of our findings, we next analysed tumour samples from a patient with *EGFR*-mutated lung adenocarcinoma who developed clonally-related disease transformation to SCLC following treatment with the EGFR-targeting tyrosine kinase inhibitor (TKI) erlotinib, which is a recognised mechanism of acquired resistance to targeted anti-cancer therapies[409,410]. In the absence of inactivating mutations in MHC-I APP genes, the areas of SCLC transformation exhibited significant downregulation of MHC-I and other pathway components (**Figure 3.7**), which was associated with resistance to subsequent immune checkpoint inhibition. Although arising in the context of selective pressure from TKI therapy, this phenomenon demonstrates how lineage switching in cancer (in this case, transformation to a neuroendocrine phenotype) can also modulate MHC-I expression and enable immune escape.

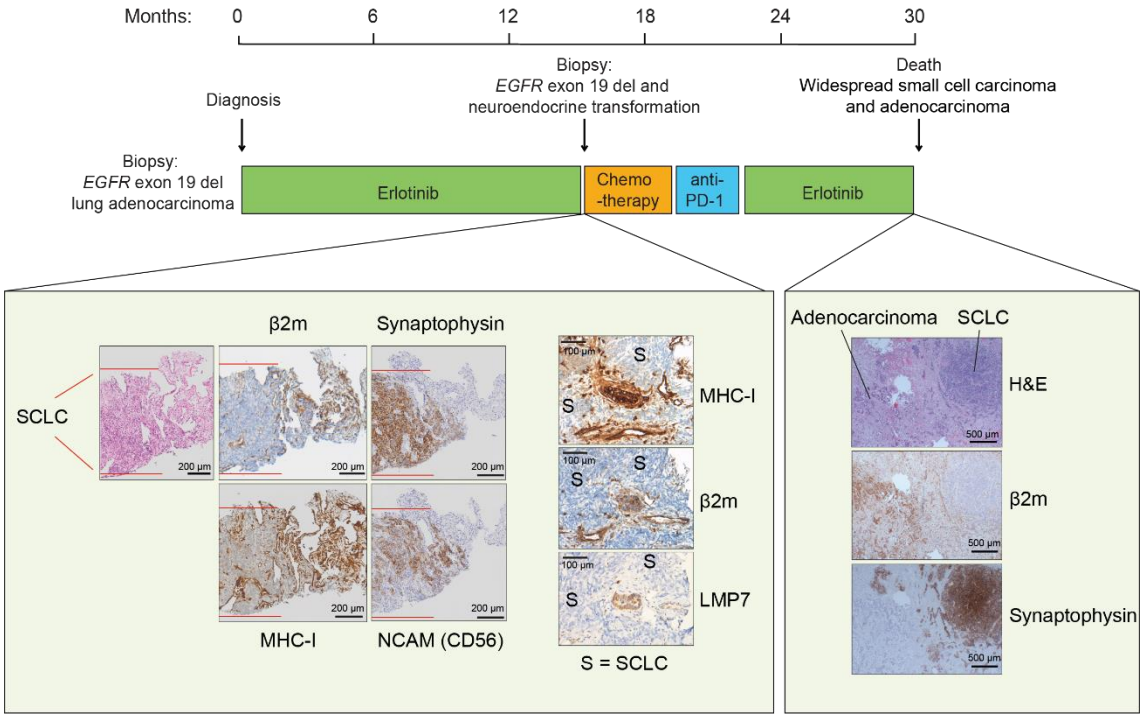

Figure 3.7. MHC-I downregulation arising from neuroendocrine transformation of lung adenocarcinoma to SCLC.

Biopsy at disease progression (left) and post-mortem histology (right). Immunohistochemistry was performed for neuroendocrine markers (synaptophysin and NCAM) and MHC-I APP components (MHC-I, β2M and LMP7). Areas of neuroendocrine transformation to SCLC, illustrated by synaptophysin and NCAM positivity, are indicated between the red lines. Experiment performed by A/Prof Marian Burr.

3.3 Discussion

Given the potential efficacy and broad applicability of cancer immunotherapies, identifying and understanding mechanisms of resistance are critical to optimising the therapeutic benefit that patients can derive. In contrast to genomic mechanisms of immune evasion, such as inactivating *B2M* mutations that disable tumour cell MHC-I expression and antigen presentation, non-genomic mechanisms are potentially reversible and consequently of particular translational interest.

In this work, I identify that the epigenetic complex PRC2 facilitates MHC-I repression in cancer cells by maintaining MHC-I APP genes in a transcriptionally silent, bivalent chromatin state. This is a physiological process seen in embryonic stem cells and neural progenitor cells, which likely developed to protect these populations from elimination by autoreactive T cells[411], but is co-opted by cancers of neuroendocrine origin to evade adaptive immune responses. Interestingly, this lineage-specific phenomenon is conserved across species, as seen in mouse SCLC and transmissible Tasmanian devil facial tumours. It is also noteworthy that neuroendocrine malignancies such as SCLC typically exhibit a highly aggressive clinical course with propensity for early and widespread metastasis, which is indicative of ineffective immune control. Given SCLC cells are characterised by high mutational burden, which promotes neoantigen formation and immunogenicity, this underscores the critical importance of tumour cell MHC-I expression and antigen presentation in facilitating anti-cancer immunosurveillance.

While it has previously been established that PRC2 targeting can indirectly enhance tumour immunogenicity through ERV reactivation and stimulation of a cell-intrinsic interferon response[397], my findings contribute to an emerging body of literature demonstrating that PRC2 also directly inhibits anti-cancer immune responses through repression of MHC-I genes. PRC2-mediated MHC-I repression is targetable by currently available small molecule inhibitors to efficiently restore MHC-I expression and sensitivity to T cell-mediated killing, providing the scientific rationale for combining PRC2 inhibitors and immune checkpoint blockade in clinical trials of these malignancies.

The opportunity to contribute to this project gave me valuable exposure to a range of basic scientific techniques and provided a solid methodological foundation for the subsequent work in my PhD, which will be described in the following two chapters.

Chapter 4 – Identifying regulators of MHC-II expression in AML

4.1 Introduction

Acute myeloid leukaemia (AML) is an aggressive haematological malignancy characterised by poor long-term outcomes – the overall 5-year survival rate is approximately 25% and is even lower in patients with advanced age and/or adverse genetic features. The therapeutic armamentarium has remained largely unchanged despite decades of research, with the optimal treatment strategy for younger, fit patients comprising intensive induction chemotherapy with cytarabine and an anthracycline, followed by consolidation with further chemotherapy cycles or alloSCT depending on a patient's risk of relapse as predicted by disease mutational profile[244]. Although associated with significant potential for treatment-related morbidity and mortality, alloSCT offers the best chance of durable remission through immunological disease control[412], particularly for adverse-risk patients. In spite of this, approximately 40-50% of alloSCT patients develop leukaemic relapse, of which the majority will eventually succumb to progressive, refractory disease.

While recent sequencing studies have clearly mapped out the subclonal nature of AML and the changes in mutational architecture that occur in response to therapeutic pressures like chemotherapy and alloSCT[413,414], it is unclear in most cases how these mutations drive acquired resistance and escape from the immunological GVL effect. Previous case reports and small case series have described loss or downregulation of MHC-I and/or MHC-II in leukaemic blasts at relapse post-alloSCT[415-417], which was linked in one case to focal deletion of a region of chromosome 6p encoding several MHC-I genes[417]. In another case series, relapse following haploidentical alloSCT was due to acquired uniparental disomy of chromosome 6p, resulting in the loss of mismatched HLA antigens on mutant leukaemic blasts[418]. This is not seen in patients who undergo alloSCT from a closely HLA-matched donor[419], confirming the specificity of this escape mechanism from immune pressure exerted by the allograft.

Considering the small number of reported cases of genomic evolution directly contributing to MHC loss or downregulation, it is possible that epigenetic mechanisms facilitate post-alloSCT immune escape in a significant proportion of patients. This hypothesis is supported by a *New England Journal of Medicine* paper published in 2018[420], which analysed paired patient samples collected at the time of initial presentation and following post-alloSCT relapse. Although whole exome sequencing did not identify acquisition of mutations in immune-related genes at relapse, RNA sequencing demonstrated downregulation of multiple genes involved in MHC-II antigen processing and presentation, which was reversible with interferon-γ stimulation. These findings

were confirmed in a subsequent *Nature Medicine* paper[421], which independently verified MHC-II loss through CIITA downregulation as a key recurring feature in post-transplantation relapse samples and showed that this led to abrogated T cell responses *in vitro*.

While these two publications implicate tumour cell MHC-II expression, and by extension $CD4^+$ T cell function, in GVL-mediated immunosurveillance, the molecular mechanisms by which MHC-II is regulated to contribute to immune escape remained unknown. Given the similarities with our work on MHC class I downregulation, I was well-placed to try and answer this key biological question as an essential first step towards designing targeted salvage therapies aimed at bolstering the immune response and improving survival outcomes in AML patients who have an otherwise dismal prognosis.

4.2 Results

4.2.1 Whole-genome CRISPR screens in MHC-II negative AML cell lines

To identify potential regulators of MHC-II expression in AML, I first performed whole-genome CRISPR screens in MOLM13 and OCI-AML3, which are two AML cell lines of myelomonocytic lineage with constitutively low MHC-II expression in the absence of IFN-γ stimulation (**Figure 4.1**). Notably, MOLM13 and OCI-AML3 collectively encompass mutations in *DNMT3A*, *NPM1* and *FLT3*, which are the most common oncogenic drivers in AML[370]. The CRISPR screens were performed with the Bassik Lab Human CRISPR-Cas9 Deletion Library used for the MHC-I screens – the library sgRNAs are expressed in the pMCB320 lentiviral sgRNA vector, which encodes puromycin and mCherry selection markers.

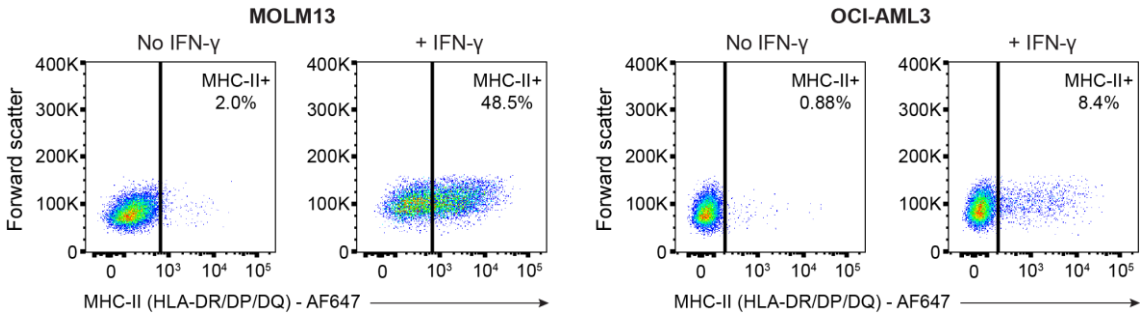

Figure 4.1. MHC-II expression in MOLM13 and OCI-AML3 cells.

Cell surface MHC-II expression in MOLM13 and OCI-AML3 cells in the presence or absence of IFN-γ 25 ng/mL for 48 hours. Representative of 3 experiments.

Since the number of viral particles that enter each cell is stochastic and dependent on the ratio of viral particles to target cells, a common feature of CRISPR screens is transduction of the target cells at a low multiplicity of infection (MOI), typically between 0.3 and 0.5, in order to minimise the number of cells that are infected by more than one sgRNA. This aims to ensure that only one gene is disrupted per cell and avoids any confounding effect of different sgRNAs interacting within a given cell. To achieve an MOI of 0.3, viral titration studies were performed to determine the optimal volume of virus needed to infect 30% of target cells, determined by mCherry positivity in an unselected population at 72 hours post-transduction (**Figure 4.2**). Importantly, the titration studies were performed under the same transduction conditions planned for the screens, using 3 x 10^6 cells in each well of a 12-well plate and with centrifugation (at 900g for 90 minutes) as well as the transduction reagent polybrene to improve efficiency. Based on this experiment, 50 µL of library virus was used per well in the MOLM13 screens and 200 µL of library virus was used per well in the OCI-AML3 screens.

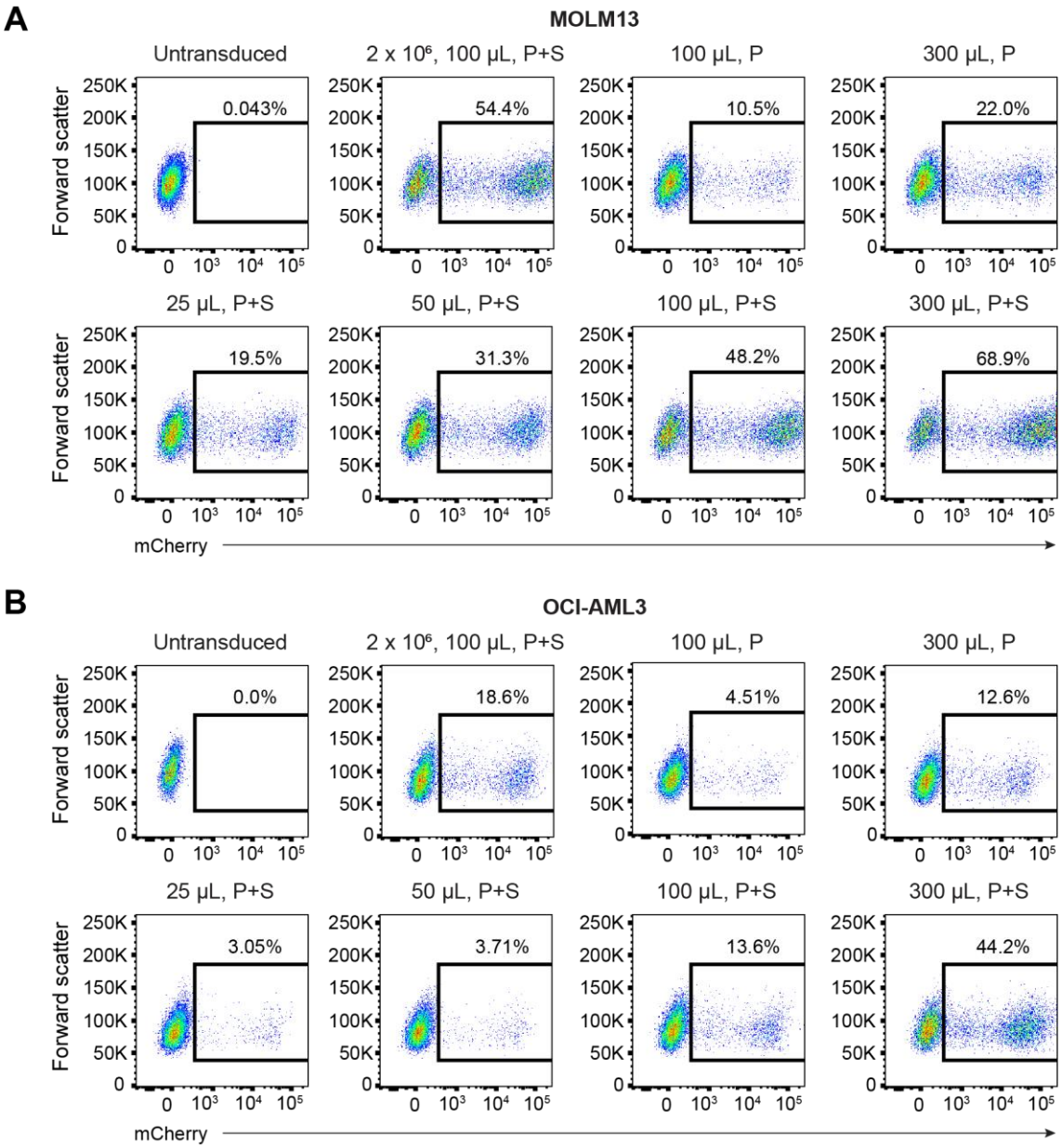

Figure 4.2. Titration of whole-genome library virus in human AML cell lines.

(A and B) mCherry expression in MOLM13 (A) and OCI-AML3 (B) cells transduced with specified volumes of pooled library virus. Except where indicated, 3 x 10^6 cells were transduced. P, polybrene 8 µg/mL. S = spinfection (centrifugation at 900 g x 90 minutes).

Parental MOLM13 and OCI-AML cells were then transduced using the pHRSIN-P_{SFFV}-Cas9-P_{PGK}-Blasticidin vector, with a minimum of 10 days of blasticidin treatment to ensure stringent selection of Cas9-expressing cells. These cells were expanded for the screens, with a total of 288 x 10^6 cells (3 x 10^6 cells per well of a 12-well plate, with 8 plates used) transduced simultaneously. At a MOI of 0.2 for both cell lines, this meant 57.6 x 10^6 cells were transduced

for each screen, giving approximately 260-fold representation of each of the ~220,000 sgRNAs in the library.

The transduced cells were pooled and expanded further prior to selection of sgRNA-expressing cells by treatment with 2 µg/mL puromycin on day +2. Serial FACS was then performed over the next 4 weeks to enrich for viable mCherry+ MHC-II+ cells, as detected by a pan-MHC-II (HLA-DR/DP/DQ) antibody. For each cell line, two sets of three sorts each were performed in parallel, with one set of cells pre-treated with IFN-γ 25 ng/mL for 48 hours prior to each sort and the other set left untreated. The pulsed IFN-γ sorts were done in case disruption of MHC-II regulators was insufficient to induce basal MHC-II expression, but was able to enhance MHC-II upregulation in response to cytokine stimulation. Sorts were conducted at days +12, +21 and +27 for the MOLM13 (no IFN-γ) cells, with minor variation for the other screen conditions due to sorter availability. After each sort, approximately half of the recovered cells were pelleted and frozen for downstream sequencing and the other half expanded for subsequent sorting. A control unsorted library population of cells was maintained in parallel and pellets of these cells were also frozen at the time of each sort. With consecutive sorts, serial enrichment of an MHC-II+ population was observed, with representative results from the MOLM13 screen in **Figure 4.3**.

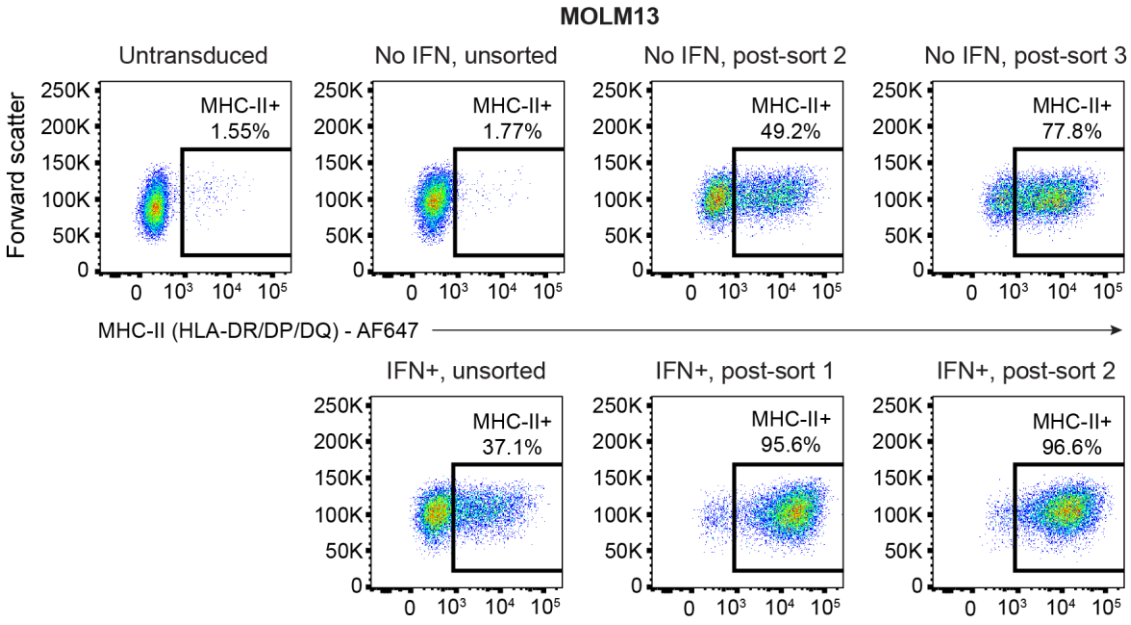

Figure 4.3. Post-sort enrichment of transduced MHC-II⁺ MOLM-13 cells.

Cell surface MHC-II expression in MOLM13 cells from indicated timepoints in the no IFN and IFN+ screens. IFN+ sorted cells were pulsed with IFN-γ 25 ng/mL for 48 hours prior to analysis.

Genomic DNA was extracted from sorted cell pellets as well as contemporaneous control library pellets using the Puregene Core Kit A (Qiagen) according to manufacturer's instructions. sgRNA sequences were amplified by two rounds of PCR, with the second round of primers containing adaptors for Illumina sequencing. Samples were sequenced with single-end 75 bp reads on an Illumina NextSeq 500, with sequenced reads trimmed and mapped to the reference sgRNA library to compute read counts for each sgRNA. The RSA algorithm[395] was used to rank genes for which targeting sgRNAs were significantly enriched in the sorted populations compared to the unsorted control populations grown in parallel.

4.2.2 Whole-genome CRISPR screen results

The results of the whole-genome CRISPR screens are shown in **Figure 4.4**. Two of the top candidate hits in both screens were F-box only protein 11 (*FBXO11*), a substrate recognition component of the SKP1-CUL1-F-box (SCF) E3 ubiquitin ligase complex, and Ras-responsive element binding protein 1 (*RREB1*), a zinc finger transcription factor.

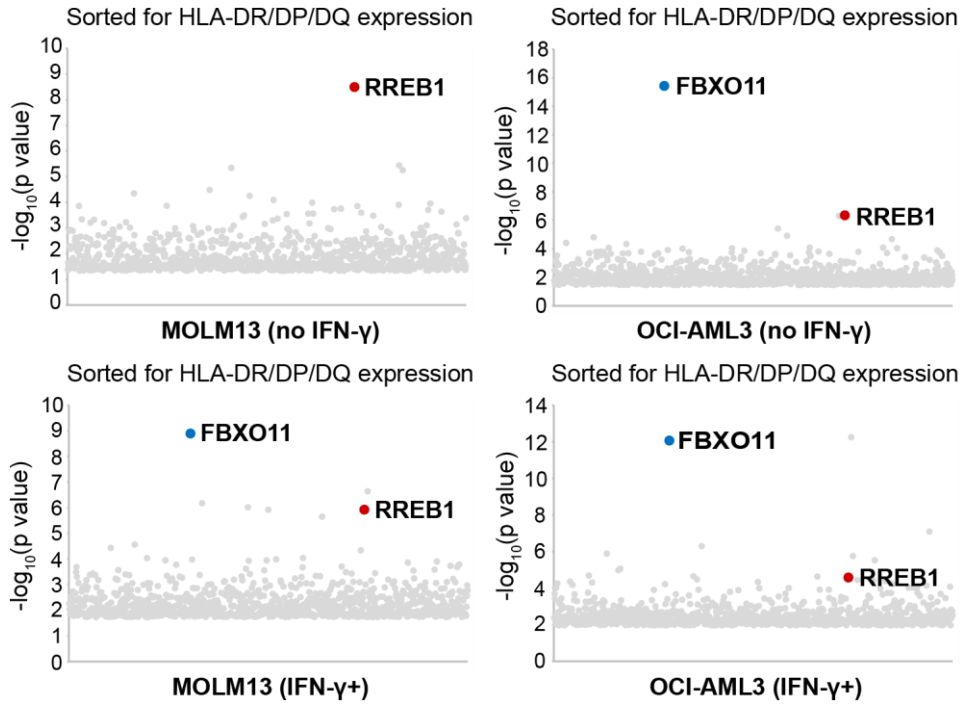

Figure 4.4. Whole-genome CRISPR screen results.

For IFN-γ+ sorts, cells were pulsed with IFN-γ 25 ng/mL for 48 hours prior to each sort. Bubble plots show the top 1,000 enriched genes identified. p values were calculated using the RSA algorithm[395]. OCI-AML3 screen performed by Dr Sylvain Garciaz.

These screen hits were validated through single-gene KO in MOLM13 and OCI-AML3 cells, as well as in MV4-11 cells, another AML cell line with distinct driver mutations. Both *RREB1* and *FBXO11* KO induced MHC-II upregulation in these cell lines, which was potentiated by IFN-γ stimulation (**Figures 4.5A-C**). Additionally, combined KO of *RREB1* and *FBXO11* further increased MHC-II expression (**Figure 4.5D**) with no significant effect on surface MHC-I levels or transcription of key genes within the MHC-I APP (**Figures 4.5D and 4.5E**).

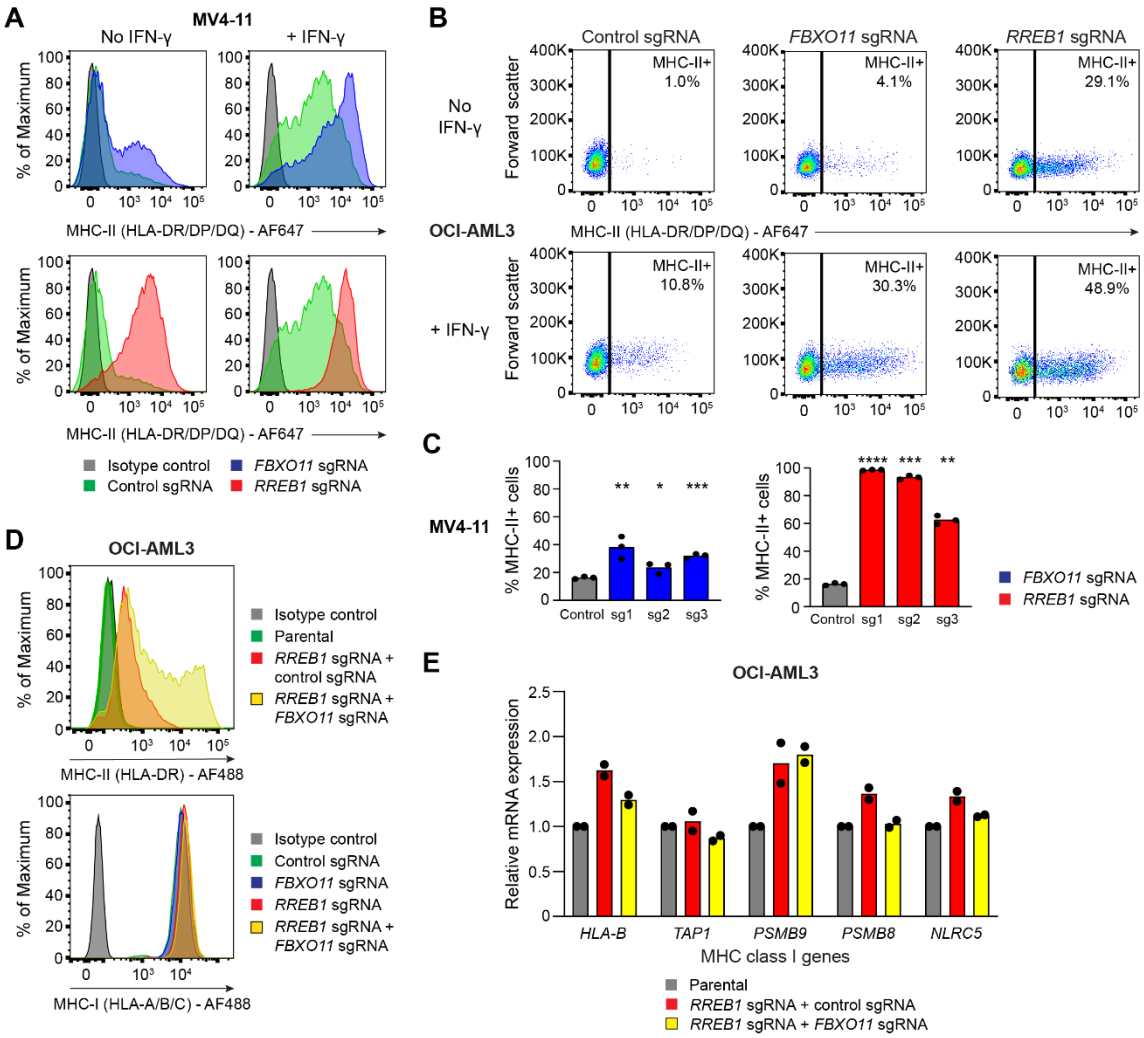

Figure 4.5. Validation of whole-genome CRISPR screen hits.

(A and B) Cell surface MHC-II expression in MV4-11 Cas9 cells (A) and OCI-AML3 Cas9 cells (B) transduced with a pool of 3 sgRNAs targeting the indicated genes or a control sgRNA, in the presence of absence of IFN-γ 10 ng/mL (MV4-11) or 25 ng/mL (OCI-AML3) for 48 hours. Representative plots from 3 experiments. **(C)** Cell surface MHC-II expression in MV4-11 Cas9 cells transduced with individual sgRNAs targeting the indicated genes or a control sgRNA. Bars depict the mean percentage of MHC-II+ cells from 3 independent experiments indicated by points. Statistical analysis by unpaired t test compared with control cells; * $p < 0.05$,

** p < 0.01, *** p < 0.001, **** p < 0.0001. **(D)** Cell surface MHC-I and MHC-II expression in OCI-AML3 cells transduced with sgRNAs targeting the indicated genes and/or a control sgRNA. Representative plots from 2 experiments. **(E)** mRNA expression of MHC-I pathway genes in OCI-AML3 cells transduced with sgRNA targeting the indicated genes. Bars depict mean fold change in expression from 3 independent experiments and points indicate the mean of technical triplicates from individual experiments.

While these results confirmed RREB1 and FBXO11 are significant negative regulators of MHC-II expression, the underlying mechanisms for both remained unclear. RREB1 has been reported to function as both a transcriptional activator[422-425] and repressor[426-429] and is particularly recognised in mediating EMT through TGF-β and RAS signalling[424]. Notably, it has also been described as a negative regulator of the non-classical MHC-I molecule HLA-G[427], which is thought to mediate immune tolerance due to its expression in fetal tissues and ability to inhibit NK and T cell-mediated cytotoxicity[430]. With respect to its repressive function, RREB1 was found to associate with CtBP co-repressor complex proteins through immunoprecipitation-mass spectrometry (IP-MS) studies[318], raising the possibility of this complex being involved in MHC-II regulation, although no CtBP complex components were identified in my whole-genome screens.

FBXO11 is an F-box protein, which constitutes the substrate recognition component of SCF multi-subunit E3 ubiquitin ligase complexes that catalyse polyubiquitination of proteins and target them for proteasomal degradation. Established targets of FBXO11 include BCL6[431], through which it controls B cell development within germinal centres[432], as well as BLIMP-1[339], which is essential for terminal differentiation of B cells into plasma cells. However, given AML cells with low MHC-II expression exhibit silencing of multiple MHC-II genes, the protein target of FBXO11-mediated regulation was not evident.

We and others have shown that PRC2 coordinates MHC-I silencing across multiple cancer types[361,433,434]. Although it has previously been proposed that PRC2 may contribute to MHC-II silencing in diffuse large B cell lymphoma[434] and AML[435], no polycomb complex proteins were identified as hits within my genome-wide screens. I therefore sought to clarify whether PRC2 was a major negative regulator of MHC-II expression in AML. Treatment of human AML cell lines and a murine MLL-AF9-driven AML cell line with EPZ-011989, a potent and selective EZH2 inhibitor (**Figure 4.6A**), demonstrated only a minimal increase in baseline MHC-II expression and

no substantial enhancement of MHC-II following IFN-γ stimulation (**Figure 4.6B**). Notably, previous studies implicating PRC2 in MHC-II repression in AML failed to demonstrate H3K27me3 at MHC-II genes[435], raising the prospect that alternative mechanisms such as viral mimicry, a well-established consequence of PRC2 inhibition[397], may indirectly activate MHC-II through a cell-intrinsic interferon response. Consistent with this, chromatin immunoprecipitation sequencing (ChIP-seq) data for H3K27me3 in AML cells[436] revealed minimal H3K27me3 deposition at MHC-II pathway genes compared to known polycomb target genes (**Figure 4.6C**). Collectively, these data indicate that PRC2 is not the dominant negative regulator of MHC-II expression in AML and that RREB1 and FBXO11 likely operate through PRC2-independent mechanisms.

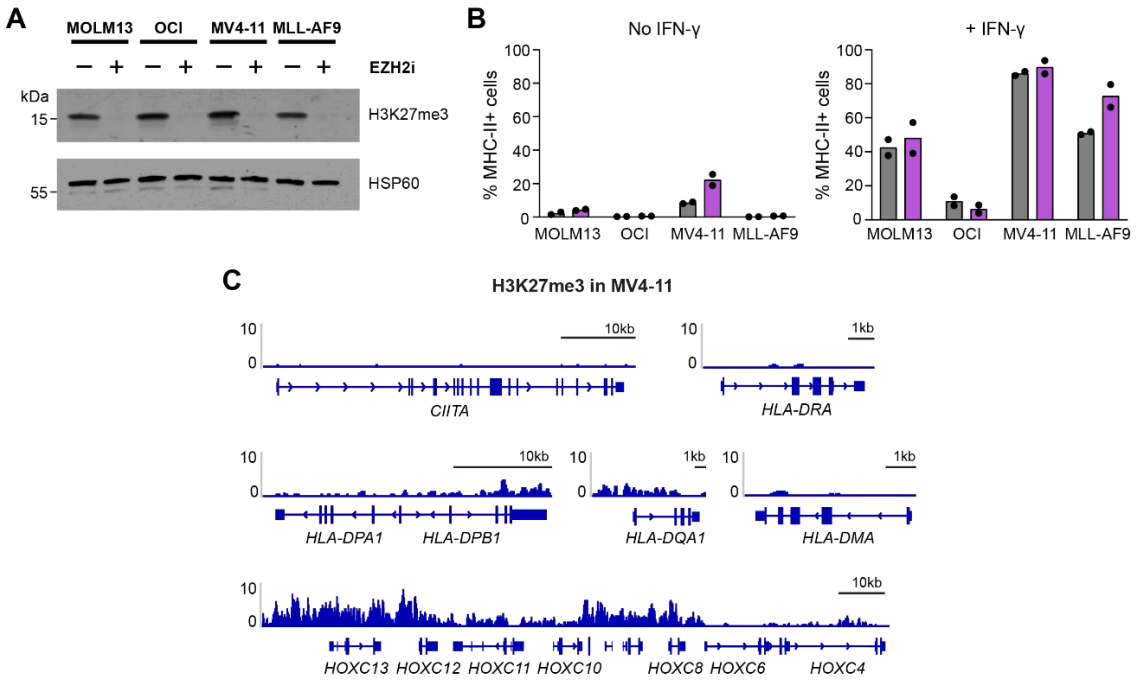

Figure 4.6. PRC2 inhibition fails to significantly increase MHC-II expression in human and mouse AML cell lines.

(A) Immunoblot of the indicated cell lines treated with EZH2 inhibitor (EPZ-011989 3μM) or vehicle control for 7 days. **(B)** Cell surface MHC-II expression in the indicated cell lines treated with EZH2 inhibitor (EPZ-011989 3μM) for 7 days, in the presence or absence of human IFN-γ 25 ng/mL (MOLM13 and OCI-AML3), human IFN-γ 10 ng/mL (MV4-11) or mouse IFN-γ 10 ng/mL (MLL-AF9) for 48 hours. Bars depict the mean percentage of MHC-II$^+$ cells from 3 independent experiments indicated by points. **(C)** Chromatin immunoprecipitation (ChIP) sequencing showing H3K27me3 levels at MHC-II genes and the HoxC cluster. Data are from GEO: GSM1513828[436]. Y axes indicate reads per million (rpm).

I therefore decided to repeat the positive-selection screens in MOLM13 and OCI-AML3 cells using a smaller, focused library targeting epigenetic regulators and transcription factors, as the smaller library size and consequently higher sgRNA fold representation can provide greater resolution to discern interacting proteins that may be co-operating to regulate MHC-II. I also planned to perform a corresponding CRISPR screen in a murine AML cell line using a targeted epigenetic library, given that the mechanism of MHC-II repression may be conserved across species, as seen with PRC2 in MHC-I regulation.

4.2.3 Targeted CRISPR screens using mouse epigenetic libraries

For the mouse CRISPR screens, I utilised a murine model of AML created through expression of an MLL-AF9 fusion construct in c-KIT-selected haematopoietic progenitor cells from C57/Bl6 mice, which also lacks MHC-II expression in the absence of IFN-γ stimulation (**Figure 4.7A**). As with MOLM13 and OCI-AML3, parental MLL-AF9 cells were then transduced with the pHRSIN-P_{SFFV}-Cas9-P_{PGK}-Blasticidin vector and selected with blasticidin for 10 days. Cas9-expressing MLL-AF9 cells were expanded and transduced with two sublibraries from a whole-genome mouse library provided as a kind gift from Professor Johannes Zuber (IMP, Vienna). These sublibraries collectively comprise ~14,000 sgRNA (6 sgRNA per gene) targeting established chromatin modifiers and transcription factors. The sgRNA were expressed in a lentiviral vector encoding neomycin and mCherry selection markers.

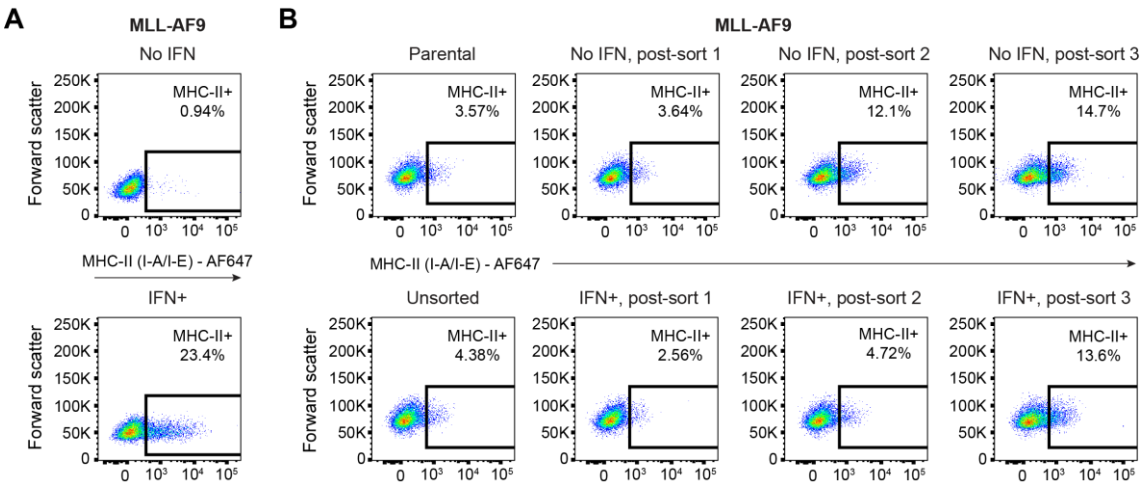

Figure 4.7. Targeted epigenetic screens in MLL-AF9 cells.

(A) Cell surface MHC-II expression in MLL-AF9 cells in the presence or absence of mouse IFN-γ 10 ng/mL for 24 hours. **(B)** Cell surface MHC-II expression in MLL-AF9 cells from indicated timepoints in the no IFN and IFN+ screens.

A total of 96 x 10^6 MLL-AF9 cells were transduced with pooled library virus (100 µL for 2 x 10^6 cells per well of a 12-well plate) and selected with neomycin 0.5 mg/mL for 1 week, starting from day +2. At an MOI of 0.3, this provided approximately 2,000 fold representation of each sgRNA in the library. Cells were serially sorted to enrich a mCherry+, MHC-II+ population (**Figure 4.7B**), with one set of cells pulsed with high-dose mouse IFN-γ (20 ng/mL for 48 hours) prior to each sort. Pellets of sorted cells and unsorted control library cells were frozen after each sort.

Genomic DNA was extracted from sorted and control cell pellets and sgRNA sequences were amplified by two-step PCR, with the first round PCR adding sample barcodes and both PCR steps adding adapters for Illumina sequencing. Samples were sequenced with single-end 75 bp reads on an Illumina NextSeq 500 and analysed, as previously outlined for the whole-genome screens, to determine which targeting sgRNAs were significantly enriched in the sorted populations compared to the unsorted control populations grown in parallel.

4.2.4 Targeted CRISPR screens using human epigenetic libraries

For the human targeted CRISPR screens, pooled lentivirus was produced as described in **Sections 2.2.5 to 2.2.9** from two custom libraries curated by members of the Dawson laboratory, which were designed to target known chromatin modifiers and transcription factors. These libraries comprise a total of ~15,300 sgRNA with 6 targeting sgRNA per gene, as well as sets of non-targeting and safe control sgRNA. The sgRNA were expressed in the pKLV-U6gRNA(BbsI)-$Puro_{2A}$-BFP lentiviral vector, which encodes puromycin and BFP selection markers.

MOLM13 and OCI-AML3 were again used for these screens, with a total of 96 x 10^6/L cells (2 x 10^6 cells per well of a 12-well plate x 4 plates) of each line transduced. Based on titration studies (**Figures 4.8A and 4.8B**), 300 µL of virus was used per well for MOLM13 and 150 µL per well for OCI-AML3. With an MOI of 0.3, this provided approximately 1,900 fold representation of each sgRNA in the library.

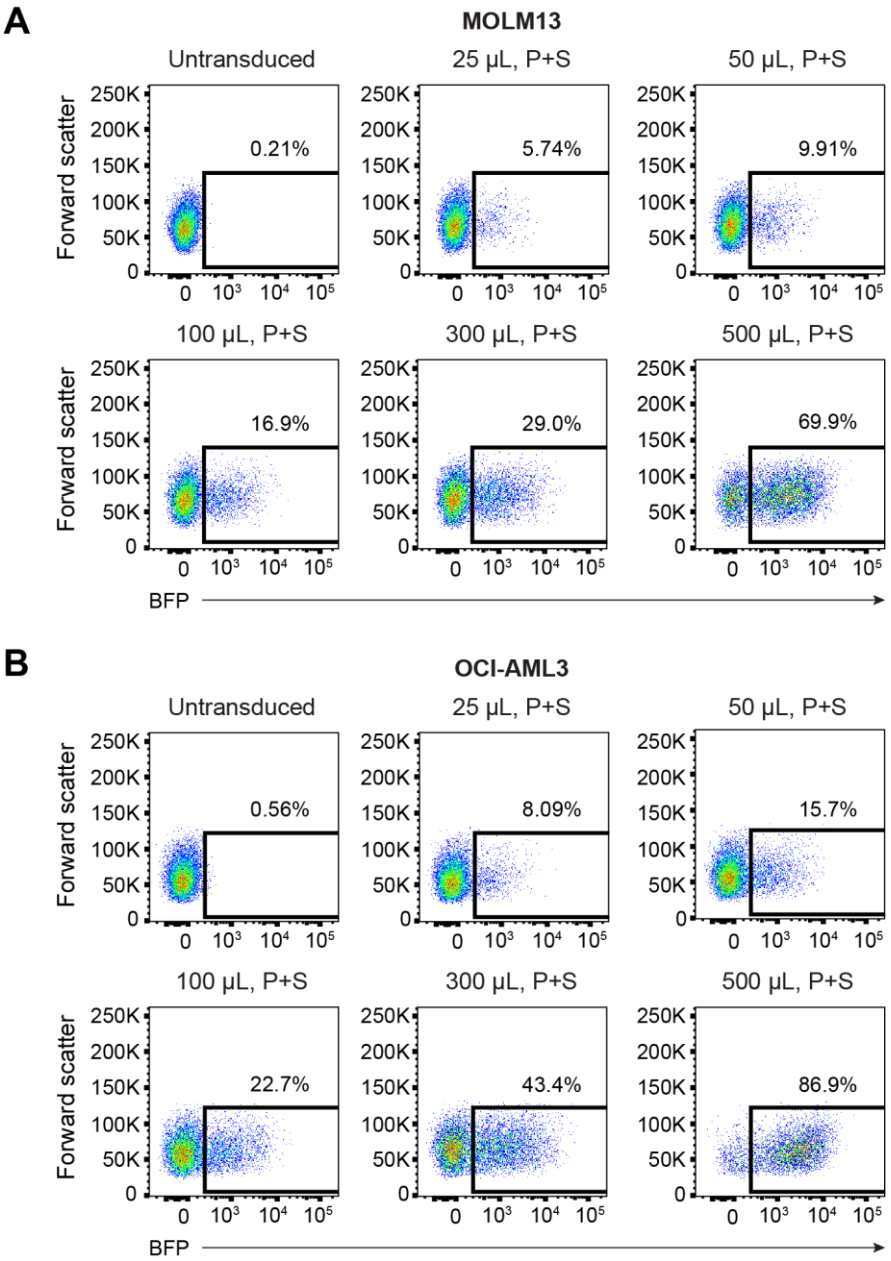

Figure 4.8. Titration of targeted epigenetic library virus in human AML cells.

(A and B) BFP expression in MOLM13 (A) and OCI-AML3 (B) cells transduced with specified volumes of pooled library virus. P, polybrene 8 µg/mL. S = spinfection (centrifugation at 900 g x 90 minutes).

Transduced cells were selected with puromycin 2 µg/mL on day +2 and then serially sorted to enrich a BFP+, MHC-II+ population (**Figures 4.9A and 4.9B**), with one set of cells pulsed with IFN-γ 25 ng/mL for 48 hours prior to each sort. Pellets of sorted cells and unsorted control library cells were frozen after each sort, with genomic DNA extracted, sequenced and analysed in the same way as the whole-genome screens.

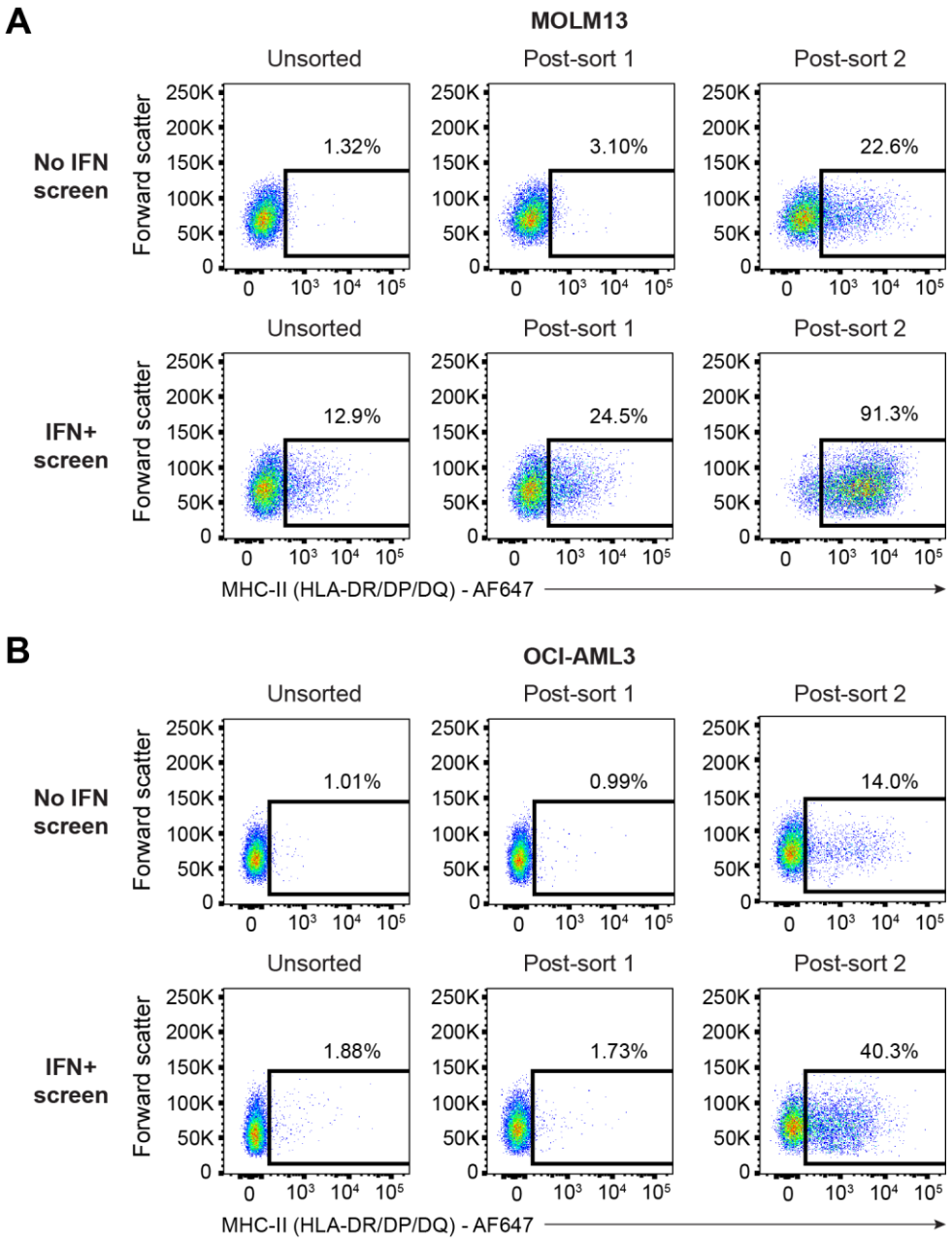

Figure 4.9. Targeted epigenetic screens in human AML cells.

(A and B) Cell surface MHC-II expression in MOLM13 (A) and OCI-AML3 (B) cells from indicated timepoints in the no IFN and IFN+ screens. Cells from the IFN+ screen were pulsed with IFN-γ 25 ng/mL for 48 hours prior to analysis.

4.2.5 Targeted CRISPR screen results

Results of the targeted mouse screens are shown in **Figure 4.10A**. Two of the top hits in these screens were *Zfp217* and *Rcor1* (CoREST), which form an accessory CtBP complex together with LSD1 (KDM1A) and HDAC1/2 to facilitate transcriptional repression via removal of activating chromatin marks, including H3K4 methylation and histone acetylation[437,438]. Both *Zfp217* and

Rcor1 KO increased MHC-II expression in response to IFN-γ stimulation, although basal MHC-II levels were essentially unaffected (**Figure 4.10B**). Notably, the other components of this subcomplex did not read out in these screens, which likely reflects the functional redundancy observed between HDAC1 and HDAC2, as well as the significant toxicity induced by *KDM1A* KO in these cells.

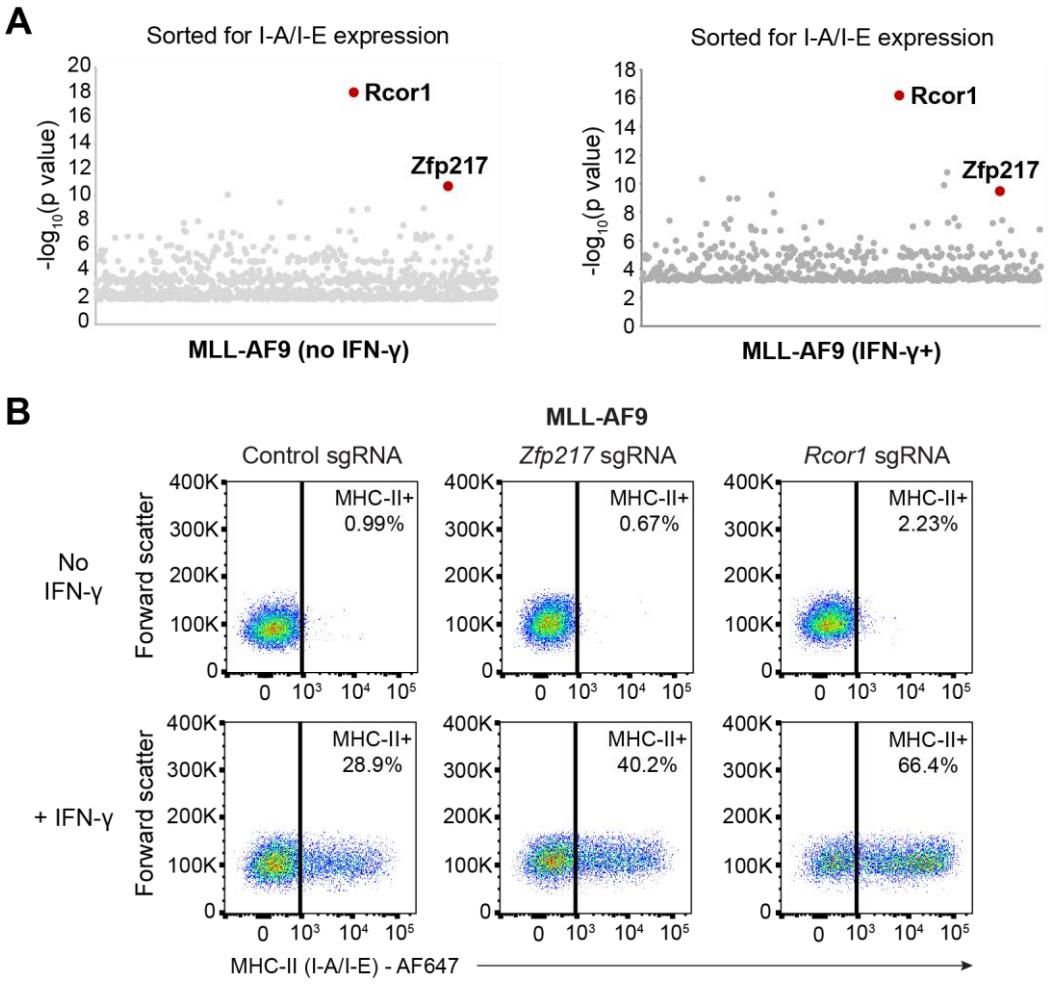

Figure 4.10. Results of the targeted epigenetic screens in MLL-AF9 cells.

(A) For IFN+ sorts, cells were pulsed with mouse IFN-γ 10 ng/mL for 48 hours prior to each sort. Bubble plots show the top 1,000 genes identified. p values were calculated using the RSA algorithm[395]. **(B)** Cell surface MHC-II expression in MLL-AF9 Cas9 cells transduced with a pool of 2 sgRNAs targeting the indicated genes or a control sgRNA, in the presence of absence of mouse IFN-γ 10 ng/mL for 48 hours. Representative data from 3 experiments.

Results of the targeted human screens are shown in **Figure 4.11A**. Consistent with the whole-genome screens, *RREB1* and *FBXO11* again emerged as top hits, together with multiple components of the CtBP complex (**Figure 4.11B**). In vertebrates, the CtBP complex comprises a

core homodimer or heterodimer of CtBP1 and CtBP2, which are highly homologous and functionally redundant proteins, likely explaining why sgRNA targeting these two genes were not enriched in my screens. CtBP1 and CtBP2 interact with a range of transcriptional regulators through two conserved binding motifs, namely a PLDLS motif found on DNA-binding transcription factors such as RREB1 or adaptor proteins like WIZ, and an RRT motif present on other DNA-binding proteins like ZNF217 and RIZ1. This enables the CtBP complex to localise to DNA-bound transcription factors and then recruit adaptor proteins and chromatin modifiers that facilitate its repressive function, including histone methyltransferases (EHMT1 and EHMT2), HDAC1/2 and LSD1[439]. Remarkably, the additional hits identified in my targeted CRISPR screens linked the transcription factor RREB1, the PLDLS-containing adapter protein WIZ, the chromatin reader CDYL and the histone methyltransferases EHMT1 and EHMT2 as the specific CtBP complex that facilitates MHC-II repression. This was validated through single gene KO of non-redundant complex members, which induced MHC-II expression even in the absence of IFN-γ stimulation (**Figure 4.11C**).

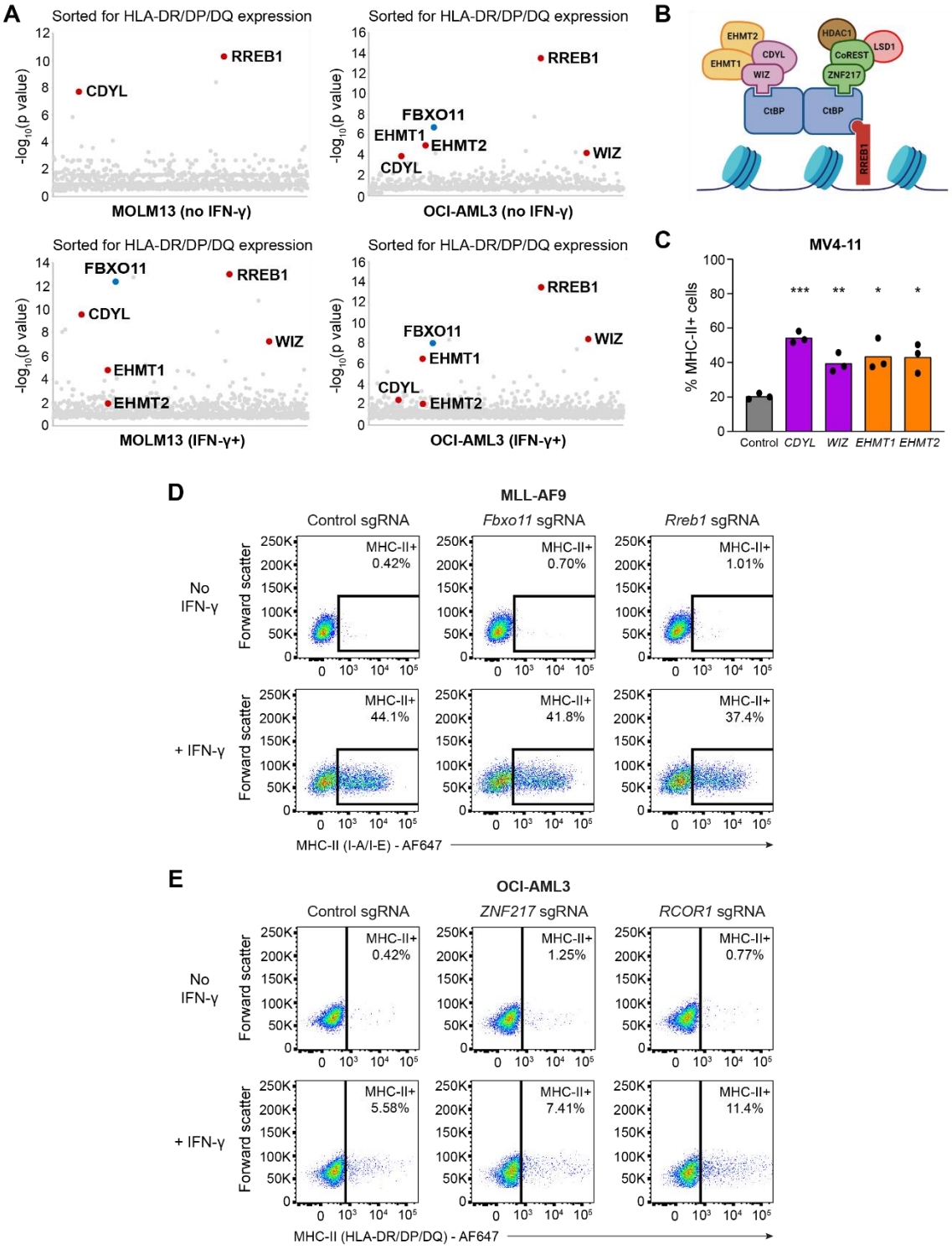

Figure 4.11. Results of the targeted epigenetic screens in human AML cells.

(A) For IFN+ sorts, cells were pulsed with IFN-γ 25 ng/mL for 48 hours prior to each sort. Bubble plots show the top 1,000 genes identified. p values were calculated using the RSA algorithm[395]. **(B)** Schematic representation of the CtBP co-repressor complex. **(C)** Cell surface MHC-II expression in MV4-11 Cas9 cells transduced by a pool of 2 sgRNAs targeting the indicated genes or a control sgRNA. Bars depict the mean percentage of MHC-II+ cells from 3

independent experiments indicated by points. Statistical analysis by unpaired t test compared with control cells: * $p < 0.05$, ** $p < 0.01$, *** $p < 0.001$. **(D)** Cell surface MHC-II expression in MLL-AF9 Cas9 cells transduced by a pool of 2 sgRNAs targeting the indicated genes or a control sgRNA, in the presence or absence of mouse IFN-γ 10 ng/mL for 48 hours. **(E)** Cell surface MHC-II expression in OCI-AML3 Cas9 cells transduced by a pool of 2 sgRNAs targeting the indicated genes or a control sgRNA, in the presence or absence of IFN-γ 25 ng/mL for 48 hours.

These findings implicate the CtBP co-repressor complex as the key transcriptional regulator of MHC-II in AML. Interestingly, while genetic screens in both human and mouse AML cell lines identified CtBP complex components, the main hits from both screens did not cross-validate – specifically, *Rreb1* and *Fbxo11* KO did not induce MHC-II expression in MLL-AF9 cells (**Figure 4.11D**) and *ZNF217* and *RCOR1* KO similarly had no effect in human AML cells (**Figure 4.11E**). This suggests that different facultative complex members are involved in MHC-II repression for each species. Furthermore, the MHC-II DNA-binding element for the CtBP complex in mouse (corresponding to RREB1 in human) remained unknown. Nevertheless, given the higher clinical relevance, I decided to focus on understanding the mechanisms of MHC-II regulation by the CtBP complex and FBXO11 in human cells and the potential translational impact of targeting these processes to enhance anti-leukaemic immune responses. These mechanistic and functional aspects of my project are described in Chapter 5.

Chapter 5 – Inhibition of the CtBP complex and FBXO11 enhances MHC-II expression and anti-cancer immune responses

5.1 Results

5.1.1 Transcriptional silencing of MHC-II is mediated by the CtBP complex

Having established through my CRISPR screens that the CtBP complex is involved in MHC-II repression, I wished to confirm the presence of CtBP complex members at MHC-II genes. In support of this, ChIP-seq assays localised WIZ to MHC-II pathway genes but not *NLRC5*, the key transcriptional regulator of MHC-I expression[42] (**Figure 5.1A**). Although chromatin profiling techniques (ChIP-seq and CUT&RUN) for additional CtBP complex members were unsuccessful, WIZ is not known to associate with any other epigenetic complexes (**Figure 5.1B**) and therefore the WIZ ChIP-seq findings are likely indicative of specific CtBP complex binding to MHC-II genes.

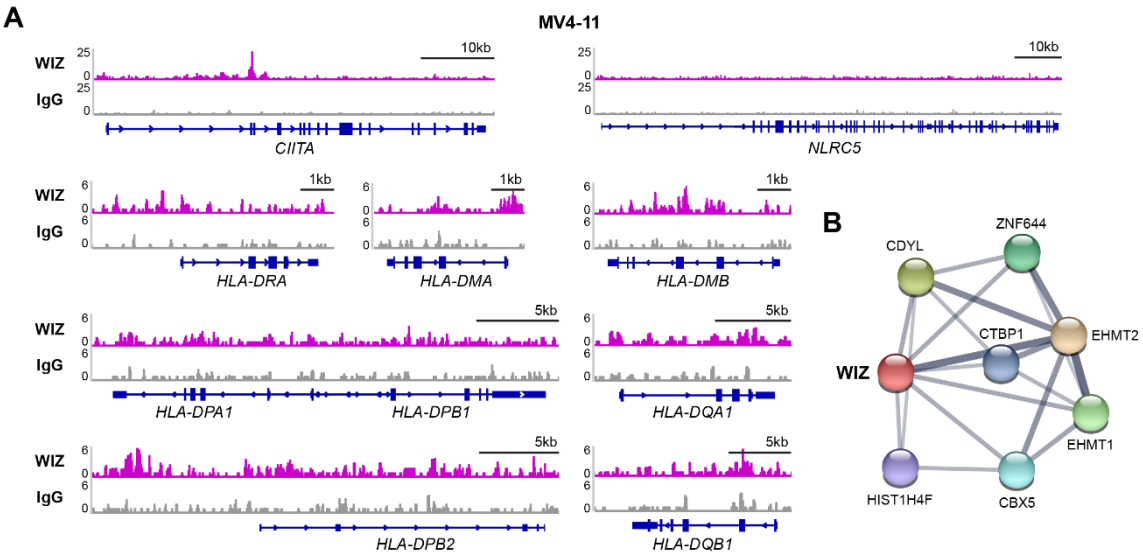

Figure 5.1. WIZ localises specifically to MHC-II pathway genes.

(A) Chromatin immunoprecipitation sequencing (ChIP-seq) plots for WIZ in MV4-11 cells at *NLRC5* and MHC-II pathway genes. **(B)** STRING network analysis of known direct protein interactors with WIZ.

I next wanted to determine the functional consequences of selectively inhibiting the catalytic components of this CtBP complex. EHMT1 and EHMT2 form a heteromer and cooperatively facilitate H3K9me1 and H3K9me2 formation *in vivo*[289]. I therefore treated AML cells with A-366 and UNC0638, which are two chemically distinct, potent and selective inhibitors of both EHMT1 and EHMT2[440,441] that independently induced dose-dependent MHC-II upregulation and potentiation of IFN-γ sensitivity (**Figures 5.2A-C**), mirroring CRISPR-mediated KO of *EHMT1* and *EHMT2* (**Figure 4.10C**). As H3K9me2 is associated with dynamic gene repression within facultative heterochromatin and euchromatin[291,442], I assessed H3K9me2 levels at MHC-II

pathway genes, including the key transcriptional regulator *CIITA*. These data demonstrate that MHC-II pathway genes are marked by H3K9me2 at baseline and that the re-expression of MHC-II following EHMT1/2 inhibition is associated with depletion of H3K9me2 at these genes (**Figure 5.2D**). Importantly, H3K27me3 is not seen at MHC-II genes, nor does A-366 treatment alter H3K27me3 levels at known PRC2 target genes (**Figure 5.2D**). These findings confirm the key role of the CtBP complex in regulating MHC-II through the repressive activity of the histone methyltransferases EHMT1/2.

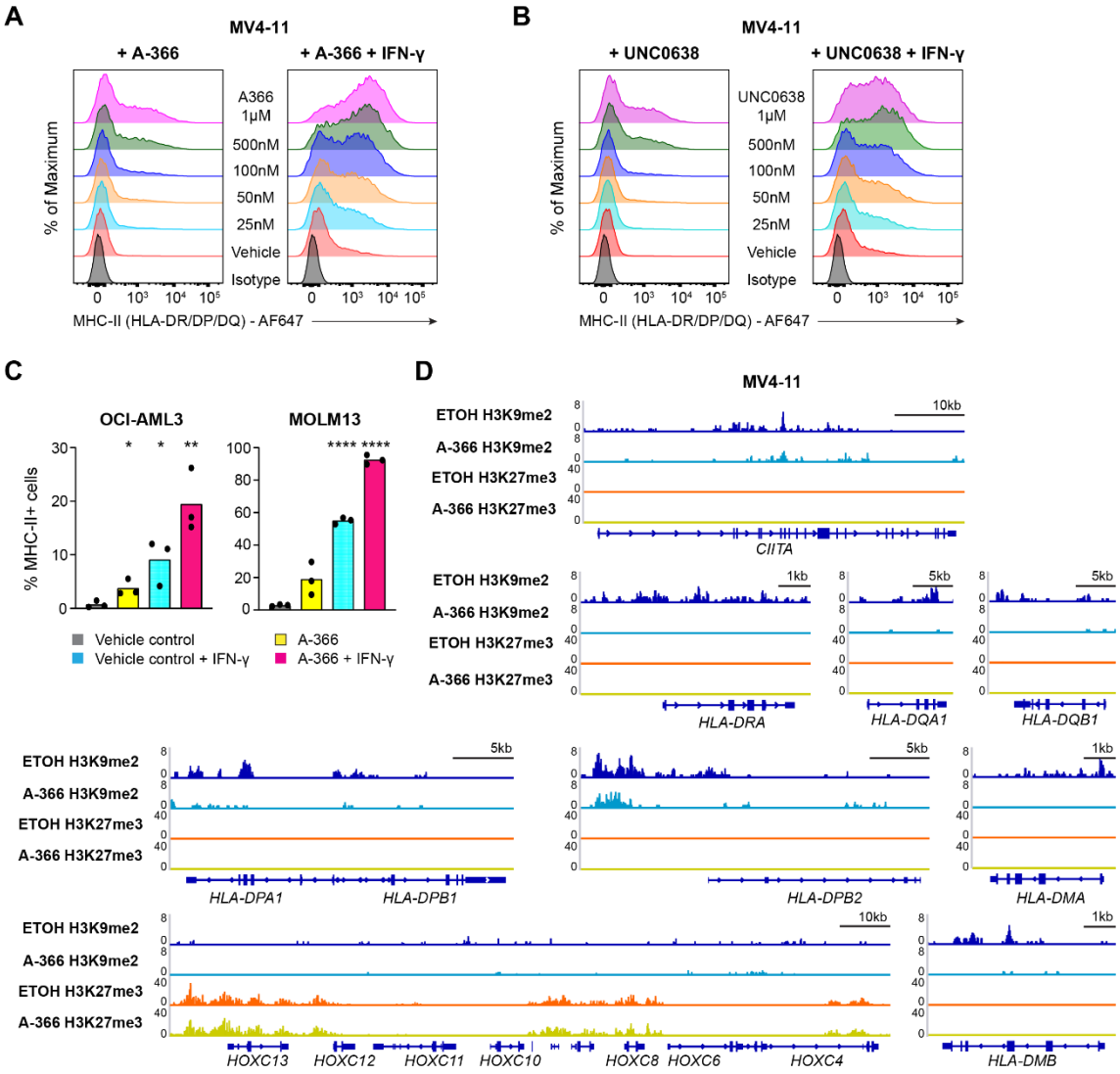

Figure 5.2. The CtBP complex regulates MHC-II pathway genes through the repressive activity of EHMT1 and EHMT2.

(A and B) Cell surface MHC-II expression in MV4-11 cells treated with the EHMT1/2 inhibitors A-366 (A) and UNC0638 (B) at the indicated doses or vehicle control in the presence or absence of IFN-γ 10 ng/mL for 24 hours. Representative plots from 2 experiments. **(C)** Cell surface MHC-II expression in MOLM13 and OCI-AML3 cells treated with EHMT1/2 inhibitor (A-

366 1μM) or vehicle control, in the presence or absence of IFN-γ 25 ng/mL for 48 hours. Bars depict the mean percentage of MHC-II^{+} cells from 3 independent experiments indicated by points. Statistical analysis by unpaired t test compared to control cells; p value * < 0.05, ** < 0.01, **** < 0.0001. **(D)** CUT&Tag chromatin profiling of H3K9me2 and H3K27me3 at MHC-II genes in MV4-11 cells treated with A-366 1μM or vehicle control (ETOH) for 7 days. The HoxC cluster is included as a positive H3K27me3 control.

It is increasingly recognised that therapies targeting epigenetic inhibitors, particularly those involved in transcriptional repression, can reactivate ERVs, triggering a type I IFN response and subsequent MHC upregulation[174,175,443]. To assess whether MHC-II upregulation following CtBP complex disruption was principally due to enhanced IFN signalling, I generated MV4-11 cells with CRISPR-mediated disruption of *STAT1* (**Figure 5.3A**), a transcription factor that is a key component of the canonical type I and type II IFN pathway[444,445]. Loss of STAT1 had no effect on the level of MHC-II upregulation induced by both *RREB1* KO and A-366 treatment (**Figure 5.3B**), confirming that CtBP complex targeting de-represses MHC-II independent of IFN signalling due to ERV re-activation and viral mimicry.

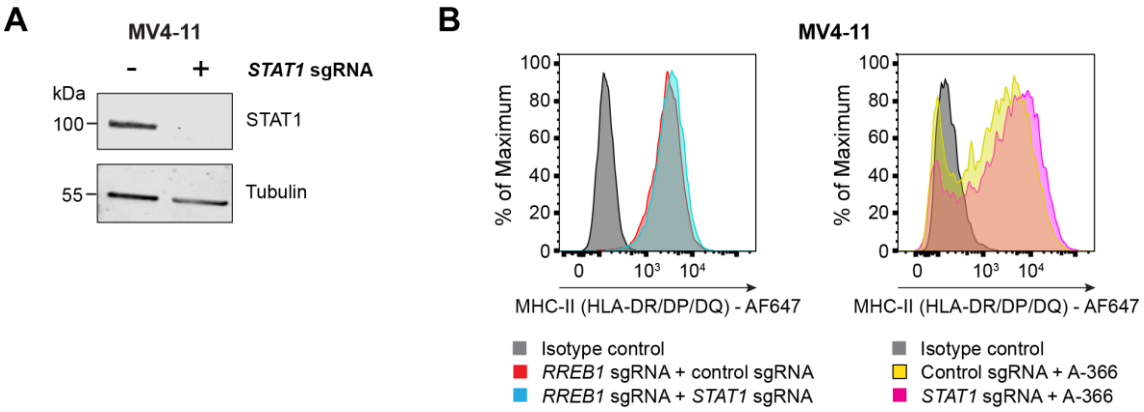

Figure 5.3. CtBP complex targeting de-represses MHC-II independent of IFN signalling. **(A)** Immunoblot of MV4-11 Cas9 cells transduced with a pool of 2 sgRNAs targeting *STAT1* or a control sgRNA. **(B)** Cell surface MHC-II expression in MV4-11 *RREB1* KO cells transduced with a pool of 2 sgRNAs targeting *STAT1* or a control sgRNA, and MV4-11 *STAT1* KO or control cells treated with A-366 1μM for 7 days. Representative plots from 2 experiments.

5.1.2 The CtBP complex and FBXO11 are specific and synergistic repressors of surface MHC-II expression

As loss of the RREB1-containing CtBP complex increases basal expression of MHC-II genes and potentiates the induction of these genes by inflammatory cytokines, I sought to investigate the specificity of the gene expression changes induced by functional disruption of this complex in the presence and absence of IFN-γ. Strikingly, the most highly upregulated genes following *RREB1* KO in AML included multiple genes encoding MHC-II alleles, as well as the MHC-II transactivator CIITA (**Figures 5.4A-C**). CIITA is the master regulator of tissue-specific MHC-II expression and binds the proximal promoter of all classical MHC-II genes (encoding the HLA-DR, HLA-DP and HLA-DQ isotypes), as well as other MHC-II pathway genes including *CD74* (which encodes the invariant chain), *HLA-DM* and *HLA-DO*. Notably, I did not identify increased expression of any genes involved in the MHC-I antigen processing and presentation pathway following loss of RREB1[361], including the non-classical MHC-I allele HLA-G (**Figure 5.4D**), of which RREB1 is a known regulator[427]. Gene set enrichment analysis also predominantly highlighted terms driven by MHC-II gene upregulation, with no significant change in pathways relating to intracellular signalling, cell death or cell cycle progression (**Figure 5.4E**). In conjunction with my WIZ ChIP-seq (**Figure 5.1A**) and H3K9me2 data (**Figure 5.2D**), these findings implicate the RREB1-containing CtBP complex as a major and selective transcriptional repressor of MHC-II genes.

A

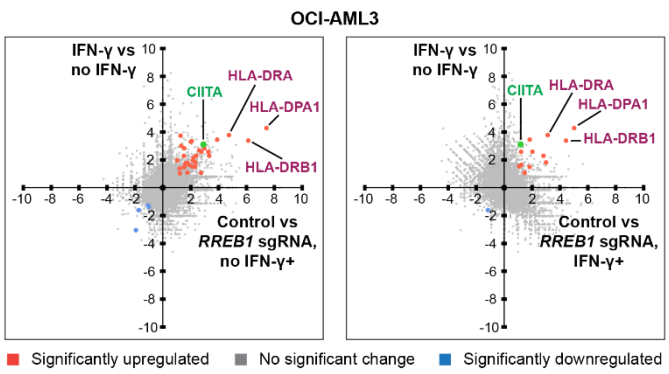

B

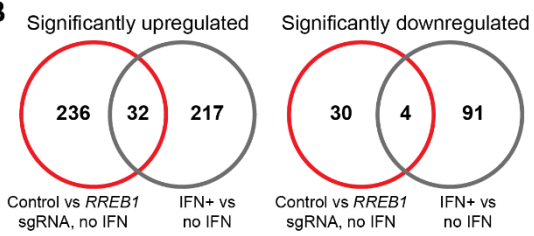

Significantly upregulated in both conditions:

Gene	log_2FC Control vs *RREB1* sgRNA, no IFN	p value Control vs *RREB1* sgRNA, no IFN	log_2FC IFN+ vs no IFN	p value IFN+ vs no IFN
HLA-DPA1	7.439	7.198E-08	4.285	8.301E-03
HLA-DRB1	6.133	1.876E-21	3.384	1.633E-06
HLA-DRA	4.748	6.391E-29	3.780	2.662E-18
AGT	3.903	1.576E-06	3.456	2.477E-05
OTOF	3.329	6.774E-07	2.298	1.912E-03
FAM134B	3.265	4.942E-05	2.584	2.415E-03
KYNU	2.984	1.968E-02	2.841	2.342E-02
CIITA	2.917	3.670E-03	3.108	1.019E-03
PROCR	2.767	1.965E-08	2.579	1.652E-07
MS4A3	2.747	2.082E-13	1.067	3.375E-02
SLC22A23	2.612	1.806E-02	2.688	1.023E-02
NLGN3	2.404	1.435E-02	2.305	1.688E-02
CLU	2.337	1.966E-06	1.820	5.147E-04
KRT81	2.328	2.905E-09	1.501	6.277E-04
IL18BP	2.192	1.432E-02	2.159	1.313E-02
RNF207	2.165	1.475E-02	1.953	2.911E-02
KIF26B	2.105	9.693E-08	1.536	3.143E-04
IL12RB1	2.075	3.164E-06	3.354	1.114E-17
C5orf42	2.008	1.921E-03	3.302	9.331E-10
PRKAR2B	1.894	4.421E-14	1.637	1.575E-10
lnc-BCL2L11-3:1	1.779	2.241E-02	1.785	1.708E-02
LINC00899	1.770	4.766E-05	1.083	3.677E-02
SMARCD3	1.626	9.882E-03	1.750	3.127E-03
SULT1A3	1.545	5.376E-03	1.506	5.647E-03
LINC00599	1.542	5.760E-03	2.830	3.758E-10
SPHK2	1.526	4.010E-02	1.467	4.425E-02
MRAS	1.512	3.545E-04	2.292	4.308E-10
SLAMF8	1.322	1.529E-03	3.006	7.281E-20
APOL4	1.275	3.687E-03	3.744	8.452E-31
FGR	1.227	3.366E-03	1.037	1.746E-02
LINC-PINT:25	1.210	4.243E-02	1.381	1.096E-02
HEG1	1.030	1.059E-02	1.971	6.907E-10

Significantly downregulated in both conditions:

Gene	log_2FC Control vs *RREB1* sgRNA, no IFN	p value Control vs *RREB1* sgRNA, no IFN	log_2FC IFN+ vs no IFN	p value IFN+ vs no IFN
GJA1	-1.926	4.217E-07	-3.047	4.010E-11
MT1H	-1.723	3.343E-19	-1.601	1.055E-16
RN7SK	-1.056	1.532E-06	-1.264	8.438E-09
RGCC	-1.003	1.810E-02	-1.371	6.423E-04

C

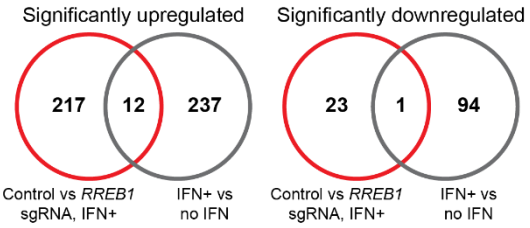

Significantly upregulated in both conditions:

Gene	log_2FC Control vs *RREB1* sgRNA, IFN+	p value Control vs *RREB1* sgRNA, IFN+	log_2FC IFN+ vs no IFN	p value IFN+ vs no IFN
HLA-DPA1	5.020	1.386E-21	4.285	8.301E-03
HLA-DRB1	4.437	3.165E-95	3.384	1.633E-06
HLA-DRA	3.123	1.810E-103	3.780	2.662E-18
CLU	3.006	1.120E-25	1.820	5.147E-04
OTOF	2.823	1.306E-14	2.298	1.912E-03
FAM134B	2.028	8.844E-06	2.584	2.415E-03
AGT	1.833	5.600E-07	3.456	2.477E-05
KRT81	1.824	1.162E-10	1.501	6.277E-04
MS4A3	1.468	7.982E-06	1.067	3.375E-02
PRKAR2B	1.227	9.110E-11	1.637	1.575E-10
PROCR	1.211	1.181E-04	2.579	1.652E-07
KIF26B	1.073	2.031E-03	1.536	3.143E-04

Significantly downregulated in both conditions:

Gene	log_2FC Control vs *RREB1* sgRNA, IFN+	p value Control vs *RREB1* sgRNA, IFN+	log_2FC IFN+ vs no IFN	p value IFN+ vs no IFN
MT1H	-1.167	6.840E-05	-1.601	1.055E-16

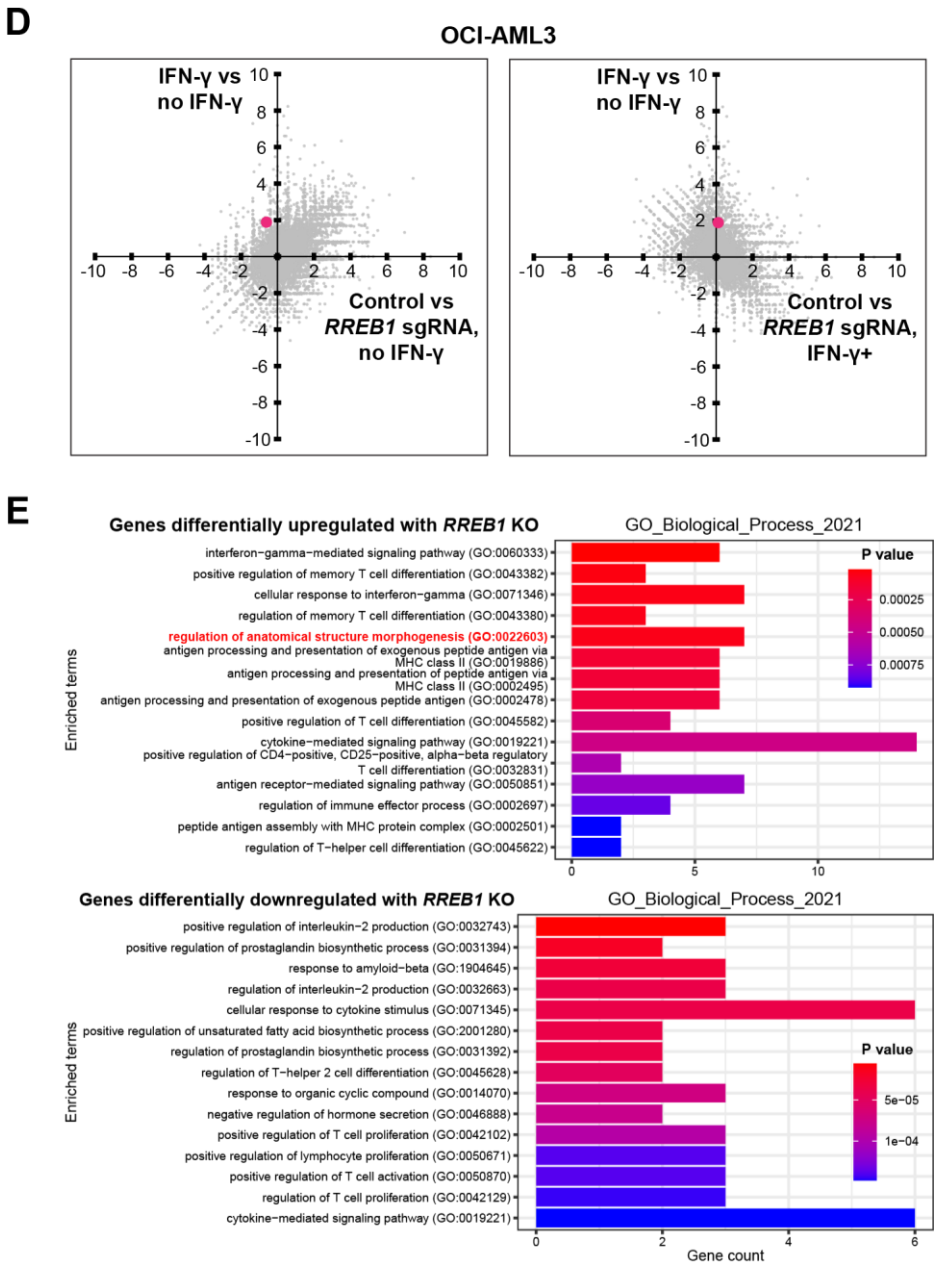

Figure 5.4. Gene expression changes induced by *RREB1* KO.

(A) RNA-seq correlation plots showing differential gene expression in OCI-AML3 cells in the presence or absence of IFN-γ 25 ng/mL for 48 hours (Y-axis) and OCI-AML3 Cas9 cells transduced with control or *RREB1* sgRNA in the presence or absence of IFN-γ 25 ng/mL for 48 hours (X-axis). Fold change > 1.0 and false discovery rate < 0.05 for highlighted genes (in blue and orange) with significant differential gene expression. *CIITA* is labelled separately in green and reaches significance only in the *RREB1* sgRNA, no IFN-γ analysis. **(B and C)** Venn diagrams show the number of significant differentially expressed genes in OCI-AML3 cells in the presence or absence of IFN-γ 25 ng/mL for 48 hours and OCI-AML3 cells transduced with control and *RREB1* sgRNA (B) and with IFN-γ 25 ng/mL for 48 hours (C). Genes that are significantly upregulated or downregulated (defined as fold change > 1.0 and false discovery

rate < 0.05) in both conditions are listed, with MHC-II pathway genes highlighted. **(D)** RNA-seq correlation plots showing differential gene expression in OCI-AML3 cells in the presence or absence of IFN-γ 25 ng/mL for 48 hours (Y-axis) and OCI-AML3 Cas9 cells transduced with control and *RREB1* sgRNA in the presence or absence of IFN-γ 25 ng/mL for 48 hours (X-axis). *HLA-G* is highlighted. **(E)** Gene set enrichment analysis performed on all differentially upregulated and downregulated genes with *RREB1* KO. For genes differentially upregulated with *RREB1* KO, the term highlighted in red is the only one not associated with MHC-II pathway genes.

I next utilised RNA-sequencing to determine the transcriptional consequences of FBXO11 loss. Here I found that FBXO11 depletion in AML cells significantly increased expression of only a small subset of genes (30 genes in IFN-γ-treated cells, 45 genes in untreated cells). Importantly, these included multiple classical MHC-II genes but, in contrast to *RREB1* KO, *CIITA* expression did not increase following *FBXO11* KO (**Figures 5.5A-C**). Given the importance of CIITA in coordinating the transcriptional activation of MHC-II pathway genes, these data raised the possibility that FBXO11 may regulate CIITA protein stability. Consistent with this, the MHC-II upregulation that follows FBXO11 loss is most dramatic following IFN-γ stimulation (**Figure 4.5A-B**), which is known to induce *CIITA* gene expression. Validation of the RNA-seq findings by RT-qPCR in a different AML cell line further confirmed that, while loss of RREB1 led to activation of both *CIITA* and MHC-II gene expression, *FBXO11* KO led to activation of downstream MHC-II genes with no change in CIITA mRNA levels (**Figure 5.5D**). To further investigate FBXO11-mediated post-translational regulation of CIITA, I expressed CIITA cDNA in AML cells under the control of a viral promoter, which drives stable MHC-II expression with no corresponding effect on MHC-I (**Figure 5.5E**). Depletion of FBXO11 in these cells led to a substantial accumulation of CIITA protein with a corresponding increase in cell surface MHC-II (**Figures 5.5F and 5.5G**). Together these data suggest that loss of FBXO11 increases cell surface MHC-II in leukaemia cells due to stabilization of CIITA protein, which drives enhanced expression of multiple MHC-II genes.

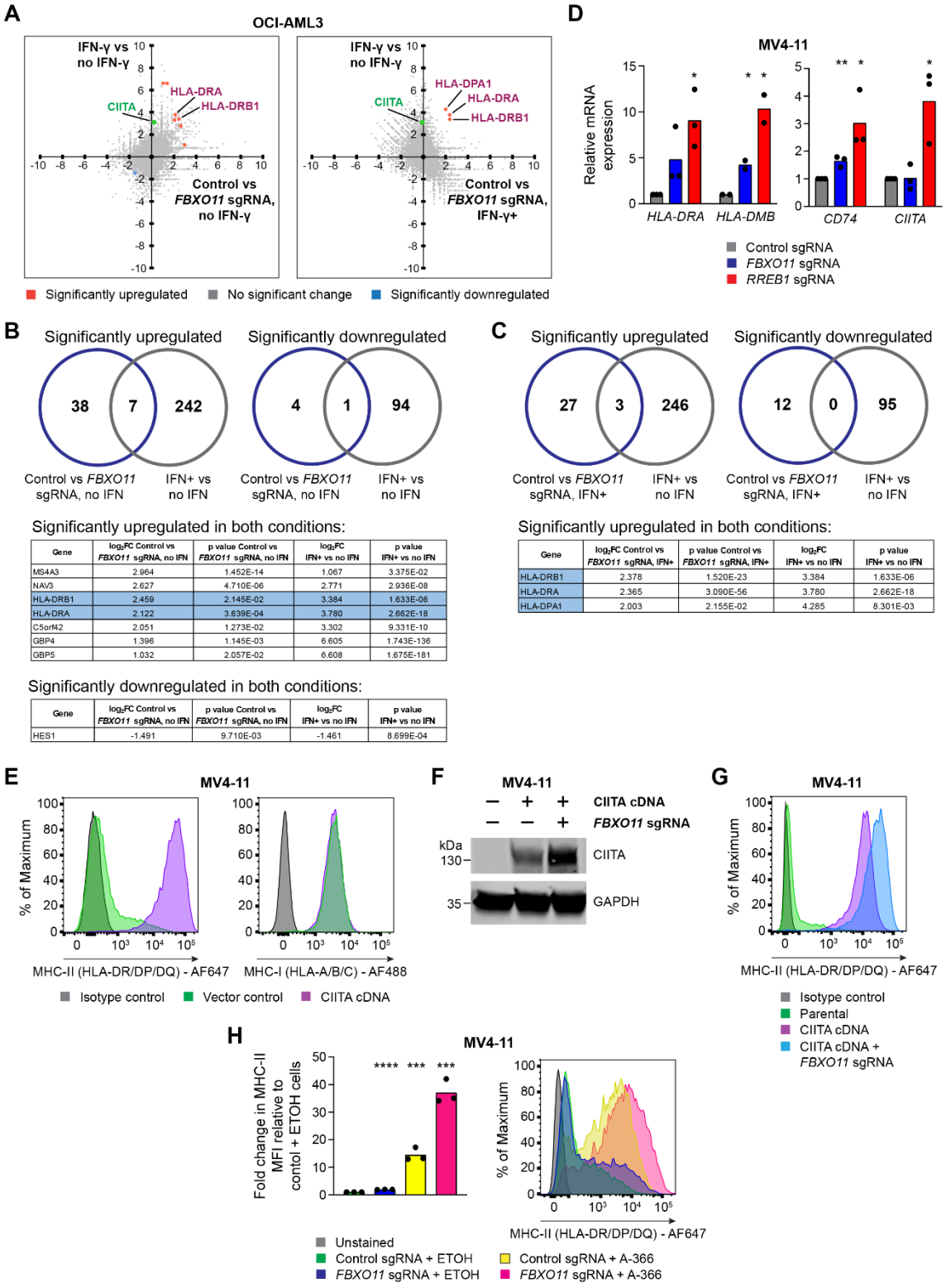

Figure 5.5. FBXO11 loss increases surface MHC-II expression through stabilisation of CIITA.

(A) RNA-seq correlation plots showing differential gene expression in OCI-AML3 cells in the presence or absence of IFN-γ 25 ng/mL for 48 hours (Y-axis) and OCI-AML3 Cas9 cells transduced with control or *FBXO11* sgRNA in the presence or absence of IFN-γ 25 ng/mL for 48 hours (X-axis). Fold change > 1.0 and false discovery rate < 0.05 for highlighted genes (in blue

and orange) with significant differential gene expression. *CIITA* is labelled separately in green and does not reach significance in either plot. **(B and C)** Venn diagrams show the number of significant differentially expressed genes in OCI-AML3 cells in the presence or absence of IFN-γ 25 ng/mL for 48 hours and OCI-AML3 cells transduced with control and *FBXO11* sgRNA (B) and with IFN-γ 25 ng/mL for 48 hours (C). Genes that are significantly upregulated or downregulated (defined as fold change > 1.0 and false discovery rate < 0.05) in both conditions are listed, with MHC-II pathway genes highlighted. **(D)** mRNA expression of MHC-II genes in MV4-11 Cas9 cells transduced with control, *FBXO11* or *RREB1* sgRNA. Bars depict mean fold change in expression from 3 independent experiments and points indicate the mean of technical triplicates from individual experiments. Statistical analysis by unpaired t test compared to control cells, with significant changes indicated; p value * < 0.05, ** < 0.01. **(E)** Cell surface MHC-II and MHC-I expression in MV4-11 cells transduced with a retroviral vector encoding CIITA cDNA or vector control. Representative data from 3 experiments. **(F and G)** Immunoblot (F) and cell surface MHC-II expression (G) in MV4-11 Cas9 cells transduced with a retroviral vector encoding CIITA cDNA and with or without *FBXO11* sgRNA. Representative data from 2 experiments. **(H)** Cell surface MHC-II expression and mean fold change in median fluorescence intensity (MFI) in MV4-11 Cas9 cells transduced with control or *FBXO11* sgRNA and treated with EHMT1/2 inhibitor (A-366 1μM) or vehicle control (ETOH) for 7 days. Bars depict mean fold change in MFI from 3 independent experiments indicated by points. Statistical analysis by unpaired t test compared to control sgRNA + ETOH cells, with significant changes indicated; p value *** < 0.001, **** < 0.0001.

Since my results had demonstrated a role for the CtBP complex in transcriptional repression of CIITA and FBXO11 as a specific regulator of CIITA protein stability, I predicted that combined targeting of these non-overlapping repressive mechanisms would synergistically induce high level MHC-II expression. As expected, depletion of FBXO11 further increased MHC-II expression in *RREB1* KO cells (**Figure 4.5D**) and also enhanced the MHC-II upregulation induced by pharmacological EHMT1/2 inhibition (**Figure 5.5H**). My data therefore establish that the CtBP complex and FBXO11 are highly selective and synergistic regulators of MHC-II expression in AML, and provide valuable insights into potential therapeutic strategies to facilitate re-expression of MHC-II in the setting of post-alloSCT relapse.

5.1.3 CtBP complex and FBXO11 targeting enhance MHC-II expression in non-haematological cancers

The established prognostic importance of tumour cell MHC-II expression in immunotherapy responses is illustrated through RNA-seq analysis of biopsy samples from cohorts of melanoma patients treated with immune checkpoint inhibitors[446] (**Figure 5.6A**), which demonstrated significant variability in MHC-II levels and a strong correlation of higher expression of MHC-II pathway genes with therapeutic response. I therefore evaluated the effect of disrupting CtBP complex and FBXO11 function in melanoma cell lines with variable levels of cell surface MHC-II (**Figure 5.6B**), which is representative of the heterogeneity for MHC-II expression seen in this disease[163].

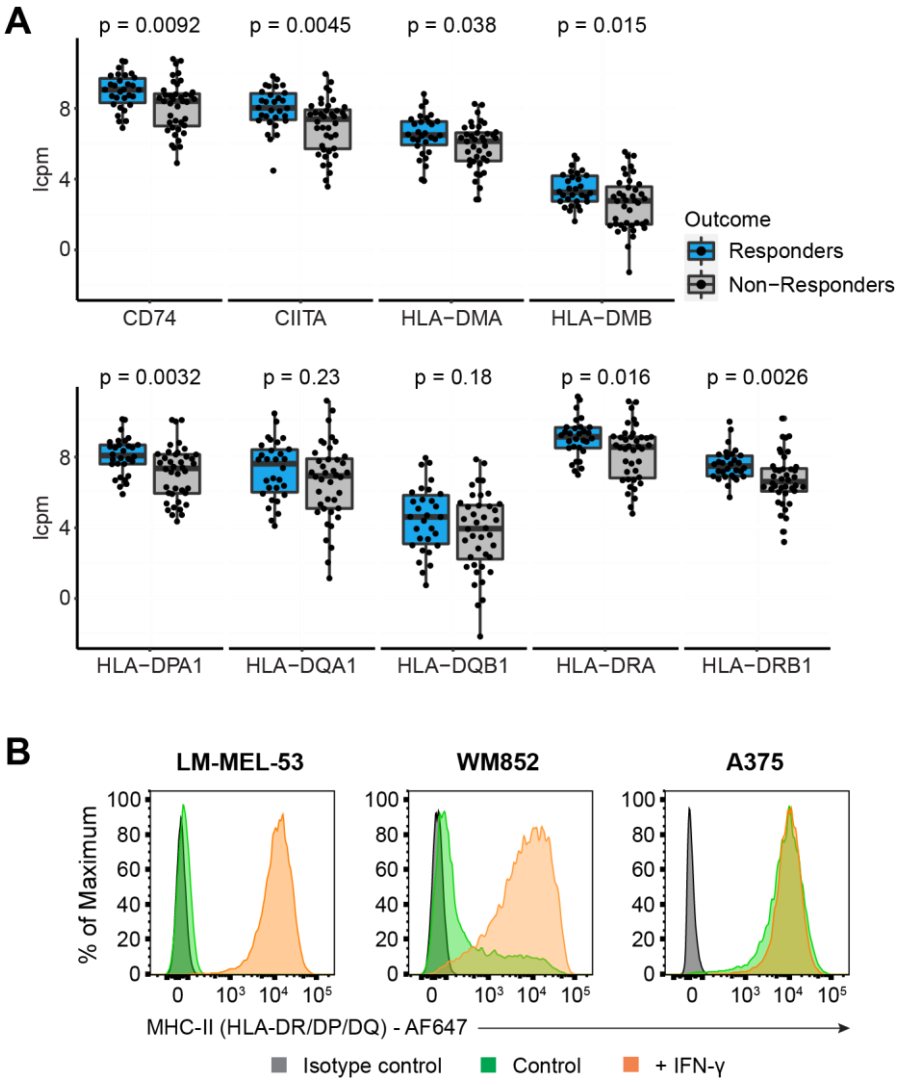

Figure 5.6. Tumour cell MHC-II expression correlates with immunotherapy response in melanoma.

(A) mRNA expression of MHC-II genes in tumour biopsy samples from melanoma patients treated with immune checkpoint inhibitors. The upper limit, centre and lower limit of each box denotes the upper quartile, median and lower quartile of the data, respectively. P values were calculated using the Wilcoxon rank-sum test. Data are from ENA: PRJEB23709[446]. Y axes indicate log_2 counts per million (lcpm). **(B)** Cell surface MHC-II expression in LM-MEL-53, WM852 and A375 cells, in the presence or absence of IFN-γ 10 ng/mL for 48 hours. Representative data from 2 experiments.

Mirroring my findings in AML, deletion of FBXO11 in melanoma cell lines with basal expression of MHC-II led to accumulation of endogenous CIITA and a corresponding increase in cell surface MHC-II (**Figures 5.7A-D**). In contrast, in LM-MEL-53 cells where MHC-II is silenced, increased MHC-II upregulation following *FBXO11* KO was only evident following induction of basal CIITA expression in response to IFN-γ treatment (**Figure 5.7E**).

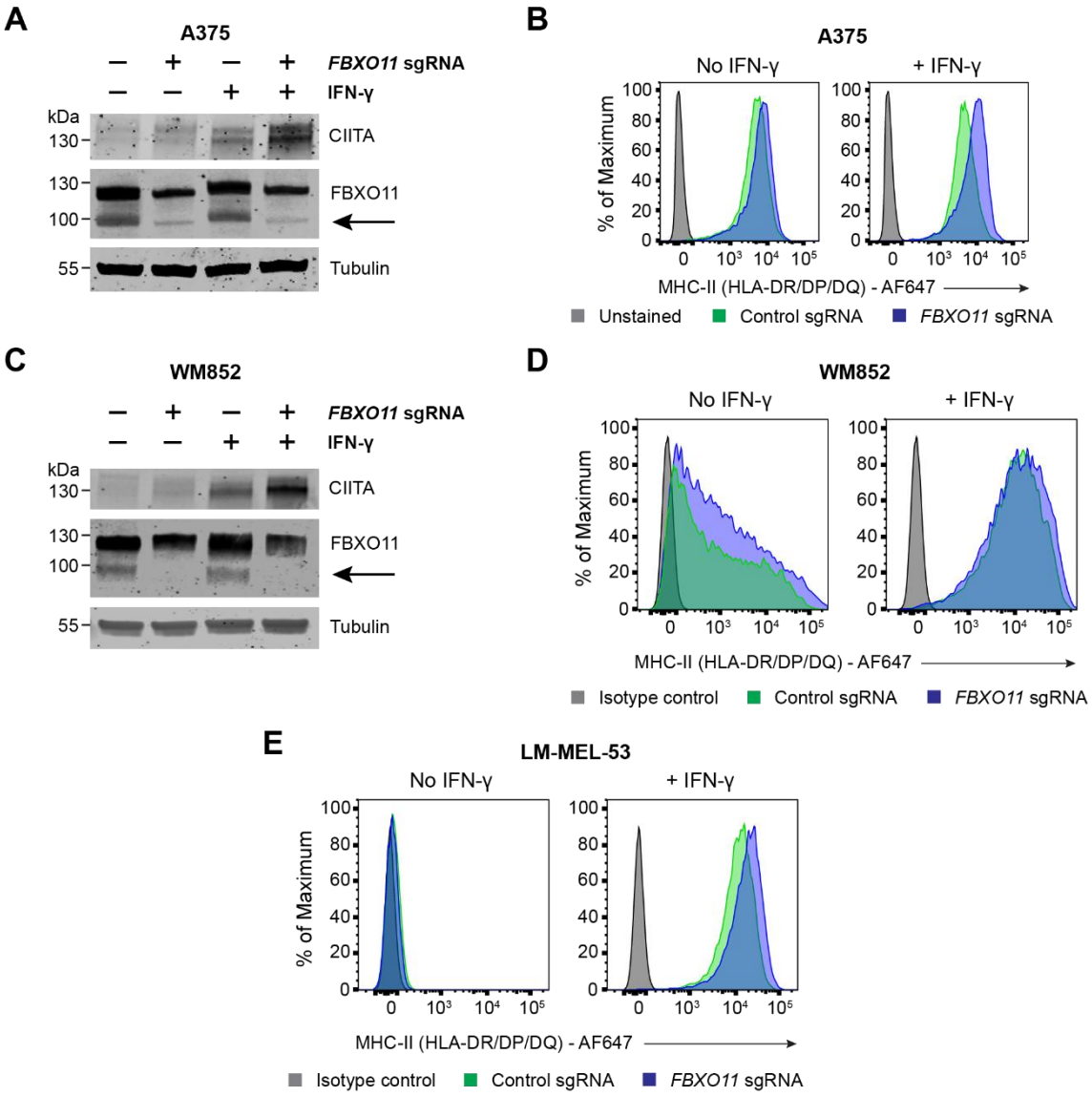

Figure 5.7. FBXO11 targeting in melanoma cells.

(A and B) Immunoblot (A) and cell surface MHC-II expression (B) in A375 cells transduced with a retroviral vector encoding CIITA cDNA with or without *FBXO11* sgRNA, in the presence or absence of IFN-γ 10 ng/mL for 48 hours. Representative data from 2 experiments. **(C and D)** Immunoblot (C) and cell surface MHC-II expression (D) in WM852 cells transduced with a retroviral vector encoding CIITA cDNA with or without *FBXO11* sgRNA, in the presence or absence of IFN-γ 10 ng/mL for 48 hours. Representative data from 2 experiments. **(E)** Cell surface MHC-II expression in LM-MEL-53 cells transduced with control or *FBXO11* sgRNA, in the presence or absence of IFN-γ 10 ng/mL for 48 hours. Representative data from 2 experiments. Experiments performed by Ms Juliana Gomez and Dr Nishi Kumari.

Similar to my observations in AML, targeting the catalytic activity of the EHMT1/2-containing CtBP complex with A-366 led to enhanced MHC-II expression in these cells, which was further augmented by concurrent *FBXO11* KO (**Figure 5.8A**), with no effect on MHC-I levels (**Figure 5.8B**). Modest MHC-II upregulation was also seen in WM852 and A375 cells treated with A-366 (**Figures 5.8C and 5.8D**), corresponding with the lesser degree of basal MHC-II repression in these cells. These data reinforce the specificity of CtBP complex and FBXO11-mediated MHC-II repression, and broaden the applicability of treatments targeting these repressive mechanisms to upregulate tumour-specific MHC-II and potentially enhance melanoma responses to immune checkpoint inhibition.

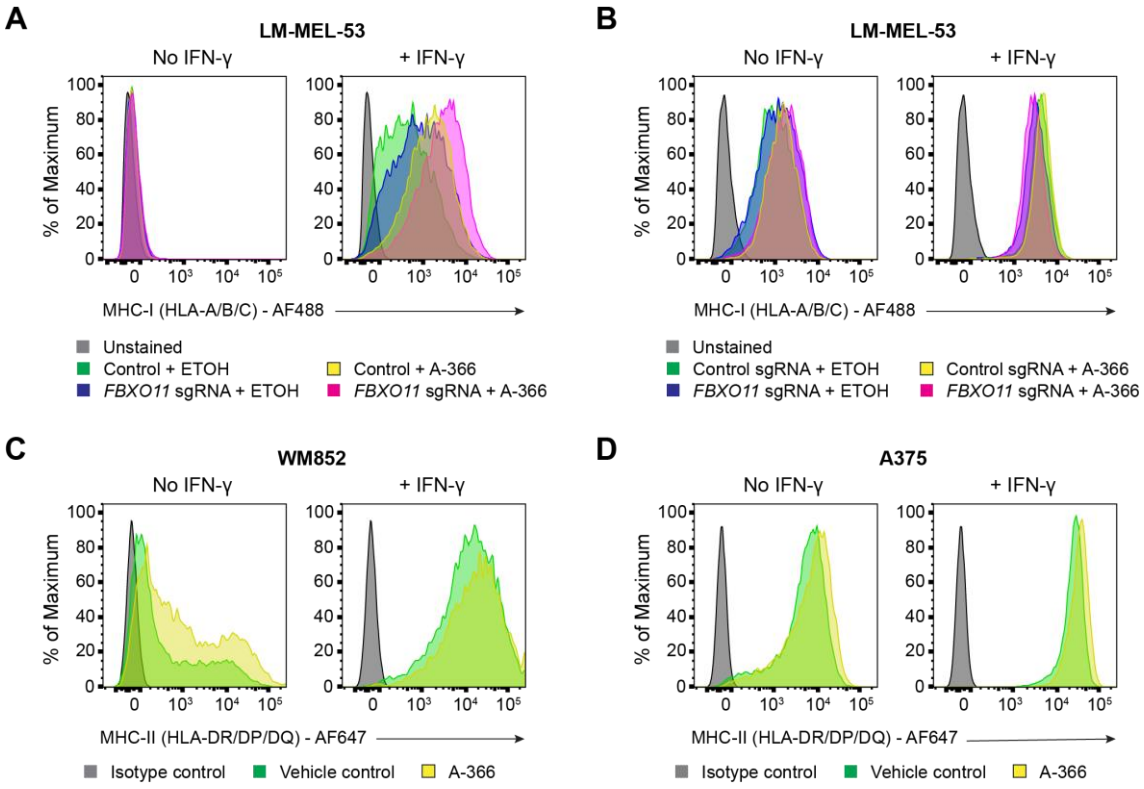

Figure 5.8. CtBP complex and FBXO11 targeting in melanoma cells.

(A and B) Cell surface MHC-II (A) and MHC-I (B) expression in LM-MEL-53 Cas9 cells transduced with control or *FBXO11* sgRNA and treated with EHMT1/2 inhibitor (A-366 3µM) or vehicle control for 7 days, in the presence or absence of IFN-γ 10 ng/mL for 48 hours. Representative data from 2 experiments. **(C and D)** Cell surface MHC-II expression in WM852 (C) and A375 (D) cells treated with EHMT1/2 inhibitor (A-366 3µM) or vehicle control for 7 days, in the presence or absence of IFN-γ 10 ng/mL for 48 hours. Representative data from 2 experiments. Experiments performed by Ms Juliana Gomez and Dr Nishi Kumari.

5.1.4 FBXO11 interacts with CIITA and promotes CIITA ubiquitination

In order to further characterize the mechanism through which FBXO11 regulates CIITA protein stability, I generated LM-MEL-53 cells expressing epitope-tagged CIITA. As seen in MV4-11 cells (**Figures 5.5F and 5.5G**), genetic disruption of FBXO11 resulted in significant CIITA accumulation (**Figures 5.9A and 5.9B**). Increased CIITA levels were also observed following co-expression of an FBXO11 mutant (**Figure 5.9C**) in which the F-box domain (aa71-116) has been deleted, thereby abolishing binding to the remainder of the SCF ubiquitin ligase complex but leaving the substrate recognition domain intact[339]. The FBXO11ΔFbox mutant showed increased nuclear localization compared to wildtype FBXO11 (**Figure 5.9D**), potentially reflecting impaired binding to SCF complex components within the cytoplasm. Expression of FBXO11ΔFbox increased the nuclear localization of co-expressed CIITA and dual staining revealed high CIITA and FBXO11ΔFbox co-localization (**Figures 5.9D-F**). These findings suggested that FBXO11ΔFbox may bind and stabilize CIITA by inhibiting its recruitment to the SCF ubiquitin ligase complex and subsequent degradation.

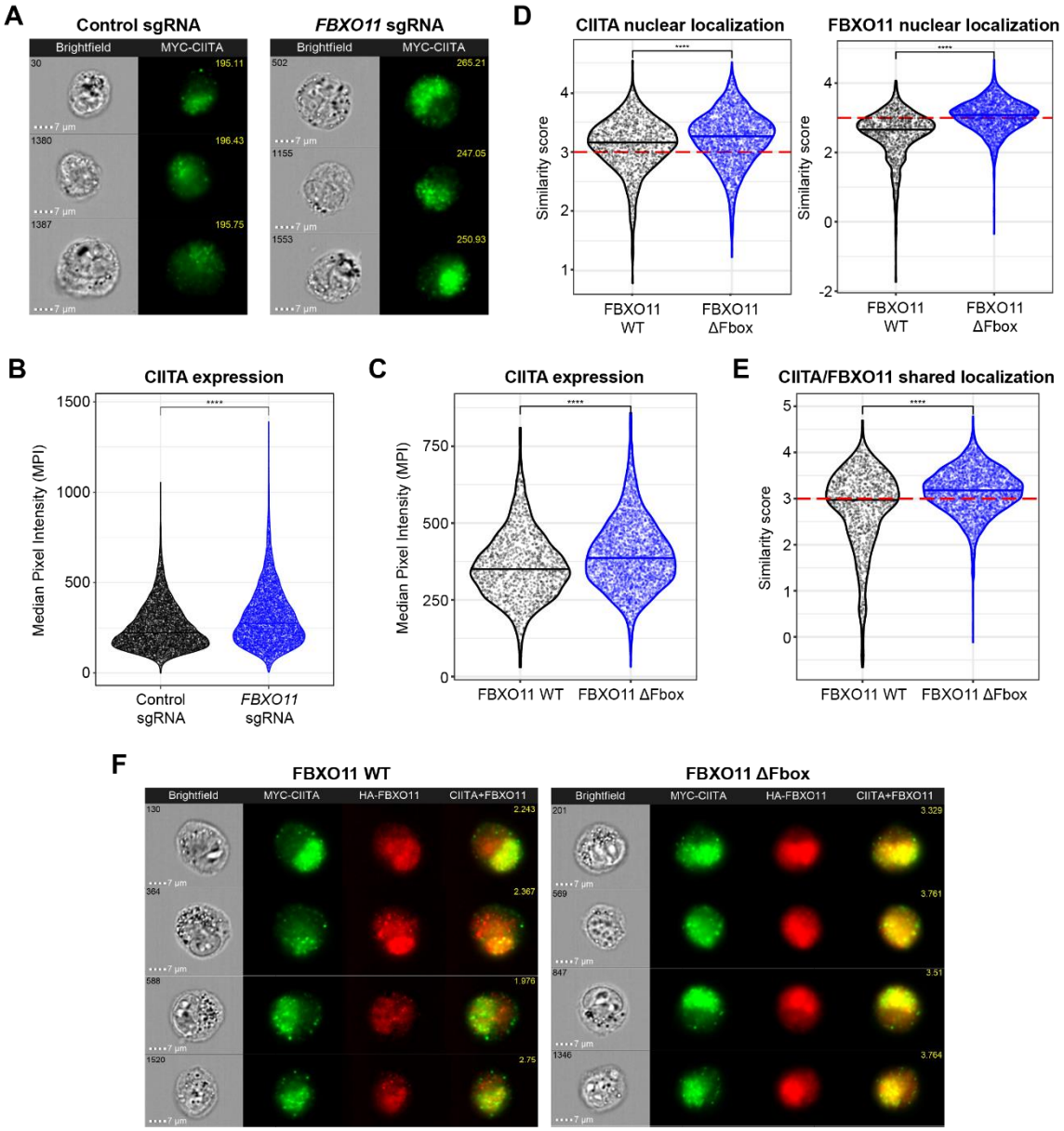

Figure 5.9. FBXO11 co-localises with CIITA and its loss promotes nuclear accumulation of CIITA.

(A) Representative images showing brightfield microscopy (cell number at top left) and Myc-CIITA expression (median pixel intensity [MPI] value at top right) in LM-MEL-53 Cas9 cells transduced with control or *FBXO11* sgRNA. **(B)** Myc-CIITA expression measured as MPI in LM-MEL-53 Cas9 cells transduced with control or *FBXO11* sgRNA. Each data point represents a single cell measured and bars represent the group median. Statistical significance was calculated using Dunn's test with Bonferroni correction for multiple comparisons. **** = $p < 0.0001$. Representative data from 2 experiments. **(C)** Myc-CIITA expression measured as MPI in LM-MEL-53 cells expressing FBXO11 WT or FBXO11 ΔFbox. Each data point represents a single cell measured and bars represent the group median. Statistical significance was calculated using Dunn's test with Bonferroni correction for multiple comparisons. **** = p <

0.0001. Representative data from 2 experiments. **(D)** Summary of CIITA and FBXO11 nuclear localization in LM-MEL-53 cells expressing FBXO11 WT or FBXO11 ΔFbox. High shared localization with DAPI defined by similarity score ≥ 3 (red dotted line), as previously described[345-347]. Statistical significance was calculated using Dunn's test with Bonferroni correction for multiple comparisons. **** = $p < 0.0001$. **(E)** Summary of shared localization between CIITA and FBXO11 in LM-MEL-53 cells expressing FBXO11 WT or FBXO11 ΔFbox. High shared localization defined by similarity score ≥ 3 (red dotted line). Statistical significance was calculated using Dunn's test with Bonferroni correction for multiple comparisons. **** = $p < 0.0001$. Representative data from 2 experiments. **(F)** Representative images showing brightfield microscopy (cell number at top left), as well as CIITA and FBXO11 expression (similarity score at top right) in LM-MEL-53 cells expressing FBXO11 WT or FBXO11 ΔFbox. Experiments performed by Dr Chelisa Cardinez and Ms Juliana Gomez.

To more directly investigate whether CIITA and FBXO11 interact, I immunoprecipitated CIITA from CIITA-expressing LM-MEL-53 cells, which revealed co-immunoprecipitation of FBXO11 (**Figure 5.10A**). Consistent with the significant nuclear co-localization of CIITA and FBXO11ΔFbox, and the known function of the F-box in selectively binding Skp1 to target bound substrates for degradation, interaction between CIITA and FBXO11ΔFbox was readily detected. Supporting the specificity of this interaction, endogenous FBXO11 could also be detected in association with CIITA (**Figure 5.10B**). Incubation of cells with the proteasome inhibitor MG-132 led to accumulation of polyubiquitinated CIITA, indicating turnover of CIITA via proteasome-mediated degradation. Whilst total levels of CIITA were increased in the absence of FBXO11 (**Figures 5.7A, 5.9A-B and 5.10C**), knockout of FBXO11 led to a reduction in polyubiquitinated CIITA in MG-132-treated cells, supporting a role for FBXO11 in targeting CIITA for polyubiquitination and degradation by the proteasome (**Figure 5.10C**). These findings collectively establish FBXO11 as part of a key ubiquitin ligase complex regulating CIITA protein stability via proteasomal degradation. The stabilization of CIITA subsequently leads to enhanced downstream transcriptional activation of CIITA-regulated MHC-II genes and increased cell surface MHC-II expression.

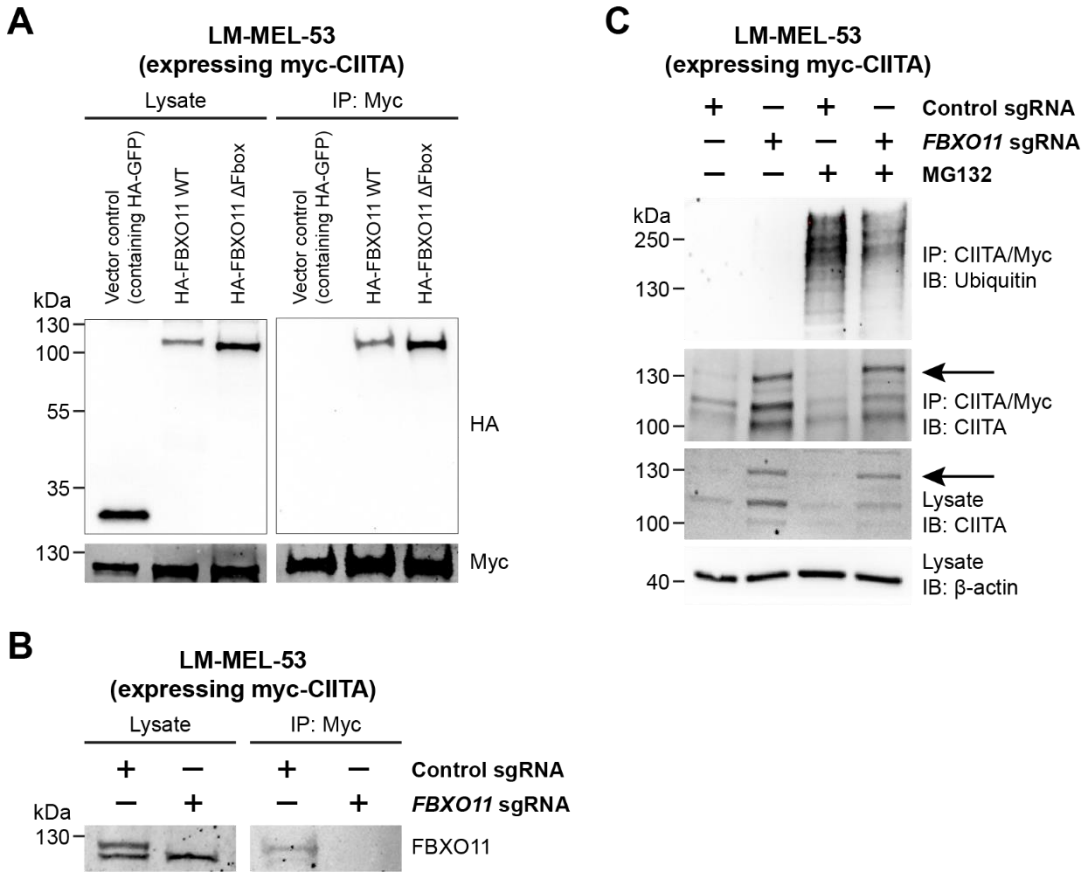

Figure 5.10. FBXO11 promotes CIITA ubiquitination.

(A) Immunoprecipitation of myc-CIITA from lysates of LM-MEL-53 cells expressing FBXO11 WT or FBXO11 ΔFbox, analysed by immunoblot. Lysate, 5% of input. Experiments performed twice. **(B)** Immunoprecipitation of myc-CIITA from lysates of LM-MEL-53 Cas9 cells transduced with control or *FBXO11* sgRNA, analysed by immunoblot. Lysate, 5% of input. Experiments performed twice. **(C)** Immunoprecipitation of myc-CIITA from lysates of LM-MEL-53 Cas9 cells transduced with control or *FBXO11* sgRNA and with or without MG-132 treatment, analysed by immunoblot. Lysate, 5% of input. Experiments performed twice. Experiments performed by Ms Juliana Gomez, Dr Nishi Kumari and Dr Chelisa Cardinez.

5.1.5 MHC-II expression on leukaemic blasts facilitates adaptive anti-cancer immune surveillance

To explore the contribution of tumour cell MHC-II expression to immunological anti-leukaemia responses, I investigated whether MHC-II upregulation could be induced in a mouse model of AML. Although deletion of *Fbxo11* and *Rreb1* (**Figure 4.10D**) and A-366 treatment (**Figure 5.11A**) did not increase surface MHC-II levels, expression of CIITA cDNA resulted in significant and selective MHC-II upregulation (**Figures 5.11B and 5.11C**) in mouse AML cells, enabling us to

specifically test the functional effects of leukaemia MHC-II expression using genetically matched immune effector cells.

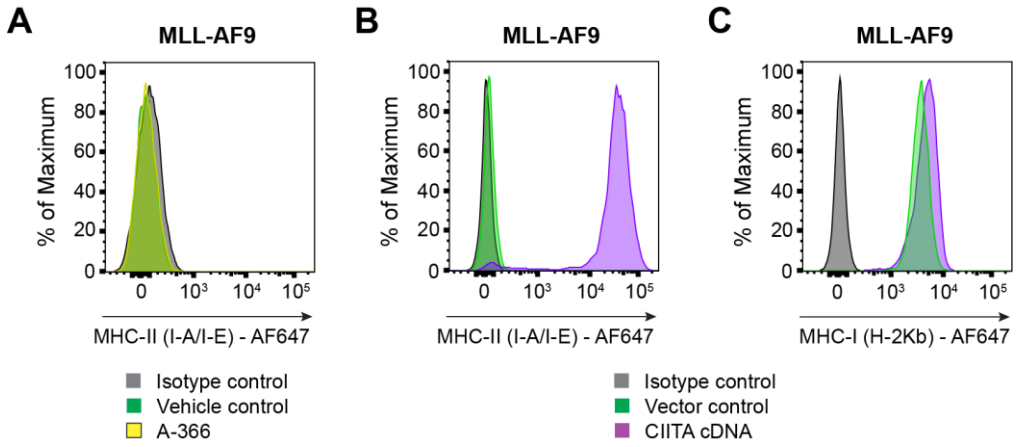

Figure 5.11. CIITA overexpression specifically induces MHC-II upregulation in MLL-AF9 cells. **(A)** Cell surface MHC-II expression in MLL-AF9 cells treated with EHMT1/2 inhibitor (A-366 1µM) or vehicle control for 7 days. Representative data from 3 experiments. **(B and C)** Cell surface MHC-II (B) and MHC-I (C) expression in MLL-AF9 cells transduced with a retroviral vector encoding CIITA cDNA or vector control. Representative data from 3 experiments.

To investigate whether restoring MHC-II in MHC-II-negative AML cells is sufficient to stimulate antigen-dependent T cell responses, I engineered mouse leukaemia cells to express full-length OVA with a green fluorescent protein (GFP) reporter, as well as CIITA. These OVA-expressing MHC-II$^+$ cells were then used for *in vitro* co-culture experiments on the Incucyte SX5 Live-Cell Analysis System, allowing objective real-time tracking of AML cell proliferation and killing using a combination of phase contrast imaging and detection of GFP fluorescence (**Figure 5.12A**). Co-culture with CD4$^+$ OT-II T cells, which specifically recognize processed peptides derived from OVA protein and presented on mouse MHC-II, significantly reduced the number of OVA-expressing MHC-II$^+$ MLL-AF9 cells compared to OVA-expressing cells that were negative for MHC-II (**Figure 5.12B**). High-level release of pro-inflammatory cytokines were also observed following co-culture of CD4$^+$ OT-II T cells with OVA-expressing MHC-II$^+$ leukaemia cells (**Figure 5.12C**) compared to leukaemia cells expressing either OVA or MHC-II alone, providing confirmation of antigen- and MHC-II-dependent T cell activation. Tumour cell-specific MHC-II expression also significantly potentiated CD8$^+$ T cell killing in combined co-cultures of OVA-expressing leukaemia cells with CD8$^+$ OT-I T cells and CD4$^+$ OT-II T cells (**Figure 5.12D**), suggesting a role for promotion of CD4$^+$ T cell help in addition to direct CD4$^+$ T cell cytotoxicity.

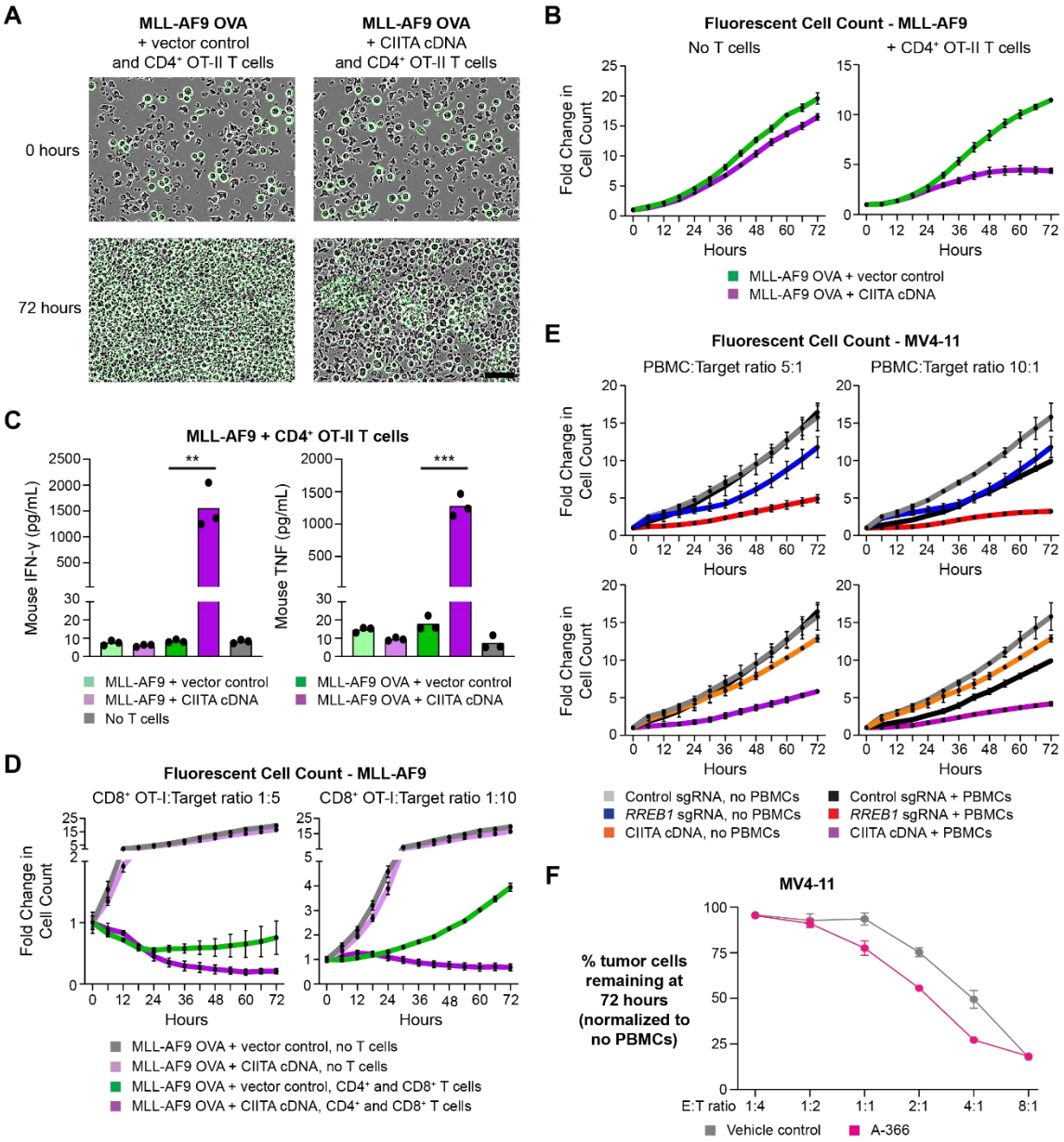

Figure 5.12. MHC-II expression on leukaemic blasts facilitates adaptive anti-cancer immune responses.

(A) Phase contrast microscopy of MLL-AF9 OVA-expressing cells transduced with a retroviral vector encoding CIITA cDNA or vector control, during co-culture with CD4$^+$ OT-II T cells at an E:T ratio of 4:1. GFP-expressing cells are shown with the overlaid green object mask, based on automated detection using the Incucyte SX5 platform. Scale bar, 50µm. **(B)** Fold change of fluorescent cell count for MLL-AF9 OVA-expressing cells transduced with a retroviral vector encoding CIITA cDNA or vector control, following co-culture with CD4$^+$ OT-II T cells at an effector:target (E:T) ratio of 4:1. Plots show mean ± SEM of technical triplicates from a representative experiment, performed twice. **(C)** Cytometric bead array (CBA) assay for T cell cytokines following 24 hour co-culture of OT-II CD4$^+$ T cells with MLL-AF9 cells expressing OVA

peptide and/or CIITA cDNA or vector control, at an E:T ratio of 2:1. Bars depict the mean of technical triplicates from a representative experiment, performed twice. Statistical analysis by unpaired t test compared to respective vector control cells, with significant changes indicated; p value ** < 0.01, *** < 0.001. **(D)** Fold change of fluorescent cell count for MLL-AF9 OVA-expressing cells transduced with a retroviral vector encoding CIITA cDNA or vector control, following co-culture with $CD4^+$ OT-II T cells at an E:T ratio of 4:1 and $CD8^+$ T cells at the indicated E:T ratios. Plots show mean ± SEM of technical triplicates from a representative experiment, performed twice. **(E)** Fold change of fluorescent cell count for MV4-11 Cas9 cells transduced with *RREB1* sgRNA, a retroviral vector encoding CIITA cDNA or vector control, following co-culture with human peripheral blood mononuclear cells (PBMC) at the indicated E:T ratios. Plots show mean ± SEM of technical triplicates from a representative experiment, performed twice. **(F)** Percent remaining live MV4-11 cells following 72 hour co-culture with human $CD4^+$ T cells at the indicated E:T ratios. Cells were treated with A366 1µM or vehicle control for the duration of the experiment. Plots show mean ± SEM of technical triplicates from a representative experiment, performed twice. Experiments in panel F performed by Dr Jamie Kuzich.

These findings were validated using co-cultures of human PBMCs with *RREB1* KO, CIITA-expressing or A-366-treated MV4-11 cells, all of which resulted in clear reduction of MHC-II^+ AML cells compared to control cells with low MHC-II expression (**Figures 5.12E and 5.12F**). Importantly, EHMT1/2 inhibition had no effect on human T cell subset composition (**Figure 5.13A**) or effector function (**Figure 5.13B**), reinforcing the specificity of CtBP complex targeting in augmenting anti-tumour immunity via upregulation of tumour cell MHC-II expression.

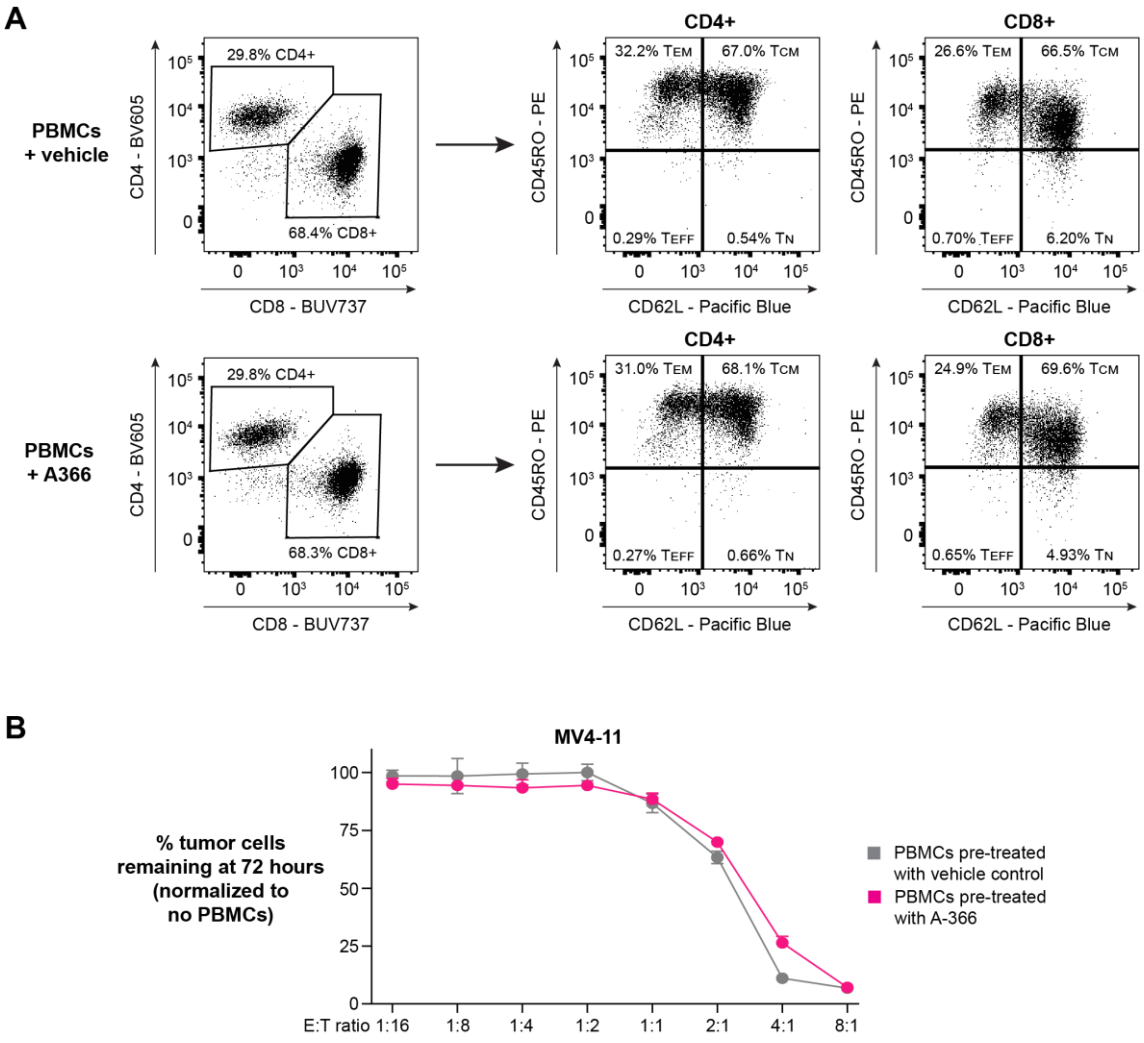

Figure 5.13. EHMT1/2 inhibition does not affect T cell subset composition or function.

(A) T cell subset analysis in human PBMCs treated with A-366 1µM or vehicle control for 5-7 days. Data is shown from a representative experiment, performed twice. **(B)** Percent remaining live MV4-11 cells following 72 hour incubation with human PBMCs at the indicated E:T ratios. PBMCs were pre-treated with A366 1µM or vehicle control for 5-7 days prior to co-culture. Plots show mean ± SEM of technical triplicates from a representative experiment, performed twice. Experiments in panel B performed by Dr Jamie Kuzich.

Taken together, these data show that, despite their impaired capacity for differentiation, both human and murine leukaemic blasts can process and present antigen via a functional MHC-II pathway, leading to antigen-dependent $CD4^+$ T cell activation and potent anti-tumour immune effects. While my results demonstrate that either genetic or pharmacological CtBP complex disruption is sufficient to increase MHC-II expression and T cell-mediated killing, the potential role for targeting FBXO11 in isolation was comparatively more modest (**Figures 4.5A-C and 5.5B**). This is consistent with its role in post-translational regulation of CIITA, which is absent or

lowly expressed in MHC-II deficient cells and requires activation through disruption of the CtBP complex or stimulation with inflammatory cytokines.

The evaluation of immune responses in patient-derived or human cell line xenografts is clouded by the xenogenic immune environment. Moreover, when unmatched PBMCs are used as immune effectors in these assays, there is also likely a potent allogeneic effect that would mask the ability to evaluate the selective functional consequences of MHC-II expression. Therefore, to determine whether tumour cell MHC-II expression promotes immune-mediated clearance of MHC-matched AML *in vivo*, I chose to utilize the transplantation of mouse leukaemia cells into genetically matched recipients with an identical MHC-I and MHC-II haplotype. As EHMT1/2 inhibitors do not regulate MHC-II expression in mice, I instead transplanted an equal ratio of control GFP$^+$ leukaemia cells (MHC-I^{high}) and mCherry$^+$ CIITA-expressing leukaemia cells (MHC-I^{high} + MHC-II^{high}) into immunocompetent mice (**Figure 5.14A**) and then assessed the relative proportion of GFP$^+$ and mCherry$^+$ cells contributing to resulting leukaemia (**Figure 5.14B**). Remarkably, the leukaemic composition in all five mice showed a marked predominance of GFP$^+$ cells (**Figure 5.14C**), consistent with immune clearance of the mCherry$^+$ MHC-II$^+$ compartment. Although an important limitation of this *in vivo* model is an inability to fully replicate the GVL effect induced by alloSCT, it nevertheless underscores the biological relevance of MHC-II in driving immune-mediated anti-leukaemia responses in an MHC-matched setting.

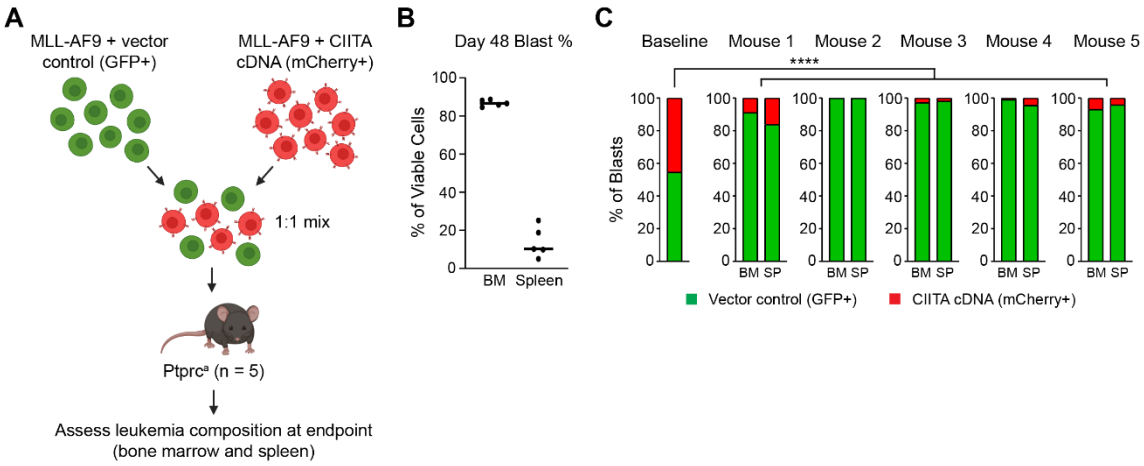

Figure 5.14. MHC-II$^+$ blasts are efficiently cleared in an *in vivo* syngeneic model of AML. **(A)** Overview of *in vivo* competition assay, utilizing MLL-AF9 cells transduced with GFP vector control or a retroviral vector encoding mCherry and CIITA cDNA. **(B)** Percentage of leukaemic blasts in bone marrow (BM) and spleen at disease endpoint. Bars represent the mean percentage of leukaemic blasts from each mouse indicated by points. **(C)** Proportion of GFP$^+$ control and mCherry$^+$ CIITA-expressing cells in bone marrow (BM) and spleen (SP) at disease

endpoint. Two-tailed binomial test was performed to compare expected and observed proportions in each sample compared to the baseline proportion of GFP^+ and $mCherry^+$ cells injected. **** = $p < 0.0001$.

Finally, to illustrate the relevance of my findings to primary human leukaemia samples, I assessed the effect of inhibiting EHMT1/2, the catalytic component of the CtBP complex, in primary AML cells with low basal levels of MHC-II expression. Consistent with my findings in human AML cell lines, A-366 treatment of leukaemic blasts from two patients induced significant MHC-II upregulation, even in the absence of IFN-γ stimulation (**Figures 5.15A and 5.15B**). Although inhibition of epigenetic complexes is often associated with a diverse range of gene expression changes, I found that EHMT1/2 inhibition in human AML cells is remarkably specific. Despite increasing MHC-II cell surface expression, single-cell RNA sequencing following A-366 treatment did not reveal a global change in the transcriptional landscape of the treated cells, which clustered together with the control population (**Figures 5.15C and 5.15D**). Strikingly, when I assessed the global gene expression changes in both patient samples, I observed highly selective upregulation of only MHC-II pathway genes (**Figures 5.15E-5.15H**). These data confirm that CtBP-mediated repression is a targetable mechanism of MHC-II silencing in human AML. Moreover, the lack of widespread gene expression changes in the tumour cells alongside the preserved T cell function in the presence of EHMT1/2 inhibition (**Figures 5.13A and 5.13B**) provide the rationale for clinical implementation of this therapeutic strategy to circumvent leukaemic immune escape.

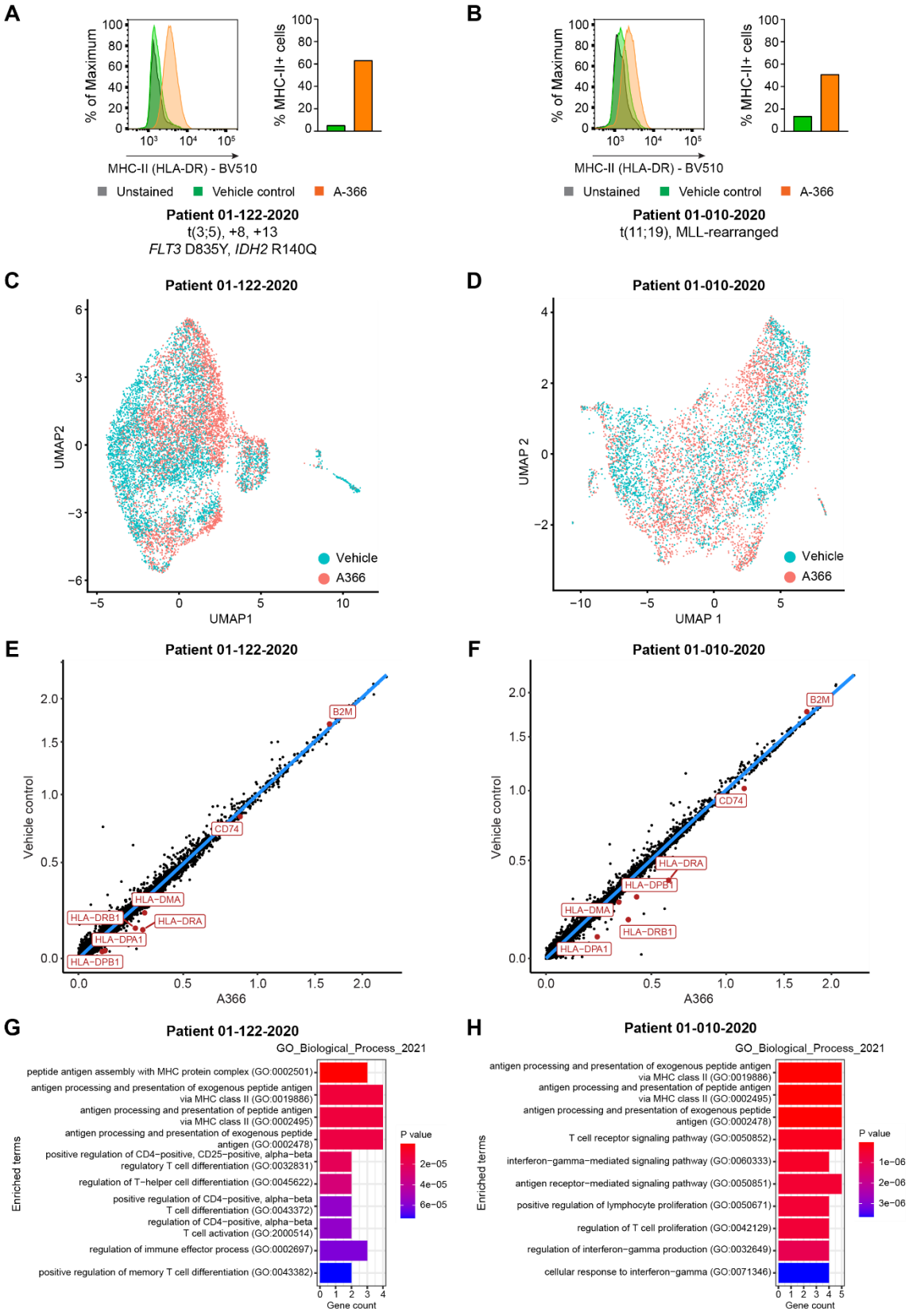

Figure 5.15. Pharmacological EHMT1/2 inhibition selectively induces MHC-II upregulation in primary AML cells.

(A and B) Cell surface MHC-II expression in primary AML cells from patients treated with EHMT1/2 inhibitor (A-366 1μM) or vehicle control for 5-7 days. Data is shown from a representative experiment, performed twice. **(C and D)** UMAP projections of primary AML cells treated with EHMT1/2 inhibitor (A-366 1μM) or vehicle control for 5-7 days. Cells are highlighted by treatment. **(E and F)** Scatterplots showing normalized gene expression in primary AML cells treated with EHMT1/2 inhibitor (A-366 1μM) or vehicle control for 5-7 days. MHC-II pathway genes and *B2M* are highlighted. **(G and H)** Gene set enrichment analysis performed on all genes differentially upregulated with A-366 treatment in primary AML cells. Experiments in panels A and B performed by Dr Doen Ming Ong and Dr Fiona Brown.

5.2 Discussion

The ability of alloSCT to maintain durable remissions in a proportion of AML patients, even those with adverse-risk prognostic features, highlights the considerable power of the GVL effect. Consequently, for patients who relapse post-alloSCT, immunomodulatory therapies that attempt to reinstate and augment GVL responses represent a logical and promising salvage strategy. However, currently available interventions, such as donor lymphocyte infusion, only benefit a minority and carry a significant risk of exacerbating graft-versus-host disease with attendant treatment-related morbidity and/or mortality[447,448].

My findings help to address this critical unmet need by identifying fundamental mechanisms of MHC-II repression in AML that can be exploited to evade the GVL effect. From a translational perspective, I show that currently available small molecule inhibitors of EHMT1/2 efficiently reverse CtBP-mediated MHC-II silencing, supporting clinical trials of these inhibitors in post-alloSCT relapse, particularly when MHC-II is lowly expressed on the emergent measurable residual disease. I elucidate the role of MHC-II in driving the adaptive immune responses underpinning the GVL effect, demonstrating that MHC-II$^+$ leukaemic blasts can activate CD4$^+$ T cells in an antigen-dependent manner, stimulating CD4$^+$ T cell-mediated cytotoxicity as well as potentiation of CD8$^+$ effector T cell function. The ability to potently and selectively induce MHC-II re-expression in leukaemic blasts provides a unique opportunity to enhance GVL responses. Targeting these specific repressive mechanisms also enables MHC-II upregulation in non-haematological cancer cells, broadening the scope of my findings and raising the prospect that these adjunctive therapeutic approaches to increase MHC-II expression could enhance immunotherapy responses, particularly with combinatorial inhibition of various immune checkpoints.

Chapter 6 – Summary and general discussion

6.1 Identifying and targeting epigenetic mechanisms of cancer immune evasion

Given the ability of immunotherapies to induce complete and durable anti-cancer responses, broadening their applicability by optimising the proportion of patients who respond and minimising the emergence of resistance are critical priorities for the field. A key first step to achieving these goals is a detailed understanding of the mechanisms underpinning cancer immune evasion, with the aim of obtaining insights into how these can be subverted.

In contrast to genomic mutations that inactivate *B2M* or the interferon signalling pathway[2], epigenetic mechanisms of MHC-I and MHC-II repression are potentially targetable to restore antigen presentation by tumour cells and promote adaptive immune responses. The work in this thesis identified key non-genomic mechanisms of MHC-I and MHC-II downregulation in cancer: firstly, the PRC2 complex mediates transcriptional repression of MHC-I, while the CtBP co-repressor complex silences MHC-II pathway genes and the FBXO11-containing E3 ubiquitin ligase complex controls protein stability of CIITA, the master regulator of MHC-II expression. Importantly, MHC-I levels are unaffected by CtBP complex targeting while MHC-II levels are unaffected by PRC2 inhibition, illustrating how these two distinct chromatin repressive complexes independently regulate MHC-I and MHC-II expression. The compartmentalisation of these processes underscores the importance of delineating the mechanisms of immune evasion in a given cancer context in order to guide appropriate intervention.

From a translational perspective, I show that currently available small molecule inhibitors of these repressive complexes efficiently reverse MHC-I and MHC-II silencing in deficient tumour cells, even in the absence of interferon stimulation. In the context of MHC-I, this can be utilised as an adjunctive strategy to pre-treat intrinsically resistant cancers that lack MHC-I and sensitise them to checkpoint inhibitor therapy. The prognostic significance of tumour-specific MHC-II expression implies that induction of MHC-II upregulation may also enhance immunotherapy responses. However, for MHC-II the therapeutic applications are potentially broader, as CtBP complex targeting additionally represents a novel strategy to restore the GVL effect and salvage post-alloSCT relapse of AML, particularly when MHC-II is lowly expressed on the emergent measurable disease. This is particularly attractive given the specificity of EHMT1/2 inhibitors in inducing MHC-II upregulation on leukaemic blasts, which may uniquely augment GVL responses without concurrent exacerbation of GVHD, as can be seen with existing immunomodulatory

strategies such as DLI or lenalidomide[449-451]. Nevertheless, while these strategies are highly promising conceptually, validation through clinical trials is still required to establish *in vivo* efficacy and determine optimal combinatorial strategies that maximise disease eradication while minimising selection pressure and emergence of therapeutic resistance.

6.2 The increasingly recognised role of MHC-II in anti-cancer immunity

In addition to uncovering non-genomic regulators of antigen presentation in cancer, I also contribute to the expanding body of literature supporting a fundamental role for tumour-specific MHC-II expression in promoting adaptive anti-cancer immune responses. Using an *in vitro* model of AML, I show in Chapter 5 of this thesis that MHC-II upregulation on leukaemic blasts stimulates antigen-dependent $CD4^+$ T cell activation, which not only augments the classical helper function of these cells but also induces direct $CD4^+$ T cell-mediated cytotoxicity. Despite the challenges involved with attempting to fully recapitulate alloSCT in a mouse model, my competition assay also clearly illustrates that MHC-II expression facilitates *in vivo* immune clearance of AML, supporting the functional relevance of my findings.

Several important, related biological questions remain unanswered. Firstly, while the existence of cytotoxic $CD4^+$ T cells is now well recognised, particularly in the setting of viral infection and immunity[452], it remains less clear how much they contribute to anti-cancer immune responses and how they can be optimally utilised for therapeutic benefit. Interestingly, a recently published analysis of patients with chronic lymphocytic leukaemia who achieved long-term remissions following CAR-T cell therapy identified persistence of a dominant $CD4^+$ CAR-T clone that demonstrated cytotoxic properties and ongoing functional activation, thereby likely being responsible for maintaining disease control[97]. Although CAR-T cells are MHC-independent, case reports also describe regression of melanoma and epithelial cancers induced by expansion and re-infusion of autologous tumour-infiltrating $CD4^+$ T cells that specifically recognise cancer-associated antigens[453,454]. Other strategies to try and induce *in vivo* cytotoxic $CD4^+$ T cell differentiation, such as HDAC inhibition[455] or vaccination[456,457], also merit exploration.

Secondly, given that optimal adaptive immune responses require coordinated $CD4^+$ and $CD8^+$ T cell function, it is notable that the two initial studies evaluating post-alloSCT relapse of AML specifically identified MHC-II (and not MHC-I) downregulation as a recurring phenomenon[420,421].

Although I and others have shown how MHC-II expression on leukaemic blasts promotes $CD4^+$ T cell-mediated immunity[435], further work is required to establish whether this is specific to the GVL effect in AML or whether strategies to induce tumour cell MHC-II expression may also be viable for other haematological malignancies treatable with alloSCT, such as lymphoma and plasma cell myeloma.

Thirdly, while the MHC-II work in this thesis has focused on its primary role in antigen presentation to $CD4^+$ T cells, its impact on other aspects of immune function also require consideration. For instance, MHC-II is a natural ligand for the T cell inhibitory co-receptor LAG-3 and its binding to LAG-3 has been shown to restrict adaptive immune responses and promote cancer survival[458,459]. Accordingly, increasing tumour cell MHC-II expression in isolation may be detrimental in *in vivo* or clinical settings where tumour-infiltrating lymphocytes exhibit high LAG-3 expression, although this could be overcome by emerging monoclonal antibody therapies targeting LAG-3, especially in combination with other checkpoint inhibitors.

6.3 Future directions

This thesis encapsulates the strong synergy between the clinical and scientific domains, whereby clinical observations and obstacles (in this case, immunotherapy resistance) drive the discovery of fundamental biological insights and novel therapeutic strategies that can subsequently be trialled at the bedside. As outlined above, my findings provide the rationale for early phase clinical trials of EHMT1/2 inhibitors to treat patients with AML relapse following alloSCT, potentially in combination with other forms of immunomodulation to augment GVL responses. While potent and selective EHMT1/2 inhibitors such as A-366 and UNC0638 already exist and were effective in my pre-clinical models, they have suboptimal bioavailability *in vivo*[460] and therefore modified compounds may be required to overcome this issue prior to clinical trials. Another worthwhile target for drug development is FBXO11, for which no current pharmacological inhibitors exist – while it is possible to non-specifically inhibit proteasomal function using inhibitors such as bortezomib, it is unknown whether this can replicate the effect of specific disruption of the FBXO11-containing E3 ubiquitin ligase complex and whether there are potentially detrimental off-target effects. Being able to leverage the established synergy between CtBP complex targeting and FBXO11 KO through dual small molecule inhibition may be therapeutically advantageous in the appropriate clinical context.

Finally, while it is hoped that the work in this thesis will translate into meaningful improvements in patient outcomes, there are many other mechanisms of cancer immune evasion for which effective interventions are greatly needed. The intrinsic nature of cancer evolution and near inevitability of emergence of therapeutic resistance mandate ongoing clinical and scientific research to ensure that the field also continues to adapt and progress within an exciting era of precision oncology, aspiring to provide patients with optimal, tailored care that is as dynamic as the diseases they fight.

Chapter 7 – References

1 Waldman, A. D., Fritz, J. M. & Lenardo, M. J. A guide to cancer immunotherapy: from T cell basic science to clinical practice. *Nature Reviews Immunology* **20**, 651-668, doi:10.1038/s41577-020-0306-5 (2020).

2 Sharma, P., Hu-Lieskovan, S., Wargo, J. A. & Ribas, A. Primary, Adaptive and Acquired Resistance to Cancer Immunotherapy. *Cell* **168**, 707-723, doi:10.1016/j.cell.2017.01.017 (2017).

3 Hogg, S. J., Beavis, P. A., Dawson, M. A. & Johnstone, R. W. Targeting the epigenetic regulation of antitumour immunity. *Nature Reviews Drug Discovery* **19**, 776-800, doi:10.1038/s41573-020-0077-5 (2020).

4 Charles A. Janeway, J. & Medzhitov, R. Innate Immune Recognition. *Annu Rev Immunol* **20**, 197-216, doi:10.1146/annurev.immunol.20.083001.084359 (2002).

5 Matzinger, P. Tolerance, Danger, and the Extended Family. *Annu. Rev. Immunol.* **12**, 991-1045, doi:10.1146/annurev.iy.12.040194.005015 (1994).

6 Chaplin, D. D. Overview of the immune response. *J. Allergy Clin. Immunol.* **125**, S3-S23, doi:10.1016/j.jaci.2009.12.980 (2010).

7 Marshall, J. S., Warrington, R., Watson, W. & Kim, H. L. An introduction to immunology and immunopathology. *Allergy, Asthma & Clinical Immunology* **14**, 49, doi:10.1186/s13223-018-0278-1 (2018).

8 Janeway, C. A. Approaching the Asymptote? Evolution and Revolution in Immunology. *Cold Spring Harb Symp Quant Biol* **54**, 1-13, doi:10.1101/sqb.1989.054.01.003 (1989).

9 Tang, D., Kang, R., Coyne, C. B., Zeh, H. J. & Lotze, M. T. PAMPs and DAMPs: signal 0s that spur autophagy and immunity. *Immunol. Rev.* **249**, 158-175, doi:10.1111/j.1600-065X.2012.01146.x (2012).

10 Kono, H. & Rock, K. L. How dying cells alert the immune system to danger. *Nature Reviews Immunology* **8**, 279-289, doi:10.1038/nri2215 (2008).

11 Arnold, D. E. & Heimall, J. R. A Review of Chronic Granulomatous Disease. *Advances in Therapy* **34**, 2543-2557, doi:10.1007/s12325-017-0636-2 (2017).

12 Brack, C., Hirama, M., Lenhard-Schuller, R. & Tonegawa, S. A complete immunoglobulin gene is created by somatic recombination. *Cell* **15**, 1-14, doi:10.1016/0092-8674(78)90078-8 (1978).

13 Papavasiliou, F. N. & Schatz, D. G. Somatic Hypermutation of Immunoglobulin Genes: Merging Mechanisms for Genetic Diversity. *Cell* **109**, S35-S44, doi:10.1016/S0092-8674(02)00706-7 (2002).

14 Stavnezer, J., Jeroen E.J. Guikema & Schrader, C. E. Mechanism and Regulation of Class Switch Recombination. *Annu. Rev. Immunol.* **26**, 261-292, doi:10.1146/annurev.immunol.26.021607.090248 (2008).

15 LeBien, T. W. & Tedder, T. F. B lymphocytes: how they develop and function. *Blood* **112**, 1570-1580, doi:10.1182/blood-2008-02-078071 (2008).

16 Klein, L., Kyewski, B., Allen, P. M. & Hogquist, K. A. Positive and negative selection of the T cell repertoire: what thymocytes see (and don't see). *Nature Reviews Immunology* **14**, 377-391, doi:10.1038/nri3667 (2014).

17 Kumar, B. V., Connors, T. J. & Farber, D. L. Human T Cell Development, Localization, and Function throughout Life. *Immunity* **48**, 202-213, doi:10.1016/j.immuni.2018.01.007 (2018).

18 Zhang, N. & Bevan, M. J. CD8+ T Cells: Foot Soldiers of the Immune System. *Immunity* **35**, 161-168, doi:10.1016/j.immuni.2011.07.010 (2011).

19 Luckheeram, R. V., Zhou, R., Verma, A. D. & Xia, B. CD4+T Cells: Differentiation and Functions. *Clinical and Developmental Immunology* **2012**, 925135, doi:10.1155/2012/925135 (2012).
20 Zhu, J., Yamane, H. & Paul, W. E. Differentiation of Effector CD4 T Cell Populations. *Annual Review of Immunology* **28**, 445-489, doi:10.1146/annurev-immunol-030409-101212 (2010).
21 Jameson, S. C. & Masopust, D. Diversity in T Cell Memory: An Embarrassment of Riches. *Immunity* **31**, 859-871, doi:10.1016/j.immuni.2009.11.007 (2009).
22 Dustin, M. L. The immunological synapse. *Cancer Immunol Res* **2**, 1023-1033, doi:10.1158/2326-6066.CIR-14-0161 (2014).
23 Chen, L. & Flies, D. B. Molecular mechanisms of T cell co-stimulation and co-inhibition. *Nature Reviews Immunology* **13**, 227-242, doi:10.1038/nri3405 (2013).
24 Zhu, Y., Yao, S. & Chen, L. Cell Surface Signaling Molecules in the Control of Immune Responses: A Tide Model. *Immunity* **34**, 466-478, doi:10.1016/j.immuni.2011.04.008 (2011).
25 Curtsinger, J. M. & Mescher, M. F. Inflammatory cytokines as a third signal for T cell activation. *Current Opinion in Immunology* **22**, 333-340, doi:10.1016/j.coi.2010.02.013 (2010).
26 Voskoboinik, I., Whisstock, J. C. & Trapani, J. A. Perforin and granzymes: function, dysfunction and human pathology. *Nature Reviews Immunology* **15**, 388-400, doi:10.1038/nri3839 (2015).
27 Ben-Sasson, S. Z. *et al.* IL-1 acts directly on CD4 T cells to enhance their antigen-driven expansion and differentiation. *Proc Natl Acad Sci* **106**, 7119-7124, doi:10.1073/pnas.0902745106 (2009).
28 Schorle, H., Holtschke, T., Hünig, T., Schimpl, A. & Horak, I. Development and function of T cells in mice rendered interleukin-2 deficient by gene targeting. *Nature* **352**, 621-624, doi:10.1038/352621a0 (1991).
29 Kochan, G., Escors, D., Breckpot, K. & Guerrero-Setas, D. Role of non-classical MHC class I molecules in cancer immunosuppression. *OncoImmunology* **2**, e26491, doi:10.4161/onci.26491 (2013).
30 Wieczorek, M. *et al.* Major Histocompatibility Complex (MHC) Class I and MHC Class II Proteins: Conformational Plasticity in Antigen Presentation. *Front Immunol* **8**, doi:10.3389/fimmu.2017.00292 (2017).
31 Neefjes, J., Jongsma, M. L. M., Paul, P. & Bakke, O. Towards a systems understanding of MHC class I and MHC class II antigen presentation. *Nature Reviews Immunology* **11**, 823, doi:10.1038/nri3084 (2011).
32 Szeto, C., Lobos, C. A., Nguyen, A. T. & Gras, S. TCR Recognition of Peptide–MHC-I: Rule Makers and Breakers. *Int J Mol Sci* **22**, 68 (2021).
33 Bartee, E., Mansouri, M., Nerenberg, B. T. H., Gouveia, K. & Früh, K. Downregulation of Major Histocompatibility Complex Class I by Human Ubiquitin Ligases Related to Viral Immune Evasion Proteins. *J Virol* **78**, 1109-1120, doi:10.1128/JVI.78.3.1109-1120.2004 (2004).
34 Chicz, R. M. *et al.* Predominant naturally processed peptides bound to HLA-DR1 are derived from MHC-related molecules and are heterogeneous in size. *Nature* **358**, 764-768, doi:10.1038/358764a0 (1992).
35 Shin, J.-S. *et al.* Surface expression of MHC class II in dendritic cells is controlled by regulated ubiquitination. *Nature* **444**, 115-118, doi:10.1038/nature05261 (2006).
36 van Niel, G. *et al.* Dendritic Cells Regulate Exposure of MHC Class II at Their Plasma Membrane by Oligoubiquitination. *Immunity* **25**, 885-894, doi:10.1016/j.immuni.2006.11.001 (2006).

37 Matsuki, Y. *et al.* Novel regulation of MHC class II function in B cells. *The EMBO Journal* **26**, 846-854, doi:10.1038/sj.emboj.7601556 (2007).
38 Gauvreau, M.-É. *et al.* Sorting of MHC Class II Molecules into Exosomes through a Ubiquitin-Independent Pathway. *Traffic* **10**, 1518-1527, doi:10.1111/j.1600-0854.2009.00948.x (2009).
39 Segura, E. *et al.* ICAM-1 on exosomes from mature dendritic cells is critical for efficient naive T-cell priming. *Blood* **106**, 216-223, doi:10.1182/blood-2005-01-0220 (2005).
40 Vijayan, S., Sidiq, T., Yousuf, S., van den Elsen, P. J. & Kobayashi, K. S. Class I transactivator, NLRC5: a central player in the MHC class I pathway and cancer immune surveillance. *Immunogenetics* **71**, 273-282, doi:10.1007/s00251-019-01106-z (2019).
41 Gobin, S. J., van Zutphen, M., Westerheide, S. D., Boss, J. M. & van den Elsen, P. J. The MHC-specific enhanceosome and its role in MHC class I and beta(2)-microglobulin gene transactivation. *J Immunol* **167**, 5175-5184, doi:10.4049/jimmunol.167.9.5175 (2001).
42 Meissner, T. B. *et al.* NLR family member NLRC5 is a transcriptional regulator of MHC class I genes. *Proceedings of the National Academy of Sciences* **107**, 13794-13799, doi:10.1073/pnas.1008684107 (2010).
43 Robbins, G. R. *et al.* Regulation of Class I Major Histocompatibility Complex (MHC) by Nucleotide-binding Domain, Leucine-rich Repeat-containing (NLR) Proteins. *Journal of Biological Chemistry* **287**, 24294-24303, doi:10.1074/jbc.M112.364604 (2012).
44 Staehli, F. *et al.* NLRC5 deficiency selectively impairs MHC class I- dependent lymphocyte killing by cytotoxic T cells. *J Immunol* **188**, 3820-3828, doi:10.4049/jimmunol.1102671 (2012).
45 Biswas, A., Meissner, T. B., Kawai, T. & Kobayashi, K. S. Cutting edge: impaired MHC class I expression in mice deficient for Nlrc5/class I transactivator. *J Immunol* **189**, 516-520, doi:10.4049/jimmunol.1200064 (2012).
46 Steimle, V., Otten, L. A., Zufferey, M. & Mach, B. Complementation cloning of an MHC class II transactivator mutated in hereditary MHC class II deficiency (or bare lymphocyte syndrome). *Cell* **75**, 135-146 (1993).
47 Yoshihama, S. *et al.* NLRC5/MHC class I transactivator is a target for immune evasion in cancer. *Proceedings of the National Academy of Sciences* **113**, 5999-6004, doi:10.1073/pnas.1602069113 (2016).
48 Otten, L. A., Steimle, V., Bontron, S. & Mach, B. Quantitative control of MHC class II expression by the transactivator CIITA. *Eur. J. Immunol.* **28**, 473-478, doi:10.1002/(SICI)1521-4141(199802)28:02<473::AID-IMMU473>3.0.CO;2-E (1998).
49 Ludigs, K. *et al.* NLRC5 Exclusively Transactivates MHC Class I and Related Genes through a Distinctive SXY Module. *PLoS Genet* **11**, e1005088, doi:10.1371/journal.pgen.1005088 (2015).
50 René, C., Lozano, C. & Eliaou, J. F. Expression of classical HLA class I molecules: regulation and clinical impacts. *HLA* **87**, 338-349, doi:10.1111/tan.12787 (2016).
51 Weissman, J. D. & Singer, D. S. A complex regulatory DNA element associated with a major histocompatibility complex class I gene consists of both a silencer and an enhancer. *Mol Cell Biol* **11**, 4217-4227, doi:10.1128/mcb.11.8.4217-4227.1991 (1991).
52 Murphy, C., Nikodem, D., Howcroft, K., Weissman, J. D. & Singer, D. S. Active Repression of Major Histocompatibility Complex Class I Genes in a Human Neuroblastoma Cell Line. *Journal of Biological Chemistry* **271**, 30992-30999, doi:10.1074/jbc.271.48.30992 (1996).
53 van den Elsen, P. Expression Regulation of Major Histocompatibility Complex Class I and Class II Encoding Genes. *Front Immunol* **2**, doi:10.3389/fimmu.2011.00048 (2011).
54 Ting, J. P.-Y. & Trowsdale, J. Genetic Control of MHC Class II Expression. *Cell* **109**, S21-S33, doi:10.1016/S0092-8674(02)00696-7 (2002).

55 Waldburger, J. M., Suter, T., Fontana, A., Acha-Orbea, H. & Reith, W. Selective abrogation of major histocompatibility complex class II expression on extrahematopoietic cells in mice lacking promoter IV of the class II transactivator gene. *J Exp Med* **194**, 393-406, doi:10.1084/jem.194.4.393 (2001).

56 Osborne, A., Zhang, H., Yang, W.-M., Seto, E. & Blanck, G. Histone Deacetylase Activity Represses Gamma Interferon-Inducible HLA-DR Gene Expression following the Establishment of a DNase I-Hypersensitive Chromatin Conformation. *Molecular and Cellular Biology* **21**, 6495-6506, doi:10.1128/MCB.21.19.6495-6506.2001 (2001).

57 Kanaseki, T. *et al.* Histone deacetylation, but not hypermethylation, modifies class II transactivator and MHC class II gene expression in squamous cell carcinomas. *J Immunol* **170**, 4980-4985, doi:10.4049/jimmunol.170.10.4980 (2003).

58 Zika, E., Greer, S. F., Zhu, X.-S. & Ting, J. P.-Y. Histone Deacetylase 1/mSin3A Disrupts Gamma Interferon-Induced CIITA Function and Major Histocompatibility Complex Class II Enhanceosome Formation. *Molecular and Cellular Biology* **23**, 3091-3102, doi:10.1128/mcb.23.9.3091-3102.2003 (2003).

59 Morris, A. C., Spangler, W. E. & Boss, J. M. Methylation of class II trans-activator promoter IV: a novel mechanism of MHC class II gene control. *J Immunol* **164**, 4143-4149, doi:10.4049/jimmunol.164.8.4143 (2000).

60 van den Elsen, P. J. *et al.* Lack of CIITA expression is central to the absence of antigen presentation functions of trophoblast cells and is caused by methylation of the IFN-γ inducible promoter (PIV) of CIITA. *Human Immunology* **61**, 850-862, doi:10.1016/S0198-8859(00)00159-2 (2000).

61 Morris, A. C., Beresford, G. W., Mooney, M. R. & Boss, J. M. Kinetics of a gamma interferon response: expression and assembly of CIITA promoter IV and inhibition by methylation. *Mol Cell Biol* **22**, 4781-4791, doi:10.1128/mcb.22.13.4781-4791.2002 (2002).

62 Piskurich, J. F. *et al.* BLIMP-1 mediates extinction of major histocompatibility class II transactivator expression in plasma cells. *Nature Immunology* **1**, 526-532, doi:10.1038/82788 (2000).

63 Marin-Acevedo, J. A., Kimbrough, E. O. & Lou, Y. Next generation of immune checkpoint inhibitors and beyond. *Journal of Hematology & Oncology* **14**, 45, doi:10.1186/s13045-021-01056-8 (2021).

64 Brunet, J.-F. *et al.* A new member of the immunoglobulin superfamily—CTLA-4. *Nature* **328**, 267-270, doi:10.1038/328267a0 (1987).

65 Collins, A. V. *et al.* The Interaction Properties of Costimulatory Molecules Revisited. *Immunity* **17**, 201-210, doi:10.1016/S1074-7613(02)00362-X (2002).

66 Schneider, H. *et al.* Reversal of the TCR Stop Signal by CTLA-4. *Science* **313**, 1972-1975, doi:10.1126/science.1131078 (2006).

67 Qureshi, O. S. *et al.* Trans-Endocytosis of CD80 and CD86: A Molecular Basis for the Cell-Extrinsic Function of CTLA-4. *Science* **332**, 600-603, doi:10.1126/science.1202947 (2011).

68 Marengère, L. E. *et al.* Regulation of T cell receptor signaling by tyrosine phosphatase SYP association with CTLA-4. *Science* **272**, 1170-1173, doi:10.1126/science.272.5265.1170 (1996).

69 Chuang, E. *et al.* The CD28 and CTLA-4 receptors associate with the serine/threonine phosphatase PP2A. *Immunity* **13**, 313-322, doi:10.1016/s1074-7613(00)00031-5 (2000).

70 Greenwald, R. J., Boussiotis, V. A., Lorsbach, R. B., Abbas, A. K. & Sharpe, A. H. CTLA-4 Regulates Induction of Anergy In Vivo. *Immunity* **14**, 145-155, doi:10.1016/S1074-7613(01)00097-8 (2001).

71 Tivol, E. A. *et al.* Loss of CTLA-4 leads to massive lymphoproliferation and fatal multiorgan tissue destruction, revealing a critical negative regulatory role of CTLA-4. *Immunity* **3**, 541-547, doi:10.1016/1074-7613(95)90125-6 (1995).
72 Waterhouse, P. *et al.* Lymphoproliferative Disorders with Early Lethality in Mice Deficient in Ctla-4. *Science* **270**, 985-988, doi:10.1126/science.270.5238.985 (1995).
73 Hodi, F. S. *et al.* Biologic activity of cytotoxic T lymphocyte-associated antigen 4 antibody blockade in previously vaccinated metastatic melanoma and ovarian carcinoma patients. *Proc Natl Acad Sci U S A* **100**, 4712-4717, doi:10.1073/pnas.0830997100 (2003).
74 Phan, G. Q. *et al.* Cancer regression and autoimmunity induced by cytotoxic T lymphocyte-associated antigen 4 blockade in patients with metastatic melanoma. *Proc Natl Acad Sci U S A* **100**, 8372-8377, doi:10.1073/pnas.1533209100 (2003).
75 Seidel, J. A., Otsuka, A. & Kabashima, K. Anti-PD-1 and Anti-CTLA-4 Therapies in Cancer: Mechanisms of Action, Efficacy, and Limitations. *Front Oncol* **8**, 86, doi:10.3389/fonc.2018.00086 (2018).
76 Ishida, Y., Agata, Y., Shibahara, K. & Honjo, T. Induced expression of PD-1, a novel member of the immunoglobulin gene superfamily, upon programmed cell death. *EMBO J* **11**, 3887-3895, doi:10.1002/j.1460-2075.1992.tb05481.x (1992).
77 Agata, Y. *et al.* Expression of the PD-1 antigen on the surface of stimulated mouse T and B lymphocytes. *Int Immunol* **8**, 765-772, doi:10.1093/intimm/8.5.765 (1996).
78 Parry, R. V. *et al.* CTLA-4 and PD-1 receptors inhibit T-cell activation by distinct mechanisms. *Mol Cell Biol* **25**, 9543-9553, doi:10.1128/mcb.25.21.9543-9553.2005 (2005).
79 Freeman, G. J. *et al.* Engagement of the Pd-1 Immunoinhibitory Receptor by a Novel B7 Family Member Leads to Negative Regulation of Lymphocyte Activation. *The Journal of Experimental Medicine* **192**, 1027-1034, doi:10.1084/jem.192.7.1027 (2000).
80 Hui, E. *et al.* T cell costimulatory receptor CD28 is a primary target for PD-1-mediated inhibition. *Science* **355**, 1428-1433, doi:10.1126/science.aaf1292 (2017).
81 Barber, D. L. *et al.* Restoring function in exhausted CD8 T cells during chronic viral infection. *Nature* **439**, 682-687, doi:10.1038/nature04444 (2006).
82 Crawford, A. *et al.* Molecular and transcriptional basis of $CD4^+$ T cell dysfunction during chronic infection. *Immunity* **40**, 289-302, doi:10.1016/j.immuni.2014.01.005 (2014).
83 Fourcade, J. *et al.* Upregulation of Tim-3 and PD-1 expression is associated with tumor antigen-specific CD8+ T cell dysfunction in melanoma patients. *J Exp Med* **207**, 2175-2186, doi:10.1084/jem.20100637 (2010).
84 Matsuzaki, J. *et al.* Tumor-infiltrating NY-ESO-1-specific CD8+ T cells are negatively regulated by LAG-3 and PD-1 in human ovarian cancer. *Proc Natl Acad Sci U S A* **107**, 7875-7880, doi:10.1073/pnas.1003345107 (2010).
85 Sharpe, A. H. & Pauken, K. E. The diverse functions of the PD1 inhibitory pathway. *Nature Reviews Immunology* **18**, 153-167, doi:10.1038/nri.2017.108 (2018).
86 Topalian, S. L. *et al.* Safety, Activity, and Immune Correlates of Anti–PD-1 Antibody in Cancer. *New England Journal of Medicine* **366**, 2443-2454, doi:10.1056/NEJMoa1200690 (2012).
87 Brahmer, J. R. *et al.* Safety and Activity of Anti–PD-L1 Antibody in Patients with Advanced Cancer. *New England Journal of Medicine* **366**, 2455-2465, doi:10.1056/NEJMoa1200694 (2012).
88 Das, S. & Johnson, D. B. Immune-related adverse events and anti-tumor efficacy of immune checkpoint inhibitors. *Journal for ImmunoTherapy of Cancer* **7**, 306, doi:10.1186/s40425-019-0805-8 (2019).
89 Robert, C. A decade of immune-checkpoint inhibitors in cancer therapy. *Nature Communications* **11**, 3801, doi:10.1038/s41467-020-17670-y (2020).

90 Gogas, H. J., Kirkwood, J. M. & Sondak, V. K. Chemotherapy for metastatic melanoma. *Cancer* **109**, 455-464, doi:doi.org/10.1002/cncr.22427 (2007).
91 Larkin, J. *et al.* Five-Year Survival with Combined Nivolumab and Ipilimumab in Advanced Melanoma. *New England Journal of Medicine* **381**, 1535-1546, doi:10.1056/NEJMoa1910836 (2019).
92 Martins, F. *et al.* Adverse effects of immune-checkpoint inhibitors: epidemiology, management and surveillance. *Nature Reviews Clinical Oncology* **16**, 563-580, doi:10.1038/s41571-019-0218-0 (2019).
93 Wang, D. Y. *et al.* Fatal Toxic Effects Associated With Immune Checkpoint Inhibitors: A Systematic Review and Meta-analysis. *JAMA Oncology* **4**, 1721-1728, doi:10.1001/jamaoncol.2018.3923 (2018).
94 Finck, A. V., Blanchard, T., Roselle, C. P., Golinelli, G. & June, C. H. Engineered cellular immunotherapies in cancer and beyond. *Nature Medicine* **28**, 678-689, doi:10.1038/s41591-022-01765-8 (2022).
95 Maude, S. L. *et al.* Tisagenlecleucel in Children and Young Adults with B-Cell Lymphoblastic Leukemia. *New England Journal of Medicine* **378**, 439-448, doi:10.1056/NEJMoa1709866 (2018).
96 Locke, F. L. *et al.* Axicabtagene Ciloleucel as Second-Line Therapy for Large B-Cell Lymphoma. *New England Journal of Medicine* **386**, 640-654, doi:10.1056/NEJMoa2116133 (2021).
97 Melenhorst, J. J. *et al.* Decade-long leukaemia remissions with persistence of CD4+ CAR T cells. *Nature* **602**, 503-509, doi:10.1038/s41586-021-04390-6 (2022).
98 Hill, J. A. & Seo, S. K. How I prevent infections in patients receiving CD19-targeted chimeric antigen receptor T cells for B-cell malignancies. *Blood* **136**, 925-935, doi:10.1182/blood.2019004000 (2020).
99 Shah, N. N. & Fry, T. J. Mechanisms of resistance to CAR T cell therapy. *Nature Reviews Clinical Oncology* **16**, 372-385, doi:10.1038/s41571-019-0184-6 (2019).
100 Copelan, E. A. Hematopoietic Stem-Cell Transplantation. *N Engl J Med* **354**, 1813-1826, doi:10.1056/NEJMra052638 (2006).
101 Giralt, S. *et al.* Engraftment of allogeneic hematopoietic progenitor cells with purine analog-containing chemotherapy: harnessing graft-versus-leukemia without myeloablative therapy. *Blood* **89**, 4531-4536 (1997).
102 McSweeney, P. A. *et al.* Hematopoietic cell transplantation in older patients with hematologic malignancies: replacing high-dose cytotoxic therapy with graft-versus-tumor effects. *Blood* **97**, 3390-3400, doi:10.1182/blood.v97.11.3390 (2001).
103 Baron, F. *et al.* Graft-versus-tumor effects after allogeneic hematopoietic cell transplantation with nonmyeloablative conditioning. *Journal of clinical oncology : official journal of the American Society of Clinical Oncology* **23**, 1993-2003, doi:10.1200/jco.2005.08.136 (2005).
104 Nagler, A. & Mohty, M. In 2022, which is preferred: haploidentical or cord transplant? *Hematology* **2022**, 64-73, doi:10.1182/hematology.2022000327 (2022).
105 Gatti, R. A., Meuwissen, H. J., Allen, H. D., Hong, R. & Good, R. A. Immunological reconstitution of sex-linked lymphopenic immunological deficiency. *The Lancet* **292**, 1366-1369, doi:10.1016/S0140-6736(68)92673-1 (1968).
106 Thomas, E. D. *et al.* Allogeneic marrow grafting for hematologic malignancy using HL-A matched donor-recipient sibling pairs. *Blood* **38**, 267-287 (1971).
107 Singh, A. K. & McGuirk, J. P. Allogeneic Stem Cell Transplantation: A Historical and Scientific Overview. *Cancer Res* **76**, 6445-6451, doi:10.1158/0008-5472.Can-16-1311 (2016).

108 Lee, S. J. *et al.* High-resolution donor-recipient HLA matching contributes to the success of unrelated donor marrow transplantation. *Blood* **110**, 4576-4583, doi:10.1182/blood-2007-06-097386 (2007).
109 Weiden, P. L., Sullivan, K. M., Flournoy, N., Storb, R. & Thomas, E. D. Antileukemic Effect of Chronic Graft-versus-Host Disease. *New England Journal of Medicine* **304**, 1529-1533, doi:10.1056/nejm198106183042507 (1981).
110 Passweg, J. R. *et al.* Graft-versus-leukemia effects in T lineage and B lineage acute lymphoblastic leukemia. *Bone Marrow Transplant* **21**, 153-158, doi:10.1038/sj.bmt.1701064 (1998).
111 Horowitz, M. *et al.* Graft-versus-leukemia reactions after bone marrow transplantation. *Blood* **75**, 555-562, doi:10.1182/blood.V75.3.555.555 (1990).
112 Marmont, A. *et al.* T-cell depletion of HLA-identical transplants in leukemia. *Blood* **78**, 2120-2130, doi:10.1182/blood.V78.8.2120.2120 (1991).
113 Shlomchik, W. D. *et al.* Prevention of Graft Versus Host Disease by Inactivation of Host Antigen-Presenting Cells. *Science* **285**, 412-415, doi:10.1126/science.285.5426.412 (1999).
114 Matte, C. C. *et al.* Donor APCs are required for maximal GVHD but not for GVL. *Nature Medicine* **10**, 987-992, doi:10.1038/nm1089 (2004).
115 Mapara, M. Y. *et al.* Donor lymphocyte infusions mediate superior graft-versus-leukemia effects in mixed compared to fully allogeneic chimeras: a critical role for host antigen–presenting cells. *Blood* **100**, 1903-1909, doi:10.1182/blood-2002-01-0023 (2002).
116 Reddy, P. *et al.* A crucial role for antigen-presenting cells and alloantigen expression in graft-versus-leukemia responses. *Nature Medicine* **11**, 1244-1249, doi:10.1038/nm1309 (2005).
117 Bosch, G., Joosten, A., Kessler, J., Melief, C. & Leeksma, O. Recognition of BCR-ABL positive leukemic blasts by human CD4+ T cells elicited by primary in vitro immunization with a BCR-ABL breakpoint peptide. *Blood* **88**, 3522-3527, doi:10.1182/blood.V88.9.3522.bloodjournal8893522 (1996).
118 Yasukawa, M. *et al.* CD4+ Cytotoxic T-Cell Clones Specific for bcr-abl b3a2 Fusion Peptide Augment Colony Formation by Chronic Myelogenous Leukemia Cells in a b3a2-Specific and HLA-DR–Restricted Manner. *Blood* **92**, 3355-3361, doi:10.1182/blood.V92.9.3355 (1998).
119 Porakishvili, N. *et al.* Cytotoxic CD4+ T cells in patients with B cell chronic lymphocytic leukemia kill via a perforin-mediated pathway. *Haematologica* **89**, 435-443 (2004).
120 Khanna, R. *et al.* Class I processing-defective Burkitt's lymphoma cells are recognized efficiently by CD4+ EBV-specific CTLs. *J Immunol* **158**, 3619-3625 (1997).
121 Quezada, S. A. *et al.* Tumor-reactive CD4+ T cells develop cytotoxic activity and eradicate large established melanoma after transfer into lymphopenic hosts. *Journal of Experimental Medicine* **207**, 637-650, doi:10.1084/jem.20091918 (2010).
122 Xie, Y. *et al.* Naive tumor-specific CD4+ T cells differentiated in vivo eradicate established melanoma. *Journal of Experimental Medicine* **207**, 651-667, doi:10.1084/jem.20091921 (2010).
123 Oh, D. Y. *et al.* Intratumoral CD4+ T Cells Mediate Anti-tumor Cytotoxicity in Human Bladder Cancer. *Cell*, doi:10.1016/j.cell.2020.05.017 (2020).
124 Cachot, A. *et al.* Tumor-specific cytolytic CD4 T cells mediate immunity against human cancer. *Science Advances* **7**, eabe3348, doi:10.1126/sciadv.abe3348 (2021).
125 Schürch, C., Riether, C., Amrein, M. A. & Ochsenbein, A. F. Cytotoxic T cells induce proliferation of chronic myeloid leukemia stem cells by secreting interferon-γ. *J Exp Med* **210**, 605-621, doi:10.1084/jem.20121229 (2013).
126 Michallet, M. *et al.* Allogeneic Hematopoietic Stem-Cell Transplantation After Nonmyeloablative Preparative Regimens: Impact of Pretransplantation and

Posttransplantation Factors on Outcome. *Journal of Clinical Oncology* **19**, 3340-3349, doi:10.1200/JCO.2001.19.14.3340 (2001).

127 Ruggeri, L. *et al.* Effectiveness of Donor Natural Killer Cell Alloreactivity in Mismatched Hematopoietic Transplants. *Science* **295**, 2097-2100, doi:10.1126/science.1068440 (2002).

128 Gill, S., Olson, J. A. & Negrin, R. S. Natural Killer Cells in Allogeneic Transplantation: Effect on Engraftment, Graft- versus-Tumor, and Graft-versus-Host Responses. *Biol. Blood Marrow Transplant.* **15**, 765-776, doi:10.1016/j.bbmt.2009.01.019 (2009).

129 Albertsson, P. A. *et al.* NK cells and the tumour microenvironment: implications for NK-cell function and anti-tumour activity. *Trends in Immunology* **24**, 603-609, doi:10.1016/j.it.2003.09.007 (2003).

130 Nowbakht, P. *et al.* Ligands for natural killer cell-activating receptors are expressed upon the maturation of normal myelomonocytic cells but at low levels in acute myeloid leukemias. *Blood* **105**, 3615-3622, doi:10.1182/blood-2004-07-2585 (2005).

131 Pende, D. *et al.* Analysis of the receptor-ligand interactions in the natural killer-mediated lysis of freshly isolated myeloid or lymphoblastic leukemias: evidence for the involvement of the Poliovirus receptor (CD155) and Nectin-2 (CD112). *Blood* **105**, 2066-2073, doi:10.1182/blood-2004-09-3548 (2005).

132 Romanski, A. *et al.* Mechanisms of resistance to natural killer cell-mediated cytotoxicity in acute lymphoblastic leukemia. *Exp Hematol* **33**, 344-352, doi:10.1016/j.exphem.2004.11.006 (2005).

133 Axelrod, M. L., Cook, R. S., Johnson, D. B. & Balko, J. M. Biological Consequences of MHC-II Expression by Tumor Cells in Cancer. *Clin. Cancer Res.* **25**, 2392-2402, doi:10.1158/1078-0432.CCR-18-3200 (2019).

134 Rimsza, L. M. *et al.* Loss of MHC class II gene and protein expression in diffuse large B-cell lymphoma is related to decreased tumor immunosurveillance and poor patient survival regardless of other prognostic factors: a follow-up study from the Leukemia and Lymphoma Molecular Profiling Project. *Blood* **103**, 4251-4258, doi:10.1182/blood-2003-07-2365 (2004).

135 Roemer, M. G. M. *et al.* Major Histocompatibility Complex Class II and Programmed Death Ligand 1 Expression Predict Outcome After Programmed Death 1 Blockade in Classic Hodgkin Lymphoma. *J. Clin. Oncol.* **36**, 942-950, doi:10.1200/JCO.2017.77.3994 (2018).

136 Johnson, A. M. *et al.* Cancer Cell–Intrinsic Expression of MHC Class II Regulates the Immune Microenvironment and Response to Anti–PD-1 Therapy in Lung Adenocarcinoma. *J. Immunol.* **204**, 2295-2307, doi:10.4049/jimmunol.1900778 (2020).

137 Forero, A. *et al.* Expression of the MHC Class II Pathway in Triple-Negative Breast Cancer Tumor Cells is Associated with a Good Prognosis and Infiltrating Lymphocytes. *Cancer Immunol. Res.* **4**, 390-399, doi:10.1158/2326-6066.CIR-15-0243 (2016).

138 Park, I. A. *et al.* Expression of the MHC class II in triple-negative breast cancer is associated with tumor-infiltrating lymphocytes and interferon signaling. *PLoS One* **12**, e0182786, doi:10.1371/journal.pone.0182786 (2017).

139 Callahan, M. J. *et al.* Increased HLA-DMB expression in the tumor epithelium is associated with increased CTL infiltration and improved prognosis in advanced-stage serous ovarian cancer. *Clin Cancer Res* **14**, 7667-7673, doi:10.1158/1078-0432.Ccr-08-0479 (2008).

140 Johnson, D. B. *et al.* Melanoma-specific MHC-II expression represents a tumour-autonomous phenotype and predicts response to anti-PD-1/PD-L1 therapy. *Nat. Commun.* **7**, 10582, doi:10.1038/ncomms10582 (2016).

141 Liu, D. *et al.* Integrative molecular and clinical modeling of clinical outcomes to PD1 blockade in patients with metastatic melanoma. *Nat. Med.* **25**, 1916-1927, doi:10.1038/s41591-019-0654-5 (2019).
142 Ostrand-Rosenberg, S., Thakur, A. & Clements, V. Rejection of mouse sarcoma cells after transfection of MHC class II genes. *J Immunol* **144**, 4068-4071 (1990).
143 Baskar, S., Clements, V. K., Glimcher, L. H., Nabavi, N. & Ostrand-Rosenberg, S. Rejection of MHC class II-transfected tumor cells requires induction of tumor-encoded B7-1 and/or B7-2 costimulatory molecules. *J Immunol* **156**, 3821-3827 (1996).
144 Panelli, M. C. *et al.* Interferon γ (IFNγ) gene transfer of an EMT6 tumor that is poorly responsive to IFNγ stimulation: increase in tumor immunogenicity is accompanied by induction of a mouse class II transactivator and class II MHC. *Cancer Immunology, Immunotherapy* **42**, 99-107, doi:10.1007/s002620050258 (1996).
145 Mortara, L. *et al.* CIITA-Induced MHC Class II Expression in Mammary Adenocarcinoma Leads to a Th1 Polarization of the Tumor Microenvironment, Tumor Rejection, and Specific Antitumor Memory. *Clinical Cancer Research* **12**, 3435-3443, doi:10.1158/1078-0432.Ccr-06-0165 (2006).
146 Bou Nasser Eddine, F. *et al.* CIITA-driven MHC class II expressing tumor cells can efficiently prime naive CD4+ TH cells in vivo and vaccinate the host against parental MHC-II-negative tumor cells. *OncoImmunology* **6**, e1261777, doi:10.1080/2162402X.2016.1261777 (2017).
147 Martin, B. K., Frelinger, J. G. & Ting, J. P. Combination gene therapy with CD86 and the MHC class II transactivator in the control of lung tumor growth. *J Immunol* **162**, 6663-6670 (1999).
148 Clements, V. K., Baskar, S., Armstrong, T. D. & Ostrand-Rosenberg, S. Invariant chain alters the malignant phenotype of MHC class II+ tumor cells. *J Immunol* **149**, 2391-2396 (1992).
149 Marine, J.-C., Dawson, S.-J. & Dawson, M. A. Non-genetic mechanisms of therapeutic resistance in cancer. *Nature Reviews Cancer* **20**, 743-756, doi:10.1038/s41568-020-00302-4 (2020).
150 Zaretsky, J. M. *et al.* Mutations Associated with Acquired Resistance to PD-1 Blockade in Melanoma. *New England Journal of Medicine* **375**, 819-829, doi:10.1056/NEJMoa1604958 (2016).
151 Sade-Feldman, M. *et al.* Resistance to checkpoint blockade therapy through inactivation of antigen presentation. *Nature Communications* **8**, 1136, doi:10.1038/s41467-017-01062-w (2017).
152 Le, D. T. *et al.* Mismatch repair deficiency predicts response of solid tumors to PD-1 blockade. *Science* **357**, 409-413, doi:10.1126/science.aan6733 (2017).
153 Gettinger, S. *et al.* Impaired HLA Class I Antigen Processing and Presentation as a Mechanism of Acquired Resistance to Immune Checkpoint Inhibitors in Lung Cancer. *Cancer Discovery* **7**, 1420-1435, doi:10.1158/2159-8290.CD-17-0593 (2017).
154 Chen, H. L. *et al.* A functionally defective allele of TAP1 results in loss of MHC class I antigen presentation in a human lung cancer. *Nat Genet* **13**, 210-213, doi:10.1038/ng0696-210 (1996).
155 Seliger, B. *et al.* Immune escape of melanoma: first evidence of structural alterations in two distinct components of the MHC class I antigen processing pathway. *Cancer Res* **61**, 8647-8650 (2001).
156 Kloor, M. *et al.* Immunoselective pressure and human leukocyte antigen class I antigen machinery defects in microsatellite unstable colorectal cancers. *Cancer Res* **65**, 6418-6424, doi:10.1158/0008-5472.Can-05-0044 (2005).
157 Chang, C.-C. *et al.* Multiple Structural and Epigenetic Defects in the Human Leukocyte Antigen Class I Antigen Presentation Pathway in a Recurrent Metastatic Melanoma

Following Immunotherapy. *Journal of Biological Chemistry* **290**, 26562-26575, doi:10.1074/jbc.M115.676130 (2015).

158 Middha, S. *et al.* Majority of B2M-Mutant and -Deficient Colorectal Carcinomas Achieve Clinical Benefit From Immune Checkpoint Inhibitor Therapy and Are Microsatellite Instability-High. *JCO Precis Oncol* **3**, doi:10.1200/po.18.00321 (2019).

159 de Vries, N. L. *et al.* γδ T cells are effectors of immunotherapy in cancers with HLA class I defects. *Nature* **613**, 743-750, doi:10.1038/s41586-022-05593-1 (2023).

160 Ye, Q. *et al.* Hypermethylation of HLA class I gene is associated with HLA class I down-regulation in human gastric cancer. *Tissue Antigens* **75**, 30-39, doi:10.1111/j.1399-0039.2009.01390.x (2010).

161 Nie, Y. *et al.* DNA hypermethylation is a mechanism for loss of expression of the HLA class I genes in human esophageal squamous cell carcinomas. *Carcinogenesis* **22**, 1615-1623, doi:10.1093/carcin/22.10.1615 (2001).

162 Yoshihama, S. *et al.* NLRC5/CITA expression correlates with efficient response to checkpoint blockade immunotherapy. *Sci Rep* **11**, 3258, doi:10.1038/s41598-021-82729-9 (2021).

163 Meyer, S. *et al.* Distinct Molecular Mechanisms of Altered HLA Class II Expression in Malignant Melanoma. *Cancers (Basel)* **13**, 3907 (2021).

164 Satoh, A. *et al.* Epigenetic inactivation of class II transactivator (CIITA) is associated with the absence of interferon-gamma-induced HLA-DR expression in colorectal and gastric cancer cells. *Oncogene* **23**, 8876-8886, doi:10.1038/sj.onc.1208144 (2004).

165 Holling, T. M., Schooten, E., Langerak, A. W. & van den Elsen, P. J. Regulation of MHC class II expression in human T-cell malignancies. *Blood* **103**, 1438-1444, doi:10.1182/blood-2003-05-1491 (2004).

166 Luo, N. *et al.* DNA methyltransferase inhibition upregulates MHC-I to potentiate cytotoxic T lymphocyte responses in breast cancer. *Nat Commun* **9**, 248, doi:10.1038/s41467-017-02630-w (2018).

167 Fonsatti, E. *et al.* Functional Up-regulation of Human Leukocyte Antigen Class I Antigens Expression by 5-aza-2′-deoxycytidine in Cutaneous Melanoma: Immunotherapeutic Implications. *Clinical Cancer Research* **13**, 3333-3338, doi:10.1158/1078-0432.Ccr-06-3091 (2007).

168 Siebenkäs, C. *et al.* Inhibiting DNA methylation activates cancer testis antigens and expression of the antigen processing and presentation machinery in colon and ovarian cancer cells. *PLoS One* **12**, e0179501, doi:10.1371/journal.pone.0179501 (2017).

169 Liu, J. H., Bian, Y. M., Xie, Y. & Lu, D. P. Epigenetic modification and preliminary investigation of the mechanism of the immune evasion of HL-60 cells. *Molecular medicine reports* **12**, 1059-1065, doi:10.3892/mmr.2015.3526 (2015).

170 Turner, T. B. *et al.* Epigenetic modifiers upregulate MHC II and impede ovarian cancer tumor growth. *Oncotarget* **8** (2017).

171 Khan, A. N. H., Gregorie, C. J. & Tomasi, T. B. Histone deacetylase inhibitors induce TAP, LMP, Tapasin genes and MHC class I antigen presentation by melanoma cells. *Cancer Immunology, Immunotherapy* **57**, 647-654, doi:10.1007/s00262-007-0402-4 (2008).

172 Sun, T. *et al.* Histone deacetylase inhibition up-regulates MHC class I to facilitate cytotoxic T lymphocyte-mediated tumor cell killing in glioma cells. *J Cancer* **10**, 5638-5645, doi:10.7150/jca.34471 (2019).

173 Londhe, P., Zhu, B., Abraham, J., Keller, C. & Davie, J. CIITA is silenced by epigenetic mechanisms that prevent the recruitment of transactivating factors in rhabdomyosarcoma cells. *Int J Cancer* **131**, E437-E448, doi:10.1002/ijc.26478 (2012).

174 Sheng, W. *et al.* LSD1 Ablation Stimulates Anti-tumor Immunity and Enables Checkpoint Blockade. *Cell* **174**, 549-563.e519, doi:10.1016/j.cell.2018.05.052 (2018).

175 Chiappinelli, K. B. *et al.* Inhibiting DNA Methylation Causes an Interferon Response in Cancer via dsRNA Including Endogenous Retroviruses. *Cell* **162**, 974-986, doi:10.1016/j.cell.2015.07.011 (2015).
176 Daskalakis, M. *et al.* Reactivation of endogenous retroviral elements via treatment with DNMT- and HDAC-inhibitors. *Cell Cycle* **17**, 811-822, doi:10.1080/15384101.2018.1442623 (2018).
177 Fennell, K. A., Bell, C. C. & Dawson, M. A. Epigenetic therapies in acute myeloid leukemia: where to from here? *Blood* **134**, 1891-1901, doi:10.1182/blood.2019003262 (2019).
178 Rosenthal, R. *et al.* Neoantigen-directed immune escape in lung cancer evolution. *Nature* **567**, 479-485, doi:10.1038/s41586-019-1032-7 (2019).
179 Lee, J. H. *et al.* Transcriptional downregulation of MHC class I and melanoma de-differentiation in resistance to PD-1 inhibition. *Nature Communications* **11**, 1897, doi:10.1038/s41467-020-15726-7 (2020).
180 Bar, J. *et al.* Transformation to small cell lung cancer as a mechanism of resistance to immunotherapy in non-small cell lung cancer. *Lung Cancer* **138**, 109-115, doi:10.1016/j.lungcan.2019.09.025 (2019).
181 Iams, W. T. *et al.* Small Cell Lung Cancer Transformation as a Mechanism of Resistance to PD-1 Therapy in KRAS-Mutant Lung Adenocarcinoma: A Report of Two Cases. *Journal of Thoracic Oncology* **14**, e45-e48, doi:10.1016/j.jtho.2018.11.031 (2019).
182 Gao, J. *et al.* Loss of IFN-γ Pathway Genes in Tumor Cells as a Mechanism of Resistance to Anti-CTLA-4 Therapy. *Cell* **167**, 397-404.e399, doi:10.1016/j.cell.2016.08.069 (2016).
183 Sucker, A. *et al.* Acquired IFNγ resistance impairs anti-tumor immunity and gives rise to T-cell-resistant melanoma lesions. *Nat Commun* **8**, 15440, doi:10.1038/ncomms15440 (2017).
184 Shin, D. S. *et al.* Primary Resistance to PD-1 Blockade Mediated by JAK1/2 Mutations. *Cancer Discovery* **7**, 188-201, doi:10.1158/2159-8290.cd-16-1223 (2017).
185 Green, M. R. *et al.* Integrative analysis reveals selective 9p24.1 amplification, increased PD-1 ligand expression, and further induction via JAK2 in nodular sclerosing Hodgkin lymphoma and primary mediastinal large B-cell lymphoma. *Blood* **116**, 3268-3277, doi:10.1182/blood-2010-05-282780 (2010).
186 Rooney, M. S., Shukla, S. A., Wu, C. J., Getz, G. & Hacohen, N. Molecular and genetic properties of tumors associated with local immune cytolytic activity. *Cell* **160**, 48-61, doi:10.1016/j.cell.2014.12.033 (2015).
187 Lastwika, K. J. *et al.* Control of PD-L1 Expression by Oncogenic Activation of the AKT-mTOR Pathway in Non-Small Cell Lung Cancer. *Cancer Res* **76**, 227-238, doi:10.1158/0008-5472.Can-14-3362 (2016).
188 Parsa, A. T. *et al.* Loss of tumor suppressor PTEN function increases B7-H1 expression and immunoresistance in glioma. *Nat Med* **13**, 84-88, doi:10.1038/nm1517 (2007).
189 Akbay, E. A. *et al.* Activation of the PD-1 pathway contributes to immune escape in EGFR-driven lung tumors. *Cancer Discov* **3**, 1355-1363, doi:10.1158/2159-8290.Cd-13-0310 (2013).
190 Casey, S. C. *et al.* MYC regulates the antitumor immune response through CD47 and PD-L1. *Science* **352**, 227-231, doi:10.1126/science.aac9935 (2016).
191 Loi, S. *et al.* RAS/MAPK Activation Is Associated with Reduced Tumor-Infiltrating Lymphocytes in Triple-Negative Breast Cancer: Therapeutic Cooperation Between MEK and PD-1/PD-L1 Immune Checkpoint Inhibitors. *Clinical Cancer Research* **22**, 1499-1509, doi:10.1158/1078-0432.Ccr-15-1125 (2016).
192 Neuwelt, A. J. *et al.* Cancer cell-intrinsic expression of MHC II in lung cancer cell lines is actively restricted by MEK/ERK signaling and epigenetic mechanisms. *J Immunother Cancer* **8**, e000441, doi:10.1136/jitc-2019-000441 (2020).

193 Peng, W. *et al.* Loss of PTEN Promotes Resistance to T Cell–Mediated Immunotherapy. *Cancer Discovery* **6**, 202-216, doi:10.1158/2159-8290.cd-15-0283 (2016).
194 Chandrasekaran, S. *et al.* Phosphoinositide 3-Kinase Signaling Can Modulate MHC Class I and II Expression. *Molecular Cancer Research* **17**, 2395-2409, doi:10.1158/1541-7786.MCR-19-0545 (2019).
195 Spranger, S., Bao, R. & Gajewski, T. F. Melanoma-intrinsic β-catenin signalling prevents anti-tumour immunity. *Nature* **523**, 231-235, doi:10.1038/nature14404 (2015).
196 Sakaguchi, S., Yamaguchi, T., Nomura, T. & Ono, M. Regulatory T Cells and Immune Tolerance. *Cell* **133**, 775-787, doi:10.1016/j.cell.2008.05.009 (2008).
197 Bates, G. J. *et al.* Quantification of regulatory T cells enables the identification of high-risk breast cancer patients and those at risk of late relapse. *Journal of clinical oncology : official journal of the American Society of Clinical Oncology* **24**, 5373-5380, doi:10.1200/jco.2006.05.9584 (2006).
198 Curiel, T. J. *et al.* Specific recruitment of regulatory T cells in ovarian carcinoma fosters immune privilege and predicts reduced survival. *Nat Med* **10**, 942-949, doi:10.1038/nm1093 (2004).
199 Sato, E. *et al.* Intraepithelial CD8+ tumor-infiltrating lymphocytes and a high CD8+/regulatory T cell ratio are associated with favorable prognosis in ovarian cancer. *Proc Natl Acad Sci U S A* **102**, 18538-18543, doi:10.1073/pnas.0509182102 (2005).
200 Saito, T. *et al.* Two FOXP3+CD4+ T cell subpopulations distinctly control the prognosis of colorectal cancers. *Nature Medicine* **22**, 679-684, doi:10.1038/nm.4086 (2016).
201 Liakou, C. I. *et al.* CTLA-4 blockade increases IFNgamma-producing CD4+ICOShi cells to shift the ratio of effector to regulatory T cells in cancer patients. *Proc Natl Acad Sci U S A* **105**, 14987-14992, doi:10.1073/pnas.0806075105 (2008).
202 Hodi, F. S. *et al.* Immunologic and clinical effects of antibody blockade of cytotoxic T lymphocyte-associated antigen 4 in previously vaccinated cancer patients. *Proc Natl Acad Sci U S A* **105**, 3005-3010, doi:10.1073/pnas.0712237105 (2008).
203 Sugiyama, D. *et al.* Anti-CCR4 mAb selectively depletes effector-type FoxP3+CD4+ regulatory T cells, evoking antitumor immune responses in humans. *Proc Natl Acad Sci U S A* **110**, 17945-17950, doi:10.1073/pnas.1316796110 (2013).
204 Huang, R.-Y., Francois, A., McGray, A. J. R., Miliotto, A. & Odunsi, K. Compensatory upregulation of PD-1, LAG-3, and CTLA-4 limits the efficacy of single-agent checkpoint blockade in metastatic ovarian cancer. *OncoImmunology* **6**, e1249561, doi:10.1080/2162402X.2016.1249561 (2017).
205 Zappasodi, R. *et al.* Rational design of anti-GITR-based combination immunotherapy. *Nature Medicine* **25**, 759-766, doi:10.1038/s41591-019-0420-8 (2019).
206 Piconese, S., Valzasina, B. & Colombo, M. P. OX40 triggering blocks suppression by regulatory T cells and facilitates tumor rejection. *J Exp Med* **205**, 825-839, doi:10.1084/jem.20071341 (2008).
207 Valzasina, B. *et al.* Triggering of OX40 (CD134) on CD4+CD25+ T cells blocks their inhibitory activity: a novel regulatory role for OX40 and its comparison with GITR. *Blood* **105**, 2845-2851, doi:10.1182/blood-2004-07-2959 (2005).
208 Veglia, F., Sanseviero, E. & Gabrilovich, D. I. Myeloid-derived suppressor cells in the era of increasing myeloid cell diversity. *Nature Reviews Immunology* **21**, 485-498, doi:10.1038/s41577-020-00490-y (2021).
209 Gabrilovich, D. I. Myeloid-Derived Suppressor Cells. *Cancer Immunology Research* **5**, 3-8, doi:10.1158/2326-6066.Cir-16-0297 (2017).
210 Yang, L. *et al.* Expansion of myeloid immune suppressor Gr+CD11b+ cells in tumor-bearing host directly promotes tumor angiogenesis. *Cancer Cell* **6**, 409-421, doi:10.1016/j.ccr.2004.08.031 (2004).

211 Yang, L. *et al.* Abrogation of TGFβ Signaling in Mammary Carcinomas Recruits Gr-1+CD11b+ Myeloid Cells that Promote Metastasis. *Cancer Cell* **13**, 23-35, doi:10.1016/j.ccr.2007.12.004 (2008).
212 Meyer, C. *et al.* Frequencies of circulating MDSC correlate with clinical outcome of melanoma patients treated with ipilimumab. *Cancer Immunol Immunother* **63**, 247-257, doi:10.1007/s00262-013-1508-5 (2014).
213 Kodumudi, K. N., Weber, A., Sarnaik, A. A. & Pilon-Thomas, S. Blockade of myeloid-derived suppressor cells after induction of lymphopenia improves adoptive T cell therapy in a murine model of melanoma. *J Immunol* **189**, 5147-5154, doi:10.4049/jimmunol.1200274 (2012).
214 Highfill, S. L. *et al.* Disruption of CXCR2-mediated MDSC tumor trafficking enhances anti-PD1 efficacy. *Sci Transl Med* **6**, 237ra267, doi:10.1126/scitranslmed.3007974 (2014).
215 Steele, C. W. *et al.* CXCR2 Inhibition Profoundly Suppresses Metastases and Augments Immunotherapy in Pancreatic Ductal Adenocarcinoma. *Cancer Cell* **29**, 832-845, doi:10.1016/j.ccell.2016.04.014 (2016).
216 Greene, S. *et al.* Inhibition of MDSC Trafficking with SX-682, a CXCR1/2 Inhibitor, Enhances NK-Cell Immunotherapy in Head and Neck Cancer Models. *Clin Cancer Res* **26**, 1420-1431, doi:10.1158/1078-0432.Ccr-19-2625 (2020).
217 Suzuki, E., Kapoor, V., Jassar, A. S., Kaiser, L. R. & Albelda, S. M. Gemcitabine selectively eliminates splenic Gr-1+/CD11b+ myeloid suppressor cells in tumor-bearing animals and enhances antitumor immune activity. *Clin Cancer Res* **11**, 6713-6721, doi:10.1158/1078-0432.Ccr-05-0883 (2005).
218 Sevko, A. *et al.* Antitumor effect of paclitaxel is mediated by inhibition of myeloid-derived suppressor cells and chronic inflammation in the spontaneous melanoma model. *J Immunol* **190**, 2464-2471, doi:10.4049/jimmunol.1202781 (2013).
219 Vincent, J. *et al.* 5-Fluorouracil selectively kills tumor-associated myeloid-derived suppressor cells resulting in enhanced T cell-dependent antitumor immunity. *Cancer Res* **70**, 3052-3061, doi:10.1158/0008-5472.Can-09-3690 (2010).
220 Nefedova, Y. *et al.* Mechanism of All-Trans Retinoic Acid Effect on Tumor-Associated Myeloid-Derived Suppressor Cells. *Cancer Research* **67**, 11021-11028, doi:10.1158/0008-5472.Can-07-2593 (2007).
221 Tobin, R. P. *et al.* Targeting myeloid-derived suppressor cells using all-trans retinoic acid in melanoma patients treated with Ipilimumab. *International Immunopharmacology* **63**, 282-291, doi:10.1016/j.intimp.2018.08.007 (2018).
222 Tavazoie, M. F. *et al.* LXR/ApoE Activation Restricts Innate Immune Suppression in Cancer. *Cell* **172**, 825-840.e818, doi:10.1016/j.cell.2017.12.026 (2018).
223 Fujita, M. *et al.* COX-2 Blockade Suppresses Gliomagenesis by Inhibiting Myeloid-Derived Suppressor Cells. *Cancer Research* **71**, 2664-2674, doi:10.1158/0008-5472.Can-10-3055 (2011).
224 Veglia, F. *et al.* Fatty acid transport protein 2 reprograms neutrophils in cancer. *Nature* **569**, 73-78, doi:10.1038/s41586-019-1118-2 (2019).
225 Mohamed, E. *et al.* The Unfolded Protein Response Mediator PERK Governs Myeloid Cell-Driven Immunosuppression in Tumors through Inhibition of STING Signaling. *Immunity* **52**, 668-682.e667, doi:10.1016/j.immuni.2020.03.004 (2020).
226 Gomez Perdiguero, E. *et al.* Tissue-resident macrophages originate from yolk-sac-derived erythro-myeloid progenitors. *Nature* **518**, 547-551, doi:10.1038/nature13989 (2015).
227 Mantovani, A., Allavena, P., Marchesi, F. & Garlanda, C. Macrophages as tools and targets in cancer therapy. *Nature Reviews Drug Discovery* **21**, 799-820, doi:10.1038/s41573-022-00520-5 (2022).

228 DeNardo, D. G. & Ruffell, B. Macrophages as regulators of tumour immunity and immunotherapy. *Nature Reviews Immunology* **19**, 369-382, doi:10.1038/s41577-019-0127-6 (2019).
229 Pan, Y., Yu, Y., Wang, X. & Zhang, T. Tumor-Associated Macrophages in Tumor Immunity. *Frontiers in Immunology* **11**, doi:10.3389/fimmu.2020.583084 (2020).
230 Yin, M. *et al.* Tumor-associated macrophages drive spheroid formation during early transcoelomic metastasis of ovarian cancer. *The Journal of Clinical Investigation* **126**, 4157-4173, doi:10.1172/JCI87252 (2016).
231 Movahedi, K. *et al.* Different Tumor Microenvironments Contain Functionally Distinct Subsets of Macrophages Derived from Ly6C(high) Monocytes. *Cancer Research* **70**, 5728-5739, doi:10.1158/0008-5472.Can-09-4672 (2010).
232 Lu, T. *et al.* Tumor-infiltrating myeloid cells induce tumor cell resistance to cytotoxic T cells in mice. *The Journal of Clinical Investigation* **121**, 4015-4029, doi:10.1172/JCI45862 (2011).
233 Kaplanov, I. *et al.* Blocking IL-1β reverses the immunosuppression in mouse breast cancer and synergizes with anti–PD-1 for tumor abrogation. *Proceedings of the National Academy of Sciences* **116**, 1361-1369, doi:10.1073/pnas.1812266115 (2019).
234 Aggen, D. H. *et al.* Blocking IL1 Beta Promotes Tumor Regression and Remodeling of the Myeloid Compartment in a Renal Cell Carcinoma Model: Multidimensional Analyses. *Clinical Cancer Research* **27**, 608-621, doi:10.1158/1078-0432.Ccr-20-1610 (2021).
235 Tengesdal, I. W. *et al.* Targeting tumor-derived NLRP3 reduces melanoma progression by limiting MDSCs expansion. *Proceedings of the National Academy of Sciences* **118**, e2000915118, doi:10.1073/pnas.2000915118 (2021).
236 Beatty, G. L. *et al.* A Phase I Study of an Agonist CD40 Monoclonal Antibody (CP-870,893) in Combination with Gemcitabine in Patients with Advanced Pancreatic Ductal Adenocarcinoma. *Clinical Cancer Research* **19**, 6286-6295, doi:10.1158/1078-0432.Ccr-13-1320 (2013).
237 Huffman, A. P., Lin, J. H., Kim, S. I., Byrne, K. T. & Vonderheide, R. H. CCL5 mediates CD40-driven CD4+ T cell tumor infiltration and immunity. *JCI Insight* **5**, doi:10.1172/jci.insight.137263 (2020).
238 Tseng, D. *et al.* Anti-CD47 antibody–mediated phagocytosis of cancer by macrophages primes an effective antitumor T-cell response. *Proceedings of the National Academy of Sciences* **110**, 11103-11108, doi:10.1073/pnas.1305569110 (2013).
239 Ring, N. G. *et al.* Anti-SIRPα antibody immunotherapy enhances neutrophil and macrophage antitumor activity. *Proceedings of the National Academy of Sciences* **114**, E10578-E10585, doi:10.1073/pnas.1710877114 (2017).
240 Zhang, M. *et al.* Anti-CD47 Treatment Stimulates Phagocytosis of Glioblastoma by M1 and M2 Polarized Macrophages and Promotes M1 Polarized Macrophages In Vivo. *PLOS ONE* **11**, e0153550, doi:10.1371/journal.pone.0153550 (2016).
241 Dawson, Mark A. & Kouzarides, T. Cancer Epigenetics: From Mechanism to Therapy. *Cell* **150**, 12-27, doi:10.1016/j.cell.2012.06.013 (2012).
242 Kouzarides, T. Chromatin Modifications and Their Function. *Cell* **128**, 693-705, doi:10.1016/j.cell.2007.02.005 (2007).
243 Rasmussen, K. D. & Helin, K. Role of TET enzymes in DNA methylation, development, and cancer. *Genes & Development* **30**, 733-750, doi:10.1101/gad.276568.115 (2016).
244 Papaemmanuil, E. *et al.* Genomic Classification and Prognosis in Acute Myeloid Leukemia. *N Engl J Med* **374**, 2209-2221, doi:10.1056/NEJMoa1516192 (2016).
245 Ley, T. J. *et al.* DNMT3A Mutations in Acute Myeloid Leukemia. *New England Journal of Medicine* **363**, 2424-2433, doi:10.1056/NEJMoa1005143 (2010).
246 Jiang, Y. *et al.* Aberrant DNA methylation is a dominant mechanism in MDS progression to AML. *Blood* **113**, 1315-1325, doi:10.1182/blood-2008-06-163246 (2009).

247 Fenaux, P. *et al.* Efficacy of azacitidine compared with that of conventional care regimens in the treatment of higher-risk myelodysplastic syndromes: a randomised, open-label, phase III study. *The Lancet Oncology* **10**, 223-232, doi:10.1016/S1470-2045(09)70003-8 (2009).
248 Dombret, H. *et al.* International phase 3 study of azacitidine vs conventional care regimens in older patients with newly diagnosed AML with >30% blasts. *Blood* **126**, 291-299, doi:10.1182/blood-2015-01-621664 (2015).
249 Margueron, R. & Reinberg, D. The Polycomb complex PRC2 and its mark in life. *Nature* **469**, 343, doi:10.1038/nature09784 (2011).
250 Schuettengruber, B., Bourbon, H.-M., Di Croce, L. & Cavalli, G. Genome Regulation by Polycomb and Trithorax: 70 Years and Counting. *Cell* **171**, 34-57, doi:10.1016/j.cell.2017.08.002 (2017).
251 Margueron, R. *et al.* Role of the polycomb protein EED in the propagation of repressive histone marks. *Nature* **461**, 762-767, doi:10.1038/nature08398 (2009).
252 Chen, S., Jiao, L., Shubbar, M., Yang, X. & Liu, X. Unique Structural Platforms of Suz12 Dictate Distinct Classes of PRC2 for Chromatin Binding. *Molecular Cell* **69**, 840-852.e845, doi:10.1016/j.molcel.2018.01.039 (2018).
253 Kasinath, V. *et al.* Structures of human PRC2 with its cofactors AEBP2 and JARID2. *Science* **359**, 940-944, doi:10.1126/science.aar5700 (2018).
254 Nowak, A. J. *et al.* Chromatin-modifying complex component Nurf55/p55 associates with histones H3 and H4 and polycomb repressive complex 2 subunit Su(z)12 through partially overlapping binding sites. *J Biol Chem* **286**, 23388-23396, doi:10.1074/jbc.M110.207407 (2011).
255 Grijzenhout, A. *et al.* Functional analysis of AEBP2, a PRC2 Polycomb protein, reveals a Trithorax phenotype in embryonic development and in ESCs. *Development* **143**, 2716-2723, doi:10.1242/dev.123935 (2016).
256 Shao, Z. *et al.* Stabilization of chromatin structure by PRC1, a Polycomb complex. *Cell* **98**, 37-46, doi:10.1016/s0092-8674(00)80604-2 (1999).
257 Tie, F. *et al.* Polycomb inhibits histone acetylation by CBP by binding directly to its catalytic domain. *Proc Natl Acad Sci U S A* **113**, E744-753, doi:10.1073/pnas.1515465113 (2016).
258 Ferrari, Karin J. *et al.* Polycomb-Dependent H3K27me1 and H3K27me2 Regulate Active Transcription and Enhancer Fidelity. *Molecular Cell* **53**, 49-62, doi:10.1016/j.molcel.2013.10.030 (2014).
259 Wani, A. H. *et al.* Chromatin topology is coupled to Polycomb group protein subnuclear organization. *Nature Communications* **7**, 10291, doi:10.1038/ncomms10291 (2016).
260 Ogiyama, Y., Schuettengruber, B., Papadopoulos, G. L., Chang, J.-M. & Cavalli, G. Polycomb-Dependent Chromatin Looping Contributes to Gene Silencing during Drosophila Development. *Molecular Cell* **71**, 73-88.e75, doi:10.1016/j.molcel.2018.05.032 (2018).
261 Lanzuolo, C., Roure, V., Dekker, J., Bantignies, F. & Orlando, V. Polycomb response elements mediate the formation of chromosome higher-order structures in the bithorax complex. *Nature Cell Biology* **9**, 1167-1174, doi:10.1038/ncb1637 (2007).
262 Varambally, S. *et al.* The polycomb group protein EZH2 is involved in progression of prostate cancer. *Nature* **419**, 624-629, doi:10.1038/nature01075 (2002).
263 Kleer, C. G. *et al.* EZH2 is a marker of aggressive breast cancer and promotes neoplastic transformation of breast epithelial cells. *Proceedings of the National Academy of Sciences* **100**, 11606-11611, doi:10.1073/pnas.1933744100 (2003).
264 McCabe, M. T. *et al.* EZH2 inhibition as a therapeutic strategy for lymphoma with EZH2-activating mutations. *Nature* **492**, 108-112, doi:10.1038/nature11606 (2012).

265 Caganova, M. *et al.* Germinal center dysregulation by histone methyltransferase EZH2 promotes lymphomagenesis. *The Journal of Clinical Investigation* **123**, 5009-5022, doi:10.1172/JCI70626 (2013).
266 Danis, E. *et al.* Ezh2 Controls an Early Hematopoietic Program and Growth and Survival Signaling in Early T Cell Precursor Acute Lymphoblastic Leukemia. *Cell Reports* **14**, 1953-1965, doi:10.1016/j.celrep.2016.01.064 (2016).
267 Ariës, I. M. *et al.* PRC2 loss induces chemoresistance by repressing apoptosis in T cell acute lymphoblastic leukemia. *Journal of Experimental Medicine* **215**, 3094-3114, doi:10.1084/jem.20180570 (2018).
268 Morschhauser, F. *et al.* Tazemetostat for patients with relapsed or refractory follicular lymphoma: an open-label, single-arm, multicentre, phase 2 trial. *The Lancet Oncology* **21**, 1433-1442, doi:10.1016/S1470-2045(20)30441-1 (2020).
269 Gounder, M. *et al.* Tazemetostat in advanced epithelioid sarcoma with loss of INI1/SMARCB1: an international, open-label, phase 2 basket study. *The Lancet Oncology* **21**, 1423-1432, doi:10.1016/S1470-2045(20)30451-4 (2020).
270 Parreno, V., Martinez, A.-M. & Cavalli, G. Mechanisms of Polycomb group protein function in cancer. *Cell Research* **32**, 231-253, doi:10.1038/s41422-021-00606-6 (2022).
271 Saksouk, N., Simboeck, E. & Déjardin, J. Constitutive heterochromatin formation and transcription in mammals. *Epigenetics & Chromatin* **8**, 3, doi:10.1186/1756-8935-8-3 (2015).
272 Bannister, A. J. *et al.* Selective recognition of methylated lysine 9 on histone H3 by the HP1 chromo domain. *Nature* **410**, 120-124, doi:10.1038/35065138 (2001).
273 Lachner, M., O'Carroll, D., Rea, S., Mechtler, K. & Jenuwein, T. Methylation of histone H3 lysine 9 creates a binding site for HP1 proteins. *Nature* **410**, 116-120, doi:10.1038/35065132 (2001).
274 Nakayama, J., Rice, J. C., Strahl, B. D., Allis, C. D. & Grewal, S. I. Role of histone H3 lysine 9 methylation in epigenetic control of heterochromatin assembly. *Science* **292**, 110-113, doi:10.1126/science.1060118 (2001).
275 Hall, I. M. *et al.* Establishment and maintenance of a heterochromatin domain. *Science* **297**, 2232-2237, doi:10.1126/science.1076466 (2002).
276 Peters, A. H. *et al.* Histone H3 lysine 9 methylation is an epigenetic imprint of facultative heterochromatin. *Nat Genet* **30**, 77-80, doi:10.1038/ng789 (2002).
277 Padeken, J., Methot, S. P. & Gasser, S. M. Establishment of H3K9-methylated heterochromatin and its functions in tissue differentiation and maintenance. *Nature Reviews Molecular Cell Biology* **23**, 623-640, doi:10.1038/s41580-022-00483-w (2022).
278 Schotta, G. *et al.* Central role of Drosophila SU(VAR)3–9 in histone H3-K9 methylation and heterochromatic gene silencing. *The EMBO Journal* **21**, 1121-1131, doi:10.1093/emboj/21.5.1121 (2002).
279 Muller, H. J. Types of visible variations induced by X-rays in Drosophila. *Journal of Genetics* **22**, 299-334, doi:10.1007/BF02984195 (1930).
280 Peters, A. H. F. M. *et al.* Loss of the Suv39h Histone Methyltransferases Impairs Mammalian Heterochromatin and Genome Stability. *Cell* **107**, 323-337, doi:10.1016/S0092-8674(01)00542-6 (2001).
281 Bulut-Karslioglu, A. *et al.* Suv39h-Dependent H3K9me3 Marks Intact Retrotransposons and Silences LINE Elements in Mouse Embryonic Stem Cells. *Molecular Cell* **55**, 277-290, doi:10.1016/j.molcel.2014.05.029 (2014).
282 Johnson, W. L. *et al.* RNA-dependent stabilization of SUV39H1 at constitutive heterochromatin. *eLife* **6**, e25299, doi:10.7554/eLife.25299 (2017).
283 Velazquez Camacho, O. *et al.* Major satellite repeat RNA stabilize heterochromatin retention of Suv39h enzymes by RNA-nucleosome association and RNA:DNA hybrid formation. *eLife* **6**, e25293, doi:10.7554/eLife.25293 (2017).

284 Ekwall, K. *et al.* Mutations in the fission yeast silencing factors clr4+ and rik1+ disrupt the localisation of the chromo domain protein Swi6p and impair centromere function. *J Cell Sci* **109**, 2637-2648, doi:10.1242/jcs.109.11.2637 (1996).

285 Harte, P. J., Wu, W., Carrasquillo, M. M. & Matera, A. G. Assignment of a novel bifurcated SET domain gene, SETDB1, to human chromosome band 1q21 by in situ hybridization and radiation hybrids. *Cytogenetic and Genome Research* **84**, 83-86, doi:10.1159/000015220 (1999).

286 Schultz, D. C., Ayyanathan, K., Negorev, D., Maul, G. G. & Rauscher, F. J. SETDB1: a novel KAP-1-associated histone H3, lysine 9-specific methyltransferase that contributes to HP1-mediated silencing of euchromatic genes by KRAB zinc-finger proteins. *Genes & Development* **16**, 919-932, doi:10.1101/gad.973302 (2002).

287 Jurkowska, R. Z. *et al.* H3K14ac is linked to methylation of H3K9 by the triple Tudor domain of SETDB1. *Nature Communications* **8**, 2057, doi:10.1038/s41467-017-02259-9 (2017).

288 Falandry, C. *et al.* CLLD8/KMT1F Is a Lysine Methyltransferase That Is Important for Chromosome Segregation. *Journal of Biological Chemistry* **285**, 20234-20241, doi:10.1074/jbc.M109.052399 (2010).

289 Tachibana, M. *et al.* Histone methyltransferases G9a and GLP form heteromeric complexes and are both crucial for methylation of euchromatin at H3-K9. *Genes Dev.* **19**, 815-826, doi:10.1101/gad.1284005 (2005).

290 Tachibana, M., Sugimoto, K., Fukushima, T. & Shinkai, Y. SET Domain-containing Protein, G9a, Is a Novel Lysine-preferring Mammalian Histone Methyltransferase with Hyperactivity and Specific Selectivity to Lysines 9 and 27 of Histone H3. *J. Biol. Chem.* **276**, 25309-25317, doi:10.1074/jbc.M101914200 (2001).

291 Tachibana, M. *et al.* G9a histone methyltransferase plays a dominant role in euchromatic histone H3 lysine 9 methylation and is essential for early embryogenesis. *Genes Dev.* **16**, 1779-1791, doi:10.1101/gad.989402 (2002).

292 Jiang, Q. *et al.* G9a Plays Distinct Roles in Maintaining DNA Methylation, Retrotransposon Silencing, and Chromatin Looping. *Cell Reports* **33**, doi:10.1016/j.celrep.2020.108315 (2020).

293 Ueda, J., Tachibana, M., Ikura, T. & Shinkai, Y. Zinc Finger Protein Wiz Links G9a/GLP Histone Methyltransferases to the Co-repressor Molecule CtBP. *J Biol Chem* **281**, 20120-20128, doi:10.1074/jbc.M603087200 (2006).

294 Mulligan, P. *et al.* CDYL Bridges REST and Histone Methyltransferases for Gene Repression and Suppression of Cellular Transformation. *Molecular Cell* **32**, 718-726, doi:10.1016/j.molcel.2008.10.025 (2008).

295 Shin, Hyun M. *et al.* Epigenetic Modifications Induced by Blimp-1 Regulate CD8+ T Cell Memory Progression during Acute Virus Infection. *Immunity* **39**, 661-675, doi:10.1016/j.immuni.2013.08.032 (2013).

296 Tong, X. *et al.* Recruitment of Histone Methyltransferase G9a Mediates Transcriptional Repression of Fgf21 Gene by E4BP4 Protein. *Journal of Biological Chemistry* **288**, 5417-5425, doi:10.1074/jbc.M112.433482 (2013).

297 Fang, S. *et al.* Coordinated Recruitment of Histone Methyltransferase G9a and Other Chromatin-Modifying Enzymes in SHP-Mediated Regulation of Hepatic Bile Acid Metabolism. *Molecular and Cellular Biology* **27**, 1407-1424, doi:10.1128/MCB.00944-06 (2007).

298 Haebe, J. R., Bergin, C. J., Sandouka, T. & Benoit, Y. D. Emerging role of G9a in cancer stemness and promises as a therapeutic target. *Oncogenesis* **10**, 76, doi:10.1038/s41389-021-00370-7 (2021).

299 Hirata, H. *et al.* Wnt antagonist gene DKK2 is epigenetically silenced and inhibits renal cancer progression through apoptotic and cell cycle pathways. *Clin Cancer Res* **15**, 5678-5687, doi:10.1158/1078-0432.Ccr-09-0558 (2009).
300 Kato, S. *et al.* Gain-of-Function Genetic Alterations of G9a Drive Oncogenesis. *Cancer Discovery* **10**, 980-997, doi:10.1158/2159-8290.CD-19-0532 (2020).
301 Kim, J. T. *et al.* Deregulation of Wnt/β-catenin signaling through genetic or epigenetic alterations in human neuroendocrine tumors. *Carcinogenesis* **34**, 953-961, doi:10.1093/carcin/bgt018 (2013).
302 Lehnertz, B. *et al.* The methyltransferase G9a regulates HoxA9-dependent transcription in AML. *Genes & Development* **28**, 317-327, doi:10.1101/gad.236794.113 (2014).
303 Mabe, N. W. *et al.* G9a Promotes Breast Cancer Recurrence through Repression of a Pro-inflammatory Program. *Cell Reports* **33**, doi:10.1016/j.celrep.2020.108341 (2020).
304 Kelly, G. M. *et al.* G9a Inhibition Enhances Checkpoint Inhibitor Blockade Response in Melanoma. *Clin Cancer Res* **27**, 2624-2635, doi:10.1158/1078-0432.CCR-20-3463 (2021).
305 Smothers, J. F. & Henikoff, S. The HP1 chromo shadow domain binds a consensus peptide pentamer. *Current Biology* **10**, 27-30, doi:10.1016/S0960-9822(99)00260-2 (2000).
306 Vakoc, C. R., Mandat, S. A., Olenchock, B. A. & Blobel, G. A. Histone H3 Lysine 9 Methylation and HP1γ Are Associated with Transcription Elongation through Mammalian Chromatin. *Molecular Cell* **19**, 381-391, doi:10.1016/j.molcel.2005.06.011 (2005).
307 Schoelz, J. M. & Riddle, N. C. Functions of HP1 proteins in transcriptional regulation. *Epigenetics & Chromatin* **15**, 14, doi:10.1186/s13072-022-00453-8 (2022).
308 Rottach, A. *et al.* The multi-domain protein Np95 connects DNA methylation and histone modification. *Nucleic Acids Research* **38**, 1796-1804, doi:10.1093/nar/gkp1152 (2009).
309 Rothbart, S. B. *et al.* Multivalent histone engagement by the linked tandem Tudor and PHD domains of UHRF1 is required for the epigenetic inheritance of DNA methylation. *Genes & Development* **27**, 1288-1298, doi:10.1101/gad.220467.113 (2013).
310 Arita, K. *et al.* Recognition of modification status on a histone H3 tail by linked histone reader modules of the epigenetic regulator UHRF1. *Proceedings of the National Academy of Sciences* **109**, 12950-12955, doi:10.1073/pnas.1203701109 (2012).
311 Yamane, K. *et al.* JHDM2A, a JmjC-Containing H3K9 Demethylase, Facilitates Transcription Activation by Androgen Receptor. *Cell* **125**, 483-495, doi:10.1016/j.cell.2006.03.027 (2006).
312 Whetstine, J. R. *et al.* Reversal of histone lysine trimethylation by the JMJD2 family of histone demethylases. *Cell* **125**, 467-481, doi:10.1016/j.cell.2006.03.028 (2006).
313 Cloos, P. A. *et al.* The putative oncogene GASC1 demethylates tri- and dimethylated lysine 9 on histone H3. *Nature* **442**, 307-311, doi:10.1038/nature04837 (2006).
314 Zhu, Z. *et al.* PHF8 is a histone H3K9me2 demethylase regulating rRNA synthesis. *Cell Res* **20**, 794-801, doi:10.1038/cr.2010.75 (2010).
315 Jeon, H. Y., Hussain, A. & Qi, J. Role of H3K9 demethylases in DNA double-strand break repair. *J Cancer Biol* **1**, 10-15, doi:10.46439/cancerbiology.1.003 (2020).
316 Boyd, J. M. *et al.* A region in the C-terminus of adenovirus 2/5 E1a protein is required for association with a cellular phosphoprotein and important for the negative modulation of T24-ras mediated transformation, tumorigenesis and metastasis. *Embo j* **12**, 469-478, doi:10.1002/j.1460-2075.1993.tb05679.x (1993).
317 Chinnadurai, G. CtBP, an Unconventional Transcriptional Corepressor in Development and Oncogenesis. *Molecular Cell* **9**, 213-224, doi:10.1016/S1097-2765(02)00443-4 (2002).

318 Shi, Y. *et al.* Coordinated histone modifications mediated by a CtBP co-repressor complex. *Nature* **422**, 735-738, doi:10.1038/nature01550 (2003).
319 Kuppuswamy, M. *et al.* Role of the PLDLS-Binding Cleft Region of CtBP1 in Recruitment of Core and Auxiliary Components of the Corepressor Complex. *Molecular and Cellular Biology* **28**, 269-281, doi:10.1128/MCB.01077-07 (2008).
320 Kovi, R. C., Paliwal, S., Pande, S. & Grossman, S. R. An ARF/CtBP2 complex regulates BH3-only gene expression and p53-independent apoptosis. *Cell Death Differ* **17**, 513-521, doi:10.1038/cdd.2009.140 (2010).
321 Guaita, S. *et al.* Snail induction of epithelial to mesenchymal transition in tumor cells is accompanied by MUC1 repression and ZEB1 expression. *J Biol Chem* **277**, 39209-39216, doi:10.1074/jbc.M206400200 (2002).
322 Eger, A. *et al.* DeltaEF1 is a transcriptional repressor of E-cadherin and regulates epithelial plasticity in breast cancer cells. *Oncogene* **24**, 2375-2385, doi:10.1038/sj.onc.1208429 (2005).
323 Peña, C. *et al.* E-cadherin and vitamin D receptor regulation by SNAIL and ZEB1 in colon cancer: clinicopathological correlations. *Hum Mol Genet* **14**, 3361-3370, doi:10.1093/hmg/ddi366 (2005).
324 Spoelstra, N. S. *et al.* The transcription factor ZEB1 is aberrantly expressed in aggressive uterine cancers. *Cancer Res* **66**, 3893-3902, doi:10.1158/0008-5472.Can-05-2881 (2006).
325 Paliwal, S. *et al.* The alternative reading frame tumor suppressor antagonizes hypoxia-induced cancer cell migration via interaction with the COOH-terminal binding protein corepressor. *Cancer Res* **67**, 9322-9329, doi:10.1158/0008-5472.Can-07-1743 (2007).
326 Sierra, J., Yoshida, T., Joazeiro, C. A. & Jones, K. A. The APC tumor suppressor counteracts beta-catenin activation and H3K4 methylation at Wnt target genes. *Genes Dev* **20**, 586-600, doi:10.1101/gad.1385806 (2006).
327 Hamada, F. & Bienz, M. The APC tumor suppressor binds to C-terminal binding protein to divert nuclear beta-catenin from TCF. *Dev Cell* **7**, 677-685, doi:10.1016/j.devcel.2004.08.022 (2004).
328 Guan, C. *et al.* CtBP2 contributes to malignant development of human esophageal squamous cell carcinoma by regulation of p16INK4A. *J Cell Biochem* **114**, 1343-1354, doi:10.1002/jcb.24475 (2013).
329 Deng, H. *et al.* CtBP1 is expressed in melanoma and represses the transcription of p16INK4a and Brca1. *J Invest Dermatol* **133**, 1294-1301, doi:10.1038/jid.2012.487 (2013).
330 Takayama, K. *et al.* Androgen-responsive long noncoding RNA CTBP1-AS promotes prostate cancer. *Embo j* **32**, 1665-1680, doi:10.1038/emboj.2013.99 (2013).
331 Poser, I., Golob, M., Weidner, M., Buettner, R. & Bosserhoff, A. K. Down-regulation of COOH-terminal binding protein expression in malignant melanomas leads to induction of MIA expression. *Cancer Res* **62**, 5962-5966 (2002).
332 Winklmeier, A., Poser, I., Hoek, K. S. & Bosserhoff, A. K. Loss of full length CtBP1 expression enhances the invasive potential of human melanoma. *BMC Cancer* **9**, 52, doi:10.1186/1471-2407-9-52 (2009).
333 Liu, Z. *et al.* A New Trend in Cancer Treatment: The Combination of Epigenetics and Immunotherapy. *Frontiers in Immunology* **13**, doi:10.3389/fimmu.2022.809761 (2022).
334 Yang, H. *et al.* Expression of PD-L1, PD-L2, PD-1 and CTLA4 in myelodysplastic syndromes is enhanced by treatment with hypomethylating agents. *Leukemia* **28**, 1280-1288, doi:10.1038/leu.2013.355 (2014).
335 Morel, D., Jeffery, D., Aspeslagh, S., Almouzni, G. & Postel-Vinay, S. Combining epigenetic drugs with other therapies for solid tumours — past lessons and future

promise. *Nature Reviews Clinical Oncology* **17**, 91-107, doi:10.1038/s41571-019-0267-4 (2020).

336 Bracken, A. P. *et al.* EZH2 is downstream of the pRB-E2F pathway, essential for proliferation and amplified in cancer. *The EMBO Journal* **22**, 5323-5335, doi:10.1093/emboj/cdg542 (2003).

337 Wang, L., Jin, Q., Lee, J.-E., Su, I.-h. & Ge, K. Histone H3K27 methyltransferase Ezh2 represses Wnt genes to facilitate adipogenesis. *Proceedings of the National Academy of Sciences* **107**, 7317-7322, doi:10.1073/pnas.1000031107 (2010).

338 Kanazawa, S., Okamoto, T. & Peterlin, B. M. Tat Competes with CIITA for the Binding to P-TEFb and Blocks the Expression of MHC Class II Genes in HIV Infection. *Immunity* **12**, 61-70, doi:10.1016/S1074-7613(00)80159-4 (2000).

339 Horn, M. *et al.* DRE-1/FBXO11-Dependent Degradation of BLMP-1/BLIMP-1 Governs C. elegans Developmental Timing and Maturation. *Dev. Cell* **28**, 697-710, doi:10.1016/j.devcel.2014.01.028 (2014).

340 Diebold, S. S., Cotten, M., Koch, N. & Zenke, M. MHC class II presentation of endogenously expressed antigens by transfected dendritic cells. *Gene Ther.* **8**, 487-493, doi:10.1038/sj.gt.3301433 (2001).

341 Chan, K. L. *et al.* Inhibition of the CtBP complex and FBXO11 enhances MHC class II expression and anti-cancer immune responses. *Cancer Cell* **40**, 1190-1206.e1199, doi:10.1016/j.ccell.2022.09.007 (2022).

342 Kim, D., Paggi, J. M., Park, C., Bennett, C. & Salzberg, S. L. Graph-based genome alignment and genotyping with HISAT2 and HISAT-genotype. *Nat. Biotechnol.* **37**, 907-915, doi:10.1038/s41587-019-0201-4 (2019).

343 Anders, S., Pyl, P. T. & Huber, W. HTSeq—a Python framework to work with high-throughput sequencing data. *Bioinformatics* **31**, 166-169, doi:10.1093/bioinformatics/btu638 (2014).

344 Love, M. I., Huber, W. & Anders, S. Moderated estimation of fold change and dispersion for RNA-seq data with DESeq2. *Genome Biol.* **15**, 550, doi:10.1186/s13059-014-0550-8 (2014).

345 Beum, P. V. *et al.* Quantitative analysis of protein co-localization on B cells opsonized with rituximab and complement using the ImageStream multispectral imaging flow cytometer. *Journal of Immunological Methods* **317**, 90-99, doi:10.1016/j.jim.2006.09.012 (2006).

346 Erie, A. J. *et al.* MHC class II upregulation and colocalization with Fas in experimental models of immune-mediated bone marrow failure. *Experimental Hematology* **39**, 837-849, doi:10.1016/j.exphem.2011.05.005 (2011).

347 George, T. C. *et al.* Quantitative measurement of nuclear translocation events using similarity analysis of multispectral cellular images obtained in flow. *Journal of Immunological Methods* **311**, 117-129, doi:10.1016/j.jim.2006.01.018 (2006).

348 Kaya-Okur, H. S. *et al.* CUT&Tag for efficient epigenomic profiling of small samples and single cells. *Nat. Commun.* **10**, 1930, doi:10.1038/s41467-019-09982-5 (2019).

349 Bolger, A. M., Lohse, M. & Usadel, B. Trimmomatic: a flexible trimmer for Illumina sequence data. *Bioinformatics* **30**, 2114-2120, doi:10.1093/bioinformatics/btu170 (2014).

350 Langmead, B. & Salzberg, S. L. Fast gapped-read alignment with Bowtie 2. *Nat. Methods* **9**, 357-359, doi:10.1038/nmeth.1923 (2012).

351 Danecek, P. *et al.* Twelve years of SAMtools and BCFtools. *GigaScience* **10**, doi:10.1093/gigascience/giab008 (2021).

352 Zhang, Y. *et al.* Model-based Analysis of ChIP-Seq (MACS). *Genome Biol.* **9**, R137, doi:10.1186/gb-2008-9-9-r137 (2008).

353 Ramírez, F., Dündar, F., Diehl, S., Grüning, B. A. & Manke, T. deepTools: a flexible platform for exploring deep-sequencing data. *Nucleic Acids Res.* **42**, W187-W191, doi:10.1093/nar/gku365 (2014).
354 Robinson, J. T. *et al.* Integrative genomics viewer. *Nat. Biotechnol.* **29**, 24-26, doi:10.1038/nbt.1754 (2011).
355 Mosmann, T. R. *et al.* Species-specificity of T cell stimulating activities of IL 2 and BSF-1 (IL 4): comparison of normal and recombinant, mouse and human IL 2 and BSF-1 (IL 4). *J Immunol* **138**, 1813-1816 (1987).
356 Stuart, T. *et al.* Comprehensive Integration of Single-Cell Data. *Cell* **177**, 1888-1902 e1821, doi:10.1016/j.cell.2019.05.031 (2019).
357 Butler, A., Hoffman, P., Smibert, P., Papalexi, E. & Satija, R. Integrating single-cell transcriptomic data across different conditions, technologies, and species. *Nat Biotechnol* **36**, 411-420, doi:10.1038/nbt.4096 (2018).
358 Stoeckius, M. *et al.* Cell Hashing with barcoded antibodies enables multiplexing and doublet detection for single cell genomics. *Genome Biol* **19**, 224, doi:10.1186/s13059-018-1603-1 (2018).
359 Hafemeister, C. & Satija, R. Normalization and variance stabilization of single-cell RNA-seq data using regularized negative binomial regression. *Genome Biol* **20**, 296, doi:10.1186/s13059-019-1874-1 (2019).
360 Becht, E. *et al.* Dimensionality reduction for visualizing single-cell data using UMAP. *Nature Biotechnology* **37**, 38-44, doi:10.1038/nbt.4314 (2019).
361 Burr, M. L. *et al.* An Evolutionarily Conserved Function of Polycomb Silences the MHC Class I Antigen Presentation Pathway and Enables Immune Evasion in Cancer. *Cancer Cell* **36**, 385-401, doi:10.1016/j.ccell.2019.08.008 (2019).
362 Hanahan, D. & Weinberg, Robert A. Hallmarks of Cancer: The Next Generation. *Cell* **144**, 646-674, doi:10.1016/j.cell.2011.02.013 (2011).
363 Wood, L. D. *et al.* The Genomic Landscapes of Human Breast and Colorectal Cancers. *Science* **318**, 1108-1113, doi:10.1126/science.1145720 (2007).
364 Ding, L. *et al.* Somatic mutations affect key pathways in lung adenocarcinoma. *Nature* **455**, 1069, doi:10.1038/nature07423 (2008).
365 Jones, S. *et al.* Core Signaling Pathways in Human Pancreatic Cancers Revealed by Global Genomic Analyses. *Science* **321**, 1801-1806, doi:10.1126/science.1164368 (2008).
366 Parsons, D. W. *et al.* An Integrated Genomic Analysis of Human Glioblastoma Multiforme. *Science* **321**, 1807-1812, doi:10.1126/science.1164382 (2008).
367 Stransky, N. *et al.* The Mutational Landscape of Head and Neck Squamous Cell Carcinoma. *Science* **333**, 1157-1160, doi:10.1126/science.1208130 (2011).
368 The Cancer Genome Atlas Research, N. *et al.* Integrated genomic analyses of ovarian carcinoma. *Nature* **474**, 609, doi:10.1038/nature10166 (2011).
369 Kandoth, C. *et al.* Mutational landscape and significance across 12 major cancer types. *Nature* **502**, 333, doi:10.1038/nature12634 (2013).
370 Cancer Genome Atlas Research, N. *et al.* Genomic and epigenomic landscapes of adult de novo acute myeloid leukemia. *N. Engl. J. Med.* **368**, 2059-2074, doi:10.1056/NEJMoa1301689 (2013).
371 The Cancer Genome Atlas Research, N. *et al.* Comprehensive molecular characterization of clear cell renal cell carcinoma. *Nature* **499**, 43, doi:10.1038/nature12222 (2013).
372 Korfi, K., Ali, S., Heward, J. A. & Fitzgibbon, J. Follicular lymphoma, a B cell malignancy addicted to epigenetic mutations. *Epigenetics* **12**, 370-377, doi:10.1080/15592294.2017.1282587 (2017).
373 Green, M. R. Chromatin modifying gene mutations in follicular lymphoma. *Blood* **131**, 595-604, doi:10.1182/blood-2017-08-737361 (2018).

374 Sperling, A. S., Gibson, C. J. & Ebert, B. L. The genetics of myelodysplastic syndrome: from clonal haematopoiesis to secondary leukaemia. *Nature Reviews Cancer* **17**, 5, doi:10.1038/nrc.2016.112 (2016).
375 Corces-Zimmerman, M. R., Hong, W.-J., Weissman, I. L., Medeiros, B. C. & Majeti, R. Preleukemic mutations in human acute myeloid leukemia affect epigenetic regulators and persist in remission. *Proceedings of the National Academy of Sciences* **111**, 2548-2553, doi:10.1073/pnas.1324297111 (2014).
376 Shlush, L. I. *et al.* Identification of pre-leukaemic haematopoietic stem cells in acute leukaemia. *Nature* **506**, 328, doi:10.1038/nature13038 (2014).
377 Duvic, M. *et al.* Phase 2 trial of oral vorinostat (suberoylanilide hydroxamic acid, SAHA) for refractory cutaneous T-cell lymphoma (CTCL). *Blood* **109**, 31-39, doi:10.1182/blood-2006-06-025999 (2007).
378 Piekarz, R. L. *et al.* Phase 2 trial of romidepsin in patients with peripheral T-cell lymphoma. *Blood* **117**, 5827-5834, doi:10.1182/blood-2010-10-312603 (2011).
379 Ribrag, V. *et al.* Phase 1 Study of Tazemetostat (EPZ-6438), an Inhibitor of Enhancer of Zeste-Homolog 2 (EZH2): Preliminary Safety and Activity in Relapsed or Refractory Non-Hodgkin Lymphoma (NHL) Patients. *Blood* **126**, 473-473 (2015).
380 Borthakur, G. *et al.* A Phase I/II Open-Label, Dose Escalation Study to Investigate the Safety, Pharmacokinetics, Pharmacodynamics and Clinical Activity of GSK525762 in Subjects with Relapsed, Refractory Hematologic Malignancies. *Blood* **128**, 5223-5223 (2016).
381 Magner, W. J. *et al.* Activation of MHC Class I, II, and CD40 Gene Expression by Histone Deacetylase Inhibitors. *The Journal of Immunology* **165**, 7017-7024, doi:10.4049/jimmunol.165.12.7017 (2000).
382 Li, H. *et al.* Immune regulation by low doses of the DNA methyltransferase inhibitor 5-azacitidine in common human epithelial cancers. *Oncotarget* **5**, 587-598, doi:10.18632/oncotarget.1782 (2014).
383 Goswami, S. *et al.* Modulation of EZH2 expression in T cells improves efficacy of anti–CTLA-4 therapy. *The Journal of Clinical Investigation* **128**, 3813-3818, doi:10.1172/JCI99760 (2018).
384 Wang, D. *et al.* Targeting EZH2 Reprograms Intratumoral Regulatory T Cells to Enhance Cancer Immunity. *Cell Reports* **23**, 3262-3274, doi:10.1016/j.celrep.2018.05.050 (2018).
385 Ishino, Y., Shinagawa, H., Makino, K., Amemura, M. & Nakata, A. Nucleotide sequence of the iap gene, responsible for alkaline phosphatase isozyme conversion in Escherichia coli, and identification of the gene product. *Journal of bacteriology* **169**, 5429-5433, doi:10.1128/jb.169.12.5429-5433.1987 (1987).
386 Mojica, F. J. M., Díez-Villaseñor, C., Soria, E. & Juez, G. Biological significance of a family of regularly spaced repeats in the genomes of Archaea, Bacteria and mitochondria. *Mol Microbiol.* **36**, 244-246, doi:10.1046/j.1365-2958.2000.01838.x (2000).
387 Barrangou, R. *et al.* CRISPR Provides Acquired Resistance Against Viruses in Prokaryotes. *Science* **315**, 1709-1712, doi:10.1126/science.1138140 (2007).
388 Deltcheva, E. *et al.* CRISPR RNA maturation by trans-encoded small RNA and host factor RNase III. *Nature* **471**, 602-607, doi:10.1038/nature09886 (2011).
389 Jinek, M. *et al.* A Programmable Dual-RNA-Guided DNA Endonuclease in Adaptive Bacterial Immunity. *Science* **337**, 816-821, doi:10.1126/science.1225829 (2012).
390 Qi, Lei S. *et al.* Repurposing CRISPR as an RNA-Guided Platform for Sequence-Specific Control of Gene Expression. *Cell* **152**, 1173-1183, doi:10.1016/j.cell.2013.02.022 (2013).
391 Cheng, A. W. *et al.* Multiplexed activation of endogenous genes by CRISPR-on, an RNA-guided transcriptional activator system. *Cell Research* **23**, 1163-1171, doi:10.1038/cr.2013.122 (2013).

392 Hsu, P. D., Lander, E. S. & Zhang, F. Development and applications of CRISPR-Cas9 for genome engineering. *Cell* **157**, 1262-1278, doi:10.1016/j.cell.2014.05.010 (2014).
393 Morgens, D. W. *et al.* Genome-scale measurement of off-target activity using Cas9 toxicity in high-throughput screens. *Nat. Commun* **8**, 15178, doi:10.1038/ncomms15178 (2017).
394 Perino, M. *et al.* MTF2 recruits Polycomb Repressive Complex 2 by helical-shape-selective DNA binding. *Nature Genetics* **50**, 1002-1010, doi:10.1038/s41588-018-0134-8 (2018).
395 König, R. *et al.* A probability-based approach for the analysis of large-scale RNAi screens. *Nat. Methods* **4**, 847-849, doi:10.1038/nmeth1089 (2007).
396 Joshi, P. *et al.* Dominant Alleles Identify SET Domain Residues Required for Histone Methyltransferase of Polycomb Repressive Complex 2. *Journal of Biological Chemistry* **283**, 27757-27766, doi:10.1074/jbc.M804442200 (2008).
397 Morel, K. L. *et al.* EZH2 inhibition activates a dsRNA–STING–interferon stress axis that potentiates response to PD-1 checkpoint blockade in prostate cancer. *Nature Cancer* **2**, 444-456, doi:10.1038/s43018-021-00185-w (2021).
398 Barretina, J. *et al.* The Cancer Cell Line Encyclopedia enables predictive modelling of anticancer drug sensitivity. *Nature* **483**, 603-607, doi:10.1038/nature11003 (2012).
399 Chen, L. *et al.* CRISPR-Cas9 screen reveals a MYCN-amplified neuroblastoma dependency on EZH2. *The Journal of Clinical Investigation* **128**, 446-462, doi:10.1172/JCI90793 (2018).
400 Gardner, E. E. *et al.* Chemosensitive Relapse in Small Cell Lung Cancer Proceeds through an EZH2-SLFN11 Axis. *Cancer Cell* **31**, 286-299, doi:10.1016/j.ccell.2017.01.006 (2017).
401 Paulson, K. G. *et al.* Acquired cancer resistance to combination immunotherapy from transcriptional loss of class I HLA. *Nature Communications* **9**, 3868, doi:10.1038/s41467-018-06300-3 (2018).
402 Siddle, H. V. *et al.* Reversible epigenetic down-regulation of MHC molecules by devil facial tumour disease illustrates immune escape by a contagious cancer. *Proc Natl Acad Sci* **110**, 5103-5108, doi:10.1073/pnas.1219920110 (2013).
403 Minoux, M. *et al.* Gene bivalency at Polycomb domains regulates cranial neural crest positional identity. *Science* **355**, eaal2913, doi:10.1126/science.aal2913 (2017).
404 Zeid, R. *et al.* Enhancer invasion shapes MYCN-dependent transcriptional amplification in neuroblastoma. *Nature Genetics* **50**, 515-523, doi:10.1038/s41588-018-0044-9 (2018).
405 Dunham, I. *et al.* An integrated encyclopedia of DNA elements in the human genome. *Nature* **489**, 57-74, doi:10.1038/nature11247 (2012).
406 Kundaje, A. *et al.* Integrative analysis of 111 reference human epigenomes. *Nature* **518**, 317-330, doi:10.1038/nature14248 (2015).
407 Bernstein, B. E. *et al.* A Bivalent Chromatin Structure Marks Key Developmental Genes in Embryonic Stem Cells. *Cell* **125**, 315-326, doi:10.1016/j.cell.2006.02.041 (2006).
408 Meuwissen, R. *et al.* Induction of small cell lung cancer by somatic inactivation of both Trp53 and Rb1 in a conditional mouse model. *Cancer Cell* **4**, 181-189, doi:10.1016/S1535-6108(03)00220-4 (2003).
409 Oser, M. G., Niederst, M. J., Sequist, L. V. & Engelman, J. A. Transformation from non-small-cell lung cancer to small-cell lung cancer: molecular drivers and cells of origin. *The Lancet Oncology* **16**, e165-e172, doi:10.1016/S1470-2045(14)71180-5 (2015).
410 Beltran, H. *et al.* Divergent clonal evolution of castration-resistant neuroendocrine prostate cancer. *Nature Medicine* **22**, 298, doi:10.1038/nm.4045 (2016).
411 Agudo, J. *et al.* Quiescent Tissue Stem Cells Evade Immune Surveillance. *Immunity* **48**, 271-285.e275, doi:10.1016/j.immuni.2018.02.001 (2018).

412 Dickinson, A. M. *et al.* Graft-versus-Leukemia Effect Following Hematopoietic Stem Cell Transplantation for Leukemia. *Front. Immunol.* **8**, doi:10.3389/fimmu.2017.00496 (2017).
413 Luskin, M. R. *et al.* Clinical Utility of Next-Generation Sequencing for Oncogenic Mutations in Patients with Acute Myeloid Leukemia Undergoing Allogeneic Stem Cell Transplantation. *Biology of Blood and Marrow Transplantation* **22**, 1961-1967, doi:10.1016/j.bbmt.2016.07.018 (2016).
414 Quek, L. *et al.* Mutational analysis of disease relapse in patients allografted for acute myeloid leukemia. *Blood Advances* **1**, 193-204, doi:10.1182/bloodadvances.2016000760 (2016).
415 Dermime, S. *et al.* Immune escape from a graft-versus-leukemia effect may play a role in the relapse of myeloid leukemias following allogeneic bone marrow transplantation. *Bone Marrow Transplant.* **19**, 989-999, doi:10.1038/sj.bmt.1700778 (1997).
416 Masuda, K. *et al.* Loss or down-regulation of HLA class I expression at the allelic level in freshly isolated leukemic blasts. *Cancer Science* **98**, 102-108, doi:10.1111/j.1349-7006.2006.00356.x (2007).
417 Stölzel, F. *et al.* Clonal Evolution Including Partial Loss of Human Leukocyte Antigen Genes Favoring Extramedullary Acute Myeloid Leukemia Relapse After Matched Related Allogeneic Hematopoietic Stem Cell Transplantation. *Transplantation* **93**, 744-749, doi:10.1097/TP.0b013e3182481113 (2012).
418 Vago, L. *et al.* Loss of Mismatched HLA in Leukemia after Stem-Cell Transplantation. *N. Engl. J. Med.* **361**, 478-488, doi:10.1056/NEJMoa0811036 (2009).
419 Hamdi, A. *et al.* Are changes in HLA Ags responsible for leukemia relapse after HLA-matched allogeneic hematopoietic SCT? *Bone Marrow Transplantation* **50**, 411, doi:10.1038/bmt.2014.285 (2015).
420 Christopher, M. J. *et al.* Immune Escape of Relapsed AML Cells after Allogeneic Transplantation. *N. Engl. J. Med.* **379**, 2330-2341, doi:10.1056/NEJMoa1808777 (2018).
421 Toffalori, C. *et al.* Immune signature drives leukemia escape and relapse after hematopoietic cell transplantation. *Nat. Med.* **25**, 603-611, doi:10.1038/s41591-019-0400-z (2019).
422 Fujimoto-Nishiyama, A., Ishii, S., Matsuda, S., Inoue, J.-i. & Yamamoto, T. A novel zinc finger protein, Finb, is a transcriptional activator and localized in nuclear bodies. *Gene* **195**, 267-275, doi:10.1016/s0378-1119(97)00172-8 (1997).
423 Yamane, T. *et al.* Transcriptional Activation of the Cholecystokinin Gene by DJ-1 through Interaction of DJ-1 with RREB1 and the Effect of DJ-1 on the Cholecystokinin Level in Mice. *PLOS ONE* **8**, e78374, doi:10.1371/journal.pone.0078374 (2013).
424 Su, J. *et al.* TGF-β orchestrates fibrogenic and developmental EMTs via the RAS effector RREB1. *Nature* **577**, 566-571, doi:10.1038/s41586-019-1897-5 (2020).
425 Ray, S. K., Li, H. J., Metzger, E., Schüle, R. & Leiter, A. B. CtBP and Associated LSD1 Are Required for Transcriptional Activation by NeuroD1 in Gastrointestinal Endocrine Cells. *Mol. Cell. Biol.* **34**, 2308-2317, doi:10.1128/mcb.01600-13 (2014).
426 Date, S. *et al.* Finb, a multiple zinc finger protein, represses transcription of the human angiotensinogen gene. *Int J Mol Med* **13**, 637-642, doi:10.3892/ijmm.13.5.637 (2004).
427 Flajollet, S., Poras, I., Carosella, E. D. & Moreau, P. RREB-1 Is a Transcriptional Repressor of HLA-G. *J. Immunol.* **183**, 6948-6959, doi:10.4049/jimmunol.0902053 (2009).
428 Milon, B. C., Agyapong, A., Bautista, R., Costello, L. C. & Franklin, R. B. Ras responsive element binding protein-1 (RREB-1) down-regulates hZIP1 expression in prostate cancer cells. *Prostate* **70**, 288-296, doi:10.1002/pros.21063 (2010).
429 Mukhopadhyay, N. K. *et al.* The Zinc Finger Protein Ras-Responsive Element Binding Protein-1 Is a Coregulator of the Androgen Receptor: Implications for the Role of the Ras

Pathway in Enhancing Androgenic Signaling in Prostate Cancer. *Mol. Endocrinol.* **21**, 2056-2070, doi:10.1210/me.2006-0503 (2007).

430 Carosella, E. D., Favier, B., Rouas-Freiss, N., Moreau, P. & LeMaoult, J. Beyond the increasing complexity of the immunomodulatory HLA-G molecule. *Blood* **111**, 4862-4870, doi:10.1182/blood-2007-12-127662 (2008).

431 Duan, S. *et al.* FBXO11 targets BCL6 for degradation and is inactivated in diffuse large B-cell lymphomas. *Nature* **481**, 90-93, doi:10.1038/nature10688 (2012).

432 Schneider, C. *et al.* FBXO11 inactivation leads to abnormal germinal-center formation and lymphoproliferative disease. *Blood* **128**, 660-666, doi:10.1182/blood-2015-11-684357 (2016).

433 Dersh, D. *et al.* Genome-wide Screens Identify Lineage- and Tumor-Specific Genes Modulating MHC-I- and MHC-II-Restricted Immunosurveillance of Human Lymphomas. *Immunity* **54**, 116-131, doi:10.1016/j.immuni.2020.11.002 (2021).

434 Ennishi, D. *et al.* Molecular and Genetic Characterization of MHC Deficiency Identifies EZH2 as Therapeutic Target for Enhancing Immune Recognition. *Cancer Discov.* **9**, 546-563, doi:10.1158/2159-8290.cd-18-1090 (2019).

435 Gambacorta, V. *et al.* Integrated Multiomic Profiling Identifies the Epigenetic Regulator PRC2 as a Therapeutic Target to Counteract Leukemia Immune Escape and Relapse. *Cancer Discovery* **12**, 1449-1461, doi:10.1158/2159-8290.CD-21-0980 (2022).

436 Göllner, S. *et al.* Loss of the histone methyltransferase EZH2 induces resistance to multiple drugs in acute myeloid leukemia. *Nat. Med.* **23**, 69-78, doi:10.1038/nm.4247 (2017).

437 Yang, M. *et al.* Structural Basis for CoREST-Dependent Demethylation of Nucleosomes by the Human LSD1 Histone Demethylase. *Molecular Cell* **23**, 377-387, doi:10.1016/j.molcel.2006.07.012 (2006).

438 Humphrey, G. W. *et al.* Stable Histone Deacetylase Complexes Distinguished by the Presence of SANT Domain Proteins CoREST/kiaa0071 and Mta-L1. *Journal of Biological Chemistry* **276**, 6817-6824, doi:10.1074/jbc.M007372200 (2001).

439 Chinnadurai, G. Transcriptional regulation by C-terminal binding proteins. *Int. J. Biochem. Cell Biol.* **39**, 1593-1607, doi:10.1016/j.biocel.2007.01.025 (2007).

440 Pappano, W. N. *et al.* The Histone Methyltransferase Inhibitor A-366 Uncovers a Role for G9a/GLP in the Epigenetics of Leukemia. *PLoS One* **10**, e0131716, doi:10.1371/journal.pone.0131716 (2015).

441 Vedadi, M. *et al.* A chemical probe selectively inhibits G9a and GLP methyltransferase activity in cells. *Nat. Chem. Biol.* **7**, 566-574, doi:10.1038/nchembio.599 (2011).

442 Peters, A. H. F. M. *et al.* Partitioning and Plasticity of Repressive Histone Methylation States in Mammalian Chromatin. *Mol. Cell* **12**, 1577-1589, doi:10.1016/S1097-2765(03)00477-5 (2003).

443 Roulois, D. *et al.* DNA-Demethylating Agents Target Colorectal Cancer Cells by Inducing Viral Mimicry by Endogenous Transcripts. *Cell* **162**, 961-973, doi:10.1016/j.cell.2015.07.056 (2015).

444 Durbin, J. E., Hackenmiller, R., Simon, M. C. & Levy, D. E. Targeted Disruption of the Mouse Stat1 Gene Results in Compromised Innate Immunity to Viral Disease. *Cell* **84**, 443-450, doi:10.1016/S0092-8674(00)81289-1 (1996).

445 Meraz, M. A. *et al.* Targeted Disruption of the Stat1 Gene in Mice Reveals Unexpected Physiologic Specificity in the JAK-STAT Signaling Pathway. *Cell* **84**, 431-442, doi:10.1016/S0092-8674(00)81288-X (1996).

446 Gide, T. N. *et al.* Distinct Immune Cell Populations Define Response to Anti-PD-1 Monotherapy and Anti-PD-1/Anti-CTLA-4 Combined Therapy. *Cancer Cell* **35**, 238-255.e236, doi:10.1016/j.ccell.2019.01.003 (2019).

447 Schmid, C. *et al.* Donor Lymphocyte Infusion in the Treatment of First Hematological Relapse After Allogeneic Stem-Cell Transplantation in Adults With Acute Myeloid Leukemia: A Retrospective Risk Factors Analysis and Comparison With Other Strategies by the EBMT Acute Leukemia Working Party. *J. Clin. Oncol.* **25**, 4938-4945, doi:10.1200/jco.2007.11.6053 (2007).

448 Miyamoto, T. *et al.* Donor Lymphocyte Infusion for Relapsed Hematological Malignancies after Unrelated Allogeneic Bone Marrow Transplantation Facilitated by the Japan Marrow Donor Program. *Biol. Blood Marrow Transplant.* **23**, 938-944, doi:10.1016/j.bbmt.2017.02.012 (2017).

449 Webster, J. A., Luznik, L. & Gojo, I. Treatment of AML Relapse After Allo-HCT. *Front Oncol.* **11**, doi:10.3389/fonc.2021.812207 (2021).

450 Kneppers, E. *et al.* Lenalidomide maintenance after nonmyeloablative allogeneic stem cell transplantation in multiple myeloma is not feasible: results of the HOVON 76 Trial. *Blood* **118**, 2413-2419, doi:10.1182/blood-2011-04-348292 (2011).

451 Katja, S. *et al.* Lenalidomide maintenance after allogeneic HSCT seems to trigger acute graft-versus-host disease in patients with high-risk myelodysplastic syndromes or acute myeloid leukemia and del(5q): results of the LENAMAINT trial. *Haematologica* **97**, e34-e35, doi:10.3324/haematol.2012.067629 (2012).

452 Cenerenti, M., Saillard, M., Romero, P. & Jandus, C. The Era of Cytotoxic CD4 T Cells. *Front Immunol* **13**, doi:10.3389/fimmu.2022.867189 (2022).

453 Hunder, N. N. *et al.* Treatment of Metastatic Melanoma with Autologous CD4+ T Cells against NY-ESO-1. *New England Journal of Medicine* **358**, 2698-2703, doi:10.1056/NEJMoa0800251 (2008).

454 Tran, E. *et al.* Cancer Immunotherapy Based on Mutation-Specific CD4+ T Cells in a Patient with Epithelial Cancer. *Science* **344**, 641-645, doi:10.1126/science.1251102 (2014).

455 Preglej, T. *et al.* Histone deacetylases 1 and 2 restrain CD4+ cytotoxic T lymphocyte differentiation. *JCI Insight* **5**, doi:10.1172/jci.insight.133393 (2020).

456 Inderberg-Suso, E.-M., Trachsel, S., Lislerud, K., Rasmussen, A.-M. & Gaudernack, G. Widespread CD4+ T-cell reactivity to novel hTERT epitopes following vaccination of cancer patients with a single hTERT peptide GV1001. *OncoImmunology* **1**, 670-686, doi:10.4161/onci.20426 (2012).

457 Anastasopoulou, E. A., Voutsas, I. F., Papamichail, M., Baxevanis, C. N. & Perez, S. A. MHC class II tetramer analyses in AE37-vaccinated prostate cancer patients reveal vaccine-specific polyfunctional and long-lasting CD4+ T-cells. *OncoImmunology* **5**, e1178439, doi:10.1080/2162402X.2016.1178439 (2016).

458 Hemon, P. *et al.* MHC Class II Engagement by Its Ligand LAG-3 (CD223) Contributes to Melanoma Resistance to Apoptosis. *J. Immunol.* **186**, 5173-5183, doi:10.4049/jimmunol.1002050 (2011).

459 Maruhashi, T. *et al.* Binding of LAG-3 to stable peptide-MHC class II limits T cell function and suppresses autoimmunity and anti-cancer immunity. *Immunity* **55**, 912-924.e918, doi:10.1016/j.immuni.2022.03.013 (2022).

460 Ang, G. C. K., Gupta, A., Yap, S. X. L., Surana, U. & Taneja, R. Potential Therapeutics Targeting Upstream Regulators and Interactors of EHMT1/2. *Cancers (Basel)* **14**, 2855 (2022).